Context-dependent gene function in *C. elegans*

Anna Way

Charlottesville, Virginia

B.S., University of Wrocław, Wrocław, Poland, 2013

M.S. University of Wrocław, Wrocław, Poland, 2016

A Dissertation presented to the Graduate Faculty

of the University of Virginia in Candidacy for the Degree of

Doctor of Philosophy

Department of Biology

University of Virginia

July 2021

_____

_____

_____

_____

_____

Contents

Abstract

Plasticity in multicellular organisms involves signaling pathways converting contexts into context-specific changes in gene expression. Contexts range from environmental changes such as seasonal or daily dietary changes to changes in the microbiome composition or the acute effect of stressors (chemical, physical or biological). Context can also refer to penetrant loss or gain of function mutations. In the lab, contexts include distinct mutant backgrounds, culture media, microbiomes, cells, and tissue types, among others. Studies have shown that context can change the phenotypic outcome of a perturbation.

Congruently, the signaling molecule-transcription factor (TF) interactions regulating these responses are also context-specific. However, when a target gene responds across contexts, the upstream TF identified in one context is often inferred to regulate it across contexts. Hence, reconciling these stable TF-target gene pair inferences with the context-specific nature of homeostatic responses is needed.

The induction of the *C. elegans* genes *lipl-1, lipl-3*, and *lipl-4* is essential to survival during fasting and is observed in many genetic contexts. We find DAF-16/FOXO mediating *lipl-4* induction in all contexts tested; hence, *lipl-4* regulation seems context-independent and compatible with across-context inferences. Contrastingly, DAF-16 activates the stress-responsive TF HSF-1 during oxidative stress, promoting *C. elegans* survival through induction of *lipl-3*. Further, the TF MXL-3 contributes to the dominance of HSF-1 at the expense of HLH-30 during oxidative stress but not during fasting. This study shows the limitations of across-context inferences and how context-specific

diverting of interactions within a network allows cells to specifically respond to many contexts with a limited number of molecular players.

In summary, context is a critical variable in gene regulation, particularly for genes promiscuously activated or repressed across multiple stresses or physiological responses. Inferring the gene regulatory pathways based on studies carried out in different contexts played an essential role in creating the current body of knowledge. However, as we aim to understand more deeply the gene regulatory pathways acting in health and disease, we need to acknowledge that inferences can be misleading and even hinder discovery.

Acknowledgement

Ph.D. was a long and challenging road and something that I could never achieve by myself. During my journey, I met many wonderful people who served as my mentors and friends during this long road. Here, I would like to thank them for all their help and everything they have done for me, and how they helped me develop through the last few years.

First, I would like to thank my thesis advisor, Professor Eyleen O'Rourke, for helping me throughout my scientific journey, her scientific expertise and support, and everything I learned from her.

I would like to thank my thesis committee: Professor Alan Bergland, Professor Sarah Siegrist, Proferson Bettina Winckler, Professor George Bloom for their advice and support during this journey and their scientific expertise in developing my project.

My lab mates. I would like to thank Dr. Vinod Mony for the great collaboration on the project that became my thesis' chapter. Vinod's positivity always brightened the lab.
I would like to thank fellow graduate students, technicians, and undergraduate trainees in our lab: Dr. Wenfan Ke, Leila Rayyan, Mary Kate Horak, Jake Saba, Michael Hilzendeger, Abbas Ghaddar, Nella Solodukhina, and especially two lab mates who became my great friends: Shawna Benjamin and Zofia Kołodziejczyk. Working with all

of you was a great pleasure. I feel grateful for having such friendly and supportive lab mates.

My undergraduate mentees: Emma Harrison, Alexandra Loperfito, Mikayla Marraccini, Najee Chaudhry, Jeannie Taylor, and Griffin Perry. Mentoring you and seeing you grow was one of the most pleasurable parts of my Ph.D. I will always cherish your friendship, and I am proud to call myself your mentor.

I would like to thank Jefferson Scholar Foundation for the financial support through Jefferson Fellowship and the great and supportive community they create. Because of the fellowship, I met many great people, both staff and Jefferson Fellows and Scholars, listened to many interesting talks, and met exciting speakers. The support from the Foundation allowed me to make one of my dreams come true and organize the first Communicating Science Conference at UVA.

The team of students that participated in organizing Communicating Science Conference. Thank you for all your time and passion in organizing this event together. I would like to thank Vanessa Bijak, vice-Chair of the conference, for sharing her passion for science communication and promoting Poland in the USA through the Polish Students Association, where we worked together.

I want to give sincere thanks and words of appreciation to Dr. Sonali Majumdar. Sonali gave me advice and tools to help me with my career development. During the career

development workshops offered by the PhD Plus program and led by Sonali, I gained tools and ways of thinking about developing my career in a way that will be fulfilling for me and match my values. I'm very grateful for this.

I would also like to extend my gratitude to Dr. Marlit Hayslett for all the help and kindness. Marlit initiated my interest in science communication that will outlast my Ph.D. journey. Working with Marlit for the last three years was a true pleasure. She always motivated me to do great work and, at the same time, provided excellent advice and expertise in the field.

I would like to thank Takarai Hideto (HYDE) and Hayashi Yoshiki for creating music that motivated and inspired me to keep going and not give up at the end of my Ph.D. journey.

Most of all, I would like to thank my husband, Randall Way. I can confidently say that I would not be writing this thesis, and I would not complete this journey if not for Randall. He is always there for me, helping in so many ways I cannot even list it all. He always finds words to uplift my spirit and motivates me to move forward. I am forever grateful for this, and this thesis is as much his as it is mine. Words are insufficient to express how grateful I am to have such a wonderful husband who believes in me more than I believe in myself.

List of Abbreviations

TF/s – Transcription Factor/s

IR – Insulin receptor (encoded by *daf-2* gene in *C. elegans*)

IIS - Insulin signaling

TGFß – Tumour Growth Factor ß pathway

mTOR – mechanistic Target of Rapamycin (kinase subunit encoded by *let-363* in *C. elegans*)

AMPK – 5'adenosine monophosphate-activated protein kinase

MXL-3 – Max-like 3 (TF)

TFEB – Transcription factor EB

HSF-1 – Heat shock factor 1 (TF)

FUdR - 5-Fluoro-2'-deoxyuridine

Chapter I: Introductory chapter

When exposed to environmental challenges, the cells of an organism need to adjust the expression of genes to overcome the environmental challenge (1). Key regulators of spatiotemporal gene expression are transcription factors (TFs). TFs are trans-acting factors that exert their control by binding to the cis-acting regulatory sequences of genes (2). Gene regulation is a very complex process. On one hand, one TF can regulate multiple genes. On the other hand, each gene can have several cis-acting sequences and TFs that act, together with enhancers and repressors, to regulate the expression of the single gene (2,3). Additionally, TFs can also compete with each other for binding to the same DNA fragment, and some TFs need to form dimers to properly interact with DNA sequences located in the promoters of the genes (4).

To allow for proper gene expression in different cells and tissues, many TFs are expressed in a tissue- or cell-specific manner and bind different genes in different cell types or conditions (5,6); thus, the regulation of any given gene can be cell-type specific (2,4). For instance, treating breast cancer line T-47D and endometrial cancer cell line ECC-1 with 17β-estradiol (E2) causes changes in gene expression that are cell type-specific. Genes induced by E2 treatments differ between cell lines with only 16% of T-47D upregulated genes and 5% of T-47D downregulated genes overlapping between both cell lines. More interestingly, there are 46 genes whose expression is opposite between ECC-1 and T-47D after the E2 treatment. Specifically, E2 treatment results in the upregulation of 39 genes in the T-47D line that are downregulated in the ECC-1 line,

whereas nine genes downregulated in T-47D are upregulated in ECC-1. These contradicting expression patterns correlated with occupancy at the ESR1 (estrogen receptor 1)-binding sites of the promoters of these genes (7). The opposite direction of the transcriptional response is surprising taking into account that E2 induces proliferation in both cell types (8,9), suggesting diverse regulatory pathways that can lead to the same phenotypic outcome.

TFs form complex networks of proteins that functionally interact with each other in ways ranging from protein-protein interactions to genetic epistatic relationships that define the expression levels of their downstream transcriptional targets. This complexity makes challenging the understanding of how TFs regulate gene expression in different contexts. However, dissecting the transcriptional regulation of genes in different contexts will get us closer to understanding the complexity of living organisms.

In an attempt to increase feasibility, the study of the regulation of genes is often approached as a sum of single linear pathways. Once linear pathways are dissected, the data from multiple studies are compiled to infer the “complete” regulation of a gene across natural or experimental conditions, here referred to as contexts. Contexts range from environmental changes such as seasonal or daily dietary changes to changes in the composition of the microbiome or the acute effect of stressors (chemical, physical or biological). Context can also refer to penetrant loss or gain of function mutations. In the

lab, contexts include distinct mutant backgrounds, culture media, microbiomes, cells, and tissue types, among others. Studies have shown that context can change the phenotypic outcome of a perturbation (e.g. mutation of a gene) all the way from innocuous to lethal (10–12). Therefore, although the inference of genetic pathways by compiling studies done in different contexts has brought to light many discoveries, or at least advanced our understanding of gene function, a growing body of evidence shows that we should be cautious about relying on such inferences because they can be flawed, and flawed inferences can be misleading or hinder discoveries. Here I used the genetic interactions between transcription factors (TFs) acting downstream of nutrient-sensing pathways to show to which extent different contexts can influence the functional interactions between genes, and ultimately the phenotype of interest.

Nutrient sensing is composed of evolutionarily conserved signaling molecules that play a role in detecting nutrient availability and relaying signals that allow cells and ultimately organisms to adjust the energy needs and energy output to the levels of energetic input. In response to nutrient availability, nutrient sensors promote growth, reproduction, and tissue maintenance (13). Likely due to the essential role of nutrients in the biochemical reactions that sustain growth and reproduction, organisms have multiple molecular pathways that sense nutrient availability and adjust organismal metabolism to the available nutrients. Further, likely due to its essential nature, nutrient sensing is highly conserved from simple organisms, like yeast, to humans (14–17). Major conserved nutrient sensors include the mechanistic target of rapamycin (mTOR) and AMP-activated

protein kinase (AMPK). In addition, in *C. elegans*, growth-factor sensors such as the insulin (IIS), Notch, and transforming growth factor β (TGF-β) receptors are often referred to as nutrient sensors because they link food availability to development and aging. When nutrients are scarce, the abundance of ligands for these membrane receptors decreases, which reduces the activity of the receptors and consequently stalls growth and delays reproduction (13,18–21). By contrast, signaling downstream of these receptors when food is available promotes growth and reproduction. Further, genetic or chemical inactivation of these growth-factor receptors is sufficient to trigger fasting-like molecular and physiological responses in *C. elegans* (15,22–33).

Importantly, the activity of AMPK, mTOR, IIS, TGF-β, and Notch is also reduced by exposure to other stressors, including oxidative stress (29,34,35), anoxia (36,37), and pathogens (38–40), among others. In addition, AMPK, mTOR, IIS, TGF-β, and Notch signaling have been found to relay insults in a cell- or tissue-type specific manner (41–45), and a network of context-specific TFs and other downstream effectors have been described to mediate the phenotypic outcome of the perturbations (46–48). An emerging body of research points to the notion that both the upstream sensors and their downstream players may distinctly modulate homeostatic responses appropriate to each context. Next, I will describe published examples that illustrate the context-dependent roles played by the aforementioned nutrient-sensing pathways and their downstream effectors.

1. Background on context-dependent gene function

1.1. Distinct roles of genes in development vs. adulthood

A theoretical framework supported by several examples of the extent to which context defines the role of genes was introduced in 1957 by George C. Williams as the antagonistic pleiotropy theory of aging (49). Antagonistic pleiotropy proposes that a given gene can have a beneficial role early in life, but the same function can be detrimental to the organism later in life. The contradicting effects for a gene would be possible due to natural selection operating on organisms before and during their reproductive period but not post-reproductively. Genes or traits that give an organism advantage before and during their reproductive period will be carried to the next generations, even if those genes are detrimental to the organism during the post-reproductive period. Within this framework, the different life stages of an organism are distinct contexts defining the phenotypic effect of a gene.

The *C. elegans* insulin receptor, DAF-2, commonly referred to as a nutrient sensor (13), is an ortholog of the mammalian insulin and IGF-1 (Insulin-like growth factor) receptors. DAF-2 is essential for normal development as *daf-2* mutants exhibit increased progeny lethality, and a null mutation is lethal (50–52). To study the role of the *daf-2* gene in later stages of development, researchers used temperature-sensitive alleles, which enables post-developmental gene inactivation by shifting worms to the non-permissive temperature (25ºC) as late larval stage 4 (L4) or young adults. In a striking example of antagonistic pleiotropy, when *daf-2* mutant animals are shifted to the non-permissive

temperature during the L4 stage or adulthood, they activate a stress-resistance program that leads to increased survivorship in a diverse range of harsh environments and extended healthspan and lifespan (53). Loss of function mutation of *daf-2* manifesting as embryonic lethality or exacerbated survival depending on the time at which the gene is inactivated exemplifies the distinct, even opposing, context-dependent effects that a gene can have on a phenotype. Further, the context-dependent function of the gene encoding the insulin receptor is conserved. Mice carrying null mutations of the IGF-1 receptors are embryonic lethal or die shortly after birth (54,55). On the other hand, adult mice with reduced IGF-1 levels exhibit increased lifespan and are resistant to oxidative stress (56–59). Additionally, reducing insulin signaling in *Drosophila* was also shown to increase lifespan (60), but a loss of zygotic insulin receptor function results in embryonic lethality and some arrested learve (61,62).

Loss of function mutants of downstream components of the insulin signaling pathway (IIS) also shows context-dependent phenotypes. For example, mutation of *C. elegans*' *age-1*, a PI3K homolog, slows down development (63), and *age-1* inactivation in the adult leads to longevity (63–65). The context-dependent function of PI3K is also evident in mammals, where mutations in PI3K result in embryonic lethality (66–68), but suppression of PI3K in adult mice leads to modest lifespan extension, improved glucose homeostasis, protects from age-related reduction in insulin sensitivity (69) and prevents cardiac aging (70).

Downstream of the insulin receptor, we can find mTOR (mechanistic Target of Rapamycin), a multiprotein complex often referred to as a master nutrient sensor. mTOR is an evolutionarily conserved kinase that senses the nutritional status of the cell and couples it to cell proliferation and growth. In nutrient-rich conditions, mTOR is active and promotes cell growth by activating anabolic processes (i.e., translation) while simultaneously inhibiting catabolic processes (i.e., autophagy). In nutrient-deficient conditions, mTOR inhibition leads to inhibition of anabolic processes and activation of catabolic processes to provide cells with energy and building blocks indispensable to survival (71).

Similar to the components of the insulin signaling pathway described above, the phenotypic output of genes involved in the mTOR pathway depends on the context. Early inactivation of *let-363*, the gene encoding the mTOR kinase subunit in *C. elegans*, leads to reduced fertility and reduced viability (72). Similarly, in mice, homozygous mTOR mutant embryos show growth arrest resulting in early post-implantation lethality (24,73). By contrast, the inactivation of *let-363* by RNAi in adult *C. elegans* results in a longer lifespan (72). Likewise, adult inactivation of *daf-15* (homolog of mammalian Rictor), a regulatory component of mTOR complex 1, extends both the mean and maximum adult life span in *C. elegans* (74), while *daf-15* inactivation during development leads to growth arrest (75). In mice, deletion of mTOR Substrate S6 Kinase 1 (S6K1) leads to resistance to age-related pathologies such as bone, immune, and motor dysfunction, loss of insulin sensitivity, and to increased lifespan (76). However, deletion of S6K1 in

younger animals leads to slow growth (76,77), and deletion of both S6K1 and S6K2 is lethal (77).

The insulin and mTOR signaling pathways are therefore examples of how the phenotypic output of genes depends on the age of the organism. Inactivation of the same gene can be lethal if inactivated during development, while if inactivated during adulthood it leads to extended lifespan and healthspan of the organism. In other words, context defines whether the gene is beneficial for the organism or detrimental.

1.2. Distinct roles of genes in different genetic backgrounds

Organisms are complex genetic networks acting within cells but interacting across cells, tissues, and organs. Disrupting one node of the network can set in motion a series of downstream perturbations. However, perturbing the same node, through for instance loss of function mutation, does not have the same effect on the phenotype in every organism. The impact of a perturbation can range from innocuous to lethal depending on the genetic background, the genetic makeup of all other genes in the organism/s of interest. A gene essentiality screen performed in two strains of *Saccharomyces cerevisiae* showed that although most of the essential genes were shared between the strains, there were also strain-specific essential genes (10). This conditional essentiality demonstrates to which extent each genome defines gene-gene and gene-environment interactions that result in strain-specific phenotypic variation, suggesting that the genetic background, here referred

to as genetic context, can determine the difference between life and death. The context-dependent nature of gene function may also explain the difficulties in predicting phenotype from the genotype of an organism.

The transcription factor (TF) TFEB and its downstream effectors BHLHE40 and BHLHE41 are examples of how simple inferences regarding gene functions may not always be correct. Carey *et al.* showed that *BHLHE40* and *BHLHE41* are targets of TFEB and that activation of TFEB is sufficient to induce *BHLHE40* and *BHLHE41 (78)*. TFEB is required to protect cells from LLME (L- leucyl-L-leucine methyl ester)-induced cell death (78), a type of cell death triggered by lysosomal membrane permeabilization (79,80). However, contrary to expectation, targeted activation of *BHLHE40* and *BHLHE41* sensitizes cells to LLME-cell death (78). These reports seem to contradict each other; however, using loss and gain of function versions of *TFEB*, *BHLHE40,* and *BHLHE41* has confirmed the results (78). Thus, given that TFEB is a positive regulator of *BHLHE40,* and *BHLHE41*, the most parsimonious hypothesis would have been that since TFEB protects cells from cell death then *BHLHE40* and *BHLHE41* would have the same effect. However, this is not the case. The experimental results show the opposite, showing the importance of being cautious when inferring gene function.

Contextualizing gene function is not only important to understand the working of biological systems, it is also relevant in biomedicine. Multiple examples of context-

dependent genotype-to-phenotype relationships can be found in the field of cancer (81). Cancer is a metabolic disease, and pathways that govern growth and nutrient sensing are altered in tumors (82). FOXO (a TF downstream of the insulin signaling pathway) is known to be a tumor suppressor (83). However, in acute myeloid leukemia, FOXO1/3/4 is necessary for cell growth, and its inhibition increases apoptosis markers and results in longer survivorship in mice with leukemia (84).

Another example of the conflicting/opposing roles of FOXO comes from studies of *C. elegans*' DAF-16, the FOXO homolog. When insulin signaling is reduced in *C. elegans*, DAF-16 is activated. Activation of DAF-16 in turn leads to extended healthspan and lifespan as well as increased stress resistance (85). Further, in the *C. elegans* germline, DAF-16 activity prevents stem cell overproliferation (86). In adult *C. elegans*, germline stem cells are the only cells that still proliferate; hence, a perturbation that leads to increased germ cell proliferation is considered tumorigenic in the worm (87,88). Therefore, one would infer that increasing DAF-16 activity in the germline would have a tumor-suppressive effect. However, demonstrating the complexity of gene-context and tissue-tissue interactions, when DAF-16 was overexpressed in the hypodermis, it caused hyper-proliferation of the germine and shorter lifespan (89). What is more, based on the canonical inhibitory effect of the insulin signaling pathway on DAF-16/FOXO (78), when the gene encoding the *C. elegans* insulin receptor *daf-2* is inactivated, one would expect further increases in DAF-16 activity. However, in Qi *et al*'s. study, *daf-2* inactivation suppressed the DAF-16-mediated germline tumor phenotype (89), suggesting

that the pro-oncogenic DAF-16 activity is positively regulated by insulin signaling. Thus, the cell-autonomous activity of DAF-16 in germline seems to have the opposite effect that cell-non autonomous activity of DAF-16 in the hypodermis. Qi *et al.* proposed the existence of two antagonistic DAF-16/FOXO functions. The first one is a cell-proliferative somatic function, and the second is an antiproliferative germline activity. In the first case, germline cell proliferation is inhibited cell-autonomously by DAF-16 in conditions of reduced IIS. In the second case, when DAF-16 is artificially activated in somatic tissues (via overexpression) in the presence of active IIS, tumor-like growth of the germline is promoted (90).

Summarizing, inferring the function of a gene and the effect of mutating it based on analysis or manipulation of the gene in other contexts can lead to flawed conclusions. This has implications, not only for basic research, but also for the use of drugs in the clinic, as some drugs may have different effects on the same cancerous mutation depending on the tissue in which this mutation occurs or the genetic background of the patient (91). Further, as described in the next sections, factors beyond the organism itself, such as its microbiota or its diet, can revert the phenotypic outcome of genes.

1.3. Environmental context

1.3.1. Stress

Animals live in ever-changing environments. They are constantly exposed to stressors, and they need to flee or adapt to those challenges by adjusting their gene expression

programs. Since the number of genes is limited, but the number of stressors and their combinations are not or less so, animals may use the same molecular players to respond to different stressors. However, depending on the context, the molecular players may activate different sets of genes, targeting those ones promoting stress-specific homeostasis.

An example of a molecule adjusting its response to the specific challenge is the TF TFEB. Carey *et al.* looked at genes activated by TFEB in two different contexts: (1) cells treated with the mTOR inhibitor Torin, and (2) cells exposed to the pathogen *Salmonella enterica* (78). In both conditions, TFEB is expected to be activated and induce the transcription of downstream targets. Indeed, that is what happened; however, the subsets of TFEB-mediated induced genes were different between conditions (78). Similarly, Lin *et al.* investigated the role that DAF-16 (mammalian FOXO) and HLH-30 (mammalian TFEB) play in longevity, oxidative and heat stress, and dauer formation (dauer is stress-resistant developmental stage of *C. elegans* alternative to the larval stage 3) (92). First, they tested the role of DAF-16/FOXO and HLH-30/TFEB in the lifespan extension of *daf-2* (insulin receptor) and *glp-1* (Notch receptor) mutants. Both TFs suppressed the longevity of *daf-2* and *glp-1* animals, and they appeared to work on the same genetic pathway as inactivation of both had almost no additive effect on lifespan. Transcriptional analysis showed that DAF-16/FOXO and HLH-30/TFEB co-regulated aging-related genes and that DAF-16/FOXO and HLH-30/TFEB can bind to the promoters of the same genes. However, this was not the case for all genes regulated by HLH-30/TFEB or DAF-

16/FOXO, since for some of them only DAF-16/FOXO or only HLH-30/TFEB binding was observed, suggesting that they may regulate gene transcription differently in different contexts. Hence, Lin *et al.* tested whether DAF-16/FOXO and HLH-30/TFEB were part of the same stress-resistance pathways as they were in the regulation of lifespan. Interestingly, DAF-16/FOXO and HLH-30/TFEB effect in heat stress were additive, but in oxidative stress, their action was not additive, suggesting that DAF-16/FOXO and HLH-30/TFEB act in the same genetic pathway during oxidative stress, but in separate pathways during heat stress. However, in a different biological process, dauer formation, DAF-16/FOXO, and HLH-30/TFEB were opposite. When researchers induced dauer formation using the thermosensitive mutant *daf-2 (e1370)*, DAF-16/FOXO, as expected, suppressed the formation of dauers. However, surprisingly, HLH-30/TFEB acted as an inhibitor, as its loss of function mutation further enhanced dauer formation in the *daf-2* mutant (92). This example shows that DAF-16/FOXO and HLH-30/TFEB action is context-dependent: the two TFs work together to promote longevity and oxidative stress survival, but in separate pathways during heat stress, and they can oppose each other during dauer formation (92).

Differential regulation of gene expression in different contexts was also shown by Heimbucher *et al.* who have shown that DAF-16/FOXO regulates *sodh-1/dod-11* in opposite ways in different contexts. First, Zhang *et al.* showed that in the *daf-2* mutant, DAF-16/FOXO mediates the transcriptional activation of *sodh-1/dod-11* (93). However, in conditions where IIS signaling is active, in *daf-16* mutants, and in chemically induced

hypoxia, the expression of *sodh-1p::rfp* was increased, suggesting DAF-16/FOXO role as a *sodh-1/dod-11* inhibitor is context-dependent (94). A similar case was described for PQM-1, a C2H2 zinc finger TF that works downstream of the IIS and cooperates with DAF-16/FOXO to regulate genes downstream of IIS (95). Loss of function mutation of *pqm-1* suppresses *daf-2* longevity (95). However, the same mutation exacerbates *daf-2*'s resistance to chemically induced anoxia (94). Taken together, the same TF can act as an inhibitor or activator of the same gene, depending on the context.

1.3.2. Diet

All living organisms need nutrients to grow, reproduce, and survive environmental challenges. However, the diet of each organism is different, creating a unique dietary context for each organism. A recent paper from our lab showed single-compound changes in the composition of the diet can change the toxicity of chemotherapeutic drugs. Specifically, single dietary supplementation of thymidine or serine can enhance the toxicity of the antimetabolite 5' fluorodeoxyuridine (FUdR) in *C. elegans* up to 100 fold (96). FUdR is a fluoropyrimidine drug commonly used to treat colon cancer and that, when added to the culture media of *C. elegans*, causes embryonic lethality or developmental delay (depending on the dose). However, most interestingly, the increase in toxicity observed when *C. elegans* are co-exposed to FUdR and non-toxic levels of serine is that if the *E. coli* normally used to feed worms in the lab are killed or genetically manipulated, then FUdR is not toxic to worms and serine does not enhance the toxicity of FUdR. Therefore, *E. coli*, which in addition to being the food source of *C. elegans* in the

lab, is the sole source of microbiota, is mediating the toxicity of the chemotherapeutic FUdR in the *C. elegans* host.

After dissecting how *E. coli* promotes FUdR toxicity in *C. elegans*, we studied how *C. elegans* responds to the FUdR and serine-enhanced FUdR toxicity. When *C. elegans* are exposed to FUdR and its diet is not supplemented with serine, RNAi against autophagy genes suppresses the toxicity of FUdR toxicity, and the expression of autophagy genes and autophagic flux was shown to be increased with worms treated with FUdR only. Further, RNAi against the upstream activators of autophagy AMPK, MSH-1, UNG-1, and PUS-1 also reduced the toxicity of FUdR. Hence, altogether, hyperactivation of autophagy seems to be the cause of death in *C. elegans* exposed to FUdR. Surprisingly it was then observed that when *C. elegans* are co-exposed to FUdR and serine, RNAi against the same autophagy genes led to enhanced toxicity, suggesting that autophagy protects from death in this context. Similarly, *pus-1* enhances the FUDR toxicity when the diet is supplemented with serine (96).

Taken together, these observations reveal an extreme example of context dependence. The sole dietary supplementation of one amino acid changes the drug toxicity mechanism to the point of reverting the role of the same molecular players in survival to drug toxicity.

1.3.3. Microbiota

The microbiota, defined as the microorganisms living inside and on multicellular organisms, plays an essential role in growth, behavior, and reproduction, among other critical animal functions (97–99). A growing body of research shows that host factors interact with the microbiota or its products, which in turn can influence or define phenotypic outcomes. Hence, in the framework proposed here, the microbiota serves as a biological context that influences gene-environment interactions to the extent of changing the phenotype.

In *C. elegans*, several studies have pointed to a range of phenotypes influenced by the microbiota. For example, as a component of the mTORC2 complex (100), Rictor (encoded by *rict-1* in *C. elegans*) modulates critical biological processes, including the rate of development, fat storage, and the rate of aging (101). However, the effect of inactivating Rictor on these phenotypes depends on the composition of the microbiota. *rict-1 C. elegans* mutants co-cultured with *E. coli* HB101 show decreased fat levels, smaller body size and brood size than wild-type worms. However, when *rict-1 C. elegans* mutants are co-cultured with *E. coli* OP50, they are fatter, bigger, and develop faster than their wild-type counterparts (101). Interestingly, *E. coli*-dependent lifespan phenotypes were also observed when Rictor was mutated in *C. elegans*, with *rict-1* mutants co-cultured with *E. coli* OP50 living shorter than wild-type animals, and *rict-1* mutants co-cultured with *E.coli* HB101 or *E.coli* HT115 living longer than wild-type worms (101,102). Similarly, overexpressing *rict-1* in worms grown on *E. coli* OP50 extends

lifespan, while overexpressing *rict-1* in worms growing on *E. coli* HT115 shortens the lifespan of *C. elegans* (102).

Mizunuma *et al*. investigated those changes further, showing that worms with inactivated *rict-1* cultured on *E. coli* HT115 bacteria were more resistant to oxidative stress than wild-type worms (103). In contrast, worms with inactivated *rict-1* cultured on *E. coli* OP50 bacteria didn't show resistance to oxidative stress. Similarly, they observed a difference in *C. elegans* lifespan that was dependent on the microbiome. *C. elegans* lifespan measured at 25ºC was consistent with previous findings by Soukas *et al.*, with *rict-1* mutants fed *E. coli* HT115 living slightly longer than wild-type worms. However, when *rict-1* mutants were kept in 20ºC or 15ºC, their lifespan was always shorter than the wild type, regardless of the *E. coli* strain (103). Altogether, these reports point to the effect of the *E. coli* strain used to feed and build the *C. elegans* microbiota on the life-history traits of this simple animal and emphasize the importance of the microbial context in defining genotype-phenotype relationships.

2. Mechanistic understanding of context-dependent gene function

When performing experiments in different contexts, it may happen that we will obtain results that at first seem contradictory, for example, a transcription factor acts as a repressor of a gene in one context and as an activator of the same gene in a different context. However, if both observations are robust and reproducible, that means there

must be a molecular mechanism underlying the opposing effects on phenotype. To unveil the molecular underpinnings of opposing genotype-phenotype relationships for the same gene, we need to go beyond describing the interaction between gene and its context, we need to look at how other genes may distinctively respond and interact with each other and with the gene of interest to ultimately yield opposing phenotypes. To achieve such in-depth understanding may require the use of computational modeling as the number of variables and potential interactions quickly grows to the billions. Computational modeling allows for synthesizing large amounts of data (e.g. all metabolic reactions) and *in silico* modeling of the interactions resulting from inactivating or hyperactivating one or more nodes (e.g. genes). However, this task is challenging. For instance, reconstructing organismal metabolism *in silico* requires including all the reactions active in each cell type of the organism (104–108), and all the possible interactions between cells that are mediated, triggered or inhibited by metabolites. However, as we described above, the activity of genes and their interactions within and across cells are affected by the context (e.g. diet or microbiota). To account for this, models need to be able to predict context-specific responses to perturbation. Only when predictive models with single-cell resolution and able to account for the effect of context become available will we be capable of predicting the effect of mutations, drug treatments, or stressors and how they define health versus disease status in complex organisms.

In this thesis, I present examples of how emergent predictive modeling coupled to experimental testing can guide the discovery of context-dependent gene functions that

may otherwise be overlooked or denied. I use the regulation of lysosomal lipolysis by the upstream nutrient sensors as an example of how computer modeling can guide the discovery and dissection of the gene-gene and gene-context interactions critical to define phenotypic outcomes.

Chapter II: Context-specific regulation of lysosomal lipolysis through network-level diverting of transcription factor interactions

The work presented in this chapter was published in the Proceedings of the National Academy of Sciences of the United States of America, as:
Mony VK[1], Drangowska-Way A[1], Albert R[1], Harrison E, Ghaddar A, Horak MK, Ke W, O'Rourke EJ. Context-specific regulation of lysosomal lipolysis through network-level diverting of transcription factor interactions. Proc Natl Acad Sci U S A. 2021 Oct 12;118(41):e2104832118. doi: 10.1073/pnas.2104832118. PMID: 34607947.
[1]V.K.M., A.D.-W., and R.A. contributed equally.

1. Abstract

Plasticity in multicellular organisms involves signaling pathways converting contexts – either natural environmental challenges, or planned lab perturbations– into context-specific changes in gene expression. Congruently, the signaling molecule-transcription factor (TF) interactions regulating these responses are also context-specific (e.g. TF_1 is activated by challenge A, but not B). However, when a target gene responds across contexts, the upstream TF identified in one context is often inferred to regulate it across contexts. Hence, reconciling these stable TF-target gene pair inferences with the context-specific nature of homeostatic responses is needed. The induction of the *C. elegans* genes *lipl-3* and *lipl-4* is essential to survival during fasting, and observed in many genetic contexts. We find DAF-16/FOXO mediating *lipl-4* induction in all contexts tested; hence, *lipl-4* regulation seems context-independent and compatible with across-context inferences. Contrastly, DAF-16-mediated regulation of *lipl-3* is context-specific. DAF-16 lessens the induction of *lipl-3* during fasting, yet it promotes it during oxidative stress. Through discrete dynamic modeling and genetic epistasis we define that DAF-16 represses HLH-30/TFEB –the main TF activating *lipl-3* during fasting. Contrastingly,

DAF-16 activates the stress-responsive TF HSF-1 during oxidative stress, which promotes *C. elegans* survival through induction of *lipl-3*. Further, the TF MXL-3 contributes to the dominance of HSF-1 at the expense of HLH-30 during oxidative stress but not during fasting. This study shows the limitations of across-context inferences, and how context-specific diverting of interactions within a network allows cells to specifically respond to a large number of contexts with a limited number of molecular players.

2. Significance Statement

Genes often encode for proteins with specialized functions (e.g. lipase). However, the function of the protein, and hence the gene, may be critical for survival in diverse contexts (e.g. fasting and oxidative stress). Hence, how are common survival genes activated in multiple contexts? Based on genetics and mathematical modeling we describe two modes of transcriptional activation: (1) convergent - a single transcriptional regulator activates the survival gene in multiple contexts; and (2) contextual - the activity/interaction of members of a network of transcriptional regulators is fine-tuned to activate the survival gene through molecular paths that are specific to a context. The results underscore the limitations of across-context molecular inferences, and suggest an economic tactic to biological resilience.

3. Introduction

Organisms constantly face environmental challenges. Mounting effective adaptive responses to these challenges requires that the cells composing the organism receive information about the occurrence and intensity of the challenge. However, in multicellular organisms, most cells are not directly exposed to the challenge. Therefore, adaptive responses involve signaling pathways that sense and translate the stimulus or stressor (input) into genomic actions orchestrated by transcription factors (TFs) that promote homeostatic changes in gene expression (output). This sensing and communication theoretically work best if signals get transmitted into the cell without any loss of information. Therefore, signaling was traditionally thought of as linear and hence undistorted (109). Now we know that signaling is far more complex, with different signaling pathways operating through independent and shared molecular components and biochemical mechanisms that ultimately repress or activate context-specific, as well as common, downstream genes. Nevertheless, we still mostly see signaling as pathways linearly linking an environmental condition or genetic perturbation (hereinafter referred to as context) to the activation of stable TF – target gene pairs that would, accordingly to its stable nature, be activated across contexts. Under this paradigm, a common inference would look as follows (**Fig. 1**): IF Context A is independently observed to: (a) change the levels of $Input_I$, (b) activate TF_1, and (c) promote induction of $Target_i$; AND in Context B, similar changes in $Input_I$ activate TF_1, which in turn induces $Target_i$; THEN we infer that Context A promotes induction of $Target_i$ through activation of TF_1. Although reasonable, the data used to build this kind of inferences are often obtained in contexts

that can be, as the real example depicted in **Fig. 1**, as disparate as feeding and fasting. Moreover, with wide-spread access to omics approaches, inferences are now made at genome scale. Consequently, hundreds of TFs have been assigned a genome-scale number of targets that too often are assumed to act downstream of a TF, not only in the tested context/s, but also across untested contexts. But, can we rely on input-output axes built upon data obtained in different contexts when we are aware that homeostatic responses are context specific?

Take for example, several transcription factors have been experimentally-validated to orchestrate adaptive responses to fasting and to genetic manipulations that mimic fasting in the nematode *Caenorhabiditis elegans*. Among the most characterized fasting-activated TFs in *C. elegans* are DAF-16 (mammalian FOXO) (110), PHA-4 (mammalian FOXA) (111), NHR-49 (mammalian PPARα) (112) and HLH-30 (mammalian TFEB) (113). Several groups, including ours, have shown that these TFs mediate the activation of the *C. elegans* lysosomal lipases *lipl-3* and *lipl-4* in contexts that are related to, but are not, fasting. For instance, *lipl-3* and *lipl-4* are induced upon inhibition of the gene encoding the insulin receptor (*daf-2*), the Notch receptor (*glp-1),* and the intracellular nutrient sensor mTOR (114–118). In *daf-2*, *glp-1*, and mTOR-deficient animals *lipl-4* induction is mediated by DAF-16. Chen *et al* suggested that DAF-16 would also mediate the induction of *lipl-3* in *daf-2* mutant animals (116). Therefore, *lipl-3* and *lipl-4* are downstream targets of several nutrient-sensing and nutrient-regulated growth pathways (*SI Appendix*, Fig S1*A*, *B*). Importantly, *lipl-3* and *lipl-4* encode for effectors of the *C.*

elegans response to fasting, as LIPL-3 and LIPL-4 mobilize lipids in food-deprived worms, and the transcriptional program that leads to their induction is essential to *C. elegans* survival to fasting (113,119). Based on the available information several inferences could be construed about the molecular pathways linking the expression of *lipl-3* and *lipl-4* to the feeding status of *C. elegans*. For instance, as mentioned above and as illustrated in **Fig. 1**, the transcription factor DAF-16 would mediate the induction of *lipl-3* downstream of reduced insulin-signaling (*daf-2* mutant) (116). Insulin signaling is reduced during fasting (120), and DAF-16 is activated during fasting (110). Hence, would DAF-16 promote the expression of *lipl-3* in fasting *C. elegans*? How would the action of DAF-16 be coordinated with HLH-30, which is so far the only TF shown to be necessary for the induction of *lipl-3* during fasting? On the other hand, if only DAF-16 or HLH-30 would mediate the response of *lipl-3* to fasting, how is the activity of the prevailing TF context-specifically favored? Further, if *lipl-3* would be activated in response to other stresses, would DAF-16, HLH-30, or other TFs execute the response in those contexts? Answering these questions would contribute to our understanding of how genes transcriptionally respond across contexts, and whether we can reconcile the wide-spread notion of stable TF-target gene pairs with the context-specific nature of molecular homeostatic responses.

In this study, we examined five signaling pathways that link nutritional status to growth in *C. elegans*. We refer to as inputs the contexts that inhibit or activate these signaling pathways (e.g. fasting, oxidative stress, or direct genetic inhibition/inactivation in the

presence of food), and as output the level of transcription of the lysosomal lipase genes *lipl-3* and *lipl-4*. We identified the transcription factors linking inputs to outputs, how the interactions between the TFs are diverted in different contexts to yield context-specific induction of the target gene, and mathematically expressed these roles via a discrete dynamic model. More broadly, the systematic investigation of the epistatic interactions between inputs, sensors, TFs, and the targets *lipl-3* and *lipl-4* demonstrates two generalizable modes of transcriptional regulation that provide a plausible economic solution to the need to mount specialized adaptive responses while minimizing the number of dedicated molecular players.

Figure. 1

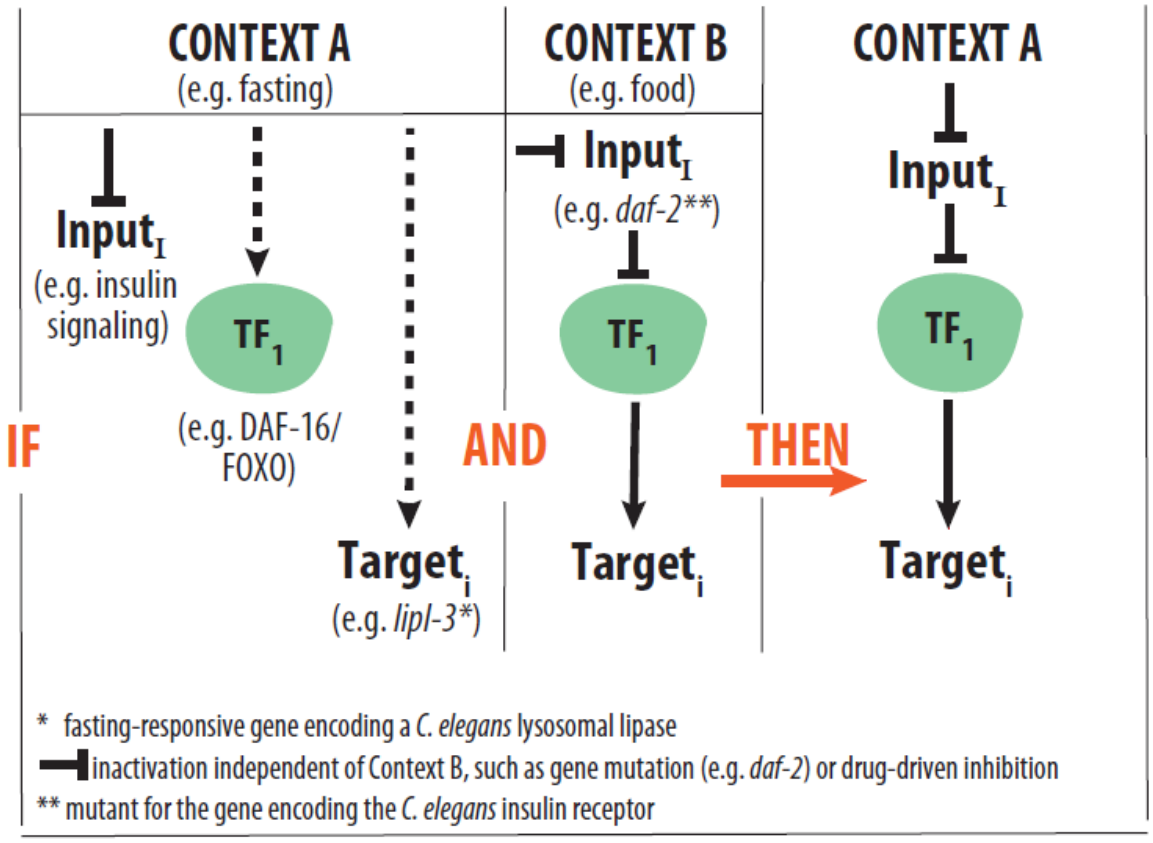
CONTEXT A
(e.g. fasting)
CONTEXT B
(e.g. food)
CONTEXT A
Input$_I$
(e.g. insulin signaling)
TF$_1$
(e.g. DAF-16/ FOXO)
Target$_i$
(e.g. *lipl-3**)
IF
Input$_I$
(e.g. *daf-2***)
TF$_1$
Target$_i$
AND
THEN
Input$_I$
TF$_1$
Target$_i$
* fasting-responsive gene encoding a *C. elegans* lysosomal lipase
inactivation independent of Context B, such as gene mutation (e.g. *daf-2*) or drug-driven inhibition
** mutant for the gene encoding the *C. elegans* insulin receptor

Fig. 1.

Schematic representation of across-context inferences. Hypothetical inference – IF in Context A the following are observed: 1) levels of $Input_I$ are reduced, 2) TF_1 is activated, and 3) $Target_i$ is induced; AND in Context B, in which $Input_I$ is artificially reduced (e.g. genetic mutation or chemical inhibition), we observe that TF_1 activates $Target_i$; THEN we would infer than in Context A the activation of $Target_i$ would be triggered by reduction of $Input_I$, and executed by TF_1. In a real-life example, the literature shows that in fasted *C. elegans* (Context A) the following happens: 1) insulin signaling is reduced (120); 2) the TF DAF-16/FOXO is activated (110); and 3) the lysosomal lipase gene *lipl-3* is induced (113). The literature also shows that in the presence of food (Context B) *C. elegans* carrying a hypomorphic mutation in the gene encoding the *C. elegans* Insulin receptor DAF-2 show activation of DAF-16 (121), and DAF-16-mediated induction of *lipl-3* (116). In this example, it would be reasonable to infer that induction of *lipl-3* during fasting is mediated by DAF-16. However, as we show in this study, although all independent observations are true, the inference is false.

4. Results

a. DAF-16 is a convergent activator of *lipl-4*

To identify the nutrient-sensing pathways and transcription factors that link food availability to the transcription of the lysosomal lipase-encoding genes *lipl-3* and *lipl-4* we planned to use genetic epistasis tests between sensors, TFs, and the targets *lipl-3* and *lipl-4* in different contexts. This required the use of thermosensitive mutants or RNA interference (RNAi) given that null mutation of several of the genes of interest leads to lethality (e.g. *let-363*, which encodes mTOR) or sterility (e.g. *glp-1*). RNAi in *C. elegans* is delivered by feeding *E . coli* expressing double stranded RNA against the gene of interest. Since different *E. coli* strains can have phenotype-changing effects on nutrient sensing pathways (101–103,122), and we had previously characterized the *lipl-3* and *lipl-4* responses to fasting using animals fed *E. coli* OP50 (113), we first show that fasting by withdrawal of an RNAi-competent derivative of OP50 (XU363) leads to induction of *lipl-3* and *lipl-4* (**Fig. 2*A***). This result indicates that RNAi-based epistasis studies of the *lipl* response to food availability can be performed using XU363-based RNAi.

We then screened for TFs mediating the induction of *lipl-4* in fasting *C. elegans* by using a candidate approach. We tested transcriptional regulators described in the literature to mediate transcriptional responses to fasting (112,113,123), calorie restriction (124), starvation-triggered dauer formation (125), and control of lipid metabolism

(114,115,126–130) . Of the 11 TFs tested we found that only *daf-16* was required for the induction of *lipl-4* during fasting (**Fig. 2*B*** and *SI Appendix,* Fig. S1*C*). This result then justified the use of *daf-16*-dependent induction as a probe to define which signaling pathways would link the feeding status of the worm to the expression of *lipl-4* (see further explanation of the rationale in *SI Appendix,* Note S1).

Using this strategy, we found *lipl-4* to be induced in feeding animals after single inhibition of insulin signaling (*daf-2(e1368*)) and single inhibition of Notch signaling (*glp-1(e2141)*) (**Fig. 2*C, D***); responses partially described by us and others for *C. elegans* feeding on *E. coli* OP50 (114,116,131). Importantly, these genetically triggered inductions were *daf-16*-dependent (**Fig. 2*C, D***). On the other hand, *lipl-4* was reported to respond to mTOR (*let-363*) RNAi when the double stranded RNAs were delivered using *E. coli* HT115 (117,118). However, we did not observe induction of *lipl-4* when double stranded RNAs against *let-363* were delivered using *E. coli* XU363 (*SI Appendix,* Fig. S1*D*), even when reduced *let-363* mRNA levels were confirmed (*SI Appendix,* Fig. S1*E*), and *lipl-3* upregulation was observed in the same samples (**Fig. 3*C***). Therefore, so far, the data suggest that Notch and insulin signaling link *lipl-4* expression to the feeding status of *C. elegans,* and that DAF-16 would be a convergent transcriptional regulator of *lipl-4*.

To test the hypothesis that the transcriptional regulation of *lipl-4* converges onto DAF-16 in multiple contexts, we tested DAF-16 role in other nutrient/growth related pathways.

Using a *C. elegans* line carrying a constitutively active form of the catalytic subunit of AMPK ($AMPK^{T172D}$), AAK-2 (132), we found no induction of *lipl-4* (*SI Appendix*, Fig. S1*F*); therefore, we were not able to test the convergent model in this context. By contrast, reducing TGF-β signaling through loss-of-function mutation of the gene encoding the TGF-β receptor *daf-1* did lead to *lipl-4* induction (**Fig. 2*E***). The classic outputs of the TGF-β pathway are DAF-3 (mammalian SMAD protein DPC4) and DAF-12 (mammalian LXR), and they both mediate responses to nutrients (133–135). However, neither of them mediated *lipl-4* induction in *daf-1* mutant *C. elegans* (*SI Appendix*, Fig. S1*G*). Instead, we found RNAi against *daf-16* being negatively epistatic to *daf-1* (**Fig. 2*E***). The action of DAF-16 on the *lipl-4* promoter is likely to be direct as DAF-16 has been detected -158bp upstream of the *lipl-4* start site in chromatin immunoprecipitation analyses (136) (*SI Appendix*, Table S3). Therefore, although our results do not rule out that other TFs may control *lipl-4* in yet-to-be-tested contexts, the data up to date enable us to propose that the transcriptional regulation of *lipl-4* exemplifies the prevalent paradigm of transcriptional control, which assumes convergence of a transcriptional response onto a stable functional TF-target gene pair that may act across contexts (**Fig. 2*F***). The convergent model supports wide-ranging inferences and meaningful extraction of general rules of transcriptional control from a relatively small number of experiments carried out in a limited number of experimental conditions.

Figure 2

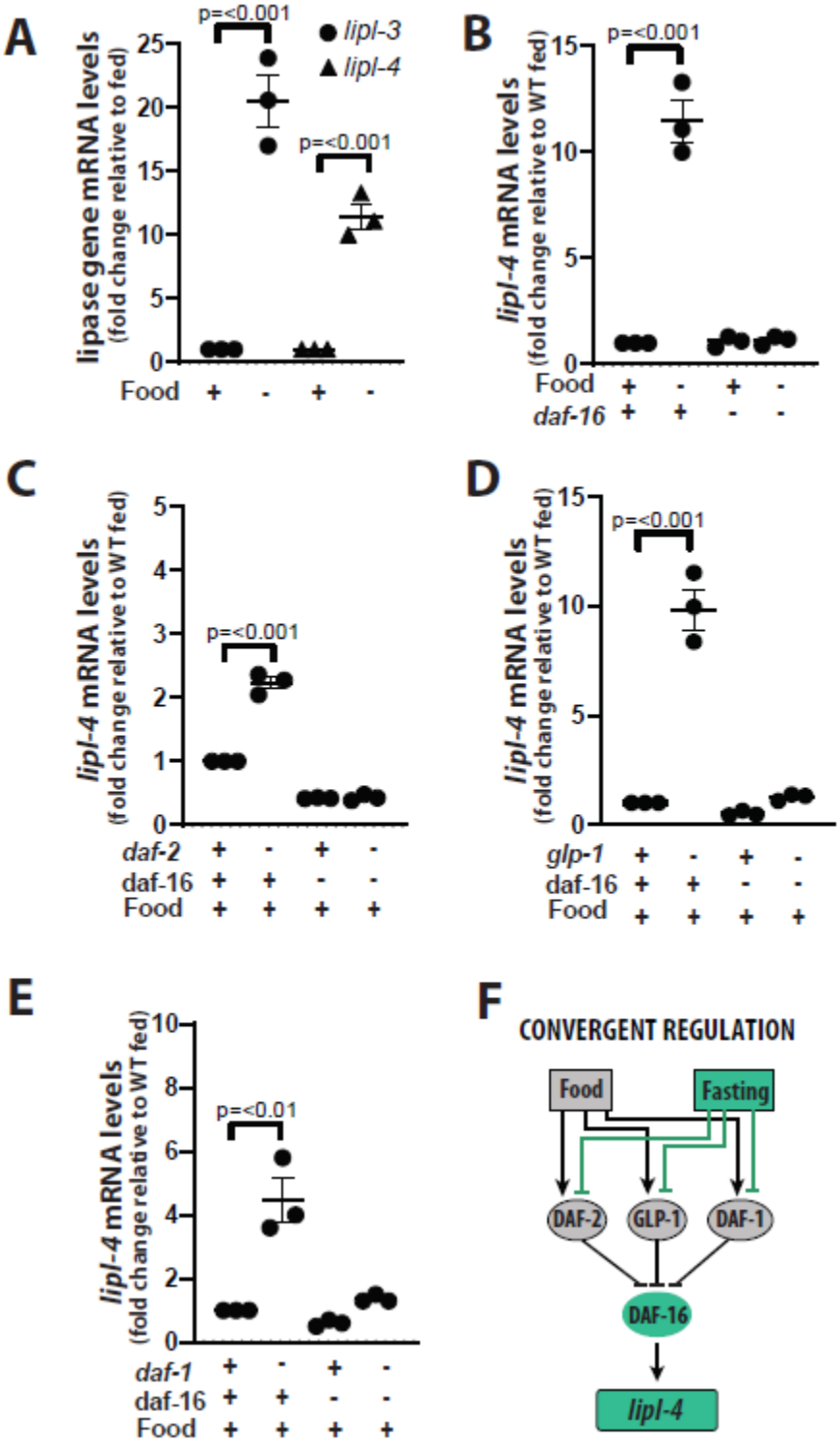
A
lipase gene mRNA levels
(fold change relative to fed)
p=<0.001
p=<0.001
lipl-3
lipl-4
Food + - + -
B
lipl-4 mRNA levels
(fold change relative to WT fed)
p=<0.001
Food + - + -
daf-16 + + - -
C
lipl-4 mRNA levels
(fold change relative to WT fed)
p=<0.001
daf-2 + - + -
daf-16 + + - -
Food + + + +
D
lipl-4 mRNA levels
(fold change relative to WT fed)
p=<0.001
glp-1 + - + -
daf-16 + + - -
Food + + + +
E
lipl-4 mRNA levels
(fold change relative to WT fed)
p=<0.01
daf-1 + - + -
daf-16 + + - -
Food + + + +
F
CONVERGENT REGULATION
Food
Fasting
DAF-2
GLP-1
DAF-1
DAF-16
lipl-4

Fig. 2.

DAF-16 is a convergent activator of *lipl-4.* (*A*-*E*) qRT-PCR analysis of gene expression in young adult *C. elegans* normalized to housekeeping gene *ama-1* or *pmp-3* and relative to untreated as denoted in Y axis is depicted. Three or more independent biological replicates are presented in all panels. Error bars denote SEM. Statistical significance assessed via one-tailed unpaired parametric t-test. Gene inactivations through mutation (gene name italicized) or RNAi (gene name in normal font) are represented with a minus sign in the treatment matrix. All RNAi treatments were started at the L1 stage. (*A*) WT animals grown on *E. coli* strain XU363 and then fasted for 6h relative to fed. N=3. (*B*) WT and *daf-16(mu86)* mutant animals fasted for 6h relative to fed. N=3. See results for other TFs in *SI Appendix*, Fig. S1C. *(C)* WT and *daf-2(e1368)* animals on empty vector control (EV) or *daf-16* RNAi bacteria from L1 stage. *(D)* WT and *glp-1(e2141)* animals on EV or *daf-16* RNAi bacteria from L1 stage. (*E*) WT and *daf-1(m40)* animals on EV or *daf-16* RNAi bacteria from L1 stage. *(F)* Model of convergent regulation of *lipl-4.* Activating interactions are depicted as arrows and inhibitory interactions as blunt arrows.

Supplementary Figure 1

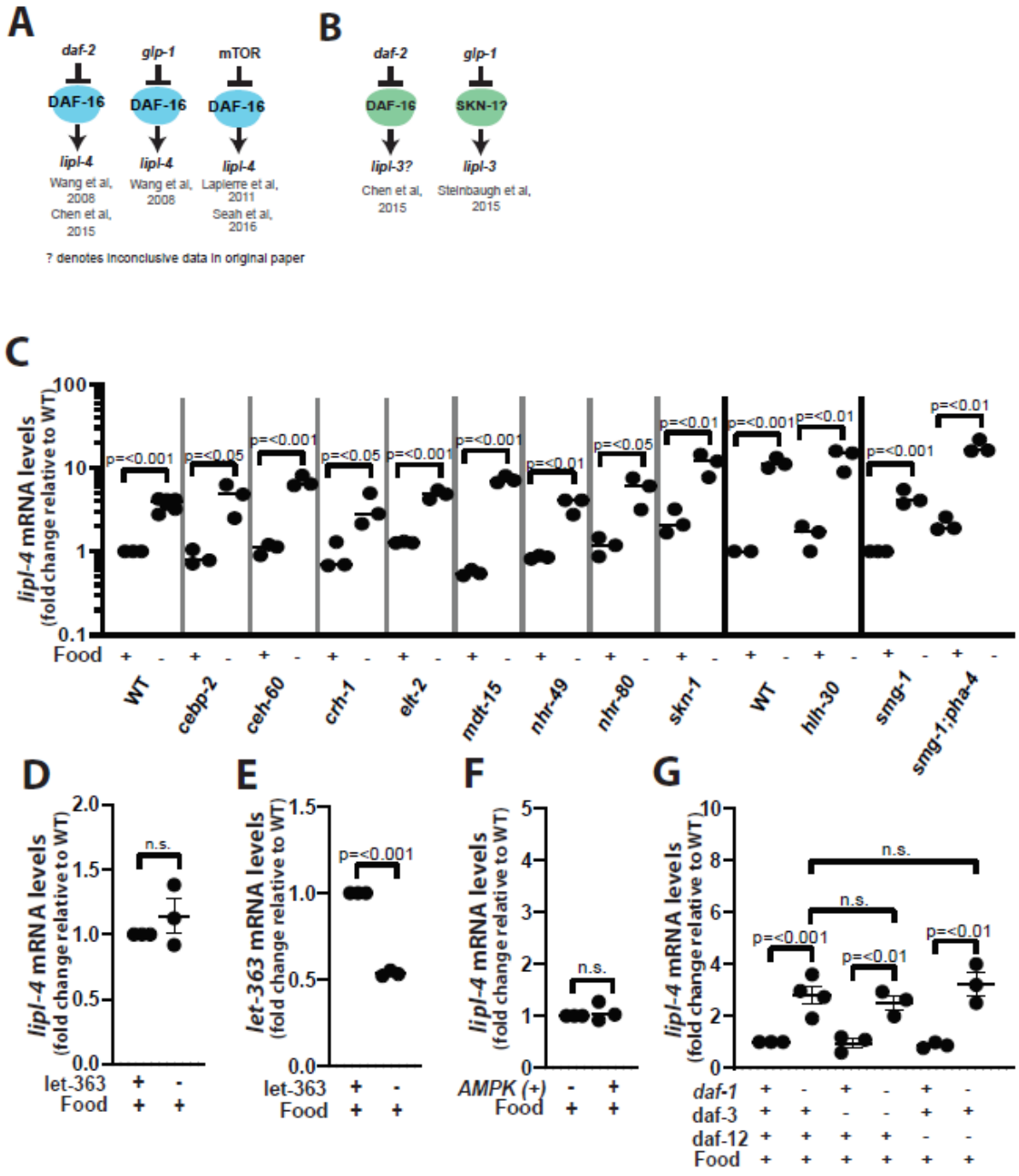

Fig. S1.

(A, B) Schematic summary of published reports on the transcriptional regulation of (A) *lipl-4* and (B) *lipl-3*. (*C-G*) qRT-PCR analysis of gene expression in young adult *C. elegans* as described in **Fig. 2**. (*C*) *lipl-4* expression in WT and TF mutant or RNAi-treated animals fasted for 6h relative to fed. For some genes independent control samples are depicted. N=3 (*D) lipl-4* expression in WT and animals treated with RNAi against *let-363*. N=3. *(E*) *let-363* expression in *let-363*-RNAi treated animals used in panel D. N=3. *(F) lipl-4* expression in WT and animals carrying a constitutively active version of $AMPK^{T172D}$ (WBM60). N=3. (*G*) *lipl-4* expression in WT and *daf-1(m40)* animals treated with empty vector control or RNAi against *daf-3* or *daf-12*. N=3.

b. Context defines the TFs regulating *lipl-3*

We then investigated the transcriptional control of *lipl-3*. We previously reported that the TF HLH-30 (mammalian TFEB) is necessary to induce the expression of *lipl-3* in fasting *C. elegans* (113). In addition, Chen *et al* suggested that DAF-16 promotes *lipl-3* induction in insulin-signaling deficient animals (*daf-2* mutant) fed *ad libitum* (116), and Steinbaugh *et al* proposed that SKN-1 promotes *lipl-3* expression in Notch-signaling deficient animals (*glp-1* mutant) fed *ad libitum* (115). Further, DAF-16 and SKN-1 were shown to generally promote the expression of lysosomal genes in *daf-2* mutant worms (137). However, it has not been directly tested whether DAF-16, SKN-1, or other fasting-responsive TFs also contribute to the induction of *lipl-3* in fasting *C. elegans*. We then tested whether additional fasting-responsive TFs contribute to *lipl-3* induction in fasting worms. Among the 11 TFs tested, we found that a few TFs affected *lipl-3* basal expression but only *hlh-30* loss of function abrogated *lipl-3* induction during fasting (**Fig. 3*A*** and *SI Appendix*, Fig. S2*A*). Unexpectedly, and opposite to the most parsimonious inference, impairing the function of *daf-16* lead to further induction of *lipl-3* in fasted worms (**Fig. 3*B***), suggesting that DAF-16 is part of a fasting-activated regulatory axis that ultimately hinders *lipl-3* induction.

As with *lipl-4*, we then used *hlh-30* dependency as the probe to define which signaling input nodes link *lipl-3* transcription to the feeding status of the worm. The assumption

here is that pathways whose sole genetic manipulation trigger an *hlh-30*-dependent induction of *lipl-3* in animals feeding *ad libitum* are likely to link *lipl-3* expresion to the feeding status of *C. elegans* (rationale described in detail in *SI Appendix,* Note S1). We did not observe *lipl-3* induction in *C. elegans* carrying a constitutively active form of the catalytic subunit of $AMPK^{T172D}$, AAK-2 (*SI Appendix,* Fig. S2*B*). However, we found that reduction of function of the intracellular nutrient sensor mTOR (*let-363* RNAi) was sufficient to promote *lipl-3* induction (**Fig. 3*C***). Since mTOR is known to be present in cells in two complexes (mTORC1 and mTORC2), each having different functions (138), we set to determine whether one or both of the mTOR complexes would be upstream of *lipl-3*. Inactivation of mTORC2 using RNAi against *rict-1* (encoding *C. elegans*'s Rictor/mTORC2) did not alter the expression levels of *lipl-3* (*SI Appendix,* Fig. S2*C*), while inactivation of mTORC1 using RNAi against *daf-15* (encoding *C. elegans*'s Raptor) resulted in induction of *lipl-3* (**Fig. 3*D***). Similarly, impairing the function of the membrane receptor *daf-1* was sufficient to promote *lipl-3* induction (**Fig. 3*E***). In addition, similar to previous reports (105,115), we found *lipl-3* induced in *daf-2* and *glp-1* mutant worms even when in our study we fed them *E. coli* XU363 (**Fig. 3*F-G***). Altogether the data suggest that mTORC1, insulin, Notch, and TGFβ signaling inhibit the expression of the lysosomal lipase *lipl-3* in fed *C. elegans*.

Published genetic epistasis analyses of *C. elegans* longevity triggered by inhibition of mTOR, *glp-1*, and *daf-2* showed that these sensors are upstream of *hlh-30 (27,92)*. Further, mTOR, *glp-1*, and *daf-2* inhibition were shown to be sufficient to promote *hlh-*

30-dependent pro-longevity responses that include induction of autophagy and lysosomal genes (27,92,137). Hence, because: 1) fasting leads to inhibition of mTOR, *glp-1*, and *daf-2*; 2) inhibition of mTOR, *glp-1*, and *daf-2* leads to activation of *hlh-30*; and 3) activated HLH-30 promotes the expression of autophagy and lysosomal genes, we hypothesized that *hlh-30* would mediate the induction of *lipl-3* in mTOR, *glp-1*, and *daf-2*-deficient *C. elegans*. Indeed, we found inhibition of mTORC1 (*daf-15* RNAi) leading to induction of *lipl-3* in an *hlh-30*-dependent manner (**Fig. 3*D***), supporting a model in which the mTORC1-HLH-30 axis links feeding status to the expression of *lipl-3* in *C. elegans*. However, opposite to the most parsimonious inferences, knock-down of *hlh-30* did not affect the induction of *lipl-3* in *daf-2* or *glp-1* mutant animals (**Fig. 3*F-G***), suggesting that a different TF or TFs would mediate *lipl-3* induction in these contexts. At this point, we detoured from our original goal, and decided to search for the TF/s promoting *lipl-3* expression in the non fasting genetic contexts *daf-2*, *glp-1* and *daf-1* (we refer to these mutants as non fasting contexts because the fasting response of *lipl-3* is *hlh-30* dependent, and induction of *lipl-3* in these genetic contexts is independent of *hlh-30*).

In search for the TF/s mediating the induction of *lipl-3* in the *daf-2* and *glp-1* contexts, we tested DAF-16, SKN-1, and PHA-4 (115,117,139–141). Chen *et al* previously suggested that the DAF-16 isoforms A and F would mediate the induction of *lipl-3* in *daf-2* animals (116). However, the published evidence was not conclusive because, as expected for some genes when using a genome-wide approach, *lipl-3* sequencing reads were not unequivocally distinguished from the reads of the adjacent gene *srw-107* (see

Supplementary Table 13 in Chen *et al* (116)). Therefore, we directly tested via qRT-PCR whether *daf-16* was epistatic to *daf-2* in the expression of *lipl-3*. Indeed, as suggested by Chen *et al*, we found that loss of *daf-16* function completely abrogated the induction of *lipl-3* in *daf-2* mutant animals (**Fig. 3*H***). On the other hand, RNAi against *skn-1* did not suppress *lipl-3* induction in *daf-2* mutant worms (*SI Appendix*, Fig. S2*D*). Then, we tested candidate TFs mediating *lipl-3* induction in the *glp-1* mutant background. We observed that knock down of *pha-4* led to further induction of *lipl-3* (*SI Appendix*, Fig. S2*E*), and that knock down of *skn-1* did not impair *lipl-3* induction (*SI Appendix*, Fig. S2*F*). The latter was unexpected because Steinbaugh *et al* previously proposed that *skn-1* promotes the induction of *lipl-3* in the *glp-1(bn18ts)* context (115). Although the use of a different *glp-1* allele (*e2141* in this study, and *bn18ts* in the previous study), the use of a different *E. coli* strain (*E. coli* XU363 in this study, and *E. coli* HT115 in Steinbaugh's study), or both could be behind *skn-1* not mediating *lipl-3* induction in our experiments, we are more inclined to think that the distinct *E coli* strains are most likely responsible for the discrepancy because distinct bacterial diets were previously shown to influence the nuclear localization of SKN-1::GFP (122). Thus, we then searched for a suppressor of *lipl-3* induction in *glp-1* mutant *C. elegans* fed *E. coli* XU363, and found that loss of *daf-16* function suppressed most of the induction in this context (**Fig. 3*I***). Thus, DAF-16 acts as an activator of *lipl-3* expression upon inhibition of insulin and Notch signaling. In addition, we had found *lipl-3* to respond to inhibition of the TGFβ pathway (**Fig. 3*E, J***). The Smad protein DAF-3 and the nuclear-hormone receptor DAF-12 contribute to the transcriptional response to inhibition of TGFβ signaling (133) (134). We fed *daf-1* mutant animals RNAi against *daf-3*, *daf-12*, and *daf-16*, and found *daf-3* to be negatively

epistatic to *daf-1* in the induction of *lipl-3* (**Fig. 3*J***), while *daf-12* knock down does not suppress *lipl-3* induction, and *daf-16* knock down further enhances *lipl-3* expression in this context (*SI Appendix*, Fig. S2*G*).

In summary (**Fig. 3*K***), HLH-30 specifically acts as a transcriptional activator of *lipl-3* downstream of the mTORC1 axis, and DAF-3 positively regulates *lipl-3* downstream of the TGFβ axis. By contrast, DAF-16 has multiple, even opposing, roles on *lipl-3* expression. DAF-16 positively regulates *lipl-3* downstream of the Insulin and Notch axes, while it negatively regulates *lipl-3* downstream of the TGFβ axis and during fasting. Therefore, the transcriptional control of *lipl-3* does not conform to a convergent model of transcriptional regulation. We propose to name contextualized transcriptional control the mode of regulation exemplified by *lipl-3*.

Figure 3

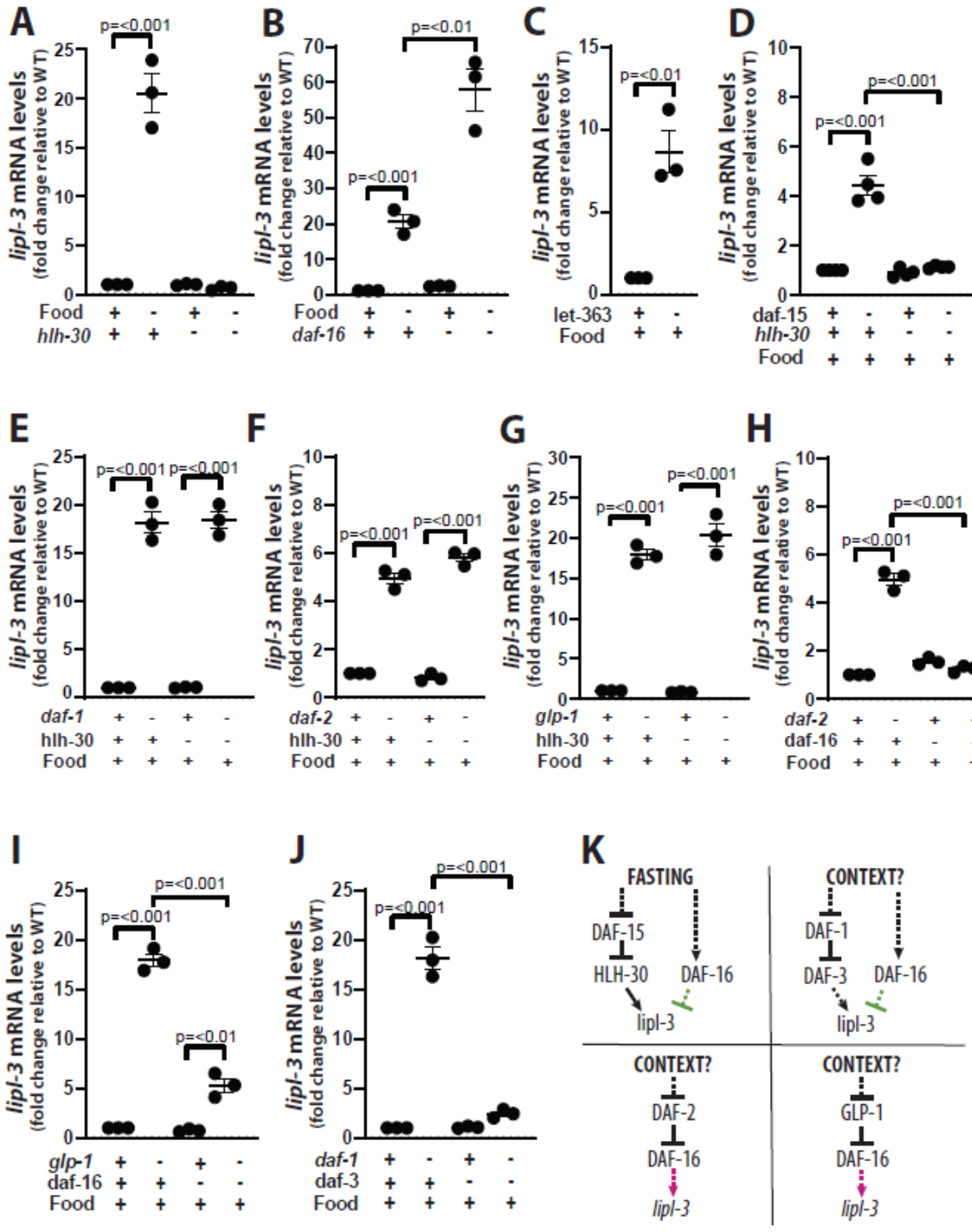
A
B
C
D
E
F
G
H
I
J
K
lipl-3 mRNA levels
(fold change relative to WT)
p=<0.001
p=<0.01
Food
hlh-30
daf-16
let-363
daf-15
daf-1
daf-2
glp-1
daf-3
FASTING
CONTEXT?
DAF-15
HLH-30
DAF-16
DAF-1
DAF-3
DAF-2
GLP-1
lipl-3

Fig. 3.

Context defines the TFs regulating *lipl-3*. (*A-J*) qRT-PCR analysis of gene expression in young adult *C. elegans* as described in **Fig. 2**. (*A*) WT and *hlh-30(tm1978)* mutant animals fasted for 6h relative to fed. N=3. (*B*) WT and *daf-16(mu86)* mutant animals fasted for 6h relative to fed. N=3.

(C) WT animals treated with empty vector control (EV) or RNAi against the gene encoding the catalytic subunit of mTOR, *let-363*. N=3. (*D*) WT and *hlh-30(tm1978)* mutant animals treated with EV or RNAi against *daf-15*, the gene encoding the essential mTORC1component RAPTOR. N=4 (*E*) WT and *daf-1(m40)* animals treated with EV or RNAi against *hlh-30*. N=3 *(F)* WT and *daf-2(e1368)* animals treated with EV or RNAi against *hlh-30*. N=3 *(G)* WT and *glp-1(e2141)* animals treated with EV or RNAi against *hlh-30*. N=3 *(H)* WT and *daf-2(e1368)* animals treated with EV or RNAi against *daf-16*. N=3. *(I)* WT and *glp-1(e2141)* animals treated with EV or RNAi against *daf-16*. N=3. *(J)* WT and *daf-1(m40)* animals treated with EV or RNAi against *daf-3*. N=3 *(K)* Schematic representation of the contextualized transcriptional control of *lipl-3* suggesting that the DAF-1-DAF-3, DAF-2-DAF-16, and GLP-1-DAF-16 axes would be important in yet-to-be-defined contexts, but not during fasting.

Supplementary Figure 2

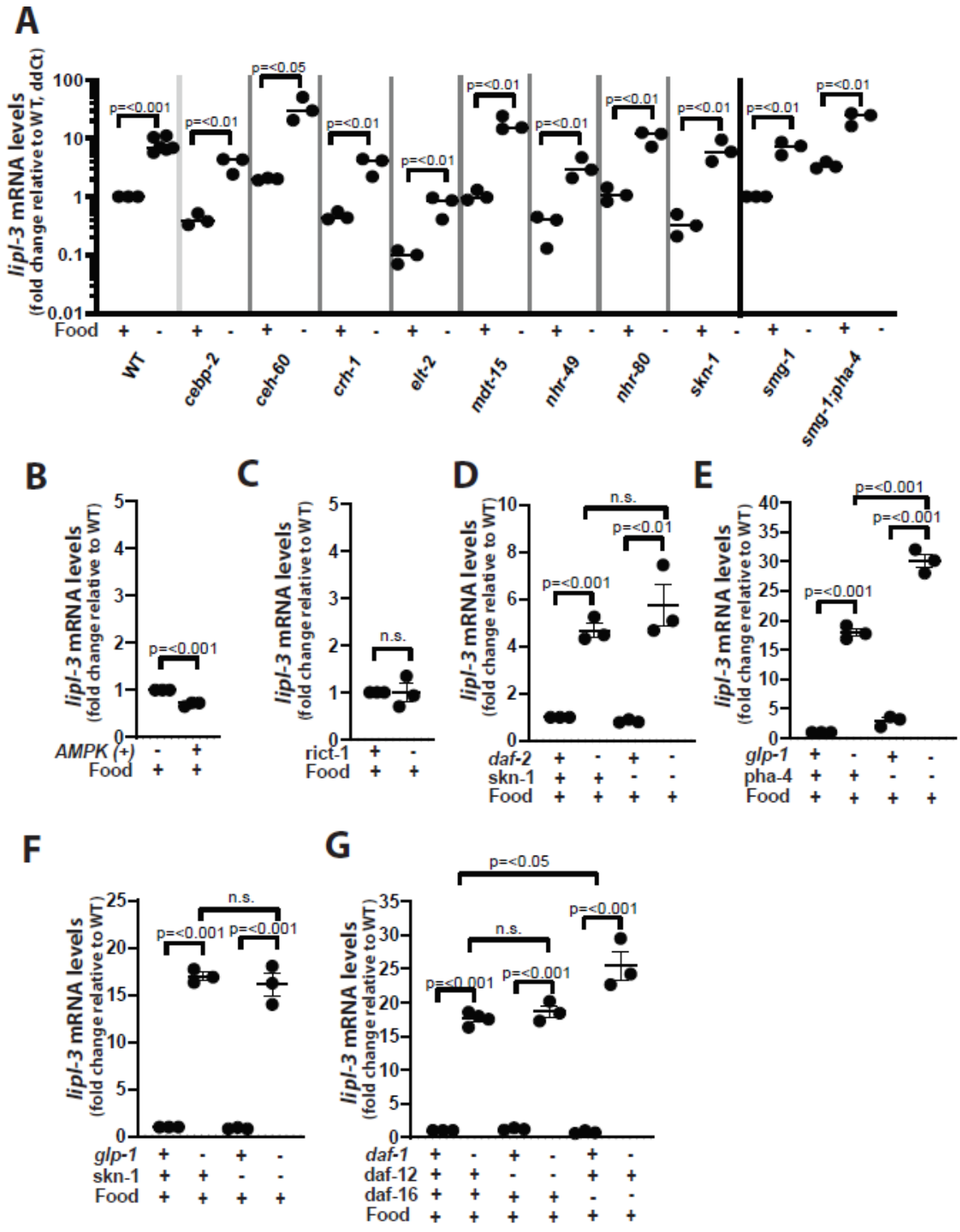

Fig. S2.

Signaling molecules and TFs not linking *lipl-3* expression to feeding status in *C. elegans.* (*A*-*G*) qRT-PCR analysis of *lipl-3* expression in young adult *C. elegans* as described in **Fig. 2**. (*A*) WT animals and TF mutants or RNAi fasted for 6h relative to fed. N=3 (*B*) WT and constitutively active AMPK^{T172D} (WBM60) animals. N=3. *(C)* WT treated with empty vector control (EV) or RNAi against *rict-1*. N=3. *(D)* WT and *daf-2(e1368)* animals treated with EV or RNAi against *skn-1*. *(E-F)* WT and *glp-1(e2141*) animals treated with EV or RNAi against (*E*) *pha-4* (N=3), or (*F*) *skn-1* (N=3). (*G*) WT and *daf-1(m40)* animals treated with EV or RNAi against *daf-12* or *daf-16*. N=3.

c. The *daf-16* - *lipl-3* activating axis promotes resistance to oxidative stress

DAF-16 activates *lipl-3* downstream of inhibited insulin and Notch signaling (**Fig. 3*H* and *I*)**, and DAF-3 downstream of inhibited TGFβ signaling (**Fig. 3*J*)**, whereas both DAF-16 and DAF-3 hinder the induction of *lipl-3* during fasting (**Fig. 3*B*** and *SI Appendix,* Fig. S3*A*). We thus hypothesized that DAF-16 and DAF-3 would promote *lipl-3* expression in a context or contexts other than fasting (Schematic in **Fig. 3K**). To start elucidating in which context/s the DAF-16-to-*lipl-3* and the DAF-3-to-*lipl-3* edges would be relevant, we tested whether *lipl-3* would transcriptionally respond to other stresses. We found *lipl-3* expression not increasing upon ER, cold, heat, salt/osmotic stress or anoxia (*SI Appendix,* Fig. S3*B*). By contrast, we found *lipl-3* responding to oxidative stress triggered by exposure to tBOOH (**Fig. 4*A***). Importantly, *lipl-3* contributes to survival in animals exposed to tBOOH (**Fig. 4*B***); hence, similar to its response to fasting, *lipl-3* induction during oxidative stress would be a physiologically relevant response in *C. elegans*.

We then used the same rationale we used to investigate the feeding-fasting axis: if *daf-3* and/or *daf-16* were mediating the response to oxidative stress, then the *lipl-3* response to oxidative stress should be *daf-3* and/or *daf-16* dependent. We found that loss of *daf-3* function did not suppress, but in fact further enhanced, the induction of *lipl-3* in animals treated with tBOOH (**Fig. 4*C***), suggesting that the *daf-1*-|*daf-3*->*lipl-3* axis would operate in contexts other than fasting or oxidative stress (**Fig. 3*K***). By contrast, loss of

daf-16 function suppressed the induction of *lipl-3* in animals treated with tBOOH (**Fig. 4*C***), suggesting that the *daf-2*-|*daf-16*->*lipl-3* and the *glp-1*-|*daf-16*->*lipl-3* axes might be part of the response to changes in the redox status in *C. elegans*. We then tested this hypothesis. The contribution of *daf-16* to resistance to oxidative stress in *daf-2* animals has been extensively documented using several oxidative stress agents (34,110,142–146), including tBOOH (92,146). Nevertheless, given the context-sensitivity of the system, we retested this observation in animals fed *E. coli* XU363. We found that *daf-16* (as expected) was negatively epistatic to *daf-2* enhanced survival to tBOOH (*SI Appendix*, Fig. S3*C***)**. More importantly, we found *lipl-3* contributing to *daf-2* resistance to oxidative stress (**Fig. 4*D*)**. Similarly, we found that both *daf-16* and *lipl-3* are negatively epistatic to *glp-1* enhanced survival to tBOOH (**Fig. 4*E, F***, respectively). Therefore, *daf-2* -| *daf-16 -> lipl-3* and *glp-1* -| *daf-16 -> lipl-3* compose input-output axes acting to maintain *C. elegans*'s redox status (**Fig. 4*G***).

A previous study suggested that DAF-16 may not be the only mediator of *lipl-3* induction during oxidative stress. Steinbaugh *et al* showed that *lipl-3* contributes to *glp-1*'s resistance to sodium arsenite (SA) (115). However, this study did not define whether *lipl-3* transcriptionally responds to SA treatment or other sources of oxidative stress. Nevertheless, based on: 1) *skn-1* being negatively epistatic to *glp-1*'s resistance to SA, and 2) *skn-1* RNAi partially suppressing the induction of *lipl-3* in *glp-1(bn18ts)* animals, this previous study inferred that the induction of *lipl-3* would be part of the adaptive response that SKN-1 orchestrates in response to SA. In our experimental setup, *glp-1*

animals showed elevated *lipl-3* expression even when *skn-1* was knocked-down (*SI Appendix,* Fig. S2*F*). Further, Oliveira *et al* described lipid metabolism as enriched among the tBOOH-induced genes that are SKN-1 independent (147). Thus, altogether, the data suggest that the *glp-1*-| *skn-1* -> *lipl-3* axis may contribute to resistance to oxidative stress via modulating the expression of *lipl-3* when the main stressor is an inorganic salt damaging the mitochondria such as SA (148), while the *glp-1*-| *daf-16* -> *lipl-3* axis may play a role in *C. elegans* survival to the organic peroxide tBOOH, which has been proposed to target cellular lipids (149). Therefore, contextualized transcriptional regulation can be as specialized as a single target gene being activated through different molecular paths when the distinction between the challenges is as small (in the context of life in nature) as different oxidant agents.

Figure 4

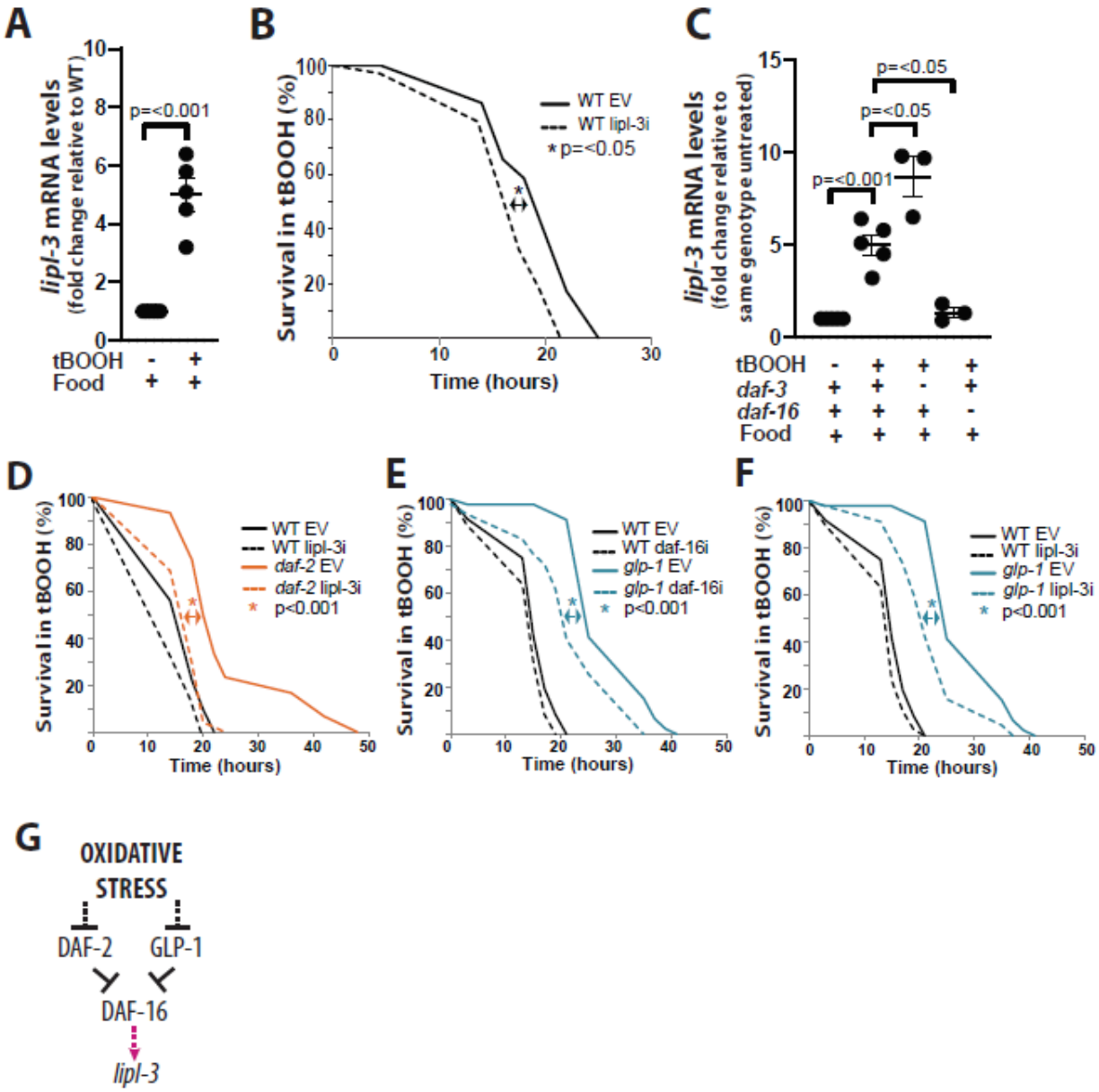
A
lipl-3 mRNA levels
(fold change relative to WT)
p=<0.001
tBOOH - +
Food + +
B
Survival in tBOOH (%)
Time (hours)
WT EV
WT lipl-3i
*p=<0.05
C
lipl-3 mRNA levels
(fold change relative to same genotype untreated)
p=<0.05
p=<0.05
p=<0.001
tBOOH - + + +
daf-3 + + - +
daf-16 + + + -
Food + + + +
D
Survival in tBOOH (%)
Time (hours)
WT EV
WT lipl-3i
daf-2 EV
daf-2 lipl-3i
* p<0.001
E
Survival in tBOOH (%)
Time (hours)
WT EV
WT daf-16i
glp-1 EV
glp-1 daf-16i
* p<0.001
F
Survival in tBOOH (%)
Time (hours)
WT EV
WT lipl-3i
glp-1 EV
glp-1 lipl-3i
* p<0.001
G
OXIDATIVE STRESS
DAF-2
GLP-1
DAF-16
lipl-3

Fig. 4.

The DAF-16 - *lipl-3* activating axis promotes resistance to oxidative stress. (*A, C*) qRT-PCR analysis of gene expression in young adult *C. elegans* as described in **Fig. 2**. (*A*) *lipl-3* expression in WT animals treated with 5mM tBOOH for 4h relative to untreated. N=5. *(C) lipl-3* expression in WT, *daf-3(mgDf90)*, and *daf-16(mu86)* mutant animals treated with tBOOH for 4h relative to untreated. N=3. *(B, D-F)* Oxidative stress survivorship assay. Wild-type animals (black), and the mutants *daf-2(e1368)* (orange) and *glp-1(e2141*) (blue), were grown from L1 on empty vector control (EV), *daf-16*, or *lipl-3* RNAi. When L3s, *daf-2* worms and their controls were transferred to 25˚C, whereas *glp-1* and their controls were incubated at 25˚C from L1s. When young adults, animals were transferred to plates containing 5mM tBOOH and scored for survivorship every 2h. N=3 (see also *SI Appendix*, Table S8) (*B*) Survivorship of WT animals treated with EV or RNAi against *lipl-3* (20˚C). (*D*) Survivorship of WT and *daf-2(e1368)* animals treated with EV or RNAi against *lipl-3* (25˚C). *(E)* Survivorship of WT and *glp-1(e2141*) animals treated with EV or RNAi against *daf-16* (25˚C). *(F)* Survivorship of WT and *glp-1(e2141*) animals treated with EV or RNAi against *lipl-3* (25˚C). *(G)* Schematic representation of the axes modulating *lipl-3* expression in response to tBOOH exposure in *C. elegans*.

Supplementary Figure 3

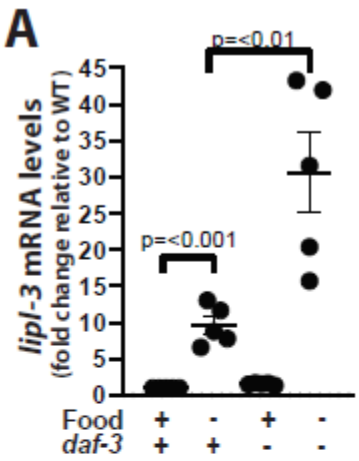

B

	lipl-3 mRNA fold change relative to untreated	± SE
ER stress	0.84	± 0.24
cold stress	0.80	± 0.07
heat stress	0.51	± 0.17
salt stress	0.36	± 0.02
anoxia	0.65	± 0.11

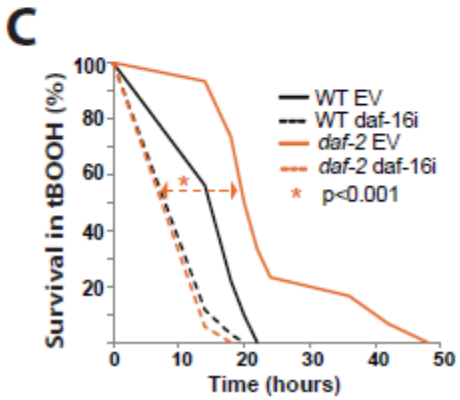

Fig. S3.

Dissecting the contextualized regulation of lipl-3. (*A-B*) qRT-PCR analysis of gene expression in young adult *C. elegans* as described in **Fig. 2**. (*A*) *lipl-3* expression in WT and *daf-3* mutant animals fasted for 6h relative to fed. N=5. (*B*) *lipl-3* expression in WT young adult animals exposed to different stresses. N=3. *(C)* Oxidative stress survivorship assay. Wild-type (black), and *daf-2(e1368)* mutant animals (orange), were grown from L1 on empty vector control or RNAi against *daf-16*. When L3s, *daf-2* worms and their corresponding controls were transferred to 25˚C. When young adults, animals were transferred to plates containing 5mM tBOOH and scored for survivorship every 2h. N=3 (see also *SI Appendix,* Table S8).

d. Literature-based network predicts multiple TF-TF functional interactions regulating *lipl-3*

We showed that DAF-16 positively regulates *lipl-3* downstream of the insulin and Notch axes and during oxidative stress, while it negatively regulates *lipl-3* downstream of the TGFβ axis and during fasting. The seemingly opposing roles that DAF-16 plays in the transcriptional regulation of *lipl-3* is a worth noting example of contextualized molecular function. Although context-dependent roles for TFs and other molecules have been described before (81,150,151), including for DAF-16 (92), the DAF-16-*lipl-3* interaction is unique in that *daf-16* has opposite functional relationships with the same target gene. This is even more intriguing when considering that the different contexts investigated here coexist in fasting animals, as lack of food leads to reduced insulin and Notch signaling and activation of DAF-16 (120,152).

We hypothesized that integrating all known interactions between sensors, TFs and *lipl-3* will allow us to understand the context-dependent interaction between DAF-16 and *lipl-3*. Hence, we decided to reconstruct *in silico* the transcriptional network predicted to regulate *lipl-3*. To this end, we performed a comprehensive literature search for pairwise functional interactions connecting: 1) sensors and nutrient-responsive TFs, 2) sensors and *lipl-3*, 3) nutrient-responsive TFs to other nutrient-responsive TFs, and 4) nutrient-responsive TFs to *lipl-3* (*SI Appendix,*Table S1). We then built a *lipl-3* regulatory network in which genes representing nutrient sensors, TFs, and *lipl-3*, are nodes and their

documented interactions are edges. We characterized each interaction by its effect on the target and recorded whether it was mediated by one or more edges. Following the principle of parsimony, we evaluated every effect requiring more than one edge, and if single edges in the network already incorporated the published observation, then we did not expressly include the multi-edge interaction in the network (see Methods). The resulting network (which we will refer to as the inferred network) consists of the most parsimonious paths that include all the known interactions among the input, the sensors, the TFs, and *lipl-3* (**Fig. 5** & *SI Appendix*, Table S2).

The resulting regulatory network shows that signaling flux initiated by food and fasting can pass onto *lipl-3* via an intricate network of TFs (**Fig. 5**). Saliently, the network predicts that SKN-1 would independently regulate *lipl-3*, and that DAF-16, DAF-3, and HSF-1 would ultimately converge onto HLH-30 to promote *lipl-3* expression. Since DAF-16, SKN-1, and DAF-3 do not mediate *lipl-3* induction during fasting (**Fig. 3*B***, *SI Appendix*, Fig. S2*A*, S3A), and HLH-30 and SKN-1 do not mediate the induction of *lipl-3* in the *glp-1* and *daf-2* mutant contexts (**Fig. 3*F***, G *SI Appendix*, Fig. S2*D*, *F*), the inferred network seems to be inaccurate. The inaccuracies are most likely resulting from the fact that to create the network we pulled together published interactions. These interactions come from experiments done in different contexts (e.g. dauer formation by festing versus response to loss of *glp-1* function in fed animals). The inaccuracies of the inferred regulatory network illustrate the limitations of a network inferred based on epistatic interactions dissected in different contexts. Nevertheless, the inferred network includes

potential functional interactions between DAF-16, DAF-3, SKN-1, HSF-1, MXL-3 and HLH-30 that may help us explain the context-dependent interactions between these TFs and *lipl-3*, and, more broadly, how context-dependent function can emerge from the same set of molecular players.

Figure 5

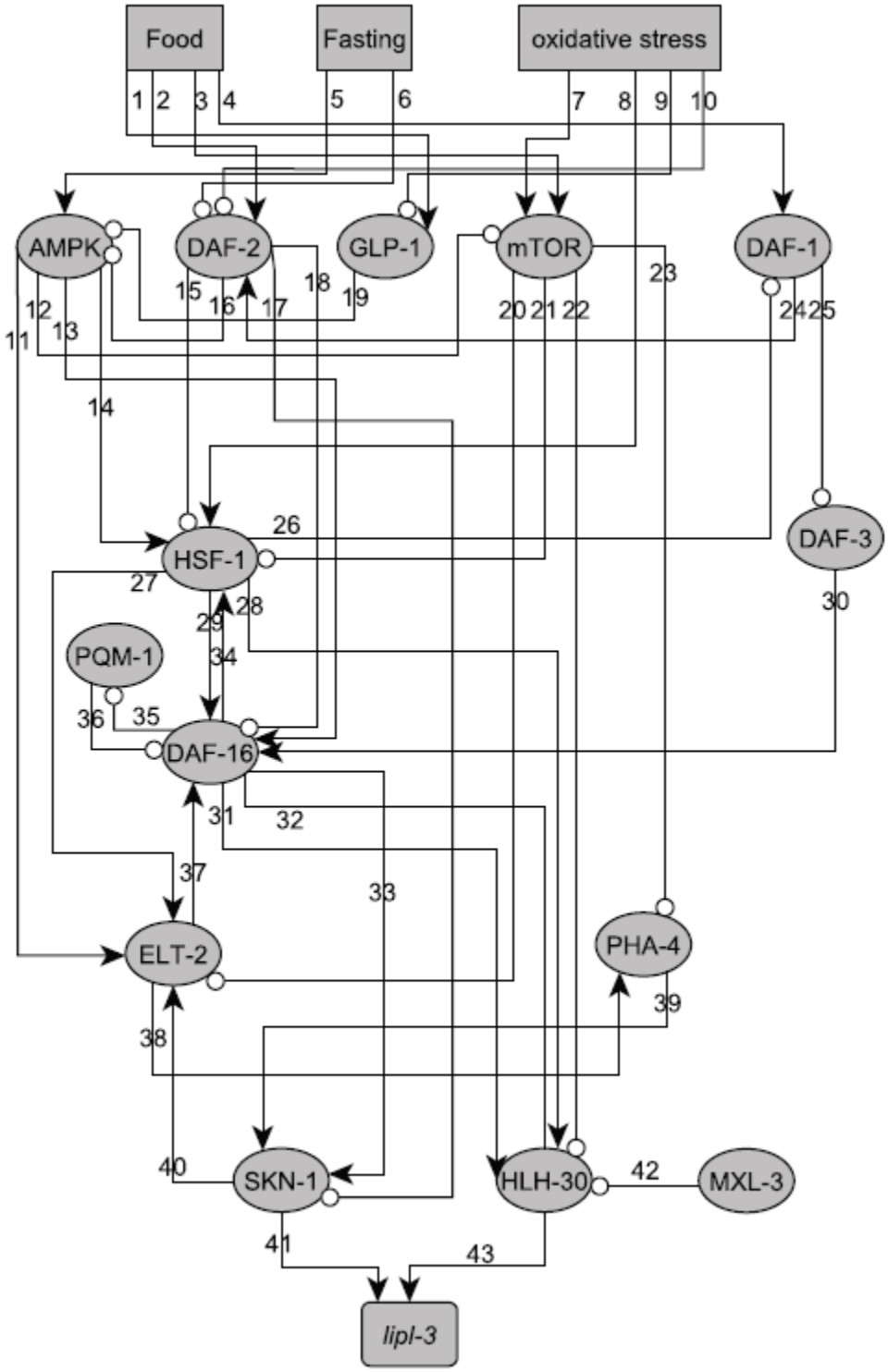
Food
Fasting
oxidative stress
1 2 3 4 5 6 7 8 9 10
AMPK
DAF-2
GLP-1
mTOR
DAF-1
11 12 13 14 15 16 17 18 19 20 21 22 23 24 25
HSF-1
DAF-3
26 27 28 29 30
PQM-1
34
35 36
DAF-16
31 32 33
37
ELT-2
PHA-4
38 39
40
SKN-1
HLH-30
42
MXL-3
41 43
lipl-3

Fig. 5.

Literature-inferred network predicts multiple TF-TF interactions regulating *lipl-3*. Representation of the nodes: 1) contexts are rectangles (e.g. fasting), proteins are ovals (nutrient sensors and TFs), and the target *lipl-3* is a rounded rectangle . The edges of the network represent documented interactions. Activating interactions are depicted as arrows and inhibitory interactions are depicted as blunt arrows. The edge labels correspond to the literature entries in *SI Appendix*, Table S2.

e. DAF-16 represses *lipl-3* expression in fed and fasted *C. elegans* via HLH-30

The generated literature-inferred network predicts that *daf-16* functionally interacts with *hlh-30* (**Fig. 5)**. Further, work from the Riedel lab demonstrated that the DAF-16 and HLH-30 proteins directly interact, and that *daf-16* and *hlh-30* can have opposing roles in the regulation of some target genes (92). However, this previous study did not focus on the roles that DAF-16 and HLH-30 play on specific target genes, and mutual regulation among *daf-16* and *hlh-30* has not been reported. Therefore, we first tested whether *daf-16* and *hlh-30* may be regulating each other. *C. elegans* overexpressing HLH-30 or carrying a loss of function mutation in *hlh-30* (allele *tm1978*) show wild-type transcriptional levels of *daf-16* (*SI Appendix*, Fig. S4*A*), as well as normal abundance and subcellular localization of DAF-16::GFP (*SI Appendix*, Fig. S4*B*), suggesting *hlh-30* does not regulate *daf-16* in our experimental setup. By contrast, loss of *daf-16* (allele *mu86*) leads to a two-fold increase in *hlh-30* mRNA levels in fed animals, and a two-fold enhancement of *hlh-30* induction during fasting when compared to fasted wild-type animals (**Fig. 6*A***). Since we previously reported that the levels of induction of *lipl-3* in fasting animals correlate with the levels of expression and activity of *hlh-30* (113), and DAF-16 seems to repress *hlh-30* expression, the results suggest that *daf-16*-mediated repression of *hlh-30* could explain the seemingly repressing role of *daf-16* in the expression of *lipl-3*. Indeed, we find that loss of function mutation of *hlh-30* suppresses the induction of *lipl-3* observed in *daf-16* fed animals and the enhancement of induction observed in *daf-16* fasted worms (**Fig. 6*B***). These results place *hlh-30* downstream of

daf-16 in the regulation of *lipl-3* in fed and fasting *C. elegans*. Further, as supported by the presence of DAF-16 binding sites upstream of every *hlh-30* isoform (*SI Appendix,* Table S3), and direct binding of DAF-16 in chromatin profiling by DNA adenine methyltransferase identification (DamID) surveys *(153)*, *hlh-30* is likely a direct target of DAF-16. Altogether, the results support a model in which DAF-16 is constitutively repressing *hlh-30*, and hence loss of function mutation of *daf-16* leads to enhanced *hlh-30* transcription and consequently *lipl-3* expression independent of the feeding status of the worm

Figure 6

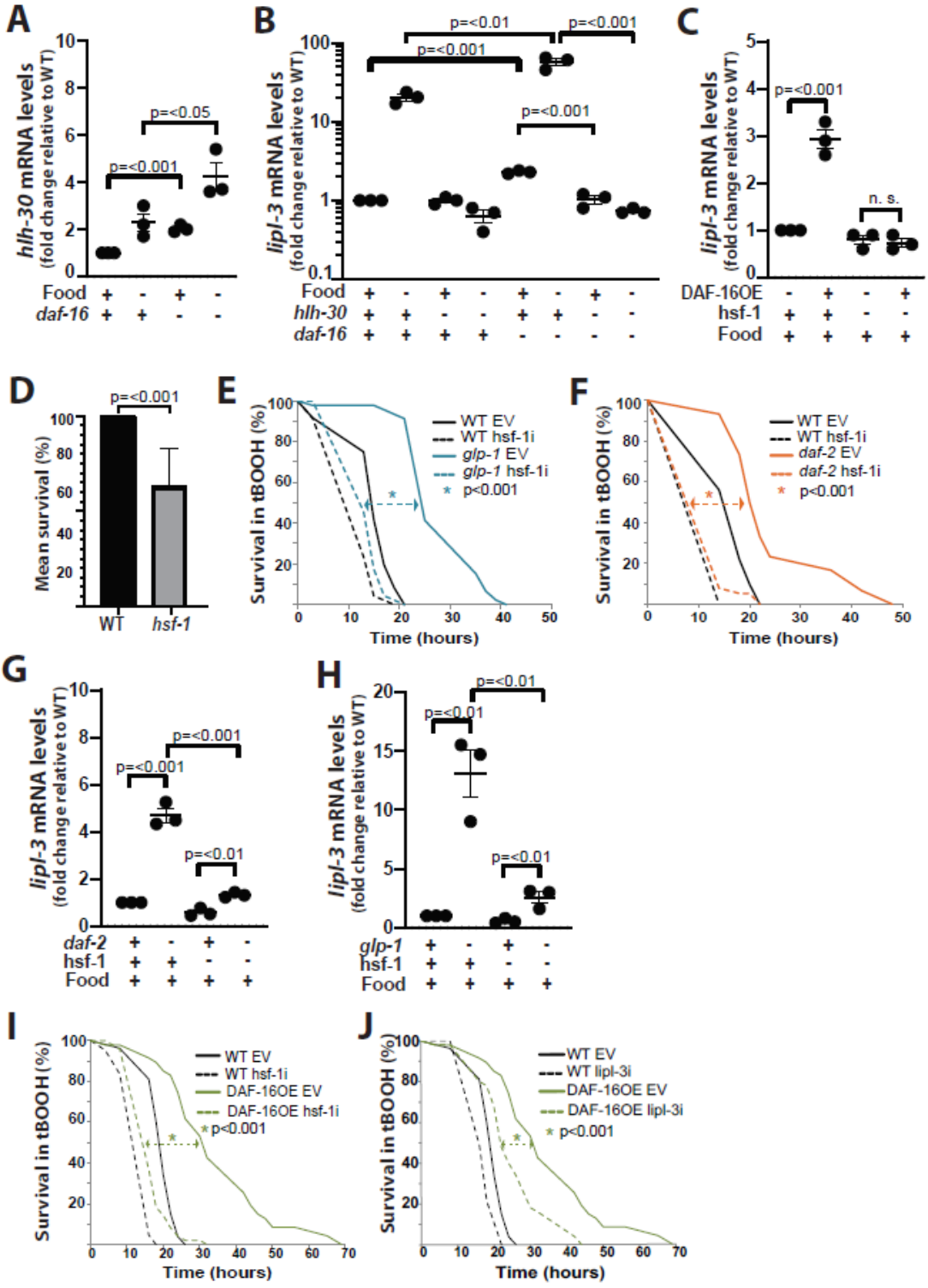
A
hlh-30 mRNA levels (fold change relative to WT)
p=<0.05
p=<0.001
Food + - + -
daf-16 + + - -
B
lipl-3 mRNA levels (fold change relative to WT)
p=<0.01
p=<0.001
p=<0.001
p=<0.001
Food + - + - + - + -
hlh-30 + + - - + + - -
daf-16 + + + + - - - -
C
lipl-3 mRNA levels (fold change relative to WT)
p=<0.001
n. s.
DAF-16OE - + - +
hsf-1 + + - -
Food + + + +
D
Mean survival (%)
p=<0.001
WT
hsf-1
E
Survival in tBOOH (%)
WT EV
WT hsf-1i
glp-1 EV
glp-1 hsf-1i
p<0.001
Time (hours)
F
Survival in tBOOH (%)
WT EV
WT hsf-1i
daf-2 EV
daf-2 hsf-1i
p<0.001
Time (hours)
G
lipl-3 mRNA levels (fold change relative to WT)
p=<0.001
p=<0.001
p=<0.01
daf-2 + - + -
hsf-1 + + - -
Food + + + +
H
lipl-3 mRNA levels (fold change relative to WT)
p=<0.01
p=<0.01
p=<0.01
glp-1 + - + -
hsf-1 + + - -
Food + + + +
I
Survival in tBOOH (%)
WT EV
WT hsf-1i
DAF-16OE EV
DAF-16OE hsf-1i
p<0.001
Time (hours)
J
Survival in tBOOH (%)
WT EV
WT lipl-3i
DAF-16OE EV
DAF-16OE lipl-3i
p<0.001
Time (hours)

Fig. 6.

DAF-16 inhibits HLH-30 and promotes HSF-1 activity. (*A-C, G, H*) qRT-PCR analysis of gene expression in young adult *C. elegans* as described in **Fig. 2**. *(E, F, I, J)* Survival to oxidative stress. When L3s, *daf-2* worms and their controls were transferred to 25˚C. *glp-1* and their controls were incubated at 25˚C from L1s. When young adults, animals were transferred to plates containing 5mM tBOOH and scored for survivorship every 2h. (*A*) *hlh-30* expression in WT and *daf-16(mu86)* animals fasted for 6h relative to fed. N=3 (*B*) *lipl-3* expression in WT, *hlh-30(tm1978), daf-16(mu86),* and *hlh-30(tm1978);daf-16(mu86)* double mutant animals fasted for 6h relative to fed. N=3 (*C*) *lipl-3* expression in WT and DAF-16OE (GR1352) animals treated empty vector control (EV) or RNAi against *hsf-1* since the L1 stage. N=3 *(D)* Mean survival of WT animals treated with EV or RNAi against *hsf-1* since the L1 stage and exposed to 5mM tBOOH at the young adult stage. Error bars denote SEM. N=3. *(E)* Survival of WT and *glp-1(e2141*) animals treated with EV or RNAi against *hsf-1* since the L1 stage and treated with tBOOH from the young adult stage. N=3 (see also *SI Appendix,* Table S8) *(F)* Survival of WT and *daf-2(e1368)* animals treated with EV or RNAi against *hsf-1* since the L1 stage and treated with tBOOH from the young adult stage. N=3 (see also *SI Appendix,* Table S8) *(G) lipl-3* expression in *daf-2(e1368)* animals treated with EV or RNAi against *hsf-1*. N=3. *(H) lipl-3* expression in *glp-1(e2141*) animals treated with EV or RNAi against *hsf-1*. N=3. *(I, J)* DAF-16OE (GR1352) animals treated with EV or RNAi against *hsf-1 (I)* or *lipl-3 (J)* since the L1 stage and treated with tBOOH from the young adult stage.N=3 (see also *SI Appendix,* Table S8).

Supplementary Figure 4

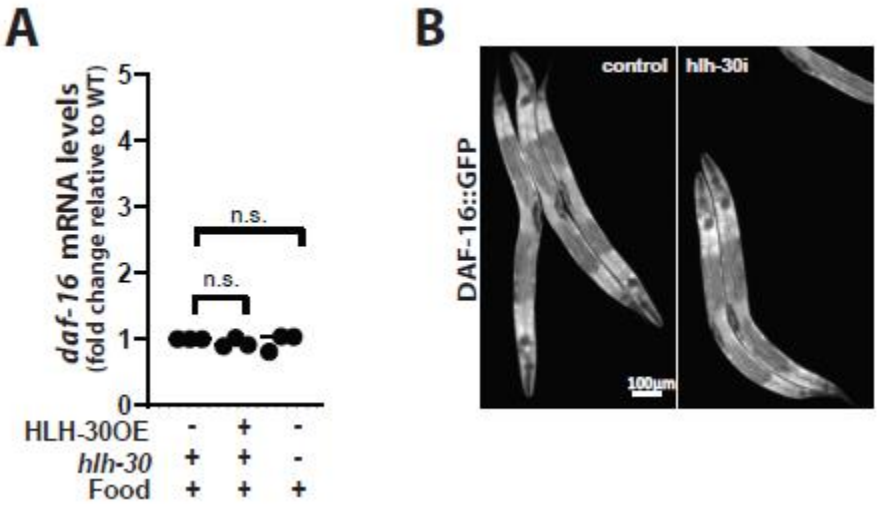

Fig. S4.

HLH-30 does not control *daf-16* expression. (*A, C, D*) qRT-PCR analysis of gene expression in young adult *C. elegans* as described in **Fig. 2**. (*A*) *daf-16* expression in *hlh-30(tm1978)* mutants and HLH-30OE animals relative to WT. N=3. *(B)* Fluorescent images of adult DAF-16::GFP (TJ356) worms treated with empty vector control or RNAi against *hlh-30* from the L1 stage.

f. DAF-16 promotes *lipl-3* induction and survival to oxidative stress via HSF-1

DAF-16 seems to act as an activator of *lipl-3* in *glp-1* and *daf-2* mutant *C. elegans* (**Fig. 3*H, I***), and in wild-type animals exposed to tBOOH (**Fig. 4*C***). However, up to 2kb upstream of the *lipl-3* coding sequence there are no DAF-16 ChIP peaks (*SI Appendix*, Table S3); importantly, the intergenic region between *lipl-3* and next upstream gene spans 875bp. Further, using yeast 1-hybrid, we previously showed that DAF-16 does not bind to the *lipl-3* promoter (113). Therefore, the evidence suggests that *daf-16* may not be directly regulating *lipl-3*. Similarly, we find no predicted DAF-3 (data not shown) or SKN-1 (*SI Appendix*, Table S3) binding sites in the *lipl-3* promoter region. By contrast, MXL-3 and HLH-30 directly bind to the *lipl-3* promoter (113). However, MXL-3 is a repressor and HLH-30 does not control *lipl-3* in the *daf-2* and *glp-1* contexts (**Fig. 3*F, G***); hence, these TFs would not be activators of *lipl-3* in *glp-1* and *daf-2* mutant *C. elegans*. Therefore, an alternative transcriptional regulator is likely to induce *lipl-3* downstream of DAF-16 in the *daf-2*, *glp-1*, and oxidative stress contexts. From the most downstream transcriptional regulators predicted to modulate the expression of *lipl-3* in our inferred network (**Fig. 5**), we are left with HSF-1 as a potential mediator of DAF-16's activating role on the *lipl-3* promoter. Importantly, HSF-1 meets three criteria to play this role: 1) HSF is a stress-responsive transcription factor; 2) there is a predicted HSF-1 binding site (154) upstream of the *lipl-3* start site (*SI Appendix*, Table S3), and 3) HSF-1 has been shown to orchestrate transcriptional responses downstream of *glp-1* and *daf-2* (155,156). Further, our inferred network places *hsf-1* downstream of *daf-16* (**Fig. 5**).

Therefore, we tested whether DAF-16 may be regulating *lipl-3* through *hsf-1*. In support of this hypothesis, we found that overexpression of DAF-16 (GR1352 line) (157) was sufficient to promote induction of *lipl-3* in fed *C. elegans* and that this induction was completely suppressed by RNAi against *hsf-1* (**Fig. 6*C***).

Physiologically, we showed above that *daf-16* and *lipl-3* contribute to survival to tBOOH in wild-type *C. elegans* (**Fig. 4*B,*** *SI Appendix,* Fig. S3*C*). Molecularly, we showed a *daf-16*-dependent induction of *lipl-3* when *C. elegans* are treated with tBOOH (**Fig. 4*C***). If, as the model and data suggest, *hsf-1* links DAF-16 activation to the induction of *lipl-3*, then *hsf-1* should also contribute to survival to oxidative stress and to the induction of *lipl-3* in *glp-1*, *daf-2*, DAF-16 overexpression, and tBOOH-treated animals. In support of the first prediction, Servello *et al* recently reported that *hsf-1* contributes to *C. elegans* resistance to peroxides (158). We independently observed that *hsf-1*-deficient animals fed *E. coli* XU363 are more sensitive to tBOOH than wild-type worms (**Fig. 6*D*-*F***). Then we tested the predicted epistatic interaction between *glp-1* and *hsf-1*, and *daf-2* and *hsf-1*. We found that loss of *hsf-1* function suppresses *glp-1* and *daf-2* resistance to tBOOH (**Fig. 6*E, F***), as well as the induction of *lipl-3* observed in these mutants (**Fig. 6*G, H***). Finally, DAF-16OE (GR1352) animals are also resistant to tBOOH, and their resistance is *hsf-1* and *lipl-3* dependent (**Fig. 6*I, J***, respectively), supporting the notion that in this context *hsf-1* acts downstream of DAF-16. Future studies may investigate whether DAF-16 directly or indirectly promotes HSF-1 activity. Altogether the data place *hsf-1* as a

mediator of the adaptive transcriptional response to oxidative stress activated downstream of the insulin and Notch pathways, and executed, at least in part, by *lipl-3*.

Our working model also proposes that HSF-1 acts as a terminal regulator of *lipl-3* in the oxidative-stress axis, which in turn predicts: 1) HSF-1 would promote *lipl-3* expression upon oxidative stress, 2) HSF-1 would be activated by oxidative stress, 3) activation of HSF-1 would be sufficient to promote *lipl-3* induction, 4) HSF-1OE animals would be resistant to oxidative stress, and 5) HSF-1OE resistance to oxidative stress would be *lipl-3* dependent. In support of the first prediction, we found *lipl-3* induction upon tBOOH treatment to be dependent on *hsf-1* (**Fig. 7*A***). In support of the second prediction, we observed HSF-1::GFP forming nuclear foci in animals treated with tBOOH (**Fig. 7*B***), a phenotype previously associated with activation of HSF-1 (159). In support of the third prediction, overexpression of HSF-1 is sufficient to promote *lipl-3* induction (**Fig. 7*C***). Since, HSF-1 overexpression is sufficient to promote *lipl-3* expression, and *lipl-3* promotes survival to oxidative stress in wild-type, *daf-2* and *glp-1 C. elegans*, we tested whether overexpression of HSF-1 would be sufficient to promote resistance to tBOOH treatment in a *lipl-3*-dependent manner. Indeed, HSF-1 overexpressing *C. elegans* are resistant to oxidative stress and this resistance is *lipl-3* dependent (**Fig. 7*D***). Together, these data demonstrate that the TF-target pair composed of *hsf-1* and *lipl-3* is a relevant contributor to the *C. elegans* response to oxidative stress. Further, the overlap between the players mediating the *lipl-3* response to tBOOH and the ones composing the *glp-1* -| *daf-16→hsf-1→lipl-3* and *daf-2* -| *daf-16→hsf-1→lipl-3* epistatic axes, allow us to

propose that these adaptive signaling axes are tuned to protect the redox status of *C. elegans*.

g. *lipl-3* promotes fat mobilization upon oxidative stress

Lipases contribute to survival to oxidative stress through two main mechanisms: 1) promoting sequestration of potentially toxic oxidized lipids, and, 2) providing energy and reducing power through fat mobilization (160,161). Experimentally, in scenario (1) the content of lipid droplets increases (162), while in scenario (2) lipid droplet content is reduced. Therefore, we tested the response of *C. elegans* major fat stores to oxidative stress using the fat-specific dye Oil red O (163,164). Supporting the notion that oxidative stress imposes an energetic demand provisioned by mobilization of fat stores, we observed a decline in Oil red O signal in animals treated with tBOOH (**Fig. 7*E***). We then tested whether *lipl-3* would contribute to fat mobilization in *C. elegans* subject to oxidative stress. Indeed, knock down of *lipl-3* impaired fat mobilization during oxidative stress (**Fig. 7*E***). Therefore, we propose that *lipl-3* contributes to survival to oxidative stress through promoting lysosomal lipolysis, and hence through providing energy to mount an effective anti-oxidant response.

Figure 7

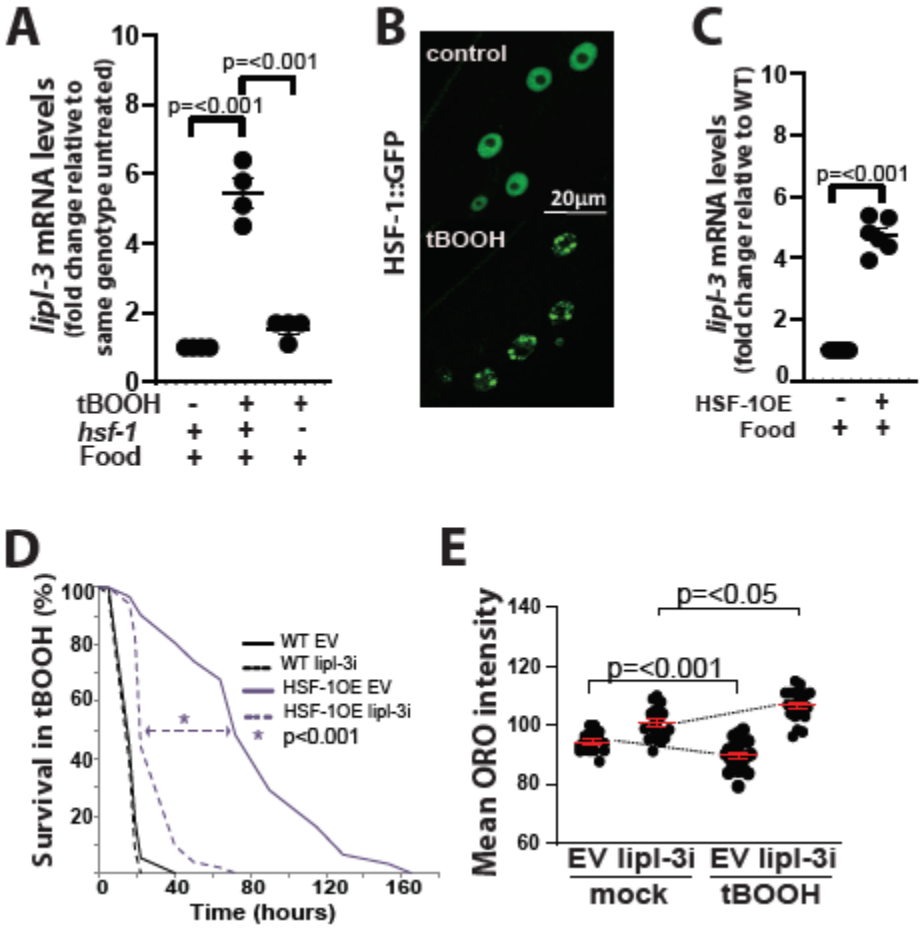
A
lipl-3 mRNA levels
(fold change relative to
same genotype untreated)
p=<0.001
p=<0.001
tBOOH
hsf-1
Food
B
HSF-1::GFP
control
20µm
tBOOH
C
lipl-3 mRNA levels
(fold change relative to WT)
p=<0.001
HSF-1OE
Food
D
Survival in tBOOH (%)
WT EV
WT lipl-3i
HSF-1OE EV
HSF-1OE lipl-3i
p<0.001
Time (hours)
E
Mean ORO intensity
p=<0.05
p=<0.001
EV lipl-3i
mock
EV lipl-3i
tBOOH

Fig. 7.

HSF-1 promotes *lipl-3* induction and *lipl-3*-mediated survival to oxidative stress. (*A, C*) qRT-PCR analysis of gene expression in young adult *C. elegans* as described in **Fig. 2**. *(A) lipl-3* expression in WT and *hsf-1(sy441)* mutant animals treated with tBOOH for 4h relative to untreated. N=4. (*B*) Confocal images of adult worms expressing HSF-1::GFP (OG497) treated for 4h with mock or 5mM tBOOH. (*C*) *lipl-3* expression in WT and HSF-1OE (AGD710) animals. N=3. (*D*) Survivorship of WT and HSF-1OE (AGD710) animals treated with empty vector control (EV) or RNAi against *lipl-3* since the L1 stage and treated with 5mM tBOOH from the young adult stage and scored for survivorship every 2h. N=3 (see also *SI Appendix,* Table S8). (E) Mean Oil red O (ORO) intensity. Wild-type animals were grown from L1 onEV or *lipl-3* RNAi. When day-1 adults animals were exposed to 0.5mM tBOOH for 4h, harvested, and stained with ORO. Statistical significance assessed via one-tailed unpaired parametric t-test. Error bars denote SEM. N=4.

h. Multipoint antagonism between the oxidative stress and fasting axes

Our data suggests that fasting favors HLH-30-mediated regulation of *lipl-3*, and oxidative stress favors HSF-1-mediated regulation of *lipl-3*. Now, how does context tilt the balance in favor of one or the other TF? This question is particularly intriguing when considering that HLH-30 and HSF-1 share upstream regulators, including *glp-1 (27,156)* , *daf-2* (27,155), and mTOR (165,166), and all of these upstream regulators are simultaneously altered during fasting and oxidative stress. Hence, how does context determine the activity of specific intermediate players, when the upstream regulators are shared?

While food is abundant, HLH-30 is enriched in the cytoplasm and *lipl-3* is expressed at low levels (113). As shown above, mTORC1 contributes to maintaining low levels of expression of *lipl-3* (**Fig. 3*D***). In addition, mTORC1 activity promotes cytoplasmic retention of TFEB, the mammalian ortholog of HLH-30 (167–171), and RNAi against *C. elegans* mTOR (*let-363*) promotes nuclear translocation of HLH-30 (27). Here we more specifically show that inhibition of mTORC1 (via *daf-15* RNAi) is sufficient to promote increased *hlh-30* expression, nuclear translocation of HLH-30, and induction of *lipl-3* (**Fig. 8*A*-*B* and 3*D***), demonstrating conservation of this regulatory axis. Therefore, one mechanism enabling HLH-30-mediated induction of *lipl-3* during fasting is inhibition of mTORC1. However, for HLH-30 to promote *lipl-3* expression, the activity of the *lipl-3* repressor MXL-3 needs to be reduced as these TFs compete for the same binding sites in the *lipl-3* promoter (113). As mTORC1 coordinates the action of several transcriptional programs (172,173), we tested the hypothesis that mTORC1 may also modulate the

activity of MXL-3. In support of this notion, RNAi against *daf-15* leads to reduced MXL-3::GFP signal in fed animals (**Fig. 8*C***), a response that mimics the MXL-3 physiological response to fasting (113). Therefore, as long as there is food and, hence, mTOR is active, HLH-30 action at the *lipl-3* promoter would be disfavored through at least three paths: 1) food → mTORC1 -| HLH-30 nuclear localization; 2) food → mTORC1 → MXL-3-mediated out-competition of HLH-30 at the *lipl-3* promoter; and 3) unknown axis -| *hlh-30* transcription. By contrast, during fasting, mTORC1 and MXL-3 activities would be reduced, and HLH-30 action on the *lipl-3* promoter would be favored.

In mammalian systems mTORC1 is activated upon oxidative stress (35), a response that, if conserved, would disfavor *C. elegans* HLH-30 action in this context. We then tested the levels of kinase activity of mTORC1 using as readout the phosphorylation of its direct target RSKS-1 (mammalian S6K) (see methods and *SI Appendix*, Note S3 for details). We observed increased levels of phosphorylated RSKS-1 in *C. elegans* treated with 5mM tBOOH for 4h relative to mock treatment (**Fig. 8*D***), supporting conservation of the mTORC1 response to oxidative stress. Further, based on the mTORC1-MXL-3 functional interaction described above, we hypothesized that increased mTORC1 activity would lead to increased activity of the HLH-30-competitor MXL-3. Supporting this hypothesis, we observed increased nuclear signal in MXL-3::GFP worms treated with tBOOH (**Fig. 8*E***). Together, the data are in line with a model in which enhanced mTORC1-MXL-3 activity would disfavor HLH-30 activity on the *lipl-3* promoter during oxidative stress.

We identified *daf-2*, *glp-1*, *daf-16*, *hsf-1* and *lipl-3* as nodes of an axis responsive to the redox status of *C. elegans* (denoted pink in **Fig. 8*J***). Hence, we asked whether these nodes would also play a role directly or indirectly in disfavoring HLH-30 action during oxidative stress. Bottom-up through the oxidative stress axis, the first player needing testing is HSF-1. Analysis of *hlh-30* expression in an *hsf-1* loss of function mutant shows induction of *hlh-30* in the untreated, and more so in tBOOH-treated animals (**Fig. 8*F***). Further, we found several potential HSF-1 binding sites up to -500bp from the *hlh-30* start site (*SI Appendix,* Table. S3), suggesting that HSF-1 may directly repress the expression of *hlh-30*. On the other hand, we found that *hsf-1* deficiency leads to loss of MXL-3::GFP signal (**Fig. 8*C***), and that HSF-1 overexpression is sufficient to promote *mxl-3* induction (**Fig. 8*G***). The presence of multiple HSF-1 binding sites up to -500 of the *mxl-3* transcriptional initiation site, suggests that HSF-1 may directly regulate *mxl-3* transcription (*SI Appendix,* Table S3). Together, the results suggest that HSF-1 would curtail HLH-30 activity through two at least two mechanisms: 1) repressing *hlh-30* expression, and 2) promoting *mxl-3* expression, which in turn would promote MXL-3-mediated out-competition of HLH-30 from the *lipl-3* promoter.

One step up in the oxidative stress axis, we find DAF-16 (**Fig. 8*J***). We showed above that DAF-16 represses *hlh-30* **(Fig. 6*A***); hence, DAF-16 drives another inhibitory edge running from the oxidative-stress to the fasting axis. On the other hand, loss of function mutation of *daf-16* does not change the expression levels of *mxl-3* (*SI Appendix*, Fig.

S5*A*), and treatment with *daf-16* RNAi does not change the abundance or localization of the MXL-3::GFP fusion protein (*SI Appendix,* Fig. S5*B*).

Finally, we reach the level of the sensors. We found that loss of *glp-1* or *daf-2* function does not increase HLH-30::GFP abundance (GFP intensity) or nuclear localization (*SI Appendix,* Fig. S5*C*), results that are in line with the lack of effect of tBOOH treatment on HLH-30::GFP expression (*SI Appendix,* Fig. S5*D*) but in contradiction with published results (92,174). On one side, we confirmed that our HLH-30::GFP transgenic line responds to stimuli such as food deprivation (*SI Appendix,* Fig. S5*D*). Further, in mammalian systems, although insulin signaling promotes mTORC1 activity (such as postpandrially), basal or reduced insulin signaling does not necessarily reduce mTORC1 activity (175). Hence, conditions in which reduced insulin signaling promotes HLH-30 nuclear translocation might do so through mTORC1-independent mechanisms. On the other hand, reduced Notch signaling does partially inhibit mTORC1 signaling in several mammalian cellular models (176). Thus, if this edge would be conserved, we would expect some mTOR inhibition in the *glp-1* mutant worms. This is an intriguing possibility, since; 1) *glp-1* mutation, but not *daf-2* mutation, leads to *mxl-3* induction (**Fig. 8*H***), which could serve a compensatory role in maintaining HLH-30 inhibited while Notch signaling is reduced; and 2) *daf-16* does not fully suppress the induction observed in *glp-1* mutant animals, leaving open the possibility to HLH-30 partially contributing to the induction observed in *glp-1* mutant worms. All other variables being equal, we hypothesize that when compared to *E. coli* OP50 or its derivatives (food source used in

our study), *E. coli* HT115 (food source used in the previous studies) may distinctively interact with the mTOR pathway. In summary, in the experimental setup tested in this study, neither *daf-2* nor *glp-1* seem to influence the fasting axis at the level of *hlh-30*, possibly because within the context of the HLH-30-*lipl-3* axis these mutations might not affect mTORC1 activity or be otherwise compensated. By contrast, we find loss of *glp-1* function promoting *mxl-3* expression (**Fig. 8*H***), and tBOOH treatment increasing MXL-3 abundance in the nucleus (**Fig. 8*E***).

Altogether, the data support the notion that the oxidative stress axis curtails the activity of HLH-30 at, at least, 3 levels (**Fig. 8*J***): 1) reduced GLP-1 activity (Notch signaling) promotes *mxl-3* expression, which in turn would outcompete HLH-30 at the *lipl-3* promoter; 2) reduced DAF-2 activity (insulin signaling) promotes DAF-16 activity, which in turn represses *hlh-30* expression, 3) increased mTORC1 activity promotes: i) retention of HLH-30 in the cytoplasm, and ii) increased activity of the HLH-30 competitor MXL-3. It is worth noting that *mxl-3* is transcriptionally controlled by the Notch axis, but not by the insulin (specifically DAF-2) signaling axis, suggesting that these signaling pathways have complementary roles in the program leading to *lipl-3* induction upon exposure to oxidative stress.

We then investigated potential effects of the fasting axis on the oxidative-stress axis. Loss of *hlh-30* function does not change the levels of expression of *hsf-1* (*SI Appendix*, Fig.

S5*E*), or the abundance or localization of HSF-1::GFP (*SI Appendix*, Fig. S5*F*). We showed above that loss of *hlh-30* function does not change the levels of expression of *daf-16* or the abundance or localization of DAF-16::GFP (*SI Appendix*, Fig. S4*A, B*), suggesting that in the tested conditions *hlh-30* does not influence the function of the terminal players in the oxidative stress axis. Similarly, loss of *mxl-3* function does not change the levels of expression of *daf-16* or the abundance or localization of DAF-16::GFP (*SI Appendix*, Fig. S5*G, H*). Contrastingly, loss of *mxl-3* function does lead to loss of HSF-1::GFP signal (**Fig. 8*I***), suggesting a two-way activating edge between MXL-3 and HSF-1 (**Fig. 8*J***). However, MXL-3 may not necessarily regulate *hsf-1* directly as no MXL-3 binding sites are found up to -5kb of the *hsf-1* transcription start site (data not shown). Finally, mTOR is the nutrient sensor linking feeding status to the activity of MXL-3 and HLH-30. Given that MXL-3 promotes HSF-1 activity (**Fig. 8*I***), and mTOR activity positively correlates with MXL-3 abundance and nuclear localization (**Fig. 8*C***), we hypothesized that mTOR may influence HSF-1 activity. In support of this notion, RNAi against *daf-15* leads to reduced HSF-1::GFP signal (**Fig. 8*I***).

Altogether, the results are in line with a model in which (**Fig. 8*J***): 1) Food promotes mTOR activity, which in turn promotes both cytoplasmic retention of HLH-30 and MXL-3 activity. Together, these factors limit the activity of HLH-30 on the *lipl-3* promoter in fed unstressed *C. elegans*; 2) Upon fasting, mTOR is inhibited and, consequently, MXL-3-mediated outcompetition of HLH-30 at the *lipl-3* promoter is reduced, and HLH-30 can translocate into the nucleus and promote the expression of *lipl-3*. 3) Upon oxidative stress

mTOR activity is enhanced, likely more tightly restricting HLH-30 translocation into the nucleus. In parallel, a combination of *glp-1* inhibition, mTOR activation, and activation of HSF-1, strengthens MXL-3 activity, which further limits HLH-30 activity at the *lipl-3* promoter. Further, MXL-3 promotes HSF-1 activity, building a self-reinforced *hlh-30*-restrictive loop. Simultaneously, the DAF-16-HSF-1 axis promotes repression of *hlh-30* expression. The network-level promoted inhibition of HLH-30 and activation of HSF-1, makes HSF-1 a prevalent *lipl-3* activator during oxidative stress. By contrast, during fasting, the edges that inhibit HLH-30 and activate HSF-1 are weakened, favoring HLH-30-mediated induction of *lipl-3*.

Finally, we asked how the experimental results we generated may fit or alter the literature- inferred network. We evaluated all the edges and nodes of the literature-inferred network and eliminated those that were contradicted by our results (see *SI Appendix,* Note S2 for a detailed explanation). This resulted in an improved network model of the transcriptional control of *lipl-3* **Fig. 8*J***. We translated the network model of **Fig. 8*J*** into a discrete dynamic model in which inputs are binary (present/absent) and the activity of proteins and mRNAs is described by three levels calibrated to the basal activity corresponding to feeding (see Methods and *SI Appendix,* Note S4). The discrete dynamic model synthesizes information from the literature and from the experiments performed in this study. For each network element (every direct or indirect regulator of *lipl-3* transcription, and *lipl-3* itself) the model describes how the regulation of the element determines its activity level. The model reproduces all of our observations in the

different contexts studied here and expresses the contextualized transcriptional control of *lipl-3* in a mathematical language (*SI Appendix*, Note S4). Together, the data presented here suggest that the opposite effect of MXL-3 on HSF-1 and HLH-30 provides the cell with an elegant mechanism for switching between the oxidative and fasting stress-responsive state. The position of the switch would be determined by the signaling status of mTORC1 (**Fig. 8*J***).

Figure 8

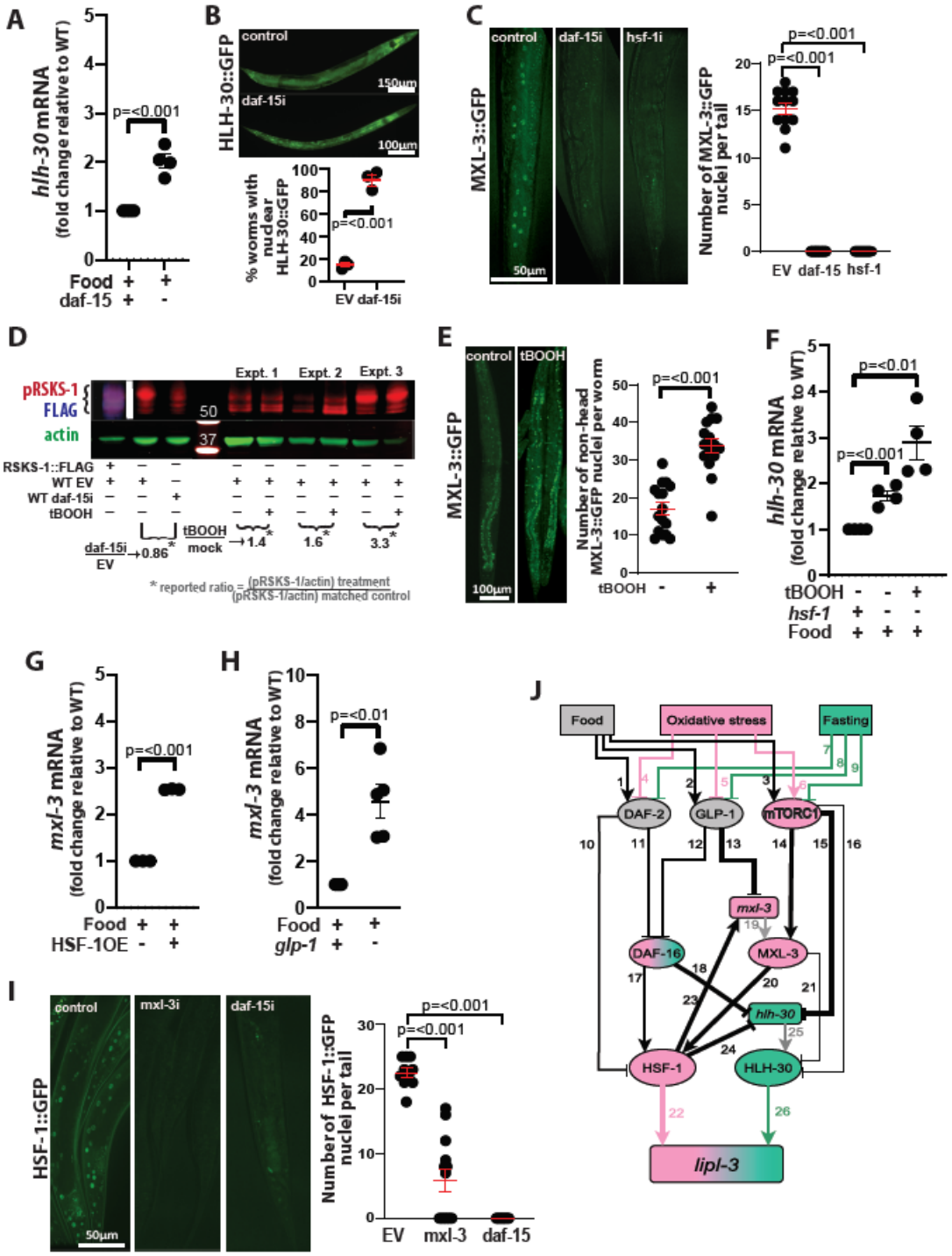
A
hlh-30 mRNA (fold change relative to WT)
p=<0.001
Food + +
daf-15 + -
B
HLH-30::GFP
control
daf-15i
150µm
100µm
% worms with nuclear HLH-30::GFP
p=<0.001
EV daf-15i
C
MXL-3::GFP
control
daf-15i
hsf-1i
50µm
Number of MXL-3::GFP nuclei per tail
p=<0.001
p=<0.001
EV daf-15 hsf-1
D
Expt. 1
Expt. 2
Expt. 3
pRSKS-1
FLAG
actin
50
37
RSKS-1::FLAG
WT EV
WT daf-15i
tBOOH
daf-15i / EV →0.86*
tBOOH / mock →1.4*
1.6*
3.3*
* reported ratio = (pRSKS-1/actin) treatment / (pRSKS-1/actin) matched control
E
MXL-3::GFP
control
tBOOH
100µm
Number of non-head MXL-3::GFP nuclei per worm
p=<0.001
tBOOH - +
F
hlh-30 mRNA (fold change relative to WT)
p=<0.01
p=<0.001
tBOOH - - +
hsf-1 + - -
Food + + +
G
mxl-3 mRNA (fold change relative to WT)
p=<0.001
Food + +
HSF-1OE - +
H
mxl-3 mRNA (fold change relative to WT)
p=<0.01
Food + +
glp-1 + -
I
HSF-1::GFP
control
mxl-3i
daf-15i
50µm
Number of HSF-1::GFP nuclei per tail
p=<0.001
p=<0.001
EV mxl-3 daf-15
J
Food
Oxidative stress
Fasting
DAF-2
GLP-1
mTORC1
mxl-3
DAF-16
MXL-3
hlh-30
HSF-1
HLH-30
lipl-3

Fig. 8.

Multipoint antagonism between the oxidative stress and fasting axes. (*A, F, G. H*) qRT-PCR analysis of gene expression in young adult *C. elegans* as detailed in **Fig. 2**. *(A) hlh-30* expression in WT animals treated with RNAi against *daf-15* from the L1 stage relative to empty vector control (EV). N=4. *(B)* Representative images of adult worms expressing HLH-30::GFP treated with EV or RNAi against *daf-15* from the L1 stage. Quantification shows the percentage of worms with GFP(+) nuclei in any tissue. Error bars denote SEM. *(C)* Representative images of adult worms expressing MXL-3::GFP treated with EV or RNAi against *daf-15* or *hsf-1* from the L1 stage. Quantification shows the mean number of GFP(+) nuclei per worm-tail. Error bars denote SEM. (*D*) Western blot assaying RSKS-1 phosphorylation status in worms treated with 5mM tBOOH. RSKS-1 bands were ascertained based on the anti-FLAG signal observed in the lysates of RSKS-1::FLAG worms (Mony V. unpublished) and from lysates of WT worms treated with RNAi against *daf-15*. (*E*) Representative images of adult worms expressing MXL-3::GFP treated with mock or 5mM tBOOH for 4h. Quantification shows the mean number of GFP(+) nuclei per worm (excluding the head). Error bars denote SEM. *(F) hlh-30* expression in WT and *hsf-1(sy441)* mutant animals treated with tBOOH for 4h relative to untreated. N=4. *(G) mxl-3* expression in WT and HSF-1(OE) animals. N=3. *(H) mxl-3* expression in WT and *glp-1(e2141)* animals. N=3. *(I)* Representative images of adult worms expressing HSF-1::GFP (OG497) treated with EV or RNAi against *mxl-3* or *daf-15* from the L1 stage. Quantification shows the mean number of GFP(+) nuclei per worm-tail. Error bars denote SEM. (*J*) Model of contextualized regulation of *lipl-3*. Shapes and arrowhead representations as in Fig. 5. The colors represent the activity of

each node in different contexts: pink refers to nodes active during oxidative stress, green denotes nodes active during fasting, and grey refers to nodes that are inactivated in both contexts. For more information see *SI Appendix,* Note S4, Table S7.

Supplementary Figure 5

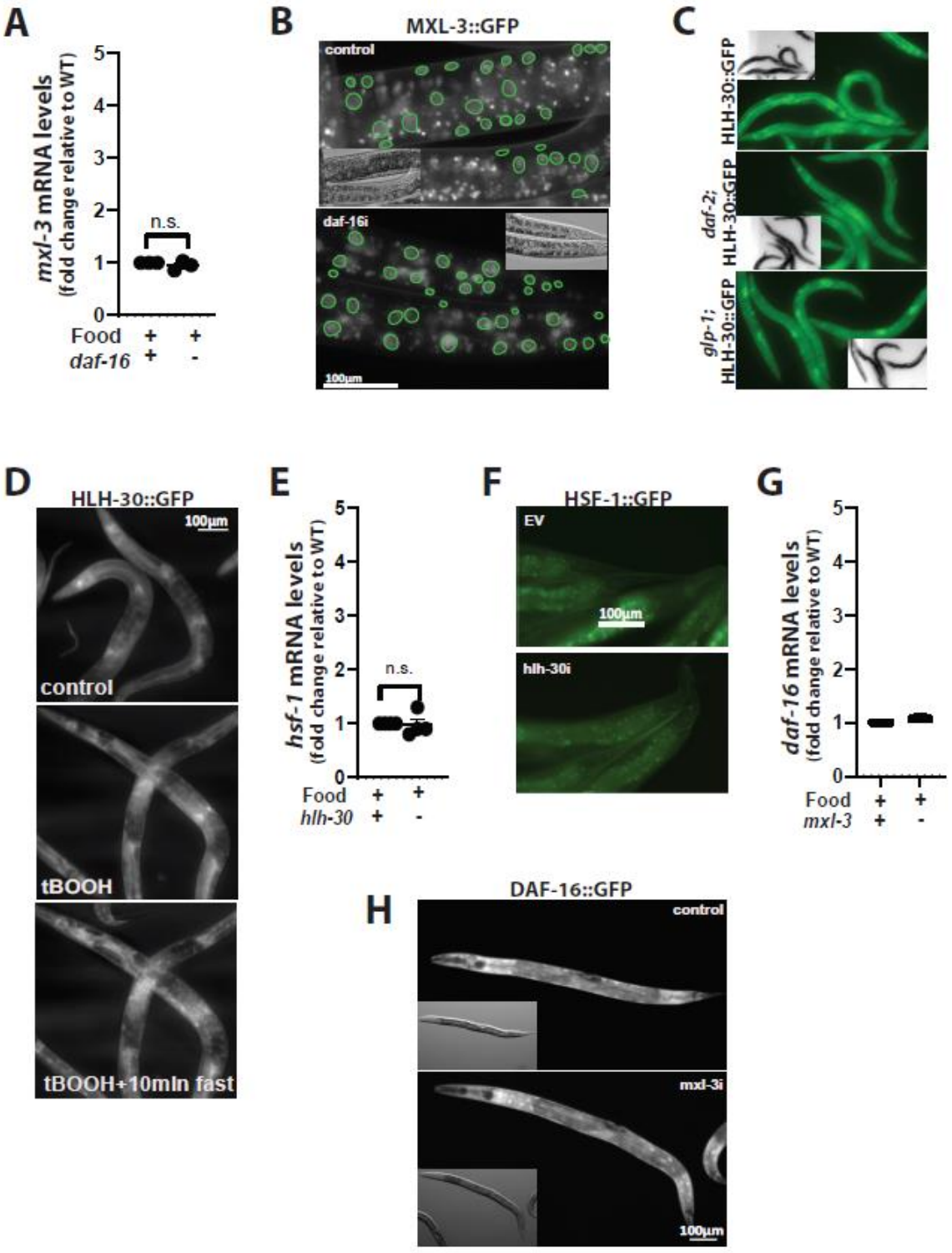

Fig. S5.
TF-TF interactions absent in relevant environmental and genetic contexts.

(*A, E, G*) qRT-PCR analysis of gene expression in young adult *C. elegans* as detailed in **Fig. 2**.

(*B, C, D, F, H*) Representative fluorescent images of adult *C. elegans* expressing (*B*) MXL-3::GFP and treated with empty vector control (EV) or RNAi against *daf-16* since the L1 stage. (*C*) HLH-30::GFP in WT, *daf-2(e1368),* or *glp-1(e2141*) mutant backgrounds [sterility visible in *glp-1* inset]. (*D*) HLH-30::GFP in untreated (top), treated with 5mM tBOOH for 4h (middle), or same animals than in the middle image but subsequently fasted for 10 min in the slide in the absence of any light source (bottom). (*F*) HSF-1::GFP (OG497) treated with EV or RNAi against *hlh-30* since the L1 stage. (*H*) DAF-16::GFP (TJ356) treated with EV or RNAi against *mxl-3* since the L1 stage.

5. Discussion

Using systematic genetic epistasis and mathematical modeling, we show here that *lipl-3* and *lipl-4* represent two distinct modes of transcriptional control. We found that *lipl-4* induction fits the linear paradigm in which a target gene is functionally linked to a specific TF across several contexts, and we name this mode of transcriptional control "convergent". By contrast, *lipl-3* induction does not conform to this paradigm. We name "contextualized" the mode of regulation represented by *lipl-3*, where the context defines the activity levels of the mediators allowing for a fine-tuned response of the target, and propose that this likely represents a prevalent mode of regulation for stress-responsive downstream effectors that contribute to plasticity in a wide range of contexts.

In general, the response of each target gene to signaling activity may be unique; hence, the mechanisms that have evolved to limit the activation of targets to their proper contexts must operate at the level of individual promoters. In developmental biology, the distinct regulation of the transcriptional response of a particular target gene is defined by "zones of competence" (177). However, to the best of our knowledge, *lipl-3* and *lipl-4* are solely expressed in the intestinal cells of *C. elegans (113,119)*, and we are studying their transcriptional regulation at a single life-stage in the ontogeny of the worm. Hence, space and time-independent information is also capable of defining alternative axes of regulation for a single gene. Our data support the notion that plasma membrane and intracellular sensor-driven modulation of TF-networks may allow cells to activate a single gene through alternative regulatory axes. DAF-3 activates *lipl-3* when TGFβ

signaling is inhibited, and likely in a yet-to-be-defined physiological context. HLH-30 promotes *lipl-3* transcription when mTORC1 function is inhibited and during fasting. HSF-1 and DAF-16 activate *lipl-3* when insulin and Notch signaling are inhibited, which would physiologically occur when animals are exposed to the oxidant tBOOH; and yet, when *C. elegans* are fasted DAF-16 appears to repress *lipl-3*. It is widely accepted that context affects the degree of activating or inhibitory action of a protein in a range from 0 to 1. However, we describe a scenario in which the environmental context can reverse the sign of the interaction.We define an intricate network of interactions between TFs (**Fig. 8*J***) that provide an explanation for the seemingly opposing roles of DAF-16 in the expression of *lipl-3*. DAF-16 represses the expression of *hlh-30*, a gene whose protein product can effectively transcribe from the *lipl-3* promoter in fasting conditions. On the other hand, DAF-16 promotes the activity of HSF-1, whose activity is promoted by inhibition of GLP-1 and DAF-2, activation of mTOR, and activation of MXL-3; all changes that are favored during oxidative stress. In a remarkable parallel to our work, the literature suggests a similar reversal for the DAF-16-*sodh-1* interaction. *sodh-1* had been identified as an effector positively regulated by DAF-16 in a *daf-2* mutant background (93) and in response to oxidative stress (178). However, it was recently reported that in wild type animals and during hypoxic stress, DAF-16 acts as a repressor of *sodh-1* (94). Although no study has yet addressed this seemingly reversal of function of DAF-16 on the *sodh-1* promoter, the published results suggest that diverting TF interactions may be an underappreciated strategy underlying plasticity.

Mechanistically, our work points to two interdependent strategies: 1) active repression of target promoter sequences in all inappropriate signaling contexts; and 2) inability of signal-regulated transcription factors to activate transcription in any but the appropriate contexts. For instance, if food is available, mTOR promotes MXL-3 repressive activity on the *lipl-3* promoter, an HLH-30 disfavoring action that is compounded by mTOR-mediated retention of HLH-30 in the cytoplasm. However, both HLH-30-inhibitory actions are relieved in the context of fasting. Significantly, HSF-1 is seemingly unaffected by MXL-3 presence at the *lipl-3* promoter, whereas HLH-30 is outcompeted; observations that are in line with the HSF-1 binding site being 410bp closer to the *lipl-3* transcription start site than the MXL-3 binding site, whereas MXL-3 and HLH-30 bind to the exact same site in the *lipl-3* promoter (113).

We recognize that our study is limited to only several players and pathways, and that the TF network we have created is not exhaustive and there is further complexity that would need to be addressed in future studies. For instance, it is worth noting that HLH-30 may mediate the response to oxidative stress of targets other than *lipl-3* (92), as well as HSF-1 may regulate the expression of other genes during fasting (179). Such strict control over target gene expression may underlie two extraordinary features of cell signaling: 1) the capacity of a single pathway to elicit a large variety of gene expression patterns, and hence to specify a large variety of cell responses using a reduced number of molecular players, and 2) the capacity of a signaling pathway to control the specification of multiple

distinct responses being directly dependent on its capacity to activate different, though perhaps overlapping, subsets of target genes in different contexts.

In summary, context is a critical variable in gene regulation; in particular for genes promiscuously activated or repressed across multiple stresses, or even physiological responses. Inferring the gene regulatory pathways based on studies carried out in different contexts played an essential role in creating the current body of knowledge. However, as we aim to understand more deeply the gene regulatory pathways acting in health and disease, we need to acknowledge that inferences can be misleading, and even hinder discovery.

6. Materials and methods

C. elegans culture

C. elegans strains in *SI Appendix*, Table S4.

Worms were fed *E. coli* OP50 or its RNAi-competent derivative *E. coli* XU363 (kind gift from Shawn Xu). We generated the XU363 clones for RNAi treatment by transforming the plasmids obtained from the Ahringer or Vidal RNAi libraries into XU363. Since the Ahringer RNAi clone against *daf-15* (RAPTOR) has only 20bp overlap with the *daf-15* ORF, we cloned a 600bp (+3519 to +4147) fragment of *daf-15* ORF in the L4440 plasmid. For all experiments, bacterial liquid cultures were started from streaks less than 10 days old, and incubated for 14-16h at 37˚C in LB. To culture RNAi clones, the LB media was supplemented with carbenicillin 50μg/mL. TO harvest, bacteria were concentrated 20x in S-buffer and seeded on NGM or RNAi (50 μg/ml carbenicillin and 1mM IPTG) plates. Synchronized hatchlings were seeded onto the plates the following day. *glp-1* mutants were incubated at 15°C from hatchlings and after 24h they were transferred to 25°C. *daf-1* and *daf-2* mutants were grown at 20°C from hatchlings to L3, and then transferred to 25°C. The parallel wild-type and/or empty vector controls for all experiments underwent the same thermal shifts as the corresponding *glp-1* or *daf-2*/*daf-1* mutants. Worms were harvested as young adults (adult vulva and ≤5 eggs inside the adult).

RNA isolation and qRT-PCR

RNA isolation was performed using TRI Reagent (Molecular Research Center) following manufacturer's recommendations. cDNA was prepared using M-MLV Reverse Transcriptase (Thermo Fisher) and oligodT primers (Thermo Fisher). qRT-PCR was performed using iTaq™ Universal SYBR® Green Supermix (BioRad). Primers were designed so that at least one of the two primers spanned across an intron. Primer list in *SI Appendix*, Table S5.

All expression values were calculated as ddCT (180) relative to internal control (*pmp-3* or *ama-1*) and normalized to wild-type or otherwise untreated control. The data were analyzed for statistical significance using one-tailed t-test in GraphPad Prism 7.

Fasting

C. elegans were grown on *E. coli* XU363 until they were young adults. Then, 50% of the worms were harvested, washed twice with S-buffer, and incubated rocking in S-buffer for 6h at 20°C. The other 50 % of the worms of each genotype served as the fed controls. All worms were harvested using S Buffer, and frozen in liquid nitrogen immediately.

Oxidative stress

Hatchlings were seeded on XU363 L4440, *lipl-3*, or *lipl-4* RNAi, and incubated at 20°C. For qRT-PCR analyses, L4 stage worms were treated with 5mM tBOOH (tert-Butyl hydroperoxide, ACROS Organics) and harvested 4h later. For survival tests, young adults were transferred to corresponding control or RNAi plates containing 5mM tBOOH; for this assay bacteria were UV-killed (5 cycles of 1mJ) right before adding tBOOH. The assay was carried out at 25°C for *glp-1* and *daf-2* animals and their corresponding wild-type controls, and at 20°C for all other genotypes and corresponding controls. The number of living animals was scored at the time intervals denoted in the figures. Animals were scored as dead if they did not respond to repeated prodding with a platinum wire. The assay was repeated a minimum of 3 independent times using ~50 animals per condition per trial. Survival curves were generated and analyzed using the Kaplan-Meier statistical test in SPSS.

Stress Panel

Hatchlings were seeded on XU363 L4440 and incubated at 20°C. When animals reached the young adult stage they were transferred to: 1) 25mM DTT for ER stress, 2) 200mM NaCl for salt stress, 3) 32°C for heat stress, 4) 10°C for cold stress, and 5) untreated control plates, and harvested 5h later. For anoxia treatment, young adults were transferred to an anaerobic chamber (sealed chamber containing an AnaeroPack® from Mitsubishi

Gas Chemical) and incubated for 8 hours. For all stresses, treated and control worms were harvested and immediately frozen in liquid nitrogen for later processing.

Western blotting

For western blotting of phosphorylated RSKS-1 (pRSKS-1), samples were prepared from 2,500 young-adult worms grown since L1s on NGM plates at 20°C. For tBOOH treatment, young adult animals were treated with mock (water) or 5mM tBOOH for 4 hours, harvested, and immediately frozen in liquid nitrogen. N=3 independent biological replicates. Frozen worm pellets were resuspended in Blue Protein Loading Dye (New England BioLabs #B7703S), heated at 85°C for 5 min, placed back in ice, and sonicated. Protein lysates were heated at 85°C for another 10 min, centrifuged at 15,000g for 15 min at 4°C, and loaded onto a 4–12% Bis-tris gel (Fisher #NP0322BOX). Gels were transferred to 0.2-µm nitrocellulose membranes and then blocked with Intercept® (TBS) Blocking Buffer (Li-Cor 927-60001). Membranes were incubated in the primary antibodies anti-P70S6Kinase 1:1000 (Cell Signaling Tech #9209), anti-actin 1:10,000 (Millipore Sigma #MAB1501), or anti-FLAG 1:10,000 (Millipore Sigma #F1804) overnight at 4 °C. Secondary antibody for anti-P70S6 Kinase was Rabbit HRP (Invitrogen #65-6120) (1:15,000). ECL Substrate (Bio-Rad #170-5060) treated blots were imaged using BioRad ChemiDoc and ChemiDoc MP Imaging Systems. For actin and FLAG, secondary antibody was Mouse Alexa Fluor (LiCor, CAT# 92632210) imaged using the Li-Cor Odyssey imager. (See more details on Western blotting procedure in Supplementary Note S3)

Network reconstruction

Literature search for known interactions between all genes tested in this study was done as follows: (1) The PubMed database was searched using the query terms: *C. elegans* + gene name 1 + gene name 2 (genes 1 & 2 are the genes possibly participating in the interaction of interest). (2) If we did not find experimental evidence supporting the queried interaction in *C. elegans*, we then searched for it in *Saccharomyces cerevisiae*, *Drosophila melanogaster*, mouse or human using the closest homologs of each gene. We also queried all gene pairs in STRING (https://string-db.org/). Based on the results of these searches, we built a table (*SI Appendix*, Table S1) in which we labeled each interaction by its effect on the target gene. We used the terms "Promote" (e.g. fasting → AMPK = promote) and "Inhibit" (e.g. *daf-2* -| *daf-16* = inhibit) to label the interactions. We also recorded whether the interaction was likely direct (e.g. a TF whose activity promotes the transcription of a target gene, and that has been shown through ChIP or similar to bind to the promoter of the target gene) or indirect (e.g. knockout of a membrane receptor leading to the upregulation of *lipl-3*). Indirect interactions are expected to have one or more mediators. Following the principle of parsimony, we considered every indirect effect (e.g. "Node A promotes node B", or A→B), and if a succession of direct interactions (a path in the network, e.g. A →C→B) already incorporated this indirect effect, then we noted that the indirect interaction (e.g. A→B) does not need to be included as an independent edge of the network. The technical term for this process is "binary transitive reduction with critical edges", and it was introduced

in (181). Using this logic, we created a version of the interaction table that lists the interactions composing the parsimonious network (*SI Appendix*, Table S2). Cytoscape (http://www.cytoscape.org/) was used to create a visual representation of the interactions (**Fig. 5**).

Network refinement

We evaluated each edge and node of the literature-based network (**Fig. 5**) and eliminated those that contradicted our results. We added two new nodes, representing the mRNAs *hlh-30* and *mxl-3*, as our experiments allowed us to separate transcriptional regulation from protein interactions. Based on our experiments we refined two edges that were incident on *hlh-30* and added four new edges, namely HSF-1 → *mxl-3* (**Fig. 8*C, F***), mTOR→ MXL-3 (**Fig. 8*C***), GLP-1 -| *mxl-3* (**Fig. 8*G***), and MXL-3 → HSF-1 (**Fig. 8*H***). A detailed explanation of each decision is given in *SI Appendix*, Note S2. The resulting refined parsimonious network is presented in **Fig. 8*I***. The documentation of each edge in this network is indicated in *SI Appendix*, Table S7.

Discrete dynamic model

We characterized each node of the network in **Fig. 8*I*** with three expression or activity levels: 1) a baseline level (0) observed in a wild type unperturbed (e.g. fed) *C. elegans*, 2) an above-baseline level (1), and 3) a below-baseline level (-1). Each node of the network was described by a regulatory function that summarizes how the node's activity level is

determined by the regulation of the node. We constructed the regulatory function based on evidence in the literature and the experiments performed in this study. The aggregation of all regulatory functions determines the system's long-term steady states under different conditions (such as feeding, fasting or oxidative stress). We evaluated the model by comparing its steady states with the biological knowledge regarding the nodes' documented status in each condition. We used the model to determine the context-dependent activities of nodes that were not directly addressed by prior or current experiments. The discrete dynamic model is described in detail in *SI Appendix*, Note S4.

Imaging

Wild-type or mutant worms were reared in XU363 L4440 or RNAi bacteria for two generations at 20˚C, and harvested as young/gravid adults except for *daf-15* RNAi, which leads to L4 arrest. Images of the response to tBOOH were taken after treating gravid worms with 5mM tBOOH for 4h. For all conditions, worms were paralyzed using levamisole (10mg/ml in S-buffer), transferred to agar pads, and imaged immediately. Imaging was carried out using a Nikon Eclipse Ti spinning disc confocal microscope, 40×/1.3NA objective. ImageJ software was used to count the number of tail or body-excluding-the-head nuclei. Tail was defined as the region posterior to the vulva. Head was defined as the area anterior to the posterior edge of the pharynx. At least 10 worms were scored for each treatment and biological replicate (minimum N=3). Statistical significance assessed via one-tailed unpaired parametric t-test. The mean ± SEM number of nuclei were plotted. Supplemental figures using MXL-3::GFP and DAF-16::GFP were

captured using Zeiss Axio Zoom.v16 dissecting microscope PlanNeoFluar Z x2.3/0.57 FWD objective, magnification x150. Supplementary figures using HLH-30::GFP and HSF-1::GFP were captured using Nikon Eclipse Ti microscope with 10x 0.45 NA objective.

ORO staining

Day-1 adults reared on XU363 L4440 control or *lipl-3* RNAi were exposed to 0.5mM tBOOH for 4h and then stained using the quick Oil Red O method (164). ORO signal was quantitated as previously described (163). Statistical significance assessed via two-tailed unpaired parametric t-test. The mean ± SEM were plotted.

7. Supplementary notes

a. Supplementary note 1 (SI Appendix, Note S1)

How can we identify the molecular players that link the transcriptional levels of a specific gene (e.g. *lipl-3*) to the feeding status of the animal? First, we can use existing information. For instance, fasting reduces the activity of a few nutrient sensors such as the insulin receptor DAF-2. Therefore, we can test whether genetic inactivation of this nutrient sensor (e.g. mutation of the encoding gene *daf-2*) is sufficient to promote the induction of the target gene of interest. However, although exciting, a positive result would not be sufficient to include DAF-2 in the regulatory axis that links the expression of *lipl-3* to the feeding status of the animal because DAF-2 activity levels are altered in many other contexts (e.g. infection, development, etc). So, how can we test whether DAF-2 is part of the signaling axis that links feeding status to the expression of *lipl-3*? We can combine the mutation of *daf-2* with a "probe" of the *lipl-3* response to fasting. If known, a useful "probe" would be the TF that mediates the actual response of *lipl-3* to fasting. For instance, the response of *lipl-3* to fasting depends on *hlh-30* but not on *daf-16* (**Fig. 3*A, B***). Thus, if the induction of *lipl-3* observed in *daf-2* mutant animals depends on *daf-16* but not on *hlh-30*, we can exclude *daf-2* as a significant player in the axis that links *lipl-3* expression to the feeding status of *C. elegans*. Using this rationale we searched for TF/s that control *lipl-3* and *lipl-4* induction during fasting and then tested whether the same TF/s would control the induction of *lipl-3* and *lipl-4* in animals with single inactivation of the nutrient sensors mTOR, Notch, Insulin and TGF-β receptors or single activation of AMPK.

b. Supplementary note 2 (SI Appendix, Note S2)

This note describes how the literature-based inferred network (**Fig. 5**) was refined to produce the parsimonious network model of **Fig. 8*J*.** The literature-based network is inconsistent with our experimental results showing that DAF-16, ELT-2, SKN-1, PHA-4, and DAF-3 do not mediate *lipl-3* induction during fasting (**Fig. 3*B***, *SI Appendix,* Fig. S2*A*, S3*A*), and that HLH-30 and SKN-1 do not mediate the induction of *lipl-3* in the *daf-2* and *glp-1* mutant contexts (**Fig. 3*F, G***, *SI Appendix,* Fig. S2*D, F*). Thus, we evaluated all the edges and nodes of the literature-based network and eliminated those that were contradicted by our results, as these edges and nodes seem not relevant to the contexts we are studying. In addition, we refined several edges, specifying their mechanism (e.g. transcriptional regulation) and effect (e.g. downregulation) and incorporated new edges in the network. In the following we explain each new edge.

The evidence regarding DAF-3 is sparse and contains inconsistencies. It is known that DAF-1 inhibits DAF-3, thus one would expect that loss-of-function mutation or repressed status of *daf-1* yields above-basal activation of DAF-3. Such a repressed status of DAF-1 is expected during fasting. Yet, *daf-3* loss of function does not diminish *lipl-3* upregulation during fasting, in fact it leads to further induction of *lipl-3* (*SI Appendix,* Fig. S3*A*). In addition, DAF-3 does not contribute to the induction of *lipl-3* in animals exposed to oxidative stress (**Fig. 4*C***). For these reasons, we do not include DAF-3 in the

network model. Even after removing the DAF-3 node the indirect inhibitory effect from *daf-1* to DAF-16 is preserved.

As SKN-1 does not mediate *lipl-3* induction during fasting, or in the *daf-2* or *glp*-1 mutant contexts (*SI Appendix*, Fig. S2*A*, *D, F*), we do not consider SKN-1 in the current version of the network model. As PHA-4 does not mediate *lipl-3* induction during fasting (*SI Appendix,* Fig. S2*A*) or in the *glp-1* mutant context (*SI Appendix* Fig. S2*E*), we omit it from the network. We also omit ELT-2, which does not mediate *lipl-3* induction during fasting (*SI Appendix*, Fig. S2*A*). The literature-documented interactions of ELT-2, PHA-4 and SKN-1 are mainly with each other. Their removal does not affect any interactions among other nodes of the network.

In the literature-based network the node AMPK mediates the effects of fasting on mTOR, HSF-1, and DAF-16. Yet, we found that constitutive activation of AMPK did not upregulate *lipl-3* (*SI Appendix,* Fig. S2*B*). This may be due to the fact that the successions of interactions (paths) between AMPK and *hlh-30* are incoherent (**Fig. 5**): there exist paths that are overall activating (because they contain an even number of inhibitory influences, for example AMPK-| mTOR-| hlh-30) and paths that are overall inhibitory (for example, AMPK →DAF-16 -| *hlh-30*). We omit AMPK from the network model and restore the inhibitory edges from fasting to mTOR and from *glp-1* to DAF-16 that were

previously deleted because of the existence of paths mediated by AMPK. This way, all the indirect effects from inputs/sensors to the rest of the network are preserved.

The node PQM-1 is included in the network based on the observation that PQM-1 inhibits the nuclear localization of DAF-16 and vice versa in a *daf-2* mutant background. Such mutual inhibition has two equilibria: one in which DAF-16 is expressed in the nucleus and PQM-1 is not and one in which PQM-1 is expressed in the nucleus and DAF-16 is not. As we found that loss of *daf-16* function completely abrogated the induction of *lipl-3* in *daf-2* mutant animals (**Fig. 3*H***), we infer that the first situation is relevant in our case. As PQM-1 does not have any other documented regulators, there is no evidence that the equilibrium would shift. For this reason, we omit PQM-1 from the network.

After the elimination of *daf-3* from the **Fig. 5** network the TGFß receptor DAF-1 has two incoming edges (from the input node Food and from HSF-1) and a single outgoing edge (to *daf-2*). The inhibitory edge from HSF-1 is based on the published observation that HSF-1 represses the expression of the TGFß-receptor ligand *daf-7*. However, a consequential effect of HSF-1 on *daf-7* in fasting adults is unlikely because *daf-7* is poorly expressed beyond the early larval stages, and in the adult *daf-7* expression is coordinatedly controlled by the feeding/fasting and the sex determination pathways *(182)*. Thus, we omit the feedback edge from HSF-1 to *daf-1*. After this simplification there is a linear path from the input Food to DAF-1 and then to the insulin receptor DAF-

2. This linear path suggests that the effects of *daf-1* and *daf-2* losses of function on downstream nodes are equivalent. Since our data show that *daf-1* and *daf-2* are not equivalent *lipl-3* regulatory axes (e.g. the *daf-1-daf-3* axis does not contribute to *lipl-3* response to fasting or oxidative stress, whereas the *daf-2-daf-16* axis does contribute to *lipl-3* induction during oxidative stress), we omit DAF-1 from the network model and connect the input Food directly to DAF-2. Nevertheless, we continue to consider *daf-1* loss of function results in the derivation of the dynamic model.

The literature-inferred network contains an activating interaction from DAF-16 to HSF-1 (citing evidence that a subset of DAF-16 targets requires HSF-1) and an activating interaction from HSF-1 to DAF-16 (citing evidence that extended lifespan due to HSF-1 overexpression requires *daf-16*). Both of these interactions are consistent with DAF-16 and HSF-1 co-regulating a target. Our experiments indicate that overexpression of DAF-16 was sufficient to promote induction of *lipl-3* in fed *C. elegans* and this induction was completely abrogated by RNAi against *hsf-1* (**Fig. 6*C***). This strongly supports the activating interaction from DAF-16 to HSF-1. We omit the edge from HSF-1 to DAF-16 from the *lipl-3* regulatory network.

We defined that HLH-30 and MXL-3 are regulated both at the transcriptional level and the protein level; hence, we represent them with two separate nodes. The nodes *hlh-30* and *mxl-3* represent the mRNAs and the nodes HLH-30 and MXL-3 represent the

respective proteins. The literature-inferred network contains a directionless edge between DAF-16 and HLH-30 based on evidence that these two proteins physically interact, and an activating edge from DAF-16 to HLH-30 based on paralogous evidence that in mouse adipocytes FOXO1 attaches to the promoters of TFEB and regulates its expression. Our experiments refine this evidence: loss of *daf-16* leads to increased *hlh-30* mRNA levels in both fed and fasting worms (**Fig. 6*A***). We did not find evidence of an effect from HLH-30 to DAF-16: HLH-30 overexpression or *hlh-30* loss of function mutation show wild-type transcriptional levels of *daf*-16 (*SI Appendix*, Fig. S4*A*), as well as normal abundance and subcellular localization of DAF-16::GFP (*SI Appendix*, Fig. S4*B*). Based on these results we include an inhibitory edge from DAF-16 to *hlh-30*.

The prior literature did not include any regulators of *mxl-3* or MXL-3. We found that loss of *glp-1* function promotes *mxl-3* expression (**Fig. 8*H***), thus we include an inhibitory edge from GLP-1 to *mxl-3*. We found that HSF-1 overexpression is sufficient to promote *mxl-3* induction **(Fig. 8*G***) and RNAi against *hsf-1* in fed animals led to reduced MXL-3 nuclear abundance (**Fig. 8*C***); thus we include an activating edge from HSF-1 to *mxl-3*. We also observed that tBOOH treatment increased MXL-3 abundance in the nucleus (**Fig. 8*E***). Conversely, RNAi against *daf-15* in fed animals leads to reduced MXL-3 nuclear abundance (**Fig. 8*C***), which led us to conclude that mTOR activates MXL-3 and mediates (together with HSF-1) the response of MXL-3 to oxidative stress. Conversely, loss of *mxl-3* function leads to loss of HSF-1::GFP signal (**Fig. 8*I***), suggesting an activating edge between MXL-3 and HSF-1.

The literature-based network contains an edge from HSF-1 to HLH-30, inferred from indirect evidence of heat shock promoting the expression of HLH-30-like targets (autophagy). Our experiments refine this edge: we observed ~two-fold induction of *hlh-30* in untreated and ~three-fold induction in tBOOH-treated *hsf-1* loss of function mutants (**Fig. 8*F***). This suggests an inhibitory relationship between HSF-1 and HLH-30. The interaction may be direct (indeed, there exist HSF-1 binding sites in the *hlh-30* promoter), or it may be mediated by DAF-16, which also inhibits *hlh-30*. Thus, we replace the activating edge from HSF-1 to HLH-30 with an inhibitory edge from HSF-1 to *hlh-30*.

The network model contains an inhibitory edge from fasting to GLP-1. This edge represents the decrease in GLP-1 activity due to lower agonist ligand abundance during fasting; in other words, this edge is the logical negation of the activating edge from food to GLP-1. The discrete dynamic model (described in *SI Appendix*, Note S4) is not affected by adding or not adding this edge, because in the model there is no separate "fasting" node but rather fasting is the state -1 of a "feeding status" input.

c. Supplementary note 3 (SI Appendix, Note S3)

Optimized Western blotting conditions for worm pRSKS-1

For western blotting of phosphorylated RSKS-1 (pRSKS-1) (**Fig. 8*D***), we validate the approach by comparing: 1) transgenic *C. elegans* carrying a FLAG-tagged version of RSKS-1 obtained by CRISPR knock-in of FLAG right before the RSKS-1 STOP codon (Mony V. and Hilzendeger M., unpublished) (anticipated result = ~62kDa band that overlaps with anti-FLAG signal), 2) WT worms grown on *E. coli* XU363 empty vector control, or 3) WT worms treated with RNAi against *daf-15* from the L1 stage (anticipated result = weaker band than WT). Frozen worm pellets were resuspended in Blue Protein Loading Dye (New England BioLabs B7703S), heated at 85°C for 5 min, placed back in ice, and sonicated with 5 pulses of 10s. Protein lysates were heated at 85C for another 10 min, centrifuged at 15,000g for 5 min at 4°C, and loaded onto each lane of a 4–12% Bis-tris gel (Fisher NP0322BOX). Samples were run for 3h at 150 V in MES-SDS running buffer. Gels were transferred to 0.2-μm nitrocellulose membranes using NuPage Transfer buffer (NP0006) with 20% methanol at 30 V for 90 min. The membranes were stained with Ponceau red to evaluate the quality of the SDS-PAGE and transfer, and then blocked with Intercept® (TBS) Blocking Buffer (Li-Cor 927-60001) with 0.1% Tween for 4 h. Due to the absence of antibodies specific to *C. elegans*, we tested commercial antibodies previously reported to yield a specific RSKS-1 band in worms: Cell Signaling Technology #9209 (Heintz Nature 2017) #9206, and Abcam #ab194521. However, only Cell Signaling Technology catalog #9209 yielded a discrete band of the predicted

~60kDa size (https://web.expasy.org), that was reduced in animals treated with RNAi against mTORC1 (*daf-15* RNAi), and that overlapped with the anti-FLAG signal when RSKS-1::FLAG lysates were run. Chemiluminescence and fluorescent bands were quantified after background subtraction using Image J. Levels of phosphorylated RSKS-1 (pRSKS-1) are reported as area x intensity of pRSKS-1 band normalized to corresponding actin band.

d. Supplementary note 4 (SI Appendix, Note S4)

The discrete dynamic model builds on the network model shown in **Fig. 8*J***. It characterizes each node of the network with up to three expression or activity levels. Each node of the network is described by a regulatory function that summarizes how the node's activity level is determined by the regulation of the node. We construct the regulatory function based on evidence in the literature and the experiments performed in this study. The aggregation of all regulatory functions determines the system's long-term steady states under different conditions (such as feeding, fasting or oxidative stress). We evaluate the model by comparing its steady states with the biological knowledge regarding the nodes' documented status in each condition. For reviews of discrete dynamic modeling (also called logical modeling) in systems biology, see (183) (184) (185) (186)

Definition of the expression or activity level of each node

The model contains two inputs: feeding status and oxidative stress. These two inputs have two levels: -1 (denoting the absence of this input) and 1 (denoting the presence of this input).

For visual clarity, the network in **Fig. 8*J*** separates feeding status into two different nodes: “food”, and its opposite, “fasting”. The discrete dynamic model represents these two situations as two different levels of the input “feeding status”. Thus, feeding condition corresponds to feeding status = 1, and fasting condition corresponds to feeding status = -1. When considering the states of both inputs, feeding status = 1 & oxidative stress = -1 indicates an *ad libitum* feeding condition in the absence of oxidative stress; we refer to this condition as “feeding”. The condition feeding status = 1 & oxidative stress = 1 indicates a condition of oxidative stress in which no restrictions on feeding were imposed; we refer to this as “oxidative stress”. The two remaining combinations represent fasting without oxidative stress – we refer to this condition as “fasting”–, and fasting in the presence of oxidative stress –for which we can only make predictions, as this condition was not experimentally tested.

The non-input nodes have one or multiple regulators. When representing the status of each node we use three expression/activity levels, we define the basal level as the level observed under a feeding condition; we denote this “level 0”. The level corresponding to

knockout or repressed status of the node is denoted -1, and the level with higher than basal expression or activity is denoted 1. Importantly, the activity status of the non-input nodes represent their impact on the transcription of *lipl-3*, and not necessarily other targets.

Principles of constructing the regulatory functions

The basic building block of the model is the regulatory function. Each node (except the inputs fasting and oxidative stress) has upstream regulatory functions that will define the future state of the node. We communicate the regulatory functions as tables. Each table contains as many columns as regulators the respective node has, plus one column to indicate the future state of the node. Each row in a table describes a single or a combination of regulator states, and the future state of the node under the described combination of regulator states. Each table also contains a final column whose entries describe the context or information that determines or constrains each row of the table.

Certain rows of each table are directly informed by experiments published in the literature or reported here. Some specific cases include the effect of *glp-1* mutation on *mxl-3* (edge 13, **Fig. 8*H***), the effect of mTOR inhibition (*daf-15* RNAi) on MXL-3 (edge 14, **Fig. 8*C***), on *hlh-30* (edge 15, **Fig. 8*A***) and on HLH-30 (edge 16, **Fig. 8*B***), the effect of HSF-1 on *mxl-3* (edge 23, **Fig. 8*C,G***) and on *hlh-30* (edge 24, **Fig. 8*F***), and the effect of MXL-3 on HLH-30 (edge 21, (113).

Other rows are inferences from experiments that measure an indirect effect, for example the effect of fasting on *lipl-3*. If the discovered edges or nodes are correctly integrated in the network, the derived regulatory functions need to recapitulate all indirect effects. An accurate network reconstruction is achieved by a process of trial and revision of populations of individual regulatory functions, analysis of the resulting indirect relationships in the model, comparison with the experimentally observed indirect relationship, and – if necessary – edge or node placement revision to improve the agreement. We mark the entries constrained by experimental knowledge in bold. Yet other rows of the regulatory functions are not constrained by experiments. We put a question mark next to the relevant entries for which experimental data has not been obtained here or previously, and predictions are likely to be inaccurate due to, for instance, opposing signs in the regulatory functions and hence the possible outcomes (e.g. *daf-16* mutant simultaneously challenged with fasting and oxidative stress).

In the following description, for simplicity, we will refer to the expression/activity level of each node as the state of the node. We denote the state of each node with the name of the node. We represent the future state of a node by putting an "*" next to the node name. Thus, "*lipl-3*" represents the current state of *lipl-3*, "*lipl-3**" represents the future state of *lipl-3*.

The model can be used to determine the dynamic changes in a system when starting from an initial state for each node (for example, the baseline state of fed worms), then a signal or perturbation is introduced (for example, the node "feeding status" is set to -1, meaning that feeding is stopped). The state of each node in the system is recalculated (for example nodes can be updated sequentially, or all at the same time) until a steady state is found in which no node state changes anymore. Alternatively, the model's steady states can be determined analytically; in this case, the steady state corresponds to the future or "response" state of each node (in other words, the steady states are the expected or observed outcomes of the regulatory functions). Here we use the second approach. Hence, the steady states of the model actually recapitulate the observed states under feeding, fasting, oxidative stress, or both. Each entry of the regulatory functions is evaluated by the criterion that the model's steady state corresponding to that condition/context needs to recapitulate the experimental information on that condition/context.

Explanation of the regulatory functions of receptor proteins

The Notch receptor GLP-1 is activated by food (edge 2) and inhibited by oxidative stress (edge 5). Thus, the basal level, which is denoted 0, is obtained in the presence of food and the absence of oxidative stress. Compared to this basal level, its lower activity in the absence of food (152), is categorized as -1. We mark this level in bold as it is based on experimentally obtained knowledge. Due to GLP's inhibition by oxidative stress (29), its state under oxidative stress is also -1. As our three-level model does not distinguish

between degrees of downregulation/inactivity, we assume that the combination of fasting and oxidative stress also results in the level -1 of GLP-1.

feeding status	oxidative stress	GLP-1*	Context
1	-1	0	feeding
-1	-1	-1	fasting
1	**1**	-1	oxidative stress
-1	1	-1	fasting + oxidative stress

The insulin receptor DAF-2 is activated by food (in a partly DAF-1 dependent way) and inhibited by oxidative stress (edge 4). The basal level is obtained in the presence of food and absence of oxidative stress. Fasting (lack of food) or oxidative stress result in lower-than-basal DAF-2 activity (120).

feeding status	oxidative stress	DAF-2*	Context
1	-1	0	feeding
-1	-1	-1	fasting
1	**1**	-1	oxidative stress
-1	1	-1	fasting + oxidative stress

Explanation of the regulatory functions for the nodes regulated by receptors

DAF-16 baseline level of activity is observed under feeding and in the absence of oxidative stress. DAF-16 is inhibited by DAF-2 (edge 11) and by GLP-1 (edge 12), and loss of function mutation of either *daf-2* or *glp-1* is sufficient to activate DAF-16 to level 1 despite feeding and lack of oxidant. The inhibited state of DAF-2 and GLP-1 due to fasting or to oxidative stress also leads to the activation and nuclear localization of DAF-16 (110).

DAF-2	GLP-1	DAF-16*	Context
0	0	0	feeding
-1	-1	**1**	fasting OR oxidative stress
-1	0	**1**	fed *daf-2* -/-
0	**-1**	**1**	fed *glp-1* -/-

The mTOR complex is activated by food (edge 3) and by oxidative stress (edge 6). Its basal level corresponds to the presence of food and the absence of oxidative stress. The fasting condition in the absence of oxidative stress yields the repressed state of mTOR. The simultaneous presence of food and oxidative stress leads to the activation of mTOR

(**Fig. 8*D***). There is currently no information about the status of mTOR in a fasting context combined with oxidative stress, thus the last entry has a question mark.

food	oxidative stress	mTOR*	Context
1	-1	0	feeding
-1	-1	**-1**	fasting
1	**1**	**1**	oxidative stress
-1	1	?	fasting + oxidative stress

Explanation of the regulatory functions of MXL-3 and HSF-1

The expression and activity of the MXL-3 protein depends on the expression of the *mxl-3* mRNA (edge 19), and the level of mTOR activity because mTOR activates MXL-3 (edge 14). We also uncover that there is a positive feedback loop between MXL-3 and HSF-1 (mediated by edges 23 and 20) (**Fig. 8*C, I***), which couples the long-term states of MXL-3 and HSF-1.

Therefore, a repressed level of *mxl-3* expression yields a repressed level of MXL-3 regardless of the status of mTOR. This obviously occurs in the *mxl-3* mutant, but also when *hsf-1* is knocked down, which leads to below-basal MXL-3 expression (**Fig. 8*C***). Contrarily, upon oxidative stress, HSF-1 is activated (it forms nuclear foci, **Fig. 7B**).

Hence, MXL-3 is expected to have higher than basal expression during oxidative stress, a prediction that we experimentally validate (**Fig. 8*E***).

As for mTOR, our experiments indicate that RNAi against *daf-15* in fed animals leads to reduced MXL-3 abundance in the nucleus (**Fig. 8*C***). As this shows that mTOR inhibition is sufficient to reduce MXL-3 activity, a repressed state of mTOR is expected to yield an inhibited state of MXL-3 upon other mTOR inhibitory perturbations. The fasting condition corresponds to an inhibited state of mTOR, and hence, we predict, of reduced MXL-3 activity. This prediction is validated by our previous work showing that MXL-3 is inactivated in fasted animals (1). On the other hand, higher than basal activity of mTOR is expected to promote above-basal activation of MXL-3, as we demonstrate in oxidative stressed animals (**Fig. 8*E, D***).

The combination of basal mTOR activity with increased *mxl-3* expression, as found in a context of the *glp-1* mutant, may lead to a near-basal, or possibly an above-basal activity of MXL-3.

mxl-3	mTOR	MXL-3*	Context
0	0	0	feeding
-1	0	**-1**	*mxl-3* -/- OR *hsf-1* -/-
1	0	**1**	HSF-1 OE

1	**1**	**1**	Oxidative stress
0	**-1**	**-1**	mTOR KD
-1	**-1**	**-1**	fasting
1	0	0?1?	*glp-1* -/-

The HSF-1::GFP signal is lost when animals are treated with RNAi against *mxl-3*; implying that MXL-3 activates HSF-1 (**Fig. 8*I***). The HSF-1::GFP signal is also lost in animals treated with RNAi against mTOR (**Fig. 8*I***), which is consistent with the repressed state of MXL-3 under mTOR inhibition. In the fasting context, *mxl-3 is* repressed and mTOR inhibited, implying an inhibited state for HSF-1. However, DAF-2 is also inhibited and, hence, the HSF-1 activator DAF-16, is activated. Thus, we predict that in this condition HSF-1 may have a near-basal level of activity on the *lipl-3* promoter and that activity may be *daf-16* dependent.

Under oxidative stress mTOR and MXL-3 are activated. Thus, the positive feedback loop between HSF-1 and MXL-3 sustains higher-than-basal activation of both. In addition, DAF-2 is repressed and hence DAF-16 can activate HSF-1 reinforcing the HSF-1-MXL-3 activatory loop. We predict that activated DAF-16 combined with a below-basal or basal level of DAF-2, and basal level of MXL-3 would sustain the activated state (level 1) of HSF-1; this situation would be found in the context of the *daf-2* mutant or DAF-16 overexpression.

DAF-2	DAF-16	MXL-3	HSF-1*	Context
0	0	0	**0**	feeding
0	0	**-1**	**-1**	*mxl-3* -/- OR mTOR KD
-1	**1**	**-1**	0?	fasting
-1	**1**	**1**	**1**	oxidative stress
-1	**1**	0	1	*daf-2* -/-
0	**1**	0	**1**	DAF-16 OE

The aggregate of all the evidence on MXL-3 and HSF-1 enables the refinement of certain predictions. During fasting, DAF-2 and GLP-1 are inhibited, but mTOR and *mxl-3* are too. Nevertheless, the presence of the activator DAF-16 makes it likely that HSF-1 has a near-basal level of activity. On the other hand, *daf-16* deficiency does not change the abundance or localization MXL-3 (*SI Appendix*, Fig. S5*A*, S5*B*), supporting the prediction that mutation of *daf-16* combined with basal MXL-3 would yield near-basal HSF-1 activity.

In a condition of oxidative stress DAF-2 is inhibited, and DAF-16, mTOR, and MXL-3 are at above-basal activation, and, hence, HSF-1 is expected to also be activated above-basal level.

DAF-2	GLP-1	DAF-16	mTOR	*mxl-3*	MXL-3	HSF-1*	Context
0	0	0	0	0	0	0	feeding
-1	**-1**	**1**	**-1**	**-1**	**-1**	0?	fasting
-1	-1	**1**	**1**	1?	**1**	**1**	oxidative stress
0	0	**-1**	0	**0**	**0**	**0**	*daf-16* -/-

Explanation of the regulatory functions of *hlh-30* and HLH-30

To be able to represent the transcriptional and post-translational regulation of HLH-30, we use two nodes, the *hlh-30* mRNA, and the HLH-30 protein. As with the other TFs, the denoted activity level of HLH-30 relates to its activity on the *lipl-3* promoter and disregards its potential action on other promoters.

The *hlh-30* gene is repressed by mTOR (edge 15), DAF-16 (edge 18) and HSF-1 (edge 24). Therefore, conditions that lead to activation of these inhibitors/repressors are expected to lead to a lower rate of *hlh-30* transcription and *vice versa*. During oxidative stress, all three inhibitors are activated. Hence, we predict a near basal or lower than basal

expression of *hlh-30* in this condition. By contrast, fasting leads to the activation of DAF-16 and the repression of mTOR. In this condition, we observed a 2-fold increase in *hlh-30* expression. The effect was stronger (~4-fold) when *daf-16* mutation was combined with fasting (**Fig 6*A***), which is in line with this condition corresponding to the repressed state of all three inhibitors.

mTOR	DAF-16	HSF-1	*hlh-30**	Context
0	0	0	0	feeding
1	**1**	**1**	-1?	oxidative stress
-1	**1**	0?	**1**	fasting
0	**-1**	0?	**1**	*daf-16*-/-
-1	**1**	0?	**1**	fasting & *daf-16*-/-

HLH-30 protein's role in the induction of *lipl-3* depends on its expression (discussed above), its subcellular localization, and its ability to bind to the *lipl-3* promoter. mTOR inhibits HLH-30 nuclear localization (edge 16, (27) and (**Fig. 8*B***)), and MXL-3 outcompetes HLH-30 at the *lipl-3* promoter (edge 21, (113)). Oxidative stress activates mTOR and MXL-3; thus HLH-30 is likely prevented from promoting the expression of *lipl-3* through a combination of cytoplasmic retention and outcompetition at the *lipl-3*

promoter in this condition. This prediction is consistent with our observation that tBOOH treatment preserves low nuclear localization of HLH-30 (*SI Appendix*, Fig. S5*D*). Animals treated with RNAi against *daf-15* show increased HLH-30::GFP nuclear localization, reduced MXL-3 abundance (**Fig. 8*C***), and induction of *lipl-3* (**Fig. 3*C, D***) . If we generalize these regulatory functions, we can predict that HLH-30 will have a higher than basal activity (level 1) in any condition with near-basal or above-basal *hlh-30* expression and repressed or near-basal mTOR and/or MXL-3 activity. In this study, we present support for this prediction in several contexts including fasting, mutation of *daf-3, daf-16,* and *hsf-1*. In previous studies, we presented results validating this prediction in the context of *mxl-3* mutation (1), and Lapierre *et al* in animals overexpressing *hlh-30* (27).

The model also predicts that *glp-1* or *daf-2* mutation yield near-basal HLH-30 activity, which is indeed what we observed (*SI Appendix*, Fig. S5*C*).

hlh-30	mTOR	MXL-3	HLH-30*	Context
0	0	0	0	feeding
-1	0	0	**-1**	*hlh-30* -/-
1	**-1**	**-1**	**1**	mTOR KD
0?	**1**	**1**	0?	Oxidative stress

0	0	0/1?	0?	*glp-1*-/- OR *daf-2*-/-
1	**-1**	**-1**	**1**	fasting
1	0	0	1	*daf-16* -/-

Putting it all together: explanation of the regulatory functions acting on the *lipl-3* promoter

The contexts in which we experimentally observed *lipl-3* upregulation can be used to evaluate the model and reduce uncertainty. Here we list the contexts in which the model recapitulates the observations:

1. *lipl-3* upregulation under fasting (**Fig. 2*A***)
2. *hlh-30* mutation suppresses above induction (**Fig. 3*A*** and **Fig. 6*B***)
3. *daf-16* loss of function does not diminish the fasting-induced upregulation of *lipl-3* (**Fig. 3*B*** and **Fig. 6*B***)
4. *lipl-3* is induced in *daf-2* mutant animals (**Fig. 3*F***)
5. mutation of *hlh-30* does not suppress above induction (**Fig. 3*F***)
6. *lipl-3* is induced in *glp-1* mutant animals (**Fig. 3*G***)
7. mutation of *hlh-30* does not suppress above induction (**Fig. 3*G***)
8. *hsf-1* and *daf-16* are responsible for the induction of *lipl-3* in the *daf-2* and *glp-1* loss of function mutants (**Fig. 3*H, I*** and **Fig. 6*G, H***). However, loss of *daf-16* function only partially suppresses the induction observed in *glp-1* worms **Fig. 3*I***,

endorsing a future search for additional transcriptional regulators of *lipl-3* in this mutant.

9. DAF-16 overexpression promotes *lipl-3* induction through *hsf-1* (**Fig. 6*C***)
10. HSF-1 overexpression is sufficient to promote *lipl-3* induction (**Fig. 7*C***)
11. *lipl-3* is induced by mTOR inhibition (*let-363* RNAi in **Fig. 3*C***) or disruption of the mTORC1 complex (*daf-15* RNAi in **Fig. 3*D***)
12. mutation of *hlh-30* does suppress above induction (**Fig. 3*D***)
13. *lipl-3* is induced in *daf-16* mutant worms (**Fig. 6*B***)
14. mutation of *hlh-30* does suppress above induction (**Fig. 6*B***). It is interesting to highlight that both the above-basal activity of DAF-16 and its loss of function induces *lipl-3* upregulation.
15. *lipl-3* is induced by oxidative stress (tBOOH treatment, **Fig. 4*A***)
16. mutation of *hsf-1* (**Fig. 7*A***) and *daf-16* (**Fig. 4*C***) suppress above induction

Therefore, without differentiating between degrees of upregulation, the evidence supports the assumption that higher-than-basal activity of either HSF or HLH-30 is sufficient to upregulate the transcription of *lipl-3*. In the tables below we use a red font to indicate the regulator (HLH-30 or HSF-1) responsible for the upregulation of *lipl-3* in each context. All the conditions lead to the activation of at most one of the two regulators.

HSF-1	HLH-30	*lipl-3**	Context
0	0	0	feeding
0	**-1**	**0**	*hlh-30 -/-*
0?	**1**	**1**	fasting
0?	**-1**	**0**	fasting + *hlh-30 -/-*
1	0?	**1**	*daf-2-/-* OR *glp-1-/-* OR DAF-16 OE OR HSF-1 OE
1	**-1**	**1**	*daf-2 -/-*; *hlh-30 -/-* OR *glp-1 -/-*; *hlh-30 -/-*
-1	-1?0?	**0**	*daf-2-/-;hsf-1-/-* OR *glp-1-/-;hsf-1-/-* OR DAF-16 OE; *hsf-1 -/-*
0	0?	**0**	*daf-2 -/-;daf-16 -/-* OR *glp-1 -/-;daf-16 -/-*
0/-1?	**1**	**1**	mTOR KD
0/-1?	**-1**	**0**	mTOR KD; *hlh-30 -/-*
0	**1**	**1**	*daf-16 -/-*
0	**-1**	**0**	*daf-16 -/-;hlh-30 -/-*
1	0?	**1**	oxidative stress
-1	0?	**0**	oxidative stress + *hsf-1 -/-*
0?	0?	**0**	oxidative stress + *daf-16 -/-*

Contextualized transcriptional control of *lipl-3*

The two contexts, fasting and oxidative stress, upregulate *lipl-3* transcription through a shared network that contains two diverging and then converging pathways. Our experiments directly identified nodes that have increased activity (compared to the basal level) under oxidative stress: HSF-1 forms nuclear foci (**Fig. 7*B***), MXL-3 has increased nuclear abundance (**Fig. 8*E***), mTOR has increased activity (**Fig. 8*D***). These nodes are marked by the same color (pink) as the node corresponding to oxidative stress. Our experiments also indicated that *lipl-3* is upregulated in both contexts (**Fig. 6*B*, Fig. 7*A***); thus we mark *lipl-3* with both colors in **Fig. 8*J*** (pink for oxidative stress and green for fasting). The discrete dynamic model allows the identification of the state of all nodes in the network under both conditions, completing the picture. The model indicates that HLH-30 is activated by fasting; it is colored in green in **Fig. 8*J***. The model also indicates the DAF-2 and GLP-1 are repressed in both fasting and oxidative stress contexts; hence, they are colored grey in **Fig. 8*J***. According to the model DAF-16 is activated above its basal level in both contexts; this is why it is painted both green and pink.

During fasting mTOR and MXL-3 are repressed, allowing HLH-30 to activate above its basal level. Conversely, under oxidative stress mTOR, MXL-3, DAF-16, and HSF-1 are activated above their basal levels and HLH-30 is repressed. The two pathways converge on *lipl-3*, as both HLH-30 and HSF-1 can upregulate *lipl-3* transcription.

Due to the inhibition of *hlh-30* and HLH-30 by the nodes activated by oxidative stress, these nodes have dual (incoherent) effects on *lipl-3*. By activating HSF-1, they mediate *lipl-3* upregulation. By inhibiting HLH-30, they inhibit *lipl-3* upregulation. Several of these nodes are active under oxidative stress and inactive under fasting, thus their dual effect is not simultaneously manifested. However, DAF-16 is active under both contexts, making its dual effect easier to discern.

8. Supplementary tables

a. Supplementary Table 1 (SI Appendix, Table S1)

input	target	Interaction[1]	Type[2]	Experimental or Inferred[3]	Can it be deleted?*	evidence	species	References
Food	lipl-3	I	I	E	Y, Food->Feeding->daf-1-|AMPK-|mTOR-|HLH-30->lipl-3	Transcr. activation upon fasting	*C. elegans*	https://www.ncbi.nlm.nih.gov/pubmed/23604316
Food	AMPK	I	I	E	Y, Food->Feeding->daf-1-|AMPK	Inhibitory postranslational modification in ad libitum		https://www.ncbi.nlm.nih.gov/pmc/articles/PMC4973318/
Food	mTOR	P	I	E	Y, Food->Feeding->daf-1-|AMPK-|mTOR	Activating postranslational modification in ad libitum	MEF	https://www.nature.com/articles/ncb2152
Food	mTOR	P	I	E		Amino Acids Regulate the Phosphorylation and Activation of p70 S6 Kinase and eIF-4E-BPs "Withdrawal of amino acids from the nutrient medium of CHO-IR cells results in a rapid deactivation of p70 S6 kinase and dephosphorylation of eIF-4E BP1,"	CHO-IR	https://www.jbc.org/content/273/23/14484.long

Food	mTOR	P	I	E		amino acids activate mTOR through Rag proteins " amino acid stimulation of cells increased the GTP loading of RagB (Fig. 3E). "In cells with a reduction in the expression ofall the Rag proteins, leucine- stimulated phosphorylation ofS6K1 was strongly reduced "	human embryonic kidney (HEK)-293T cells	https://science.sciencemag.org/content/320/5882/1496?casa_token=tCpO9sHN1XEAAAAA:oG89sJTC8rnaKmRPdo388slO0FGqG-jZqooRvMZ8f4xRmcu3_6BXvrkw2ygbKS4xY6yNmTlwB91cjg
Food	mTOR	P	I	E		Rag proteins are mTOR pathway activators, in response to amino acids Knockdown of dRagA or dRagC markedly decreased dS6K phosphorylation in response to amino acid stimulation. also "expression of dominant-negative RagAT21N and RagBT54N decreased S6K phosphorylation" "Transfection with as little as 20 ng of RagAQ66L [constitutively active] DNA markedly increased S6K phosphorylation in the absence of amino acids"	HEK293 cells	https://www.nature.com/articles/ncb1753?proof

Food	mTOR	P	I	E		ATPase is necessary for amino acid sensing by mTOR on lysosomal surface: RNAi against V-ATPase supresses S6K phosphorylation; inhibition of V-ATPase results in failure of mTOR clustering to lysosomal surface in response to amino acids; "Semi-quantitative mass spectrometric analyses ofanti-FLAG immunoprecipitates prepared from 293Tcells expressing FLAG-tagged Ragulator components (p18 or p14) or RagB revealed the presence of many subunits of the v-ATPase"	293Tcells	https://www.ncbi.nlm.nih.gov/pmc/articles/PMC3211112/
Food	DAF-12	P	I	E	Y, Food->Feeding->daf-1-|AMPK->DAF-16-|DAF-12	Food replete conditions causes ligand-bound DAF-12 which promotes reproductive development	*C. elegans*	https://dev.biologists.org/content/137/20/3501#F7
Food	DAF-16	I	I	E	Y, Food->Feeding->daf-1-|AMPK->DAF-16	Nuclear exclusion in ad libitum	*C. elegans*	https://www.ncbi.nlm.nih.gov/pubmed/11747825
Food	DAF-3	I	I	E	Y, Food->Feeding->daf-1-|DAF-3	DAF-3 antagonises daf-7 and daf-1 which is activated by food	*C. elegans*	https://www.ncbi.nlm.nih.gov/pmc/articles/PMC316611/
Food	HLH-30	I	I	E	Y, Food->Feeding->daf-1-|AMPK-|mTOR-|HLH-30	Nuclear exclusion in ad libitum	*C. elegans*	https://www.ncbi.nlm.nih.gov/pubmed/23604316
Food	NHR-49	I	I	E	Y, Food->Feeding->daf-1-|AMPK->NHR49	Transcriptional targets repressed in ad libitum	*C. elegans*	https://www.ncbi.nlm.nih.gov/pubmed/16157872

Food	SKN-1	I	I	E	Y, Food->Feeding->daf-1-|AMPK->DAF-16->SKN-1	Nuclear exclusion in ad libitum	*C. elegans*	https://www.ncbi.nlm.nih.gov/pubmed/17538612
Food	daf-1	P	I	E		Both shows the ligand daf-7 mediating food signals. DAF-1 is their receptor	*C. elegans*	https://www.ncbi.nlm.nih.gov/pubmed/8910282
Food	daf-1	P	I	E			*C. elegans*	https://www.ncbi.nlm.nih.gov/pubmed/8893028
Food	daf-1	P	I	E		Expression of *daf-1::gfp* fully rescued the adult feeding rate, fat storage, egg retention etc of daf-1 mutants	*C. elegans*	https://www.ncbi.nlm.nih.gov/pmc/articles/PMC2556218/
Food	daf-2	P	I	E		DAF-2 appears to couple nutritional status to the activation of oocyte generation.	*C. elegans*	https://www.ncbi.nlm.nih.gov/pmc/articles/PMC3829605/
Food	glp-1	P	I	E		When animal doesn't have sufficient U/T levels, it prevents it from germline proliferation, glp-1 hyperactivation promotes meiosis in germline, despite the insufficient U/T levels	*C. elegans*	https://www.ncbi.nlm.nih.gov/pmc/articles/PMC4743060/
Fasting	lipl-3	P	I	E	Y, Fasting->AMPK-|mTOR-|HLH-30->lipl-3	Transcr. activation upon fasting	*C. elegans*	https://www.ncbi.nlm.nih.gov/pubmed/23604316
Fasting	AMPK	P	D	E		AMPK required for lifespan extension via DR	*C. elegans*	http://genesdev.cshlp.org/content/18/24/3004.full

Fasting	AMPK	P	D	E		High glucose reduced phopshorylated aak-2 - catalytic subunit of AMPK	C. elegans	https://journals.plos.org/plosone/article?id=10.1371/journal.pone.0148089
Fasting	mTOR	I	I	E	Y, Fasting->AMPK-|mTOR	Intermittent Fasting induced longevity depends on mTOR/let-363	*C. elegans*	https://www.ncbi.nlm.nih.gov/pubmed/19079239
Fasting	CRH-1	P	I	E	Y, sink node	cre::gfp-mediated induction of GFP by starvation, not found in crh-1 (tz2) mutant	*C. elegans*	https://www.ncbi.nlm.nih.gov/pubmed/17021164
Fasting	CRH-1	I	I	E	Y, sink node	crh-1 expression as well as phosphorylated CREB activity is less in eat-2 compared to WT.This is based on eat-2, which is CR not fasting	*C. elegans*	https://www.ncbi.nlm.nih.gov/pmc/articles/PMC2872642/
Fasting	DAF-12	P	I	E	Y, Fasting->AMPK-|mTOR-|HLH-30-|daf-2-|DAF-12, Fasting is sufficient for DAF-12	daf-12 mutant (rh611rh411) rescues the stress resistance-phenotype of starved worms	*C. elegans*	https://www.ncbi.nlm.nih.gov/pmc/articles/PMC5322524/
Fasting	DAF-13	P	I	E	Y, source node	Unliganded daf-12 during starvation causes increases Octopamine biosynthetic gene	*C. elegans*	https://www.ncbi.nlm.nih.gov/pmc/articles/PMC4928904/
Fasting	DAF-16	P	I	E	Y, Fasting->AMPK->DAF-16	Nuclear localization upon fasting	*C. elegans*	https://www.ncbi.nlm.nih.gov/pubmed/11747825
Fasting	DAF-3	P	I	E	Y, no evidence	DAF-3 antagonized daf-1 role in feeding rate, fat storage	*C. elegans*	https://www.ncbi.nlm.nih.gov/pmc/articles/PMC2556218/

Fasting	HLH-30	P	I	E	Y, Fasting->AMPK-|mTOR-|HLH-30	Nuclear localization upon fasting	*C. elegans*	https://www.ncbi.nlm.nih.gov/pubmed/23604316
Fasting	HSF-1	P	I	E	Y, Fasting->AMPK->HSF-1, Fasting is sufficient for HSF-1 activation	hsf-1 RNAi suppressed the longevity due to bacteria dilution based dietary restriction, also bDR induced hsf-1 and daf-16 expression	*C. elegans*	https://www.ncbi.nlm.nih.gov/pubmed/19924292
Fasting	NHR-49	P	I	E	Y, Fasting->AMPK->DAF-16-> NHR-49, Fasting is sufficient for NHR-49	Transcriptional targets activated upon fasting	*C. elegans*	https://www.ncbi.nlm.nih.gov/pubmed/16157872
Fasting	PHA-4	P	I	E	Y, Fasting->AMPK-|mTOR-|PHA-4, Fasting is sufficient for PHA-4	pha-4 ts alleles unable to extend lifespan upon bacterial dilution based DR and in eat-2 mutants, pha-4 mRNA levels were increased in eat-2(ad1116) worms compared with wild-type worms	*C. elegans*	https://www.ncbi.nlm.nih.gov/pubmed/17476212
Fasting	PHA-4	P	I	E	Fasting->AMPK-|mTOR-|PHA-4, Fasting is sufficient for PHA-4	Loss of pha-4 reduces L1 starvation survival and its overexpression increases L1 starvation survival	*C. elegans*	https://www.ncbi.nlm.nih.gov/pubmed/20174564
Fasting	SKN-1	P	I	E	Y, Fasting->AMPK->DAF-16->SKN-1	Nuclear localization upon calorie restriction	*C. elegans*	https://www.ncbi.nlm.nih.gov/pubmed/17538612
Fasting	daf-2	I	I	E		daf-2 protein levels reduced after starvation	*C. elegans*	https://www.ncbi.nlm.nih.gov/pubmed/22123849
DAF-12	DAF-16	P	I	E	Y, DAF-12->DAF-3->DAF-16, this effect has no influence on lifespan	DAF-12 is required for DAF-16::GFP to translocate to nucleus when worms are grown on lophenol	*C. elegans*	http://journals.plos.org/plosbiology/article?id=10.1371/journal.pbio.0020280

DAF-12	DAF-16	P	I	E	Y, DAF-12 is effectively a source node	DAF-12 promotes DAF-16 translocation to the nucleus and larval arrest upon cholesterol starvation	*C. elegans*	https://pubmed.ncbi.nlm.nih.gov/20549717/
DAF-12	DAF-3	P	D	E	Y, DAF-12 is effectively a source node	CHip enrichment of DAF-12 on daf-3 promoter. Promoter region shows agonist dependent activation	*C. elegans*	https://www.ncbi.nlm.nih.gov/pmc/articles/PMC3140985/
DAF-12	NHR-80	P	I	E	Y, NHR-80 is effectively a sink node	daf-12 mutation partially supessses nhr-80 mRNA levels in glp-1 mutant; glp-1; daf-12 lifespan is not further extended by NHR-80 OE	*C. elegans*	http://journals.plos.org/plosbiology/article?id=10.1371/journal.pbio.1000599
DAF-12	SKN-1	I	I	E	Y, DAF-12 is effectively a source node	daf-12 RNAi increases expression and nuclear localisation of SKN-1:::GFP	*C. elegans*	http://journals.plos.org/plospathogens/article?id=10.1371/journal.ppat.1003545
DAF-12	daf-2	I	I	E	Y, DAF-12 is effectively a source node	daf-2 and daf-12 having mutaually antagoinistic effects	*C. elegans*	https://www.ncbi.nlm.nih.gov/pubmed/7789761
CEP-1	DAF-16	I	I	E	Y, sink node	RNAi or genetic knockout of the cep-1 leads to increased life span, which is dependent upon functional daf-16	*C. elegans*	https://www.ncbi.nlm.nih.gov/pubmed/17895432
DAF-16	lipl-3	P	I	E	Y, DAF-16->HSF-1->HLH-30->lipl-3	DAF-16A and DAF-16F may promote expression of lipl-3. However, done via RNA seq and reads also overlap with srw-107. Further, RNAseq results not confirmed via qRTPCR.	*C. elegans*	https://www.ncbi.nlm.nih.gov/pmc/articles/PMC4596673/

DAF-16	CRH-1	P	I	E	Y, sink node	daf-16 mutation decreases the expression of crh-1	*C. elegans*	http://journals.plos.org/plosbiology/article?id=10.1371/journal.pbio.1000372
DAF-16	HSF-1	P	I	E		subset of DAF-16 targets requires HSF-1 for expression	*C. elegans*	http://science.sciencemag.org/content/300/5622/1142.full
DAF-16	NHR-49	P	D	E	Y, NHR-49 is effectively a sink node	NHR-49 is upregulated by the activity of DAF-16	*C. elegans*	https://www.ncbi.nlm.nih.gov/pubmed/27073739
DAF-16	NHR-49	P	D	E	Y, NHR-49 is effectively a sink node	nhr-49 mRNA as well as protein levels are under the control of DAF-16 in glp-1 mutants (this paper is D evidence- better than the above paper)	*C. elegans*	https://journals.plos.org/plosgenetics/article?id=10.1371/journal.pgen.1004829
DAF-16	NHR-80	P	I	E	Y, NHR-80 is effectively a sink node	DAF-16 may modulate NHR-80 mRNA levels	*C. elegans*	https://www.ncbi.nlm.nih.gov/pubmed/21423649
DAF-16	SKN-1	P	D	E		Comparing daf-2 and daf-16; daf-2 adults using chromatin immunoprecipitation (ChIP) and PCR for skn-1 . skn-1 mutant (zu135) suppressed daf-16(oe) oxidative stress resistance. skn-1 mRNA level is increased by daf-16(oe) (zIs356)	*C. elegans*	https://www.ncbi.nlm.nih.gov/pmc/articles/PMC5595692/
DAF-16	SKN-1	P	D	E		Chip-PCR D binding on DAF-16 to skn-1 promoter. Increased skn-1 mRNA in DAF-16OE and skn-1 required for DAF-16OE OX stress resistance	*C. elegans*	https://www.ncbi.nlm.nih.gov/pubmed/28612944

DAF-3	DAF-16	P	I	E		daf-3 RNAi and daf-3 mutants caused DAF-16::GFP to be excluded from nuclei	*C. elegans*	http://www.scienceD.com/science/article/pii/S0960982207019148
DAF-16	PQM-1	Is	I	E		In daf-2 mutant background, pqm-1 inhibits nuclear localization of daf-16 and vice versa.	*C. elegans*	https://www.scienceD.com/science/article/pii/S0092867413008404?via%3Dihub#bib17
ELT-2	DAF-16	P	I	E		elt-2 RNAi treatment reduced expression of endogenous daf-16 d/f and also reduced Pdaf-16d/f::gfp expression	*C. elegans*	https://www.ncbi.nlm.nih.gov/pmc/articles/PMC4022319/
ELT-2	DAF-16	P				ELT-2 promote longevity by regulating daf-16 gene expression	*C. elegans*	https://www.ncbi.nlm.nih.gov/pmc/articles/PMC4022319/
ELT-2	NHR-49	P	I	E	Y, ELT-2 -> DAF-16 -> NHR-49	There is one TGATAA site (strong ELT-2 binding site) in the large first intron of nhr-49	*C. elegans*	http://www.scienceD.com/science/article/pii/S0012160608013560#fig6
ELT-2	NHR-80	P	I	E	Y, ELT-2 -> DAF-16 -> NHR-80	There is TGATAA site (strong ELT-2 binding site) in the promoter of nhr-80	*C. elegans*	http://www.scienceD.com/science/article/pii/S0012160608013560#fig6
ELT-2	PHA-4	P	D	E		EMSA of pha-4 gut acting promoter region with ELT-2 protein	*C. elegans*	https://www.ncbi.nlm.nih.gov/pubmed/9584117

HLH-30	lipl-3	P	D	E		Expression of lipl-3 on Fasting depends on hlh-30	*C. elegans*	https://www.ncbi.nlm.nih.gov/pmc/articles/PMC3723461/
DAF-16	HLH-30	Int	D	E		DAF-16 and HLH-30 physically interact	*C. elegans*	https://www.nature.com/articles/s41467-018-06624-0#MOESM1
HSF-1	DAF-16	P	I	E		HSF-1 OE extended lifespan requiresdaf-16	*C. elegans*	http://science.sciencemag.org/content/300/5622/1142.full
HSF-1	HLH-30	P		I		Heat shock leads to activation of HLH-30 and also induction of hlh-30-dependent autophagy genes	*C. elegans*	https://www.nature.com/articles/ncomms14337
HSF-1	ELT-2	P	I	E		HSF-1 OE has increased expression of elt-2 mRNA	*C. elegans*	http://journals.plos.org/plosgenetics/article?id=10.1371/journal.pgen.1005956#pgen-1005956-t001
HSF-1	SKN-1	P	I	I	Y, no evidence	hsf-1 mutant (sy441) recovery reduced in heat stress. skn-1 RNAi helps to rescue this, whereas wdr-23 RNAi that enhance skn-1 activation further reduced recovery.	*C. elegans*	https://www.ncbi.nlm.nih.gov/pubmed/27207646
HSF-1	daf-1	I	I	I		HSF-1 represses daf-7 expression	*C. elegans*	https://www.ncbi.nlm.nih.gov/pmc/articles/PMC3558376/

NHR-49	DAF-16	P	I	E	Y, no evidence for this Dion (only for the opposite)	nhr-49 mRNA expression depends on DAF-16 in glp-1 mutation. NHR-49::GFP nuclear translocation depends on DAF-16. NHR-49OE longevity depends on daf-16	*C. elegans*	https://www.ncbi.nlm.nih.gov/pmc/articles/PMC4256272/
NHR-49	NHR-80	Int	D	E	Y, NHR- 49 and NHR-80 are sink nodes	Pull down assay	*C. elegans*	https://www.ncbi.nlm.nih.gov/pubmed/22511885
NHR-49	HLH-30	P			Y, this evidence points to convergent effects not interaction/regulation		*C. elegans*	https://www.jimmunol.org/content/202/1_Supplement/64.6
NHR-80	DAF-12	P	I	E	Y, no evidence in the paper, "DAF-12 and NHR-80 function in concert to promote longevity"	NHR-80 does not required DAF-12 to promote longevity	*C. elegans*	https://www.ncbi.nlm.nih.gov/pubmed/21423649
NHR-80	NHR-49	Int	D	E	Y, NHR- 49 and NHR-80 are sink nodes	Pull down assay	*C. elegans*	https://www.ncbi.nlm.nih.gov/pubmed/22511885
PHA-4	DAF-16	Int	D	E	Y, contradicted by ineffectiveness of PHA4 OE in DAF-16 mutant; opposite Dion contradicted by by dispensability of PHA-4 for HSF-1 mediated lifespan extension	Yeast 2 hybrid	*C. elegans*	https://www.ncbi.nlm.nih.gov/pubmed/23791784

PHA-4	ELT-2	Int	D	E	Y, consistent with evidence for other Dion	Overlay assay. Pha-4 antibody detected ELT-2::GST	*C. elegans*	https://www.ncbi.nlm.nih.gov/pubmed/18448117
PHA-4	NHR-49	Int	D	E	Y, NHR- 49 is a sink node	Yeast 2 hybrid	*C. elegans*	https://www.ncbi.nlm.nih.gov/pubmed/23791784
PHA-4	SKN-1	P	D	E		Pha-4 could activate skn-1 as per modENCODE paper	*C. elegans*	https://www.ncbi.nlm.nih.gov/pmc/articles/PMC3032928/
SKN-1	DAF-12	I	I	E	Y, weak (no) evidence	skn-1 RNAi suppressed the enhanced pathogenic resistance of the daf-12(sa156) mutant	*C. elegans*	https://www.ncbi.nlm.nih.gov/pubmed/23990780
SKN-1	DAF-16	P	I	E	Y, SKN-1-> ELT-2->DAF-16	daf-16 RNAi significantly reduced the life span of skn-1(zu67) worms, but skn-1 RNAi treatment failed to reduce the life span of daf-16(mgDf50) worms	*C. elegans*	https://www.ncbi.nlm.nih.gov/pubmed/20624915
SKN-1	ELT-2	P	I	E		ELT-2 is downstream of SKN-1 in intestinal differentiation	*C. elegans*	https://www.ncbi.nlm.nih.gov/pmc/articles/PMC2836165/#SD1
MXL-3	lipl-3	Is	D	E	Y, the mechanism of this inhibition is MXL-3 outcompeting HLH-30	Inactivation of the MXL-3 enabled lipl-1P::GFP expression under well-fed conditions.Gene expression analyses of two mxl-3 null mutants, confirmed that MXL-3 represses lipl-1, 2, 3, 5, MXL-3 binds in yeast 1 hybrid to CACGTG (ref. 12), and this target motif is present within 500 base pairs (bp) of the transcriptional start sites of lipl-1, 2, 3, 5, MXL-3 binds to lipl-3 promoter in vivo.	*C. elegans*	https://www.nature.com/articles/ncb2741

MXL-3	HLH-30	o	D	E		MXL-3 outcompetes HLH-30/TFEB for binding to lipl-3 promoter; analysis by ChIP shows that HLH-30 is rarely associated with the promoters ofthe lipase genes in well-fed animals (Fig. 4fand SI_ChromatinIP), even when the hlh-30 gene is expressed from a high copy number array at higher levels than those observed in fasting animals; HLH-30 and MXL-3 share the same binding motif	*C. elegans*	https://www.nature.com/articles/ncb2741
PQM-1	DAF-16	Is	I	E			*C. elegans*	https://www.scienceD.com/science/article/pii/S0092867413008404?via%3Dihub#bib17
daf-2	AMPK	I	I	E		aak-2 RNAi suppresses daf-2 longevity	*C. elegans*	https://www.ncbi.nlm.nih.gov/pubmed/16626391
daf-2	AMPK	I				aak-2 RNAi suppresses daf-2 (e1368) longevity and dauer formation	*C. elegans*	https://www.ncbi.nlm.nih.gov/pubmed/15574588
daf-2	AMPK	I				daf-2 longevity partially suppressed by aakg-4 RNAi (atypical gamma isoform of AMPK)	*C. elegans*	http://journals.plos.org/plosgenetics/article?id=10.1371/journal.pgen.1004109
daf-2	AMPK	I				aak-2 mutations (rr48 and ok524) shorten daf-2 mutant longevity (e1370)	*C. elegans*	https://www.ncbi.nlm.nih.gov/pubmed/16407400

daf-2	AMPK	I				AMPK components - RNAi (aak-2, aakb-1, aakb-2, aakg-1) suppress long term anoxia viability of daf-2 (e1370) mutants	*C. elegans*	https://pubmed.ncbi.nlm.nih.gov/21304820/
daf-2	CRH-1	I	I	E	Y, sink node	crh-1 expression and phosphorylated CREB is more in daf-2 mutants (e1370)	*C. elegans*	https://www.ncbi.nlm.nih.gov/pmc/articles/PMC2872642/
daf-2	DAF-16	I	D	E		DAF-2 prevents DAF-16 translocation to nuclei	*C. elegans*	https://www.nature.com/ng/journal/v28/n2/full/ng0601_139.html
daf-2	DAF-16	I				DAF-16 mutation suppress daf-2 mutant phenotypes like dauer arrest, lifespan extension, reduced fertility and variability defects	*C. elegans*	https://www.ncbi.nlm.nih.gov/pubmed/9504918
daf-2	HLH-30	I	I	E	Y, daf-2 -| HSF1-> HLH-30	HLH-30 is required for the lifespan extension of daf-2 mutant	*C. elegans*	https://www.ncbi.nlm.nih.gov/pmc/articles/PMC3866206/
daf-2	HSF-1	I	I	E	N, mechanism is known, mediated by DDL proteins	nuclear localization after heat shock, more HSF-1 accumulates in nuclei of animals with reduced DAF-2 signalling after heat shock	*C. elegans*	http://www.scienceD.com/science/article/pii/S0092867411015728
daf-2	HSF-1	Is	I	E		hsf-1 RNAi prevents the daf-2(e1370) mutation from extending life-span	*C. elegans*	https://science.sciencemag.org/content/300/5622/1142.long

daf-2	SKN-1	I	D	E		Nucler accumulation of SKN-1::GFP in the intestinal nuclei when DAF-2 signaling reduced. skn-1 mutant (zu67) reduces oxidative stress resistance of daf-2 mutant (e1370). Also skn-1 RNAi recuses longevity of daf-2 mutant (e1368)	*C. elegans*	https://www.ncbi.nlm.nih.gov/pubmed/18358814
daf-1	AMPK	I	I	E	Y. daf-1-> daf-2-| AMPK	germline development arrest in daf-7(e1372) mutants depends on aak-2	*C. elegans*	https://www.ncbi.nlm.nih.gov/pubmed/16407400
daf-1	DAF-12	I	I	E	Y, daf-1->daf-2 -| DAF-12	daf-1 dauer phenotype suppressed by daf-12	*C. elegans*	https://www.ncbi.nlm.nih.gov/pubmed/8375650
daf-1	DAF-16	I	I	E	Y, daf-1-|AMPK->DAF-16	daf-7 mutant longevity rescued by mutation of daf-16. Daf-16::GFP is nuclear in daf-7	*C. elegans*	https://www.ncbi.nlm.nih.gov/pmc/articles/PMC3124252/
daf-1	DAF-3	I	I	E		DAF-3 is required for increased fat deposits in daf-1 mutant	*C. elegans*	https://www.ncbi.nlm.nih.gov/pubmed/18680713
daf-1	DAF-3	I				daf-3 mutation supresses the dauer constitutive mutation of daf-1	*C. elegans*	https://www.ncbi.nlm.nih.gov/pubmed/11063683
daf-1	DAF-3	I				daf-1 mutant (m40) suppresses DR longevity but rescued by daf-3 mutant (e1376)	*C. elegans*	https://www.ncbi.nlm.nih.gov/pubmed/28107363
daf-1	HSF-1	I	I	E	Y, daf-1 -> daf-2 -| HSF-1	HSF-1 also acts downstream of DAF-7/TGF-β to regulate aging and development (same paper as entry 74/51)	*C. elegans*	https://www.ncbi.nlm.nih.gov/pmc/articles/PMC3558376/

daf-1	daf-2	P	I	E		Dauer formation of TGFB pathway mutants is suppressed by daf-2/age-1 pathway mutant in a suppressor screen	*C. elegans*	http://www.genetics.org/content/156/3/1035.long
daf-1	daf-2	P				In mutants of TGF beta genes, daf-2 and insulin genes are down regulated	*C. elegans*	https://www.ncbi.nlm.nih.gov/pubmed/15380030
daf-1	glp-1	I	I	I	Y, it is an effect on the ligand	TGFbeta activation causes expression of lag-2 which is the ligand for glp-1 receptor	*C. elegans*	https://www.ncbi.nlm.nih.gov/pubmed/28811311
glp-1	lipl-3	I	I	E	Y, glp-1-|HLH-30->lipl-3	glp-1 mutant (bn18) upregulates lipl-3. lipl-3 RNAi reduced glp-1 stress resistance to Sodium arsenite	*C. elegans*	https://www.ncbi.nlm.nih.gov/pubmed/26196144
glp-1	AMPK	I	I	E		AMPK component- RNAi (aak-2, aakb-1, aakb-2, aakg-1) suppress long term anoxia viability of glp-1 (e2141) mutants	*C. elegans*	https://journals.plos.org/plosone/article?id=10.1371/journal.pone.0016790
glp-1	AMPK	I				glp-1 (lf) mutants increases and glp-1 (gf) and decreases AMPK phosphorylation	*C. elegans*	https://www.ncbi.nlm.nih.gov/pmc/articles/PMC3904953/
glp-1	mTOR	P	I	E	Y, glp-1-|AMPK-|mTOR	glp-1 mutants have reduced TOR mRNA levels	*C. elegans*	http://www.scienceD.com/science/article/pii/S0960982211008444X
glp-1	DAF-12	I	I	E	Y, glp-1 -| NHR-80 -> DAF-12, DAF-12 may be necessary for NHR-49	glp-1 mutant lifespan extension requires daf-12	*C. elegans*	https://www.scienceD.com/science/article/pii/S0092867406002376#bib16

glp-1	DAF-16	I	I	E	Y, glp-1-|AMPK->DAF-16, but we may keep this	DAF-16::GFP translocates to nucleus in glp-1 mutant	*C. elegans*	https://www.genetics.org/content/178/2/903#sec-18%20http://www.scienceD.com/science/article/pii/S0092867406002376
glp-1	ELT-2	I	I	E	Y, glp-1|AMPK..->ELT-2, glp-1 might be a necessary inhibitor of AMPK	elt-2 RNAi shortened the lifespan of glp-1 mutant by 25%	*C. elegans*	http://www.scienceD.com/science/article/pii/S1550413112005049#mmc3
						elt-2 is required for lifespan extension in glp-1 mutant	*C. elegans*	http://www.pnas.org/content/113/20/E2832.full.pdf
						ELT-2::GLP levels are increased in glp-1 mutants	*C. elegans*	http://journals.plos.org/plosgenetics/article?id=10.1371/journal.pgen.1005956
glp-1	HLH-30	I	I	E	Y, glp-1-|AMPK-|mTOR-|HLH-30	HLH-30 is required for the lifespan extension of glp-1 mutant	*C. elegans*	https://www.ncbi.nlm.nih.gov/pmc/articles/PMC3866206/
glp-1	HSF-1	I	I	E	Y, glp-1 -| DAF-16-> HSF-1	hsp-16.2::GFP induction in glp-1 mutant is suppressed in hsf-1 RNAi	*C. elegans*	https://www.ncbi.nlm.nih.gov/pubmed/23734734

						HSF-1 is required for the longevity of glp-1 animals	*C. elegans*	https://journals.plos.org/plosgenetics/article?id=10.1371/journal.pgen.0010017#pgen-0010017-t002
glp-1	NHR-49	I	I	E	Y, glp-1-|AMPK->NHR-49, glp-1 is a necessary inhibitor of NHR-49	NHR-49 mutant (nr2041) and RNAi supresses glp-1 mutant (e2141) longevity. Enhanced expression of nhr-49 mRNA and protein in glp-1 mutant	*C. elegans*	https://www.ncbi.nlm.nih.gov/pubmed/25474470
glp-1	NHR-80	I	I	E	Y, NHR-80 is a sink node	glp-1 mutant requires NHR-80 for lifespan extension, in glp-1 mutants mRNA and protein levels of NHR-80 increase	*C. elegans*	http://journals.plos.org/plosbiology/article?id=10.1371/journal.pbio.1000599
glp-1	PHA-4	Int	I	E	Y, genetic interaction, also glp-1-|AMPK-|mTOR-|PHA-4	Synthetic genetic interaction analysis	*C. elegans*	https://www.ncbi.nlm.nih.gov/pubmed/17897480
glp-1	PHA-4	I	I	E	Y, genetic interaction, also glp-1-|AMPK-|mTOR-|PHA-4	glp-1 mutantion increases pha-4 transcripts, glp-1 extended lifespan is depended on pha-4	*C. elegans*	http://www.scienceD.com/science/article/pii/S09609822110084 4X
glp-1	SKN-1	I	I	E	Y, glp-1-|AMPK->SKN-1, SKN-1 might be necessary for ELT-2	glp-1 mutant lifespan extension and stress resistance requires SKN-1	*C. elegans*	https://elifesciences.org/articles/07836#fig1
glp-1	daf-2	P	I	E	Y, refers to germline free animals, may not be relevant	glp-1(gf)shortened lifespan is extended by daf-2 RNAi	*C. elegans*	http://science.sciencemag.org/content/313/5789/971.full

mTOR	DAF-16	I	I	E	Y, mTOR-|ELT->DAF-16 or mTOR-|PHA-4->DAF-16, the evidence is contradictory on this effect	Lifespan extension in mTORC1 components is rescued by daf-16 (mgDf47) mutant	*C. elegans*	https://www.ncbi.nlm.nih.gov/pmc/articles/PMC3348514/
mTOR	ELT-2	I	D	E		yeast two hybrid; when cells are treated with rapamycin or kinase-dead Tor1p(S1972I,D2294E) mutant is used, Gln3p (ELT-2) transfers from cytoplasm to nucleus to induce Gln3p (ELT-2)-dependent genes; expression of Tor1p(S1972I)-rapamycin resistant but not Tor1p or Tor1p(S1972I, D2294E) prevented dephosphorylation of Gln3p when rapamycin was added	*S. cerevisiae*	http://www.jbc.org/content/275/46/35727.long
mTOR	HLH-30	I	D	E		HLH-30::GFP translocated to nucleus upon mTOR RNAi	*C. elegans*	https://www.nature.com/articles/ncomms3267.pdf
mTOR	HLH-30	I				rict-1 mutants have higher HLH-30 expression as well as increased targets of HLH-30 (like autophagy)	*C. elegans*	https://www.scienceD.com/science/article/pii/S0092867419301 62X?via%3Dihub#undfig1
mTOR	HSF-1	I	I	E		hsf-1 (sy441) is required for the lifespan extension of RNAi of TOR components (daf-15, ragc-1 and rapamycin)	*C. elegans*	https://www.ncbi.nlm.nih.gov/pubmed/23879233
mTOR	PHA-4	I	I	E		let-363 RNAi based longevity is rescued in pha-4 (ts) mutants	*C. elegans*	https://www.ncbi.nlm.nih.gov/pubmed/18804378

mTOR	SKN-1	I	I	E	Y, mTOR-|PHA-4->SKN-1	let-363 RNAi increases SKN-1 nuclear occupancy	*C. elegans*	https://www.ncbi.nlm.nih.gov/pubmed/22560223
AMPK	mTOR	I	D	E		Active AMPK rapidly and potently induces raptor Ser792 phosphorylation in vitro	Mouse (MEFs)	https://www.ncbi.nlm.nih.gov/pmc/articles/PMC2674027/
AMPK	DAF-16	P	D	E		AMPK Dly phosphorylates FOXO/DAF-16 in vitro (Fig 6). Lifespan extension and stress resistance of constituively active AMPK is defendent on DAF-16	*C. elegans*	https://www.ncbi.nlm.nih.gov/pmc/articles/PMC2185793/
AMPK	ELT-2	P	D	E		snf1Δ(aak-2) mutation completely abolished the ability of Gln3(ELT-2) to become phosphorylated in the absence of glucose; pull down assay-Snf1 specifically bound to GST-Gln3; Snf1 significantly phosphorylated a bacterial recombinant Gln3 in vitro	*S. cerevisiae*	http://mcb.asm.org/content/22/4/1246.long
AMPK	HSF-1	P	D	E		phosphorylation of HSF under conditions of glucose starvation, was abolished in the snf1Δ(AAK-2) strain; yeast two hybrid; in vitro kinase assays	*S. cerevisiae*	http://www.jbc.org/content/279/7/5169.long
AMPK	NHR-49	P	I	E	Y, AMPK -> DAF-16 -> NHR-49	Constitutively active aak-2 does not extend lifespan in nhr-49 mutant (n42041)	*C. elegans*	https://www.ncbi.nlm.nih.gov/pubmed/25723162
						Activation of AMPK via AICAR increased expression of nhr-49 and its targets fat-7 and acs-2	*C. elegans*	https://www.ncbi.nlm.nih.gov/pubmed/26824904
AMPK	SKN-1	P	I	E	Y, AMPK-| mTOR-| SKN1	Effect of metformin of skn-1::GFP nuclear localization is dependent on aak-2 (ok524)	*C. elegans*	https://www.ncbi.nlm.nih.gov/pubmed/20090912

oxidative stress	daf-2	I	I	E		daf-2 mutants are hyper-resistant to paraquat (oxidative stress agent)	*C. elegans*	https://www.fasebj.org/doi/full/10.1096/fasebj.13.11.1385
oxidative stress	glp-1	I	I	E		glp-1 mutants worms are hyperesistant to tBOOH (Oxidative stress inducing agent)	*C. elegans*	https://onlinelibrary.wiley.com/doi/full/10.1111/acel.12743
oxidative stress	HSF-1	P	I	E		animals grown on hsf-1 RNAi are hypersensitive to paraquat (oxidative stress inducing agent) and animals overexpressing HSF-1 are hyper-resistant	*C. elegans*	https://science.sciencemag.org/content/300/5622/1142/tab-figures-data
oxidative stress	DAF-16	P	I	E	Y, oxidative stress -| glp-1-| DAF-16	daf-16 mutant is hypersensitive to oxidative stress	*C. elegans*	https://www.nature.com/articles/s41467-018-06624-0
oxidative stress	HLH-30	P	I	E	Y, oxidative stress -| glp-1-|mTOR-| HLH-30	hlh-30 mutant is hypersensitive to oxidative stress	*C. elegans*	https://www.nature.com/articles/s41467-018-06624-0
stress	mTOR	P	I	E		oxidizing agent (diamide) increases mTOR actvity (S6K phosphorylation) while reducing agent (BAL) reduces mTOR activity similar to fasting.	HEK293T cells	https://www.jbc.org/content/280/47/39505.long
SKN-1	lipl-3	P	I	E		skn-1 mutant has lower levels of basal expression of lipl-3	*C. elegans*	https://elifesciences.org/articles/07836
16)	TFEB (HLH-30)	P	D	E		FOXO1 attaches to the promoters of TFEB and regulates its expression	mouse 3t3L1 adipocytes	https://www.ncbi.nlm.nih.gov/pmc/articles/PMC5046220/

1) Interaction: I-Inhibit, P-Promote, Int-Interacts

2) Type: I-Indirect, D-Direct
3) Experimental or Inferred: E-Experimental, I-Inferred

b. Supplementary Table 2 (SI Appendix, Table S2)

Interaction number	input	target	Interaction[1]	Type[2]	Experimental or Inferred[3]	evidence	species	References
3	Food	mTOR	P	I	E	Amino Acids Regulate the Phosphorylation and Activation of p70 S6 Kinase and eIF-4E-BPs "Withdrawal of amino acids from the nutrient medium of CHO-IR cells results in a rapid deactivation of p70 S6 kinase and dephosphorylation of eIF-4E BP1,"	CHO-IR	https://www.jbc.org/content/273/23/14484.long
3	Food	mTOR	P	I	E	amino acids activate mTOR through Rag proteins " amino acid stimulation of cells increased the GTP loading of RagB (Fig. 3E). "In cells with a reduction in the expression ofall the Rag proteins, leucine- stimulated phosphorylation ofS6K1 was strongly reduced "	human embryonic kidney (HEK)-293T cells	https://science.sciencemag.org/content/320/5882/1496?casa_token=tCpO9sHN1XEAAAAA:oG89sJTC8rnaKmRPdo388slO0FGqG-jZqooRvMZ8f4xRmcu3_6BXvrkw2ygbKS4xY6yNmTlwB91cig

3	Food	mTOR	P	I	E	Rag proteins are mTOR pathway activators, in response to amino acids Knockdown of dRagA or dRagC markedly decreased dS6K phosphorylation in response to amino acid stimulation. also "expression of dominant-negative RagAT21N and RagBT54N decreased S6K phosphorylation" "Transfection with as little as 20 ng of RagAQ66L [constitutively active] DNA markedly increased S6K phosphorylation in the absence of amino acids"	HEK293 cells	https://www.nature.com/articles/ncb1753?proof
3	Food	mTOR	P	I	E	ATPase is necessary for amino acid sensing by mTOR on lysosomal surface: RNAi against V-ATPase supresses S6K phosphorylation; inhibition of V-ATPase results in failure of mTOR clustering to lysosomal surface in response to amino acids; "Semi-quantitative mass spectrometric analyses ofanti-FLAG immunoprecipitates prepared from 293Tcells expressing FLAG-tagged Ragulator components (p18 or p14) or RagB revealed the presence of many subunits of the v-ATPase"	293Tcells	https://www.ncbi.nlm.nih.gov/pmc/articles/PMC3211112/
4	Food	daf-1	P	I	E	Both shows the ligand daf-7 mediating food signals. DAF-1 is their receptor	C. elegans	https://www.ncbi.nlm.nih.gov/pubmed/8910282
4	Food	daf-1	P	I	E		C. elegans	https://www.ncbi.nlm.nih.gov/pubmed/8893028
4	Food	daf-1	P	I	E	Expression of daf-1::gfp fully rescued the adult feeding rate, fat storage, egg retention etc of daf-1 mutants	C. elegans	https://www.ncbi.nlm.nih.gov/pmc/articles/PMC2556218/
2	Food	daf-2	P	I	E	DAF-2 appears to couple nutritional status to the activation of oocyte generation.	C. elegans	https://www.ncbi.nlm.nih.gov/pmc/articles/PMC3829605/

1	Food	glp-1	P	I	E	When animal doesn't have sufficient U/T levels, it prevents it from germline proliferation, glp-1 hyperactivation promotes meiosis in germline, despite the insufficient U/T levels	C. elegans	https://www.ncbi.nlm.nih.gov/pmc/articles/PMC4743060/
5	Fasting	AMPK	P	D	E	AMPK required for lifespan extension via DR	C. elegans	http://genesdev.cshlp.org/content/18/24/3004.full
5	Fasting	AMPK	P	D	E	High glucose reduced phopshorylated aak-2 -catalytic subunit of AMPK	C. elegans	https://journals.plos.org/plosone/article?id=10.1371/journal.pone.0148089
6	Fasting	daf-2	I	I	E	daf-2 protein levels reduced after starvation	C. elegans	https://www.ncbi.nlm.nih.gov/pubmed/22123849
34	DAF-16	HSF-1	P	I	E	subset of DAF-16 targets requires HSF-1 for expression	C. elegans	http://science.sciencemag.org/content/300/5622/1142.full
33	DAF-16	SKN-1	P	D	E	Comparing daf-2 and daf-16; daf-2 adults using chromatin immunoprecipitation (ChIP) and PCR for skn-1 . skn-1 mutant (zu135) suppressed daf-16(oe) oxidative stress resistance. skn-1 mRNA level is increased by daf-16(oe) (zIs356)	C. elegans	https://www.ncbi.nlm.nih.gov/pmc/articles/PMC5595692/
33	DAF-16	SKN-1	P	D	E	Chip-PCR direct binding on DAF-16 to skn-1 promoter. Increased skn-1 mRNA in DAF-16OE and skn-1 required for DAF-16OE OX stress resistance	C. elegans	https://www.ncbi.nlm.nih.gov/pubmed/28612944
30	DAF-3	DAF-16	P	I	E	daf-3 RNAi and daf-3 mutants caused DAF-16::GFP to be excluded from nuclei	C. elegans	http://www.sciencedirect.com/science/article/pii/S0960982207019148

35	DAF-16	PQM-1	I	I	E	In daf-2 mutant background, pqm-1 inhibits nuclear localization of daf-16 and vice versa.	C. elegans	https://www.sciencedirect.com/science/article/pii/S0092867413008404?via%3Dihub#bib17
37	ELT-2	DAF-16	P	I	E	elt-2 RNAi treatment reduced expression of endogenous daf-16 d/f and also reduced Pdaf-16d/f::gfp expression	C. elegans	https://www.ncbi.nlm.nih.gov/pmc/articles/PMC4022319/
37	ELT-2	DAF-16	P			ELT-2 promote longevity by regulating daf-16 gene expression	C. elegans	https://www.ncbi.nlm.nih.gov/pmc/articles/PMC4022319/
38	ELT-2	PHA-4	P	D	E	EMSA of pha-4 gut acting promoter region with ELT-2 protein	C. elegans	https://www.ncbi.nlm.nih.gov/pubmed/9584117
43	HLH-30	lipl-3	P	D	E	Expression of lipl-3 on Fasting depends on hlh-30	C. elegans	https://www.ncbi.nlm.nih.gov/pmc/articles/PMC3723461/
32	DAF-16	HLH-30	Interacts	D	E	DAF-16 and HLH-30 physically interact	C. elegans	https://www.nature.com/articles/s41467-018-06624-0#MOESM1
29	HSF-1	DAF-16	P	I	E	HSF-1 OE extended lifespan requiresdaf-16	C. elegans	http://science.sciencemag.org/content/300/5622/1142.full
28	HSF-1	HLH-30	P		I	Heat shock leads to activation of HLH-30 and also induction of hlh-30-dependent autophagy genes	C. elegans	https://www.nature.com/articles/ncomms14337

27	HSF-1	ELT-2	P	I	E	HSF-1 OE has increased expression of elt-2 mRNA	C. elegans	http://journals.plos.org/plosgenetics/article?id=10.1371/journal.pgen.1005956#pgen-1005956-t001
26	HSF-1	daf-1	I	I	I	HSF-1 represses daf-7 expression	C. elegans	https://www.ncbi.nlm.nih.gov/pmc/articles/PMC3558376/
39	PHA-4	SKN-1	P	D	E	Pha-4 could activate skn-1 as per modENCODE paper	C. elegans	https://www.ncbi.nlm.nih.gov/pmc/articles/PMC3032928/
40	SKN-1	ELT-2	P	I	E	ELT-2 is downstream of SKN-1 in intestinal differentiation	C. elegans	https://www.ncbi.nlm.nih.gov/pmc/articles/PMC2836165/#SD1
42	MXL-3	HLH-30	outcompetes	D	E	MXL-3 outcompetes HLH-30/TFEB for binding to lipl-3 promoter; analysis by ChIP shows that HLH-30 is rarely associated with the promoters ofthe lipase genes in well-fed animals (Fig. 4fand SI_ChromatinIP), even when the hlh-30 gene is expressed from a high copy number array at higher levels than those observed in fasting animals; HLH-30 and MXL-3 share the same binding motif	C. elegans	https://www.nature.com/articles/ncb2741

36	PQM-1	DAF-16	I	I	E		C. elegans	https://www.sciencedirect.com/science/article/pii/S0092867413008404?via%3Dihub#bib17
16	daf-2	AMPK	I	I	E	aak-2 RNAi suppresses daf-2 longevity	C. elegans	https://www.ncbi.nlm.nih.gov/pubmed/16626391
16	daf-2	AMPK	I			aak-2 RNAi suppresses daf-2 (e1368) longevity and dauer formation	C. elegans	https://www.ncbi.nlm.nih.gov/pubmed/15574588
16	daf-2	AMPK	I			daf-2 longevity partially suppressed by aakg-4 RNAi (atypical gamma isoform of AMPK)	C. elegans	http://journals.plos.org/plosgenetics/article?id=10.1371/journal.pgen.1004109
16	daf-2	AMPK	I			aak-2 mutations (rr48 and ok524) shorten daf-2 mutant longevity (e1370)	C. elegans	https://www.ncbi.nlm.nih.gov/pubmed/16407400
16	daf-2	AMPK	I			AMPK components - RNAi (aak-2, aakb-1, aakb-2, aakg-1) suppress long term anoxia viability of daf-2 (e1370) mutants	C. elegans	https://pubmed.ncbi.nlm.nih.gov/21304820/
18	daf-2	DAF-16	I	D	E	DAF-2 prevents DAF-16 translocation to nuclei	C. elegans	https://www.nature.com/ng/journal/v28/n2/full/ng0601_139.html
18	daf-2	DAF-16	I			DAF-16 mutation suppress daf-2 mutant phenotypes like dauer arrest, lifespan extension, reduced fertility and variability defects	C. elegans	https://www.ncbi.nlm.nih.gov/pubmed/9504918

15	daf-2	HSF-1	I	I	E	hsf-1 RNAi prevents the daf-2(e1370) mutation from extending life-span	C. elegans	https://science.sciencemag.org/content/300/5622/1142.long
17	daf-2	SKN-1	I	D	E	Nucler accumulation of SKN-1::GFP in the intestinal nuclei when DAF-2 signaling reduced. skn-1 mutant (zu67) reduces oxidative stress resistance of daf-2 mutant (e1370). Also skn-1 RNAi recuses longevity of daf-2 mutant (e1368)	C. elegans	https://www.ncbi.nlm.nih.gov/pubmed/18358814
25	daf-1	DAF-3	I	I	E	DAF-3 is required for increased fat deposits in daf-1 mutant	C. elegans	https://www.ncbi.nlm.nih.gov/pubmed/18680713
25	daf-1	DAF-3	I			daf-3 mutation supresses the dauer constitutive mutation of daf-1	C. elegans	https://www.ncbi.nlm.nih.gov/pubmed/11063683
25	daf-1	DAF-3	I			daf-1 mutant (m40) suppresses DR longevity but rescued by daf-3 mutant (e1376)	C. elegans	https://www.ncbi.nlm.nih.gov/pubmed/28107363
24	daf-1	daf-2	P	I	E	Dauer formation of TGFB pathway mutants is suppressed by daf-2/age-1 pathway mutant in a suppressor screen	C. elegans	http://www.genetics.org/content/156/3/1035.long
24	daf-1	daf-2	P			In mutants of TGF beta genes, daf-2 and insulin genes are down regulated	C. elegans	https://www.ncbi.nlm.nih.gov/pubmed/15380030
19	glp-1	AMPK	I	I	E	AMPK component- RNAi (aak-2, aakb-1, aakb-2, aakg-1) suppress long term anoxia viability of glp-1 (e2141) mutants	C. elegans	https://journals.plos.org/plosone/article?id=10.1371/journal.pone.0016790
19	glp-1	AMPK	I			glp-1 (lf) mutants increases and glp-1 (gf) and decreases AMPK phosphorylation	C. elegans	https://www.ncbi.nlm.nih.gov/pmc/articles/PMC3904953/

20	mTOR	ELT-2	I	D	E	yeast two hybrid; when cells are treated with rapamycin or kinase-dead Tor1p(S1972I,D2294E) mutant is used, Gln3p (ELT-2) transfers from cytoplasm to nucleus to induce Gln3p (ELT-2)-dependent genes; expression of Tor1p(S1972I)-rapamycin resistant but not Tor1p or Tor1p(S1972I, D2294E) prevented dephosphorylation of Gln3p when rapamycin was added	S. cerevisiae	http://www.jbc.org/content/275/46/35727.long
22	mTOR	HLH-30	I	D	E	HLH-30::GFP translocated to nucleus upon mTOR RNAi	C. elegans	https://www.nature.com/articles/ncomms3267.pdf
22	mTOR	HLH-30	I			rict-1 mutants have higher HLH-30 expression as well as increased targets of HLH-30 (like autophagy)	C. elegans	https://www.sciencedirect.com/science/article/pii/S009286741930162X?via%3Dihub#undfig1
21	mTOR	HSF-1	I	I	E	hsf-1 (sy441) is required for the lifespan extension of RNAi of TOR components (daf-15, ragc-1 and rapamycin)	C. elegans	https://www.ncbi.nlm.nih.gov/pubmed/23879233
23	mTOR	PHA-4	I	I	E	let-363 RNAi based longevity is rescued in pha-4 (ts) mutants	C. elegans	https://www.ncbi.nlm.nih.gov/pubmed/18804378
12	AMPK	mTOR	I	D	E	Active AMPK rapidly and potently induces raptor Ser792 phosphorylation in vitro	Mouse (MEFs)	https://www.ncbi.nlm.nih.gov/pmc/articles/PMC2674027/
13	AMPK	DAF-16	P	D	E	AMPK directly phosphorylates FOXO/DAF-16 in vitro (Fig 6). Lifespan extension and stress resistance of constituively active AMPK is defendent on DAF-16	C. elegans	https://www.ncbi.nlm.nih.gov/pmc/articles/PMC2185793/

11	AMPK	ELT-2	P	D	E	snf1Δ(aak-2) mutation completely abolished the ability of Gln3(ELT-2) to become phosphorylated in the absence of glucose; pull down assay-Snf1 specifically bound to GST-Gln3; Snf1 significantly phosphorylated a bacterial recombinant Gln3 in vitro	S. cerevisiae	http://mcb.asm.org/content/22/4/1246.long
14	AMPK	HSF-1	P	D	E	phosphorylation of HSF under conditions of glucose starvation, was abolished in the snf1Δ(AAK-2) strain; yeast two hybrid; in vitro kinase assays	S. cerevisiae	http://www.jbc.org/content/279/7/5169.long
10	oxidative stress	daf-2	I	I	E	daf-2 mutants are hyper-resistant to paraquat (oxidative stress agent)	C. elegans	https://www.fasebj.org/doi/full/10.1096/fasebj.13.11.1385
9	oxidative stress	glp-1	I	I	E	glp-1 mutants worms are hyperesistant to tBOOH (Oxidative stress inducing agent)	C. elegans	https://onlinelibrary.wiley.com/doi/full/10.1111/acel.12743
8	oxidative stress	HSF-1	P	I	E	animals grown on hsf-1 RNAi are hypersensitive to paraquat (oxidative stress inducing agent) and animals overexpressing HSF-1 are hyper-resistant	C. elegans	https://science.sciencemag.org/content/300/5622/1142/tab-figures-data
7	oxidative stress	mTOR	P	I	E	oxidizing agent (diamide) increases mTOR actvity (S6K phosphorylation) while reducing agent (BAL) reduces mTOR activity similar to fasting.	HEK293T cells	https://www.jbc.org/content/280/47/39505.long
41	SKN-1	lipl-3	P	I	E	skn-1 mutant has lower levels of basal expression of lipl-3	C. elegans	https://elifesciences.org/articles/07836
31	FOXO1 (DAF-16)	TFEB (HLH-30)	P	D	E	FOXO1 attaches to the promoters of TFEB and regulates its expression	mouse 3t3L1 adipocytes	https://www.ncbi.nlm.nih.gov/pmc/articles/PMC5046220/

1) Interaction: I-Inhibit, P-Promote, Int-Interacts

2) Type: I-Indirect, D-Direct
3) Experimental or Inferred: E-Experimental, I-Inferred

c. Supplementary Table 3 (SI Appendix, Table S3)

TRANSCRIPTION FACTOR	TARGET PROMOTER	DATA SOURCE	TF BINDING SITE/S IN PROMOTER
DAF-16	*hlh-30*	modEncode	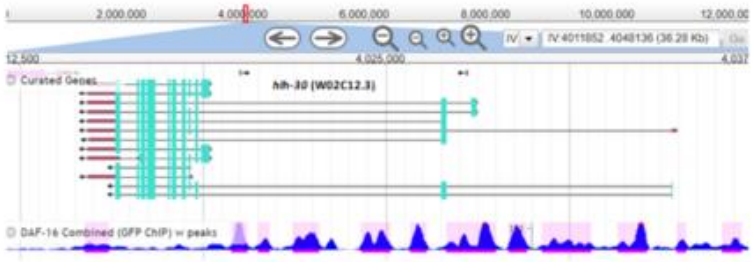
DAF-16	*lipl-3*	modEncode	
DAF-16	*lipl-4*	modEncode	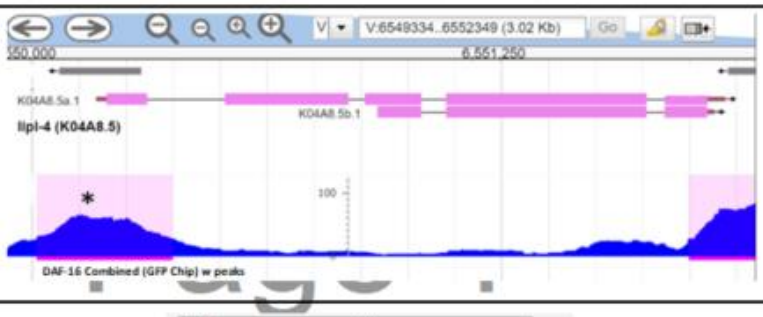
HSF-1	*lipl-3*	UCSC Genome Browser	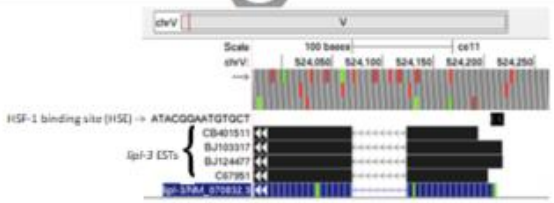
HSF-1	*hlh-30*	UCSC Genome Browser	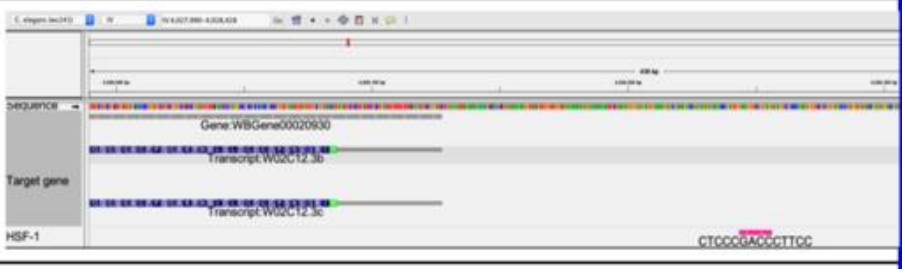

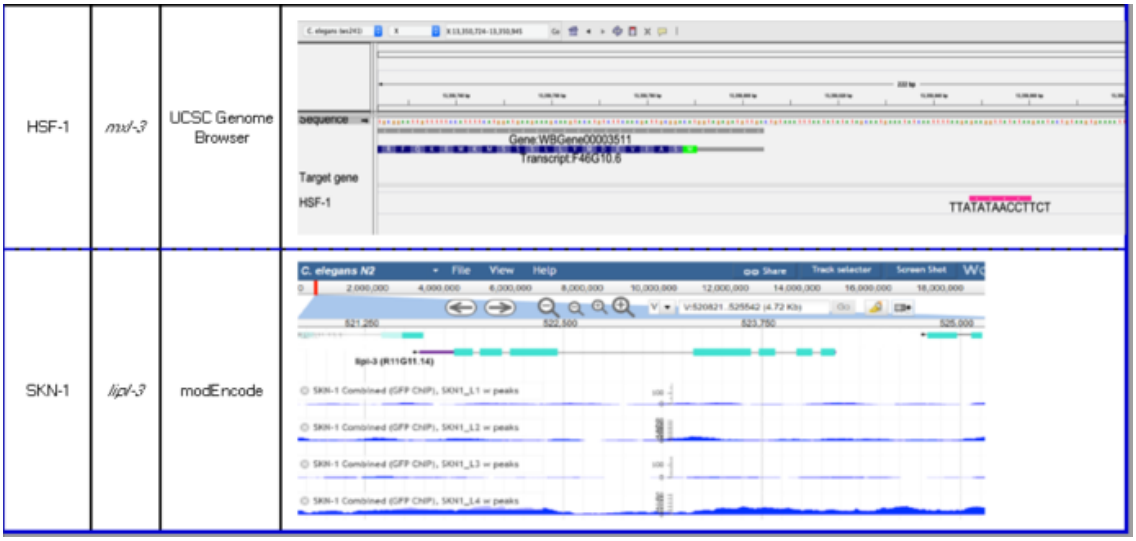

d. Supplementary Table 4 (SI Appendix, Table S4)

Published strains used in this study		
Name	**Genotype**	**Strain source**
N2 Bristol	Wild-type (WT)	CGC
CB4037	*glp-1(e2141) III*	CGC
DR40	*daf-1(m40) IV*	CGC
DR1572	*daf-2(e1368) III*	CGC
JIN1375	*hlh-30(tm1978) IV*	CGC
CF1038	*daf-16(mu86) I*	CGC
PS355	*hsf-1(sy441)I*	CGC
QV225	*skn-1(zj15) IV*	CGC
GR1311	*daf-3(mgDf90) X*	CGC
KQ1366	*rict-1(ft7) II*	CGC
VC988	*ceh-60(ok1485) X*	CGC
YT17	*crh-1(tz2) III*	CGC
XA7702	*mdt-15(tm2182) III*	CGC
RB1206	*rsks-1(ok1255) III*	CGC
STE68	*nhr-49(nr2041) I*	CGC

BX165	*nhr-80(tm1011) III*	CGC
SM190	*smg-1(cc546) I; pha-4(zu225) V*	CGC
PD8120	*smg-1(cc546) I*	CGC
WBM60	*uthIs248 [aak-2p::aak-2(genomic aa1-321)::GFP::unc-54 3'UTR + myo-2p::tdTOMATO]*	CGC
GR1352	*daf-16(mgDf47) I; xrIs87[daf-16(alpha)::GFP::daf-16B + rol-6(su1006)].*	CGC
AGD710	*uthIs235 [sur5p::hsf-1::unc-54 3'UTR + myo-2p::tdTomato::unc-54 3' UTR].*	CGC
OP433	*unc-119(tm4063) III; wgIs433 [hlh-30::TY1::EGFP::3xFLAG + unc-119(+)].*	CGC
OP745	*wgIs745 [mxl-3::TY1::EGFP::3xFLAG + unc-119(+)]. TY1::EGFP::3xFLAG*	CGC
TJ356	*zIs356 [daf-16p::daf-16a/b::GFP + rol-6(su1006)]*	CGC
OG497	*drSi13 [hsf-1p::hsf-1::GFP::unc-54 3'UTR + Cbr-unc-119(+)] II*	CGC

New strains generated for this study		
Name	**Genotype**	**Comments**
GMW 0011	OP433xCB4037 *unc-119(tm4063) III; wgIs433 [hlh-30::TY1::EGFP::3xFLAG + unc-119(+)].x glp-1(e2141) III*	This study
GMW 0012	OP433xDR1572	This study

	unc-119(tm4063) III; wgIs433 [hlh-30::TY1::EGFP::3xFLAG + unc-119(+)]x daf-2(e1368) III	
GMW 0013	CF1038xJIN1375 *daf-16 (mu86) I; hlh-30 (tm1978) IV*	This study

e. Supplementary Table 5 (SI Appendix, Table S5)

Primers

Gene	Forward primer sequence	Reverse primer sequence	Source:
ama-1	CGGAGGAGATTAAACGCAT	TGTCATGCATCTTCCACGACGAT	(113)
pmp-3	TGGCCGGATGATGGTGTCGC	ACGAACAATGCCAAAGGCCAGC	(187)
mxl-3	ATTCTTCCGATGACGATTC	CTCCCCATCAAGCAGTGGA	(113)
hlh-30	AACAATTTCAGACAGGTC	CCTGCGGTCGCGGTAATA	(113)
lipl-3	ATGGGCAGGCAAATCCACCA	AGTTGTTCTGCGCAATTATA	(113)
lipl-4	TCAAGTCGTTCAGGGAAG	TCATGTGTTATCGTCTTGAAG	(119)
let-363	CTCGGTGACAGACATCCA	AGTTACTTCCATAGCGTTGA	This work
hsf-1	TTTGCATTTTCTCGTCTCTGTC	TCTATTTCCAGCACACCTCGT	(188)
daf-16	AAAGAGCTCGTGGTGGGTTA	TTCGAGTTGAGCTTTGTAGTCG	(116)

Chapter III: Gene specificity of the context-specific regulation of lysosomal lipolysis in *C. elegans*

1. Regulation of *lipl-1* transcription downstream of nutrient sensing

Our group previously described the *C. elegans* lysosomal lipase genes *lipl-1*, *lipl-3*, and *lipl-4* as essential for survival during fasting and sufficient to promote the extension of lifespan (113,119,189). By characterizing their functions, we defined that *lipl-4* was distinct from *lipl-1* and *lipl-3* in its substrate specificity, its impact on fat mobilization, and on the main transcriptional regulators linking its transcriptional status to food availability. Upon fasting, *lipl-4* transcription is induced by the transcription factor DAF-16 (ortholog of mammalian FOXO). The consequent increase in LIPL-4 activity promotes the production of ω-3 and ω-6 PUFAs, which in turn activate autophagy, a process that promotes survival to starvation (119). On the other hand, during fasting, *lipl-1* and *lipl-3* are transcriptionally activated by HLH-30 (ortholog of mammalian TFEB) and break down the major lipid stores contained in lipid droplets in the *C. elegans* intestine through a substrate-specific type of autophagy named lipophagy (113).

As for the upstream regulators of the lysosomal lipases, we defined that *lipl-3* and *lipl-4* respond to inhibition of such membrane receptors as the insulin (*C. elegans* DAF-2), Notch (*C. elegans* GLP-1), and the TGF-β (*C. elegans* DAF-1) receptors and to intracellular nutrient sensors such as mTOR (*C. elegans* LET-363) (Fig. 2C-E, 3C-G). We showed that the regulation of *lipl-4* converges onto DAF-16/FOXO to induce its

expression during fasting and upon reduction of *daf-2*, *daf-1*, and *glp-1* function (Fig. 2). By contrast, *lipl-3* regulation is context-dependent with multiple TFs, including HLH-30/TFEB, MXL-3, DAF-16/FOXO, and HSF-1 regulating its expression (Fig. 8J). On the other hand, the transcriptional regulation of *lipl-1* remained poorly explored. All we know to date is our published demonstration that *lipl-1* is transcriptionally activated by HLH-30/TFEB during fasting, and that in the fed condition MXL-3 constitutively represses *lipl-1* (113). In this chapter, I describe our investigation on the transcriptional regulation of the lysosomal lipase *lipl-1*. Briefly, we show that *lipl-1* expression is induced in response to inhibition of *daf-2*, *glp-1*, *daf-1*, and mTOR and to constitutive activation of AMPK and caloric restriction. We also present evidence supporting context-dependent regulation of *lipl-1* expression, as TFs including HLH-30/TFEB, DAF-16/FOXO, DAF-3/SMAD4, ELT-2 and HSF-1 control *lipl-1* transcription in different genetic and environmental contexts. Most interestingly, *lipl-3* and *lipl-1* have the same anatomical and subcellular localization, role in lipid mobilization and aging. They even likely have a common evolutionary origin since their nucleotide sequences are 72% identical and their loci are both in *C. elegans*' chromosome V. Nevertheless, the transcriptional regulation of *lipl-3* and *lipl-1* is distinct, suggesting that in evolutionary terms regulatory divergence may accompany or even precede mutational divergence in the open reading frame.

a. *lipl-1* responds to the inhibition of insulin, Notch, TGF-β, and mTOR signaling, to activation of AMPK and caloric restriction

We previously showed that the expression of *lipl-1* increases during fasting (113). Here, we show that *lipl-1* is induced in *C. elegans* calorically restricted due to mutation of the gene *eat-2*, which leads to defects in pharyngeal pumping, reduced food intake, and caloric restriction (190,191) (Fig. 9A). However, fasting and caloric restriction involve complex cues sensed by many growth factors and nutrient sensors (hereinafter globally referred to as nutrient sensors) including insulin, Notch, and the TGF-β receptors, and mTOR and AMPK. Hence, we set out to define which proteins link feeding status to the activation of the transcriptional program that includes induction of *lipl-1*. To this end, we tested whether inhibition of the insulin, Notch, or TGF-β receptors, the mTOR kinase, or constitutive activation of AMPK (via a threonine to aspartic acid substitution, $AMPK^{T172D}$) (132,192) would be sufficient to promote *lipl-1* induction. Similar to *lipl-3* and *lipl-4*, inhibition of the insulin, Notch, and TGF-β receptors, and of the mTOR was sufficient to promote induction of *lipl-1* (Fig. 9A). Since mTOR is present in two different complexes (172), we then tested the potentially distinct contributions of mTORC1 and mTORC2 to the induction of *lipl-1*. When we knocked down *rict-1* (*C. elegans* RICTOR, a component of mTORC2 (172)) the induction of *lipl-1* was statistically significant but very modest, therefore we didn't investigate it further (Fig. 9B). By contrast, *lipl-1* induction upon mTORC1 inhibition through RNAi against *daf-15* (*C. elegans* RAPTOR (172)) was robust (Fig. 9B). Finally, contrary to *lipl-3* and *lipl-4* that were not induced upon constitutive activation of AMPK (Fig. S1F, S2B), *lipl-1* was

induced in AMPK^{T172D} animals (Fig. 9C). Altogether, these results show that in *C. elegans* insulin, Notch, TGF-β, mTORC1, and AMPK signaling link feeding status to the expression of *lipl-1*. The results also point to differential regulation between *lipl-1* and its paralog gene *lipl-3*.

Figure 9

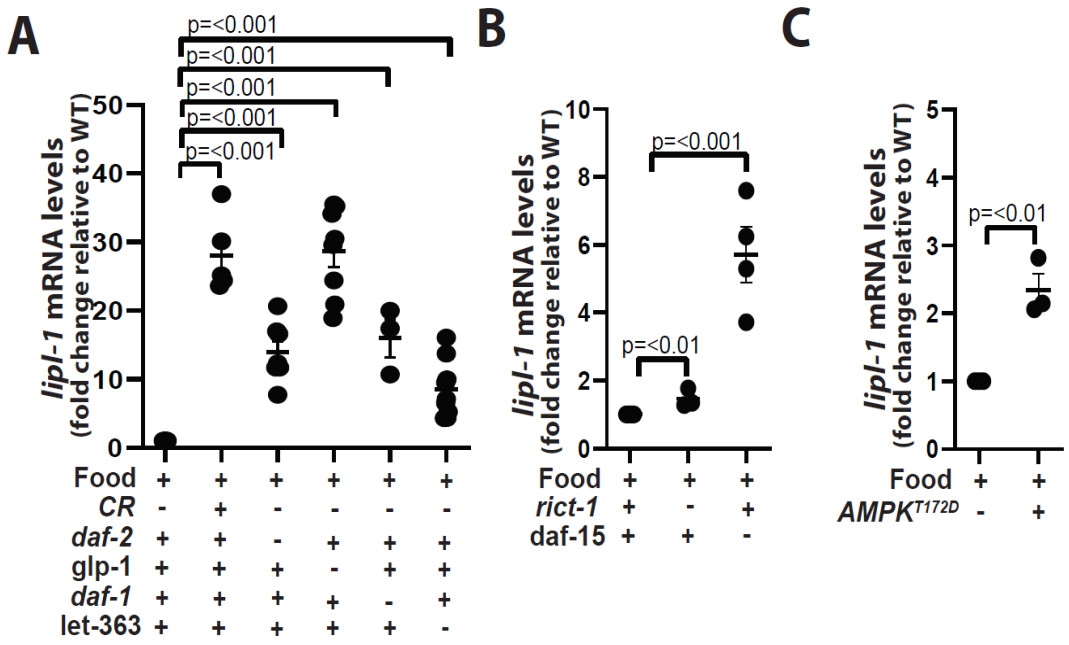
A
B
C
p=<0.001
p=<0.001
p=<0.001
p=<0.001
p=<0.001
lipl-1 mRNA levels
(fold change relative to WT)
0
10
20
30
40
50
Food + + + + + +
CR - + - - - -
daf-2 + + - + + +
glp-1 + + + - + +
daf-1 + + + + - +
let-363 + + + + + -
p=<0.001
p=<0.01
lipl-1 mRNA levels
(fold change relative to WT)
0
2
4
6
8
10
Food + + +
rict-1 + - +
daf-15 + + -
p=<0.01
lipl-1 mRNA levels
(fold change relative to WT)
0
1
2
3
4
5
Food + +
AMPK T172D - +

Fig. 9 *lipl-1* expression responds to the inhibition of insulin, Notch, TGF-β, and mTOR signaling and to the activation of AMPK

(A-C) qRT-PCR analysis of expression in young adult *C. elegans* normalized to housekeeping gene *ama-1* or *pmp-3* is shown relative to untreated as denoted in the Y-axis. Three or more independent biological replicates are presented in all panels. Error bars denote SEM. Statistical significance was assessed via a one-tailed unpaired parametric t-test. Gene inactivations through mutation (gene name italicized) or RNAi (gene name in normal font) are represented with a minus sign in the treatment matrix. All RNAi treatments were started at the L1 stage.

(A) WT, *eat-2(ad465), daf-2(e1368), glp-1(e2141), daf-1(m40)* mutants, and animals treated with RNAi against *let-363* or empty vector control from the L1 stage. N≥3

(B) WT and animals treated with RNAi against *rict-1* or *daf-15*. N≥3

(C) WT animals and animals with constitutively active AMPK ($AMPK^{T172D}$). N=3

b. HLH-30/TFEB mediates *lipl-1* induction in the mTOR and AMPK^{T172D}, but not downstream of insulin, Notch, and TGF-β signaling or in calorically restricted *C. elegans*

lipl-1 transcriptional regulation is also poorly explored. The only TF known so far to partially regulate the induction of *lipl-1* is HLH-30/TFEB during fasting (113). Therefore, we set out to test whether HLH-30/TFEB controls the expression of *lipl-1* downstream of the nutrient sensors described above. We found HLH-30/TFEB mediating the induction of *lipl-1* in *C. elegans* with constitutive activation of AMPK (AMPK^{T172D}) (Fig. 10A) and in the worms treated with RNAi against mTOR, both against the mTOR kinase (*let-363* RNAi, Fig. 10B) and against *C. elegans* RAPTOR (*daf-15* RNAi, Fig. 10C). However, just as in the case of *lipl-3* regulation, HLH-30/TFEB does not mediate *lipl-1* induction downstream of inhibited insulin, Notch, and TGF-β signaling (Fig. 10D-F), or in calorically restricted *C. elegans* (Fig. 10G, H)

Figure 10

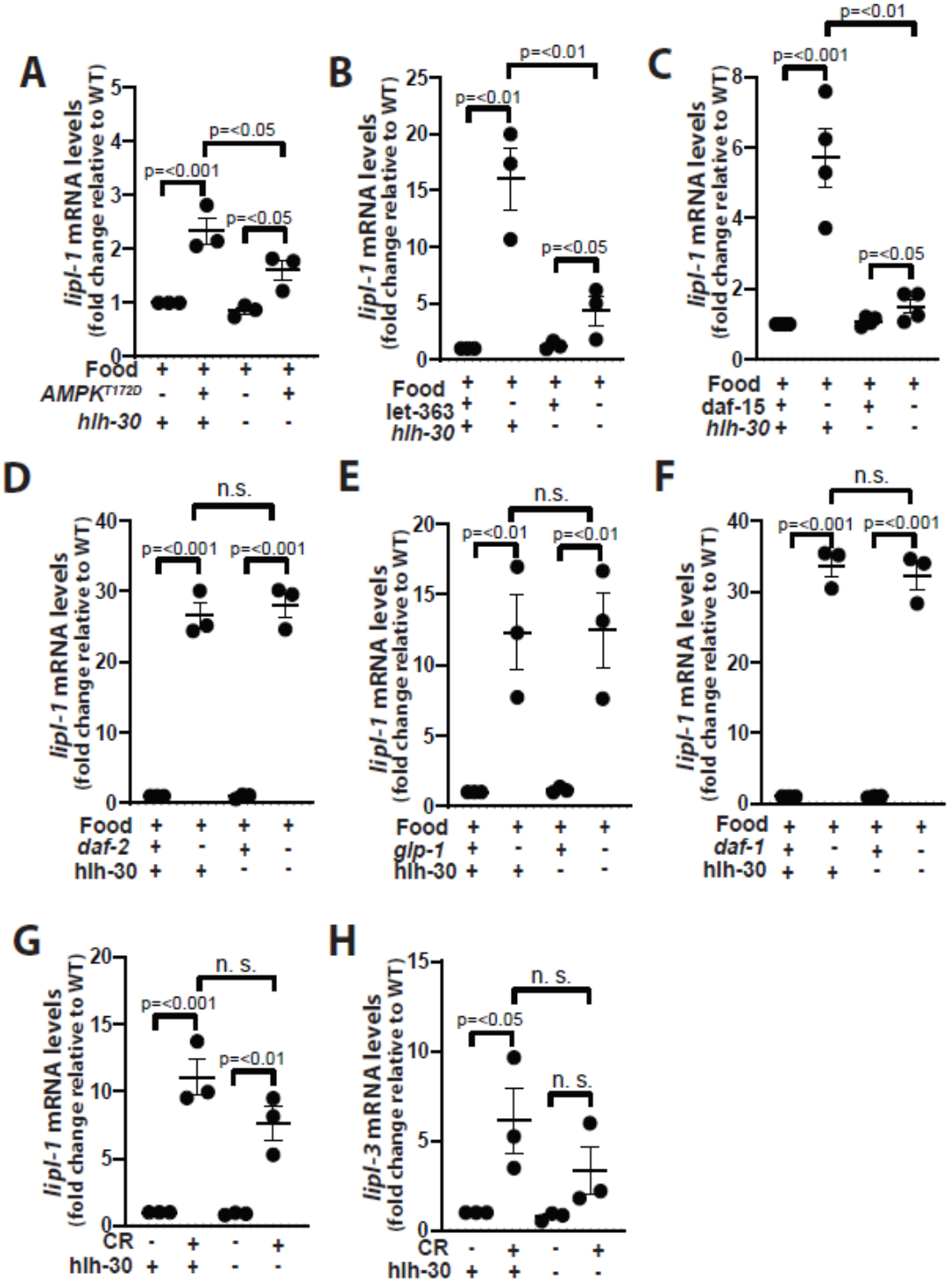
A
lipl-1 mRNA levels (fold change relative to WT)
p=<0.001
p=<0.05
p=<0.05
Food + + + +
AMPKT172D - + - +
hlh-30 + + - -
B
lipl-1 mRNA levels (fold change relative to WT)
p=<0.01
p=<0.01
p=<0.05
Food + + + +
let-363 + - + -
hlh-30 + + - -
C
lipl-1 mRNA levels (fold change relative to WT)
p=<0.001
p=<0.01
p=<0.05
Food + + + +
daf-15 + - + -
hlh-30 + + - -
D
lipl-1 mRNA levels (fold change relative to WT)
n.s.
p=<0.001
p=<0.001
Food + + + +
daf-2 + - + -
hlh-30 + + - -
E
lipl-1 mRNA levels (fold change relative to WT)
n.s.
p=<0.01
p=<0.01
Food + + + +
glp-1 + - + -
hlh-30 + + - -
F
lipl-1 mRNA levels (fold change relative to WT)
n.s.
p=<0.001
p=<0.001
Food + + + +
daf-1 + - + -
hlh-30 + + - -
G
lipl-1 mRNA levels (fold change relative to WT)
n. s.
p=<0.001
p=<0.01
CR - + - +
hlh-30 + + - -
H
lipl-3 mRNA levels (fold change relative to WT)
n. s.
p=<0.05
n. s.
CR - + - +
hlh-30 + + - -

Fig. 10 HLH-30/TFEB controls *lipl-1* downstream mTOR and AMPK activation and mTOR inhibition, but not downstream of insulin, Notch, and TGF-β signaling inhibition or caloric restriction.

(*A-F*) qRT-PCR analysis of expression in young adult *C. elegans* normalized to housekeeping gene *ama-1* or *pmp-3* is shown relative to untreated as denoted in Y-axis. Three or more independent biological replicates are presented in all panels. Error bars denote SEM. Statistical significance was assessed via a one-tailed unpaired parametric t-test. Gene inactivations through mutation (gene name italicized) or RNAi (gene name in normal font) are represented with a minus sign in the treatment matrix. All RNAi treatments were started at the L1 stage.

(A) WT animals and animals with constitutively active AMPK ($AMPK^{T172D}$) treated with RNAi against *hlh-30* or empty vector control from the L1 stage. N=3

(B, C) WT animals and *hlh-30(tm1978)* mutants treated with RNAi against *let-363 (B)* or *daf-15 (C)* or empty vector control from the L1 stage. N≥3

(D, E, F) WT, *daf-2(e1368), glp-1(e2141), daf-1(m40)* mutants, and animals treated with RNAi against *hlh-30* or empty vector control from the L1 stage. N=3

(G, H) WT animals and *eat-2(ad465)* mutants, and animals treated with RNAi against *hlh-30* or empty vector control from the L1 stage. N=3

c. DAF-16 controls *lipl-1* downstream of insulin, Notch, and TGF-β signaling, but not downstream of mTOR, AMPK and in calorically restricted *C. elegans*

DAF-16/FOXO emerged as one of the critical regulators of *lipl-3*. Therefore we decided to test whether it controlled *lipl-1* expression downstream of the nutrient sensors. DAF-16/FOXO fully suppressed the induction of *lipl-1* downstream of *daf-2* inhibition (Fig. 11A) and partly suppressed the induction of *lipl-1* in *glp-1* and *daf-1* mutant animals (Fig. 11B, C). On the other hand, *lipl-1* and *lipl-3* induction in calorically restricted and in $AMPK^{T172D}$ animals is not controlled by DAF-16/FOXO (Fig. 11D-F).

Interestingly, inactivation of *daf-16*, when either *let-363* (mTOR kinase) or *daf-15* (*C. elegans* RAPTOR) are inactivated leads to further induction of *lipl-1*, and this further induction is dependent on HLH-30/TFEB (Fig. 12A, B). This observation mirrors the transcriptional control of *lipl-3* in fasting (Fig. 6B) and in the *C. elegans* with inactivated *let-363* and *daf-15* (Fig. 12C, D), where *lipl-3* is further induced in fasted *daf-16* mutant animals, or in *C. elegans* with inactivated *let-363* or *daf-15*, and this further induction is HLH-30/TFEB dependent. Similarly, *lipl-1* is further induced in fasted *daf-16*, however, contrary to what we observe during mTOR inactivation, this further induction is not controlled by HLH-30 (Fig. 12E).

Figure 11

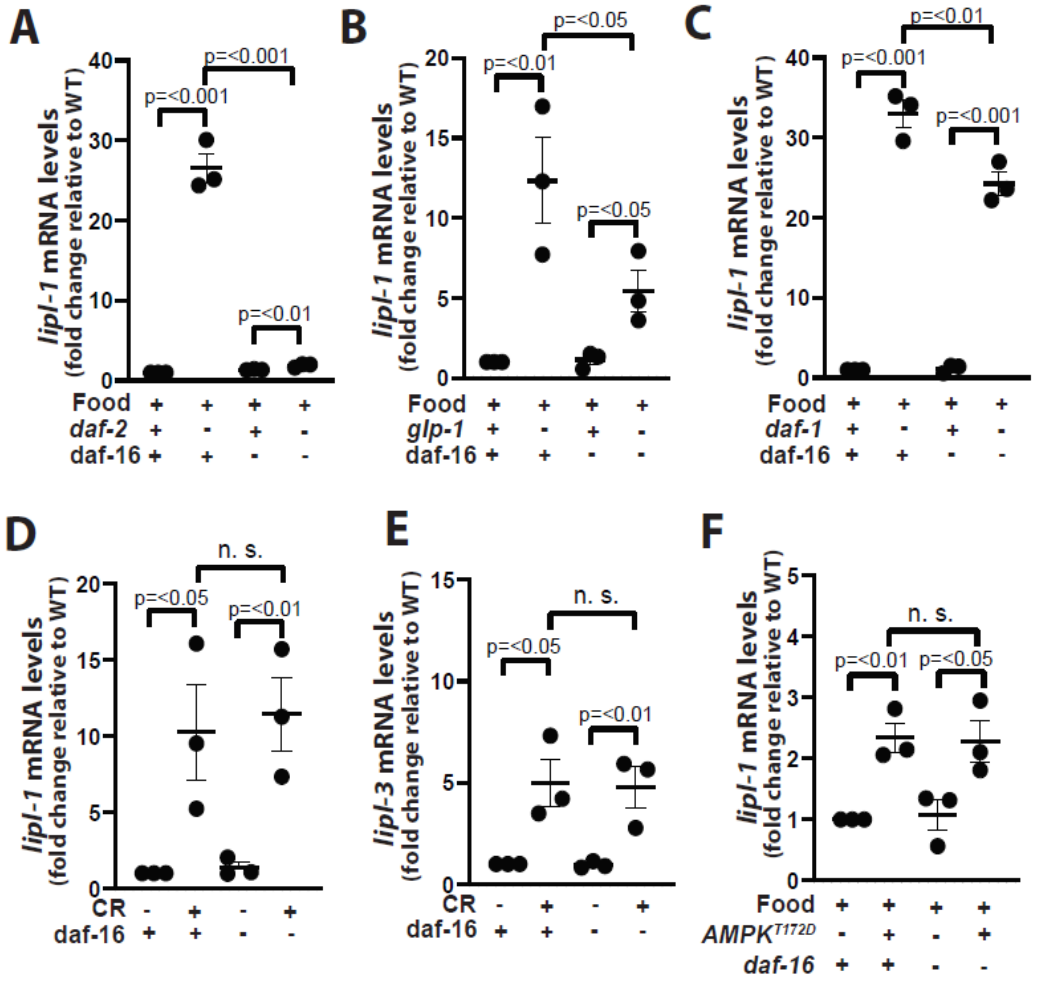
A
lipl-1 mRNA levels (fold change relative to WT)
p=<0.001
p=<0.001
p=<0.01
Food + + + +
daf-2 + - + -
daf-16 + + - -
B
lipl-1 mRNA levels (fold change relative to WT)
p=<0.05
p=<0.01
p=<0.05
Food + + + +
glp-1 + - + -
daf-16 + + - -
C
lipl-1 mRNA levels (fold change relative to WT)
p=<0.01
p=<0.001
p=<0.001
Food + + + +
daf-1 + - + -
daf-16 + + - -
D
lipl-1 mRNA levels (fold change relative to WT)
n. s.
p=<0.05
p=<0.01
CR - + - +
daf-16 + + - -
E
lipl-3 mRNA levels (fold change relative to WT)
n. s.
p=<0.05
p=<0.01
CR - + - +
daf-16 + + - -
F
lipl-1 mRNA levels (fold change relative to WT)
n. s.
p=<0.01
p=<0.05
Food + + + +
AMPKT172D - + - +
daf-16 + + - -

Fig. 11 DAF-16 controls *lipl-1* downstream of insulin, Notch, and TGF-β signaling, but not downstream of AMPK and calorically restricticted *C. elegans*

(*A-F*) qRT-PCR analysis of expression in young adult *C. elegans* normalized to housekeeping gene *ama-1* or *pmp-3* is shown relative to untreated as denoted in Y-axis. Three or more independent biological replicates are presented in all panels. Error bars denote SEM. Statistical significance was assessed via a one-tailed unpaired parametric t-test. Gene inactivations through mutation (gene name italicized) or RNAi (gene name in normal font) are represented with a minus sign in the treatment matrix. All RNAi treatments were started at the L1 stage.

(A, B, C) WT, *daf-2(e1368), glp-1(e2141), daf-1(m40)* mutants, and animals treated with RNAi against *daf-16* or empty vector control from the L1 stage. N=3

(D, E) WT animals and *eat-2(ad465)* mutants, and animals treated with RNAi against *daf-16* or empty vector control from the L1 stage. N=3

(F) WT animals and animals with constitutively active AMPK ($AMPK^{T172D}$) treated with RNAi against *daf-16* or empty vector control from the L1 stage. N=3

Figure 12

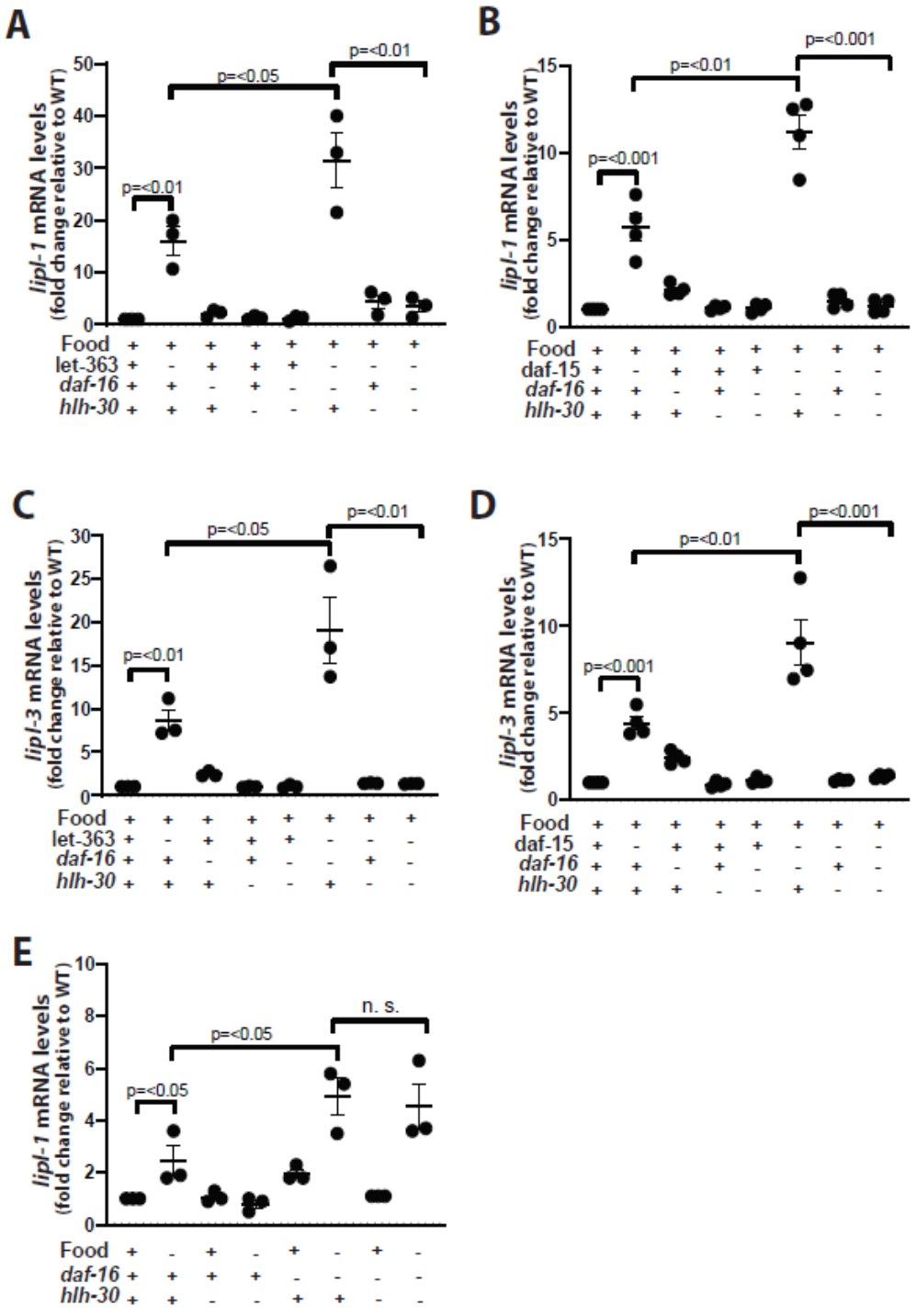
A
lipl-1 mRNA levels (fold change relative to WT)
p=<0.01
p=<0.05
p=<0.01
Food
let-363
daf-16
hlh-30
B
lipl-1 mRNA levels (fold change relative to WT)
p=<0.001
p=<0.01
p=<0.001
Food
daf-15
daf-16
hlh-30
C
lipl-3 mRNA levels (fold change relative to WT)
p=<0.01
p=<0.05
p=<0.01
Food
let-363
daf-16
hlh-30
D
lipl-3 mRNA levels (fold change relative to WT)
p=<0.001
p=<0.01
p=<0.001
Food
daf-15
daf-16
hlh-30
E
lipl-1 mRNA levels (fold change relative to WT)
p=<0.05
p=<0.05
n. s.
Food
daf-16
hlh-30

Fig. 12 DAF-16 leads to further induction of *lipl-1* downstream of mTOR inactivation or in fasted *C. elegans*

(A-E) qRT-PCR analysis of expression in young adult *C. elegans* normalized to housekeeping gene *ama-1* or *pmp-3* is shown relative to untreated as denoted in Y-axis. Three or more independent biological replicates are presented in all panels. Error bars denote SEM. Statistical significance was assessed via a one-tailed unpaired parametric t-test. Gene inactivations through mutation (gene name italicized) or RNAi (gene name in normal font) are represented with a minus sign in the treatment matrix. All RNAi treatments were started at the L1 stage.

(A-D) WT animals, *hlh-30(tm1978)* and *daf-16(mu86)* mutants treated with RNAi against *let-363 (A,C)* or *daf-15 (B,D)* or empty vector control from the L1 stage. N≥3

(E) WT animals, *hlh-30(tm1978)* and *daf-16(mu86)* mutants fasted for 6hours. N≥3

d. DAF-16/FOXO promotes *lipl-1* induction through HSF-1

Our model places HSF-1 downstream of DAF-16/FOXO in the transcriptional regulation of *lipl-3*. HSF-1 is also a likely regulator of *lipl-1* expression because we observed induction of *lipl-1* in a *C. elegans* line overexpressing HSF-1 (Fig. 13A), suggesting HSF-1 is at least sufficient to induce *lipl-1* expression. We then tested whether HSF-1 acts downstream of DAF-16/FOXO to mediate *lipl-1* induction. Indeed, *lipl-1* induction upon *daf-16* overexpression was found to be HSF-1 dependent, suggesting HSF-1 acts downstream of DAF-16/FOXO to regulate *lipl-1* expression (Fig. 13B). Additionally, induction of *lipl-1* in insulin, Notch, and TGF-β receptor mutants was also suppressed by loss of function mutation of *hsf-1* (Fig. 13C-E).

Figure 13

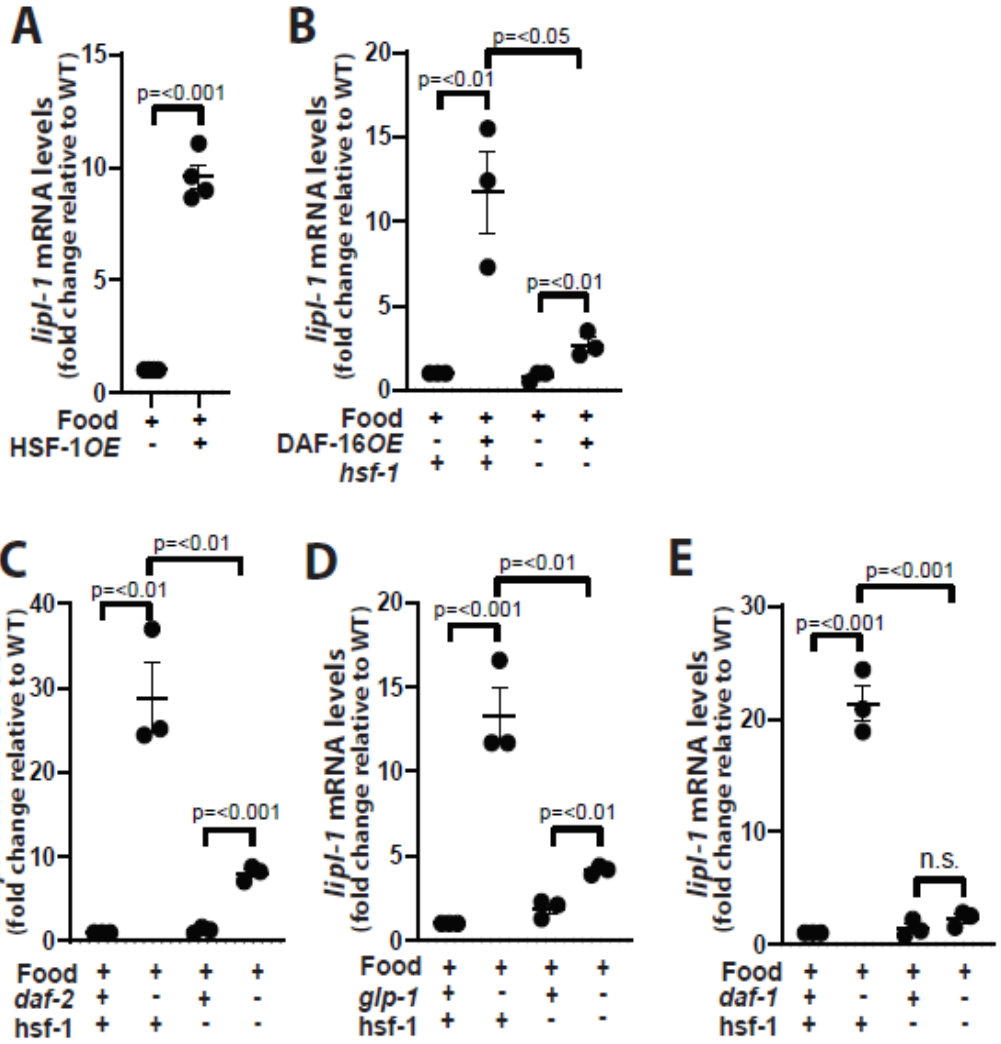
A
lipl-1 mRNA levels (fold change relative to WT)
p=<0.001
Food + +
HSF-1OE - +
B
lipl-1 mRNA levels (fold change relative to WT)
p=<0.05
p=<0.01
p=<0.01
Food + + + +
DAF-16OE - + - +
hsf-1 + + - -
C
lipl-1 mRNA levels (fold change relative to WT)
p=<0.01
p=<0.01
p=<0.001
Food + + + +
daf-2 + - + -
hsf-1 + + - -
D
lipl-1 mRNA levels (fold change relative to WT)
p=<0.01
p=<0.001
p=<0.01
Food + + + +
glp-1 + - + -
hsf-1 + + - -
E
lipl-1 mRNA levels (fold change relative to WT)
p=<0.001
p=<0.001
n.s.
Food + + + +
daf-1 + - + -
hsf-1 + + - -

Fig. 13 DAF-16/FOXO promotes *lipl-1* induction through HSF-1

(*A-E*) qRT-PCR analysis of expression in young adult *C. elegans* normalized to housekeeping gene *ama-1* or *pmp-3* is shown relative to untreated as denoted in Y axis. Three or more independent biological replicates are presented in all panels. Error bars denote SEM. Statistical significance was assessed via one-tailed unpaired parametric t-test. Gene inactivations through mutation (gene name italicized) or RNAi (gene name in normal font) are represented with a minus sign in the treatment matrix. All RNAi treatments were started at the L1 stage.

(A) WT animals and animals overexpressing HSF-1. N=3

(B) WT animals, animals overexpressing DAF-16/FOXO and DAF-16OE; *hsf-1(sy441)* double mutant. N=3

(C-E) WT, *daf-2(e1368)*, *glp-1(e2141)*, *daf-1(m40)* mutants, and animals treated with RNAi against *hsf-1* or empty vector control from the L1 stage. N=3

e. DAF-3 promotes *lipl-1* induction downstream of TGF-β signaling and SKN-1 downstream of Notch signaling

In the *daf-1* and *glp-1* mutants, DAF-16/FOXO only partially controls *lipl-1*, so there is likely another TF contributing to the *lipl-1* induction downstream of insulin and Notch signaling. We tested DAF-3 as it is one of the main effectors downstream of TGF-β (193) and it controls *lipl-3* induction downstream of *daf-1* (Fig. 3J). We also tested DAF-12, since, together with DAF-3 are the canonical TFs acting downstream of DAF-1 (193). We found that inactivation of *daf-12* leads to further enhancement of *lipl-1* expression in the *daf-1* mutant (Fig. 14A), whereas inactivation of *daf-3* almost fully suppresses *lipl-1* induction downstream of inactivated TGF-β signaling (Fig. 14B).

To determine which TF controls *lipl-1* downstream of the Notch receptor, we tested PHA-4/FOXA and SKN-1/NFR2. PHA-4/FOXA was described to control the expression of autophagy-related genes in the *C. elegans* Notch receptor mutant *glp-1* (117), and SKN-1/NFR2 was suggested to control *lipl-3* downstream of *glp-1* (115). Our results show that inactivation of PHA-4/FOXA further enhances the induction of *lipl-1* in the *glp-1* mutant (Fig. 14C), but SKN-1/NFR2 partially controls *lipl-1* expression downstream of Notch signaling (Fig. 14D), suggesting that both DAF-16/FOXO and SKN-1/NFR2 are important for the regulation of *lipl-1* downstream of Notch signaling. Whether they work in parallel or a single pathway needs further investigation.

In the case of the insulin receptor mutant *daf-2*, DAF-16/FOXO seems to be the only TF, among the tested ones that promotes the induction of *lipl-1*. We also tested DAF-12 and SKN-1/NFR2 in the *daf-2* mutant, but neither of them is necessary for induction of *lipl-1* downstream of inhibited insulin signaling (Fig. 14E, F).

Figure 14

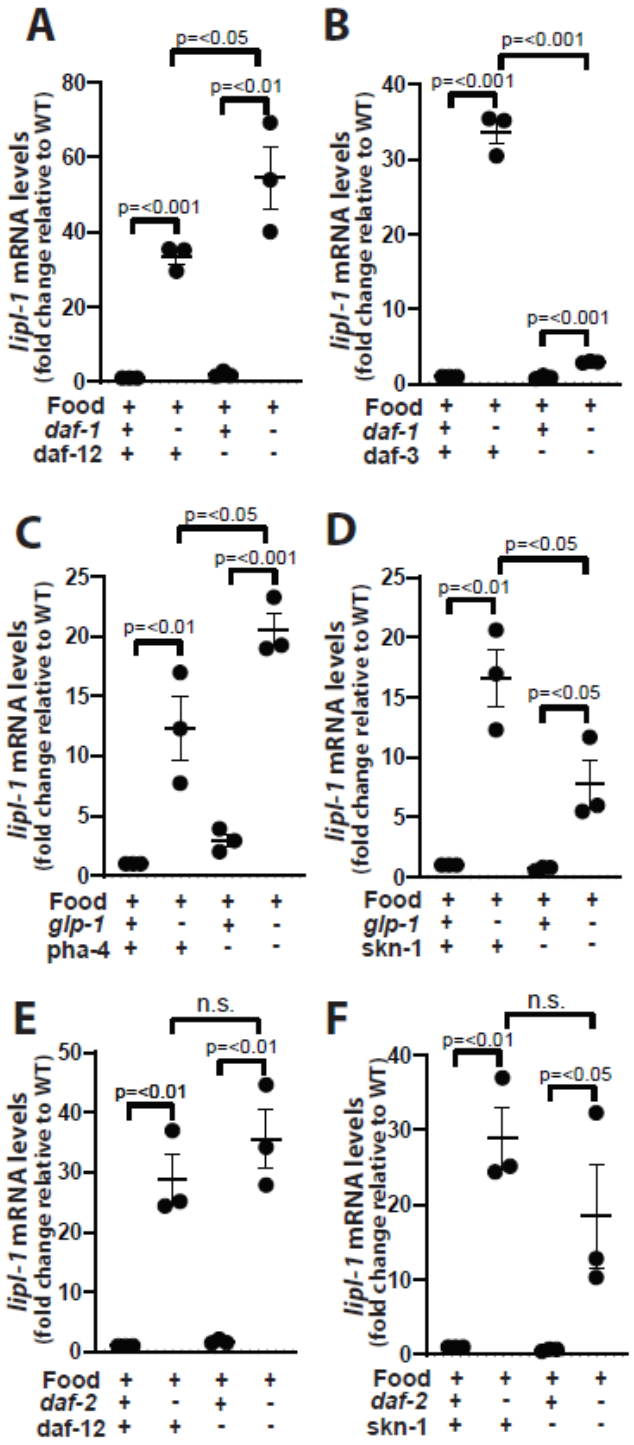
A
p=<0.05
p=<0.01
p=<0.001
lipl-1 mRNA levels (fold change relative to WT)
Food + + + +
daf-1 + - + -
daf-12 + + - -
B
p=<0.001
p=<0.001
p=<0.001
lipl-1 mRNA levels (fold change relative to WT)
Food + + + +
daf-1 + - + -
daf-3 + + - -
C
p=<0.05
p=<0.001
p=<0.01
lipl-1 mRNA levels (fold change relative to WT)
Food + + + +
glp-1 + - + -
pha-4 + + - -
D
p=<0.05
p=<0.01
p=<0.05
lipl-1 mRNA levels (fold change relative to WT)
Food + + + +
glp-1 + - + -
skn-1 + + - -
E
n.s.
p=<0.01
p=<0.01
lipl-1 mRNA levels (fold change relative to WT)
Food + + + +
daf-2 + - + -
daf-12 + + - -
F
n.s.
p=<0.01
p=<0.05
lipl-1 mRNA levels (fold change relative to WT)
Food + + + +
daf-2 + - + -
skn-1 + + - -

Fig. 14 DAF-3 promotes *lipl-1* induction downstream of TGF-β and SKN-1 downstream of Notch signaling

(*A-F*) qRT-PCR analysis of expression in young adult *C. elegans* normalized to housekeeping gene *ama-1* or *pmp-3* is shown relative to untreated as denoted in Y axis. Three or more independent biological replicates are presented in all panels. Error bars denote SEM. Statistical significance was assessed via one-tailed unpaired parametric t-test. Gene inactivations through mutation (gene name italicized) or RNAi (gene name in normal font) are represented with a minus sign in the treatment matrix. All RNAi treatments were started at the L1 stage.

(A, B) WT and *daf-1(m40)* mutants and animals treated with RNAi against *daf-12 (A)* and *daf-3 (B)* or empty vector control from the L1 stage. N=3

(C, D) WT and *glp-1(e2141)* mutants and animals treated with RNAi against *pha-4 (C)* and *skn-1 (D)* or empty vector control from the L1 stage. N=3

(E, F) WT and *daf-2(e1368)* mutants and animals treated with RNAi against *daf-12 (E)* and *skn-1 (F)* or empty vector control from the L1 stage. N=3

f. ELT-2 mediates *lipl-3* expression in calorically restricted *C. elegans*

Our previous research showed the importance of HLH-30/TFEB and DAF-16/FOXO in mediating, respectively, *lipl-3* and *lipl*-4 expression in fasting and nutrient-sensing mutants. Additionally, HLH-30/TFEB, but not DAF-16/FOXO (194), was shown to be required for the lifespan extension observed in the genetically calorically restricted *eat-2* animals (27). However, neither HLH-30/TFEB nor DAF-16/FOXO were necessary for induction of *lipl-1* in calorically restricted animals (Fig. 10G,H, 11D, E). Therefore, to find a mediator of *lipl-1* and *lipl-3* induction in calorically restricted *C. elegans*, we tested several TFs known to be involved in metabolism or lifespan extension in *eat-2* mutants including PHA-4/FOXA (124), Krüppel-like factor, KLF-1 (195), ELT-2 (196) an ortholog of human GATA4 (GATA binding protein 4), and GATA5 (GATA binding protein 5); and SKN-1 (197), an ortholog of human NFE2L1 (nuclear factor, erythroid 2 like 1); NFE2L2 (nuclear factor, erythroid 2 like 2); and NFE2L3 (nuclear factor, erythroid 2 like 3). We also tested the nuclear hormone receptor NHR-80, as the lifespan extension of *C. elegans* overexpressing *lipl-4 is* mediated by NHR-80 (189) and it has been implicated in fatty acid metabolism. However, none of the tested TFs suppressed the induction of *lipl-1* in the calorically restricted *eat-2* animals (Fig. 15A-E). In fact, *pha-4*, *klf-1* and *elt*-2 inactivation in calorically restricted animals lead to further induction of *lipl-1* (Fig. 15C-E). Therefore, further search for a TF linking *lipl-1* expression to caloric restriction in *C. elegans* is warranted. Similarly, inactivation of *pha-4* in calorically restricted worms led to further induction of *lipl-3* (Fig. 16C). By contrast, loss of *elt-2* function suppressed *lipl-3* induction in calorically restricted worms (Fig. 16A-E).

All in all, *lipl-1* and *lipl-3* are induced in calorically restricted *C. elegans*. Although we have not yet identified the TF mediating the induction of *lipl-1* in this condition, having found ELT-2 as the mediator of *lipl-3* induction in calorically restricted *C. elegans*, further points to the distinctive transcription regulation of *lipl-1* and *lipl-3* in *C. elegans*.

Figure 15

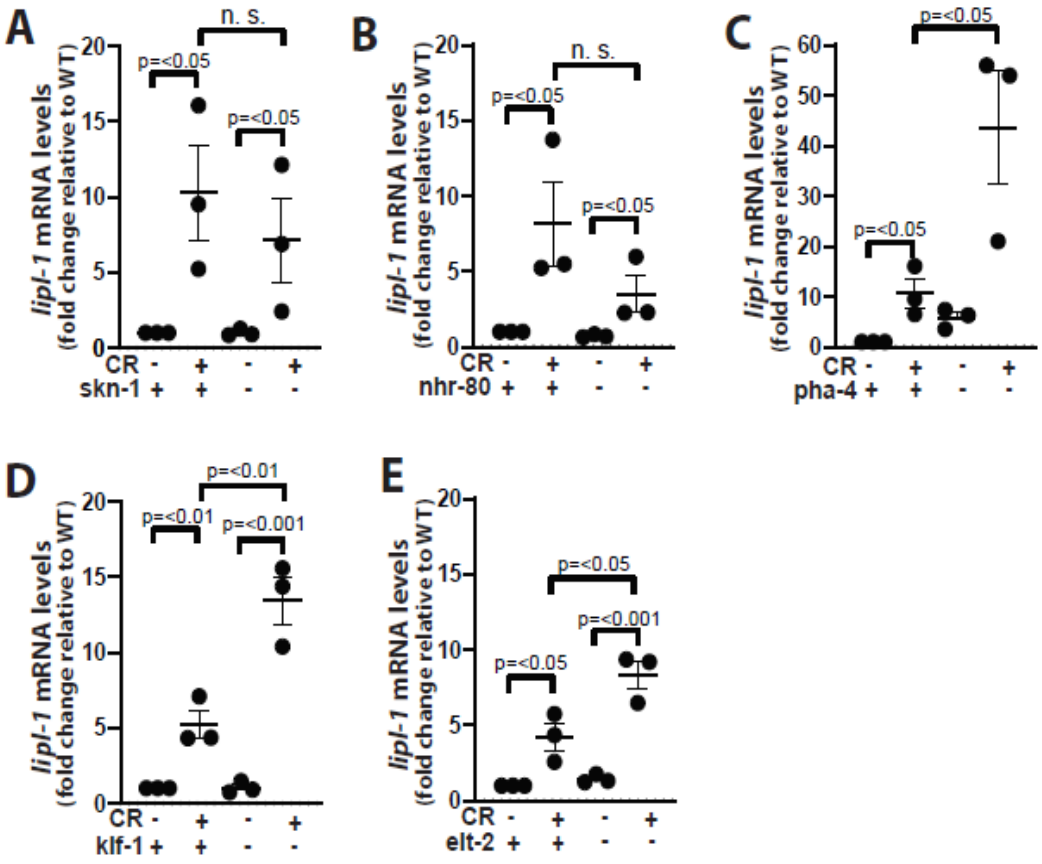
A
B
C
D
E
lipl-1 mRNA levels
(fold change relative to WT)
n. s.
p=<0.05
p=<0.01
p=<0.001
CR
skn-1
nhr-80
pha-4
klf-1
elt-2

Fig. 15 PHA-4, KLF-1 and ELT-2 inactivation in calorically restricted animals leads to enhanced activation of lipl-1 in eat-2 mutants

(*A*-*G*) qRT-PCR analysis of expression in young adult *C. elegans* normalized to housekeeping gene *ama-1* or *pmp-3* is shown relative to untreated as denoted in Y axis. Three or more independent biological replicates are presented in all panels. Error bars denote SEM. Statistical significance was assessed via one-tailed unpaired parametric t-test. Gene inactivations through mutation (gene name italicized) or RNAi (gene name in normal font) are represented with a minus sign in the treatment matrix. All RNAi treatments were started at the L1 stage.

(A-G) WT, *eat-2 (ad465)* mutants and animals treated with RNAi against *skn-1 (A), nhr-80 (B), pha-4 (C), klf-1 (D), elt-2(E)* or empty vector control from the L1 stage. N=3

Figure 16

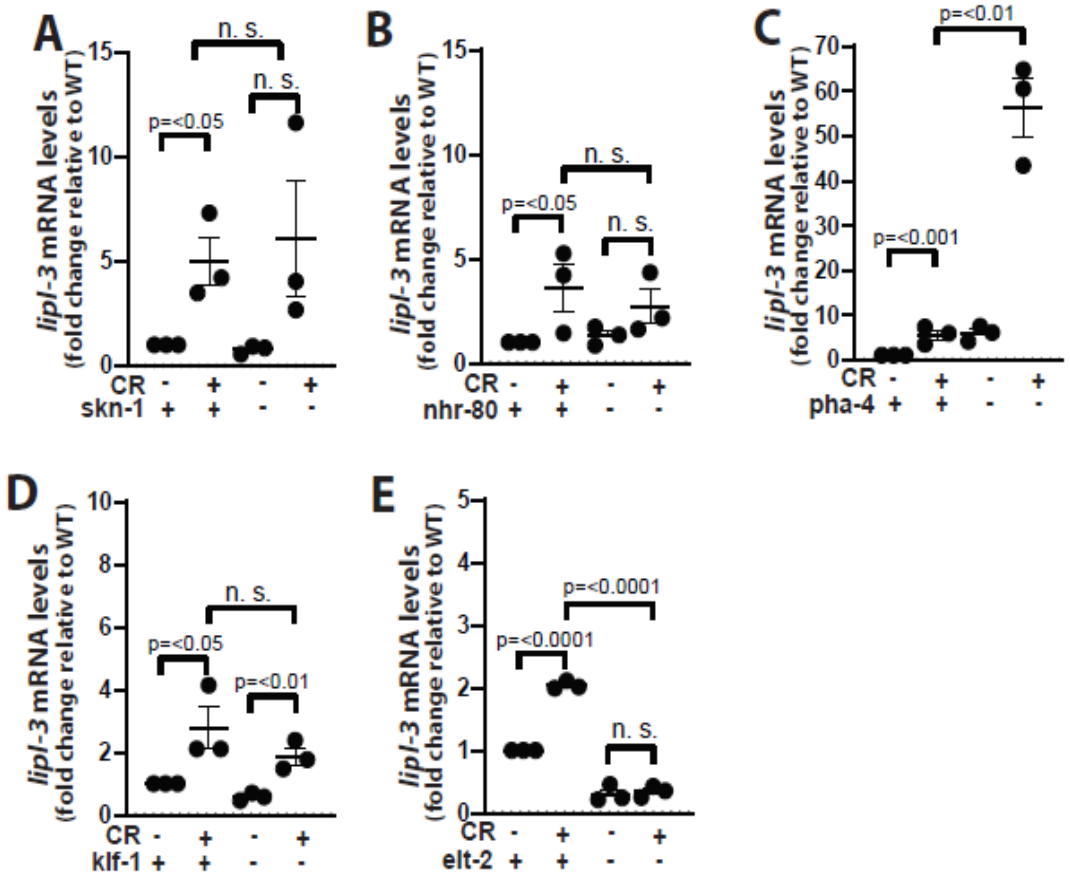
A
B
C
D
E
lipl-3 mRNA levels (fold change relative to WT)
n. s.
p=<0.05
p=<0.01
p=<0.001
p=<0.0001
CR
skn-1
nhr-80
pha-4
klf-1
elt-2

Fig. 16 ELT-2 is mediating *lipl-3* expression in calorically restricted *C. elegans*

(*A-G*) qRT-PCR analysis of expression in young adult *C. elegans* normalized to housekeeping gene *ama-1* or *pmp-3* is shown relative to untreated as denoted in Y axis. Three or more independent biological replicates are presented in all panels. Error bars denote SEM. Statistical significance was assessed via one-tailed unpaired parametric t-test. Gene inactivations through mutation (gene name italicized) or RNAi (gene name in normal font) are represented with a minus sign in the treatment matrix. All RNAi treatments were started at the L1 stage.

(A-G) WT, *eat-2 (ad465)* mutants and animals treated with RNAi against *skn-1 (A), nhr-80 (B), pha-4 (C), klf-1 (D), elt-2 (E)* or empty vector control from the L1 stage. N=3

g. Conclusions

lipl-1 and *lipl-3* were both described to have a role in breaking down the major lipid stores contained in lipid droplets in the intestine of *C. elegans* through a substrate-specific type of autophagy named lipophagy (113). Although we found similarities in the regulation of *lipl-1* and *lipl-3*, there are also several differences.

A notable similarity is that HLH-30/TFEB regulates *lipl-1* and *lipl-3* expression downstream of mTOR, but not downstream of insulin, Notch and TGF-β. Additionally, DAF-16/FOXO mediates *lipl-1* and *lipl-3* expression downstream of insulin and Notch signaling, but seemingly represses these genes in the context of fasting and mTOR inactivation. Further, the superinduction observed in *daf-16* mutants treated with RNAi against mTOR or *daf-15* is mediated by HLH-30/TFEB for both lipase genes. Also similar to the pathways linking fasting to *lipl-3* induction, *lipl-1* induction is mediated by HSF-1 downstream of insulin and Notch signaling, and HSF-1 appears to act downstream of DAF-16 in the regulation of *lipl-1*.

There are also differences between the regulation of *lipl-1* and *lipl-3*. Contrary to *lipl-3*, *lipl-1* is induced by constitutive activation of AMPK ($AMPK^{T172D}$) and it is controlled by HLH-30/TFEB in this context. In the *daf-1* mutant context, *lipl-1* and *lipl-3* induction is mediated by DAF-3. However, *lipl-1* induction is also partially mediated by DAF-16/FOXO downstream of *daf-1*, while inactivation of *daf-16* in the *daf-1* mutant context

leads to further induction of *lipl-3*. Also, DAF-12 does not play a role in *lipl-3* expression downstream of TGF-β, while it further enhances *lipl-1* expression in the *daf-1* context.

We also see differences between *lipl-1* and *lipl-3* regulation in the context of *glp-1*. We have shown that *lipl-3* expression is not affected by SKN-1 in the *glp-1* context. However, in the case of *lipl-1* we see that SKN-1 partially mediates *lipl-1* induction in *glp-1* animals. On the other hand, PHA-4/FOXA leads to further induction of both *lipl-1* and *lipl-3* in the *glp-1* context.

lipl-1 and *lipl-3* are also induced in calorically restricted *eat-2* worms. We were not able to identify the TF mediating *lipl-1* induction in *eat-2* animals; however, inactivation of the TFs *pha-4*, *klf-1* and *elt-2* led to even further induction of *lipl-1* in calorically restricted worms. Out of these 3 TFs, two affected the expression of *lipl-3* in a different manner than the expression of *lipl-1*. First, KLF-1 does not lead to further induction of *lipl-3* in calorically restricted worms, and it doesn't play a role in its induction. Second, ELT-2 regulates *lipl-3* in an opposite manner than *lipl-1* and is the sole TF that we identified mediating *lipl-3* induction in calorically restricted worms.

All in all, despite their similar roles in fat metabolism and aging, and their seemingly recent duplication, the regulation of the genes *lipl-1* and *lipl-3* differs at least in some contexts. It would be worth investigating whether *lipl-1* plays a role in the oxidative

stress in *C. elegans* just as *lipl-3* does. Even though a role for *lipl-1* in oxidative stress is likely, the distinct regulation in the *glp-1* and TGF□ contexts suggests that *lipl-1* regulation during oxidative stress may differ from that of *lipl-3*. Additionally, it would be worth investigating how the TFs that mediate the *lipl-1* expression interact with each other in different contexts and define which TFs have the capacity to bind directly to the *lipl-1* promoter to regulate its expression.

Chapter IV: Microbiota influences chemotherapeutic toxicity in *C. elegans*

1. Introduction

Multicellular organisms, including humans, live in co-evolutionary association with microorganisms that reside on and in their bodies and are known as microbiota. The composition of the microbiota differs between organisms of the same species (198), creating a unique microbial context for each organism. The microbiota is essential for the multicellular organisms that host them. It contributes factors ranging from nutrients to signals that promote development, defense from harmful microbes, and even alter behavior. Together host and microbiota are referred to as a holobiont.

In particular, the microbiota's composition and its functional capacities profoundly impact the host's metabolism and in turn its health status. For example, the microbes residing in the gastrointestinal tract of mammals and their metabolic capacities define the rate of development of the host and the likelihood of it developing diseases ranging from obesity to neurodegeneration (199,200). Nevertheless, current knowledge of the impact of host-microbiota interactions is mostly descriptive, mainly due to the complexity and the scarcity of tools to dissect these interactions *in vivo* with molecular resolution. Exceptionally, given its genetic tractability, the holobiont composed of *Escherichia coli* and *Caenorhabditis elegans* can help fill this knowledge gap.

The soil nematode *Caenorhabditis elegans* is a suitable model to gain a molecular-level understanding of the differences in host phenotypes caused by microbiota-host interactions. A healthy microbiota is indispensable for *C. elegans*' growth and reproduction (201,202). In the wild, *C. elegans* is found in association with a complex microbiota. Nevertheless, the naturally occurring microbiota can be replaced in the lab by a single-species microbiota. *C. elegans* that are grown with single species microbiotas show rates of development, reproduction, and aging that resemble the average parameters observed when co-culturing *C. elegans* with the complex mixtures of microbes associated with them in natural environments (203). Most commonly, in laboratory conditions, *C. elegans* is co-cultured with a single non-pathogenic *E. coli* strain out of the following options:

1. *E. coli* OP50, a B-derived *E. coli* strain initially chosen for *C. elegans* research because it forms a thin lawn that allows for optimal visualization of live *C. elegans* under the dissecting scope (204);

2. *E. coli* HB101, a B and K-12 hybrid *E. coli* strain that forms thicker lawns than OP50 (205);

3. *E. coli* HT115, a K-12-derived strain (206) that is competent to deliver double-stranded RNAs (dsRNA), and hence is used to perform RNA interference (RNAi) through feeding in the worm;

Each of the above *E. coli* strains creates a different environmental context for *C. elegans.* They distinctively affect life-history traits, including lifespan (101,207,208), the

response to stressors (103), and the metabolism of drugs added to the medium (209,210). Further, in some cases, using one instead of another one of these *E. coli* strains as the microbiota can change *C. elegans*' phenotypes to the extreme of being opposite, as documented for the Rictor mutant (101). Rictor is a conserved component of the mTORC2 (mechanistic Target of Rapamycin) complex with a profound impact on fat metabolism, cell survival, and cytoskeletal organization (211). *C. elegans*' Rictor mutants (*rict-1*) cultured on *E. coli* HB101 show less fat, smaller body area, smaller brood size, and longer egg-to-egg time than wild-type worms cultured on *E. coli* HB101. However, when cultured on *E. coli* OP50, the same *rict-1* mutant allele leads to increase fat accumulation, larger body size, reduced egg-to-egg time, and larger brood size than wild-type worms cultured on *E. coli* OP50 (101). Further, an independent study by Mizunuma *et al.* reports that worms with RNAi inactivated *rict-1* cultured on *E. coli* HT115 are more resistant to oxidative stress and live slightly longer than wild-type worms; whereas RNAi inactivation of *rict-1* leads to reduced oxidative stress resistance and shorter lifespan if worms are cultured on *E. coli* OP50. These reports show to which extent the microbial context influences the host's life-history traits. However, how the different *E. coli* strains distinctively influence the growth, fat, and aging phenotypes of the *rict-1* mutant worms remain to be elucidated (101,103). Similar to these examples, most published studies of microbiota-host interactions are descriptive, as they do not identify the microbe's and host's molecular mechanisms that define the phenotypic outcome of the microbiota-host interactions. To break this knowledge barrier, our lab took on the challenge of elucidating how the microbiota defines the toxicity of the chemotherapeutic drug 5'-fluorodeoxyuridine in *C. elegans*.

5’-fluorodeoxyuridine (FUdR) is an analog of the thymidine precursor 5’ deoxyuridine. *C. elegans* treated with high doses (>3µg/mL) of FUdR are sterile, as the chemotherapeutic prevents the development of the progeny. Serendipitously we observed that *C. elegans* treated with 3.1µg/mL of FUdR while cultured on *E. coli* OP50 or HT115 showed, as expected, 100% sterility (Fig. 17A). On the other hand, the toxicity of FUdR in *C. elegans* was mild to undetectable in worms cultured on *E. coli* HB101 (Fig. 17A). *E. coli* can degrade FUdR (212). Thus, the most parsimonious hypothesis was that *E. coli* HB101 was degrading FUdR more efficiently than *E. coli* OP50 or HT115. However, heat-killing the bacteria showed that killing *E. coli* HB101 did not increase the sterility in *C. elegans*, while heat-killing OP50 or HT115 reduced the toxicity (Fig. 17C), demonstrating that *E. coli* OP50 or HT115 are actively promoting FUdR toxicity in the host (96).

To identify the microbe’s metabolic pathways responsible for FUdR toxicity in *C. elegans*, we performed a three-way FUdR-*E. coli*-*C. elegans* genetic screen. We used the *E. coli* knock-out clones from the Keio collection (213). The Keio collection was made in *E.coli* BW25113 background which is a K-12-derived strain (214); hence, we first measure the toxicity of FUdR in *C. elegans* cultured on *E.coli* BW25113. The toxicity of FUdR in *C. elegans* cultured on *E.coli* BW25113 was severe and comparable to *C. elegans* cultured on *E. coli* OP50 and HT115 (Fig. 17D).

For the genetic screen, aimed at identifying the *E. coli* molecular pathway/s that promote FUdR toxicity in the worm, we cultured *C. elegans* on the Keio library mutants and the wild-type (WT) *E.coli* BW25113 strain as negative control, and then added FUdR. If an *E. coli* gene (knocked out in the Keio mutant clone) was encoding a protein critical to the capacity of *E coli* to promote FUdR toxicity in *C. elegans*, we would observe reduced or no sterility (toxicity) in worms cultured in that *E. coli* knock-out clone. Using this rationale, we identified *E. coli* genes that, when knocked out, suppress FUdR toxicity in *C. elegans* (suppressor genes), meaning they are required for *E. coli* BW25113 to promote FUdR toxicity in *C. elegans*. We also identified *E. coli* genes that when knocked out, further increase FUdR toxicity in *C. elegans* (enhancer genes). Put together through metabolic modeling, we found out that most hit genes (suppressors and enhancers) belong to the pyrimidine ribonucleotide salvage pathway (Fig. 17E). The *E. coli* KO clones that suppress toxicity in *C. elegans* include *deoA*, *udp upp*, and *udk* (orange font in Fig. 17F); enzymes necessary to convert FUdR into FUMP (fluorouracil monophosphate). By contrast, KO of enzymes diverting FUdR from its conversion into FUMP (*Ndk, YjjG, Tdk*) enhances *E. coli*-mediated FUdR toxicity (green font Fig.17F). The hypothesis was then that when FUdR is added to the medium, it hijacks the *E. coli* pyrimidine ribonucleotide salvage pathway, which FUdR into its ribonucleotide derivative FUMP (Fig. 17F). I then contributed to biochemically testing the hypothesis that the *E.coli* strains OP50 and HT115 produce more FUMP than *E.coli* HB101 when exposed to the same dose of FUdR.

We tested this hypothesis through LCMS-based metabolomic profiling of the three *E. coli* strains. After analyzing four independent biological replicates of the 3 *E coli* strains mock or FUdR-treated, we identified several metabolites that correlated with the capacity of the *E.coli* strains to promote FUdR toxicity in *C. elegans*, including thymidine and serine, which were further characterized (96). However, critical to our hypothesis, and in tune with the predictions of our model, we observed that *E. coli* HB101 shows lower levels of FUMP compared to *E. coli* OP50 or HT115 treated with the same dose of FUdR (Fig. 17G). Therefore, we asked the question: What genomic differences between the three *E. coli* strains are responsible for the difference in their capacities to convert FUdR into its toxic derivative FUMP? In other words, what genes are missing from *E. coli* HB101 that make this strain less capable of converting FUdR to FUMP. To answer this, we employed *E. coli* genome sequencing coupled with modeling the *E. coli* metabolism. We aimed to create *E. coli* metabolic models able to predict the phenotypic outcome of biomedically relevant host-microbe interactions.

Figure 17

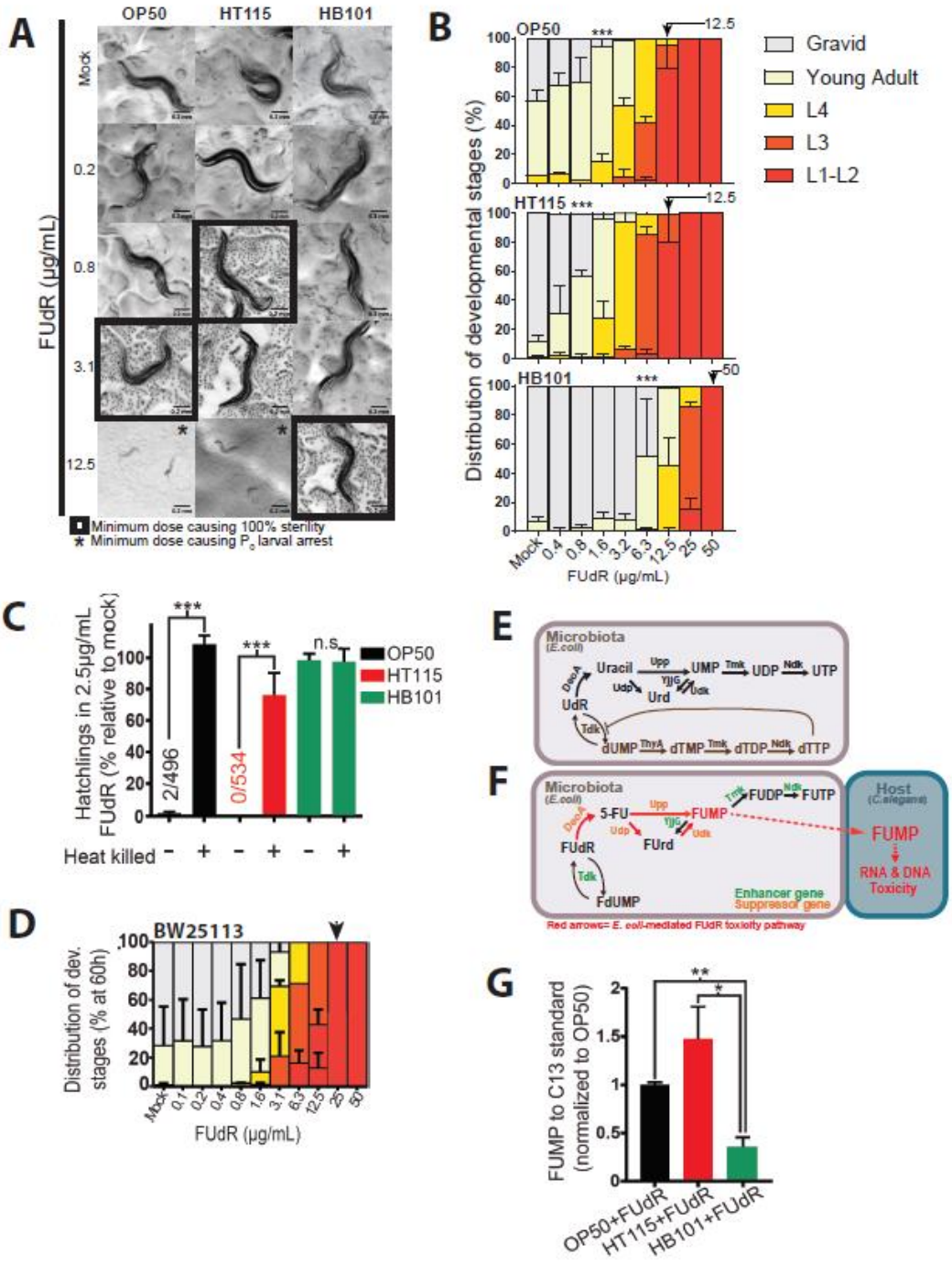
A
OP50
HT115
HB101
Mock
0.2
0.8
3.1
12.5
FUdR (µg/mL)
Minimum dose causing 100% sterility
Minimum dose causing P0 larval arrest
B
OP50
HT115
HB101
***
12.5
50
Gravid
Young Adult
L4
L3
L1-L2
Distribution of developmental stages (%)
Mock
0.4
0.8
1.6
3.2
6.3
12.5
25
50
FUdR (µg/mL)
C
Hatchlings in 2.5µg/mL FUdR (% relative to mock)
2/496
0/534
n.s
OP50
HT115
HB101
Heat killed
D
BW25113
Distribution of dev. stages (% at 60h)
FUdR (µg/mL)
E
Microbiota
(E.coli)
Uracil
UMP
UDP
UTP
UdR
Urd
dUMP
dTMP
dTDP
dTTP
F
Microbiota
(E.coli)
5-FU
FUMP
FUDP
FUTP
FUdR
FUrd
FdUMP
Host
(C.elegans)
FUMP
RNA & DNA Toxicity
Enhancer gene
Suppressor gene
Red arrows= E. coli-mediated FUdR toxicity pathway
G
FUMP to C13 standard (normalized to OP50)
**
*
OP50+FUdR
HT115+FUdR
HB101+FUdR

Fig. 17 The microbe variant defines whether the same dose of FUdR is innocuous or lethal.

(A) Worms fed different *E. coli* strains show up to 16-fold difference in FUdR-induced sterility (20°C). Quantification of hatchlings at the most differential dose (3.1µg/mL) is shown to the right. Images representing N ≥10 are depicted. Quantification from N=3, but the result confirmed ≥10 times. Error bars represent S.E.M. credit Jake Saba.

(B) Worms fed different E. coli strains show up to a 4-fold difference in FUdR-induced developmental arrest (20°C). Key to the right. Asterisks denote the minimum FUdR dose showing a significantly delayed developmental rate ($p<0.001$) relative to mock treated for each strain. Black arrowheads indicate minimum dose rendering ≥50% arrest as L1-L2s after 60h at 20°C. Whole dose-response curve N=2; minimum dose eliciting differential arrest confirmed ≥10 times, credit Jake Saba.

(C) Killing E. coli abrogates the E. coli-defined FUdR-toxicity difference in the host. Antibiotic cleaned L4 worms were transferred to 2.5µg/mL FUdR plates seeded with heat-killed *E. coli* bacteria, and hatchlings were counted 36h later. N=4. credit Jake Saba.

(D) FUdR dose response (developmental delay) curves are displayed for worms cultured on BW25113. Arrowheads indicate the minimum FUdR concentration required for >50% of

worms to arrest as L1-L2. N=2. credit Jake Saba.

(E) Schematic of pyrimidine ribonucleotide salvage pathway (black font) and dTMP de novo synthesis pathway (brown font). Adapted from Ke *at el.* (96)

(F) Model of *E. coli*-mediated FUdR-to-FUMP toxicity pathway. Adapted from Ke *at el (96)*

(G) Levels of FUMP, the predicted major toxic derivative of FUdR, correlate with degree of

toxicity observed in worms fed the 3 lab *E. coli* strains. LC/MS-determined FUMP abundance

relative to the C13 standard and normalized to OP50 within each biological replicate is depicted.

N=3.

2. Results

2.1. *E.coli* genome sequencing allows for the building of strain-specific *E. coli* models

E. coli metabolizes FUdR to its more toxic derivative FUMP. FUMP is toxic to *C. elegans,* and exposure to FUMP results in embryonic lethality. Different *E. coli* strains have distinct capacities to metabolize FUdR into FUMP, which manifests in varied levels of sterility in *C. elegans* exposed to the same dose of FUdR but cultured on different *E. coli* strains. Therefore, we asked the question: What genomic differences between the *E. coli* strains account for their differential capacities to convert FUdR into FUMP? In our specific case study, what genes are missing from *E. coli* HB101 that make this strain less capable of converting FUdR to FUMP? Furthermore, can genome sequencing of the microbiota coupled to metabolic modeling allow us to predict the phenotypic outcome of a host-microbe interaction?

To identify the genomic differences between *E. coli* strains that may define their differential capacities to promote FUdR toxicity in *C. elegans*, we sequenced the genomes of *E. coli* HB101, OP50, and HT115 at >100X coverage and assembly N50 >80,000 (NCBI Bio Project Accession #PRJNA394610). We also retrieved the publicly available genome sequence of *E. coli* BW25113 and *E. coli* MG1655; the latter being a K-12 derived strain that served as a reference strain for creating the first *in silico* metabolic model of *E. coli* (215). With the genome sequences in hand and information

regarding *E. coli* metabolism available in the databases BiGG (216), KEGG (217), PubChem (218,219), and Biocyc (220,221), our collaborators in Dr. Nathan Lewis's team at UCSD built metabolic models for each strain.

2.2. *E. coli* strains commonly used to culture *C. elegans* have different metabolic capacities

To identify the genomic differences between *E. coli* strains that may define their differential capacities to promote FUdR toxicity in *C. elegans*, we sequenced the genomes of *E. coli* HB101, OP50, and HT115 at >100X coverage and assembly N50 >80,000 (NCBI Bio Project Accession #PRJNA394610). We also retrieved the publicly available genome sequence of *E. coli* BW25113 and *E. coli* MG1655, the latter being a K-12 derived strain that served as a reference strain for creating the first *in silico* metabolic model of *E. coli* (215). With the genome sequences in hand and information regarding *E. coli* metabolism available in the databases BiGG (216), KEGG (217), PubChem (218,219), and Biocyc (220,221), our collaborators in Dr. Nathan Lewis's team at UCSD built metabolic models for each strain..

The first type of discrepancy is when the model predicts that bacteria will not grow on a given carbon source, but the experimental data show that bacteria actually grow. From the modeling perspective, this would be a false negative. Most likely, an enzyme, transporter, or reaction is missing from the model. It is possible that a missing component

of the model was not described in the literature before, such as an unknown enzymatic activity, and therefore we have not added it to the model. Another possibility is that a known enzymatic activity is carried out by an uncharacterized protein class, whose primary sequence does not allow us to link it to the enzymatic function missing in the model. Another reason for modeling-false negatives can be incorrect reaction directionality, wrongly included biomass components, wrongly excluded exogenous substrates, or too stringent regulation during modeling. In the latter case, modeling conditions will be relaxed to fit the experimental data since the goal is to develop a model that is consistent with the experimental data.

The second type of inconsistency is modeling-false positives. False positives occur when the model predicts growth of bacteria in a particular condition, but experimental data show that the bacteria cannot grow in that condition. Reasons for false positives include wrongly included metabolic capacity for a given gene/enzyme, incorrect reaction directionality, wrongly included components for biomass growth, or too loosely defined regulation. In this case, we will need to remove reactions or genes from the metabolic network or change the network's parameters. There are many reactions/genes that, when removed from the model, will result in lack of growth of the bacteria. The challenge is to find the correct reactions or genes to be removed. There are already computational tools that aid in this search (222).

Using the commercially available phenotypic screening system BIOLOGS (223), I experimentally tested the predictions of the models. BIOLOGS plates allow testing of bacteria growth on minimal media supplemented with known concentrations of single or combined metabolites. In the BIOLOG plates that I specifically used, each well has only one carbon source. I performed 3 independent biological replicates testing 285 growth conditions for each of the 4 previously untested *E. coli* strains (HT115, OP50, HB101, and BW25113). In parallel I tested in all the same conditions the previously characterized *E. coli* strain, MG1655, as our "experimental accuracy" control. Based on the criteria defined above, our collaborators will be able to identify false positives and false negatives predicted by the model. Findings on the growth capacities of the 5 strains are summarized in Table 1. Our collaborators will use my experimental data to refine the models of the 4 strains previously lacking models.

When comparing the *E. coli* strains' metabolic models, we found 32 genes uniquely absent or present in *E. coli* OP50, 16 genes unique to *E. coli* HT115, and 37 genes unique to *E. coli* HB101 (complete list of uniquely absent or present genes in Table 2). Importantly, from the 4 *E. coli* strains we modeled, we had defined that *E. coli* HB101 had the lowest capacity to mediate FUdR toxicity. Based on our previous experiments, we knew that the severity of the toxicity in *C. elegans* depends on the active bioconversion of FUdR into its toxic derivative FUMP carried out by *E. coli*. Then, we hypothesized that with this knowledge and the models in hand, we could pinpoint the genetic differences between *E. coli* HB101 and the other strains that made HB101 a

poorer FUdR convertor. We identified 36 gene functions that were absent in *E. coli* HB101 when compared to *E. coli* HT115, OP50, and BW25113. From those, we identified two *E. coli* genes directly linked to nucleotide metabolism, *crp* and *gpt*, that were predicted to be uniquely absent in HB101 and hence were likely to be responsible, at least partially, for the lower capacity of HB101 to convert FUdR into FUMP.

Crp is a cAMP-responsive transcription factor. Cpr regulates the expression of many *E. coli* genes, including *deoA* and *udp*, 2 genes we demonstrated to be required in *E coli* to promote FUdR toxicity in *C. elegans* (Fig. 17F). *E. coli* HB101 version of *crp* has a point mutation that substitutes hydrophilic threonine in position 127 to aliphatic isoleucine. It has been previously shown that substitution of threonine in position 127 significantly decreases Crp's ability to activate transcription (224). Therefore, we hypothesized that reduced Crp transcriptional activity in *E. coli* would lead to a reduced FUdR toxicity in *C. elegans*. To test this hypothesis, we used *E. coli* BW25113 *cpr* mutant, and I initiated the process of knocking out *crp* in the OP50 and HT115 backgrounds. If *E. coli* Crp is critical to FUdR toxicity in *C. elegans*, we should observe increased fertility in worms treated with FUdR when cultured in the *crp*-KO derivatives of BW25113, OP50, and HT115. Indeed, when comparing hatchling survival, we observed a >40% increased in fertility in worms treated with FUdR while cultured on BW25113-*crp* KO when compared to wild-type BW25113 (Fig. 18B). These results demonstrate the critical role of *E. coli* Crp in promoting FUdR toxicity in *C. elegans*, and point to the value of

sequencing the microbes's genome (microbiome) to predict the phenotypic outcome of host-microbe interactions.

gpt encodes a purine-salvage enzyme responsible for the conversion of inosine, xanthine and guanosine, into inosine monophosphate (IMP), xanthosine monophosphate (XMP) and guanosine monophosphate (GMP), respectively (225) (Fig. 15B). IMP, XMP, and GMP are substrates of the YjjG enzyme, YjjG can also use FUMP as a substrate to convert it into the less toxic derivative fluorouridine (FUrd) (226,227). Hence, in a condition where there is less IMP, XMP, and GMP (as in the *gpt* mutant), E coli can more effectively convert FUMP into FUrd, which would reduce the amount of FUMP, and hence toxicity in the host (Fig. 18C). To define whether reduced Gpt activity in *E. coli* may be sufficient to reduce FUdR toxicity in *C. elegans*, once again, we tested the capacity to mediate toxicity of a *gpt* mutant built in the *E. coli* BW25113, which is otherwise capable to promote toxicity in *C. elegans*. Indeed, we observed that single knock out of *gpt* in *E. coli* BW25113 was sufficient to reduce FUdR toxicity by ~20% in *C. elegans* (Fig. 18D).

To further test our hypothesis that *gpt* and *crp* are responsible for the lower capacity of HB101 to mediate FUdR toxicity in *C. elegans*, I complemented *E. coli* HB101 with plasmids expressing functional copies of *crp* or *gpt*. Complementing *E. coli* HB101 with functional copies of *crp* or *gpt* resulted in increased FUdR toxicity in *C.*

elegans, which manifested as 65% and 51% more dead embryos and 58% and 48% fewer hatchlings, respectively, than those observed in worms cultured on the ancestral *E.coli* HB101 strain (Fig. 18E). However, the severity of the toxicity was reduced compared to the toxicity observed in worms cultured in *E. coli* HT115 or OP50; hence, in the future, we need to obtain *E. coli* HB101 bacteria co-expressing wild type versions of both *crp* and *gpt*. Nevertheless, the data confirm that *crp* and *gpt* contribute to *E. coli*-mediated FUdR toxicity in *C. elegans*, and support the notion that combining microbe genome sequencing with metabolic modeling may allow us to predict the health outcome of microbe-host interactions.

Figure 18

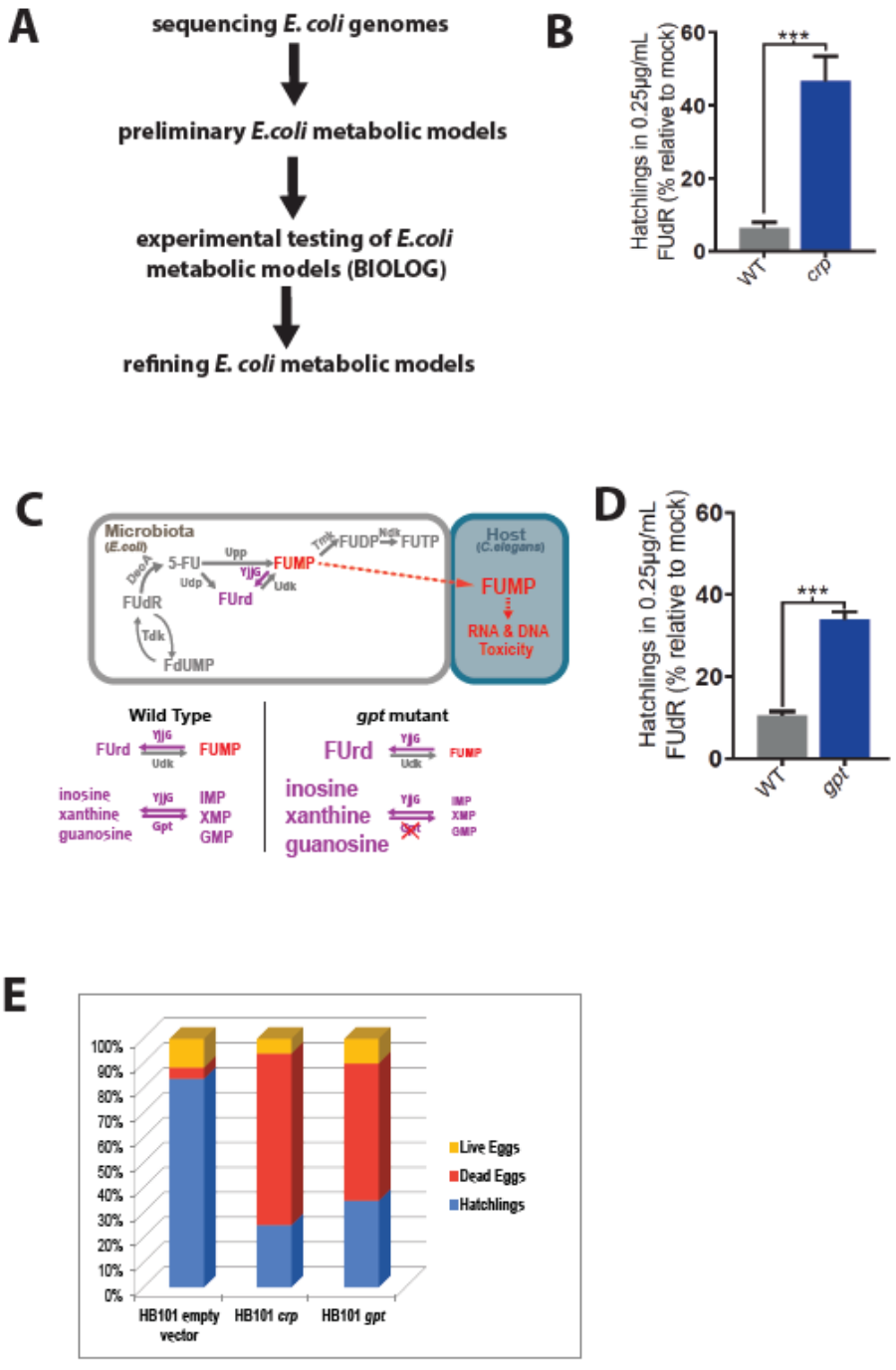
A
sequencing E. coli genomes
preliminary E.coli metabolic models
experimental testing of E.coli metabolic models (BIOLOG)
refining E. coli metabolic models
B
Hatchlings in 0.25µg/mL FUdR (% relative to mock)
60
40
20
0
***
WT
crp
C
Microbiota (E.coli)
Host (C.elegans)
5-FU
Upp
FUMP
FUDP
FUTP
FUdR
FUrd
FdUMP
Tdk
Udk
Ndk
FUMP
RNA & DNA Toxicity
Wild Type
gpt mutant
FUrd
FUMP
inosine
xanthine
guanosine
IMP
XMP
GMP
yjjG
Gpt
D
Hatchlings in 0.25µg/mL FUdR (% relative to mock)
60
40
20
0
***
WT
gpt
E
100%
90%
80%
70%
60%
50%
40%
30%
20%
10%
0%
HB101 empty vector
HB101 crp
HB101 gpt
Live Eggs
Dead Eggs
Hatchlings

Fig. 18 *crp* and *gpt* influence the capacity of *E. coli* HB101 to mediate FUdR toxicity

(A) Outline of the *E. coli* metabolic model building workflow

(B) Loss of the cAMP-regulated transcription factor crp is sufficient to partially suppress BW25113-mediated FUdR toxicity. FUdR 0.25μg/mL 25°C. N=2. credit Jake Saba

(C) Relation between pyrimidine salvage pathway and Gpt. Adapted from Ke *et al.* (96)

(D) Loss of the ribonucleoside monophosphate synthesis enzyme gpt is sufficient to partially suppress BW25113-mediated FUdR toxicity. FUdR 0.25μg/mL 25°C. N=2. credit Jake Saba

(E) Quantification of the number of hatchlings, dead eggs and live eggs in *C. elegans* co-cultured with *E. coli* HB101 complemented with the plasmids expressing *crp*, *gpt* or empty vector, with FUdR added to the plate (0.5 μl/ml).

3. Future directions

Metabolic network modeling has proven useful in developing new strains of microorganisms, understanding drug resistance, and aiding in drug discovery (228–230). Metabolic networks for microorganisms (i.e., *E. coli* (228)) and cells in culture (i.e., CHO cells (231)) have been created. Multicellular organisms follow with two *C. elegans*' metabolic networks created in 2016 (232,233) and a second version of the human metabolic network released in 2016 (recon 2) (234) and a third (recon3D) in early 2018 (235). Due to the microbiota's critical role in host health, models representing the interactions between humans and its microbiota have been created recently (236).

The data obtained in this study has potential for translation to the clinic. The mechanistic understanding of the drug-microbiome-host interaction presented here can be incorporated into mammalian microbiome-host models that may assist chemotherapeutic dosing in the future. Therefore, it would be worth sequencing the microbiome of cancer patients' treated with fluoropyrimidines and defining whether we can predict the toxicity of the treatment based on the predicted metabolic capabilities of each patient's unique microbiome. Another benefit of our work is creating metabolic models of the *E. coli* strains commonly used in *C. elegans* research, which can accelerate further research into other microbiome-host interactions potentially relevant to mammalian health.

4. Materials and Methods

Measuring bacterial growth using BIOLOGS plates

E. coli bacteria strains were grown overnight in the rich media (LB). On the next day, 1/100 dilutions were made, and bacteria were allowed to grow until reaching OD of ~0.25-0.5. Bacteria were transferred to 1.5ml Eppendorf tubes and centrifuged for 1 min at 10,000 rcf. Supernatant was removed, and bacteria were washed 4x in sterile water (this is to wash out all rich culture media). After discarding the last wash, bacteria were suspended in 1mL inoculating fluid (IF-0). To the *E. coli*, OP50 suspension uracil suspension was added to the final concentration of 0.5 mg/mL. 100µl of bacteria suspension was added to each well of BIOLOG plates. Additionally, for PM3 and PM4 plates 2M sodium succinate/200uM ferric citrate (100X) was added. Plates were incubated with the lid on and Breath Easy cover at 37C with max shaking (750rpm), and OD was measured every 12h for four days.

FUdR toxicity assay

C. elegans were grown on NGM plates with FUdR (concentration of FudR is indicated in each figure) from the L1 larvae stage until adulthood. Once the *C. elegans* on the control plates were able to lay eggs and the progeny had enough time to hatch, images were taken, and the number of eggs and hatchlings was quantified.

5. Tables

Table 1. Growth (measured by OD) of the *E.coli* strains MG1655, BW25113, OP50, HT115, HB101 on different metabolites

	MG1655	BW25113	OP50	HT115	HB101
L-Arabinose	0.36	0.02	0.36	0.19	0.11
N-Acetyl-DGlucosamine	0.22	0.26	0.39	0.19	0.14
D-Saccharic Acid	0.30	0.30	0.14	0.28	0.13
Succinic Acid	0.24	0.27	0.23	0.15	0.16
D-Galactose	0.37	0.37	0.46	0.26	0.20
L-Aspartic Acid	0.34	0.34	0.26	0.02	0.15
L-Proline	0.53	0.52	0.43	0.13	0.19
D-Alanine	0.45	0.47	0.26	0.37	0.19
D-Trehalose	0.26	0.31	0.39	0.25	0.20
D-Mannose	0.25	0.30	0.36	0.20	0.15
Dulcitol	0.34	0.42	0.40	0.02	0.12
D-Serine	0.21	0.23	0.23	0.20	0.19
D-Sorbitol	0.32	0.39	0.43	0.33	0.24
Glycerol	0.23	0.25	0.26	0.21	0.18
L-Fucose	0.23	0.30	0.17	0.34	0.21
D-Glucuronic Acid	0.35	0.32	0.39	0.31	0.19
D-Gluconic Acid	0.42	0.35	0.42	0.36	0.20
D,L-α-GlycerolPhosphate	0.20	0.20	0.30	0.14	0.10
D-Xylose	0.31	0.38	0.39	0.26	0.14
L-Lactic Acid	0.17	0.20	0.19	0.14	0.17
Formic Acid	0.02	0.09	0.08	0.02	0.06
D-Mannitol	0.22	0.23	0.37	0.24	0.16
L-Glutamic Acid	0.07	0.13	0.44	0.03	0.12
D-Glucose-6- Phosphate	0.38	0.36	0.38	0.29	0.23
D-Galactonic Acid-γ-Lactone	0.34	0.36	0.37	0.36	0.21
D,L-Malic Acid	0.36	0.34	0.31	0.09	0.14
D-Ribose	0.20	0.23	0.41	0.24	0.13
Tween 20	0.05	0.05	0.07	0.07	0.12
L-Rhamnose	0.26	0.08	0.37	0.25	0.24
D-Fructose	0.24	0.27	0.37	0.23	0.15
Acetic Acid	0.19	0.18	0.11	0.12	0.11
α-D-Glucose	0.21	0.22	0.45	0.21	0.17
Maltose	0.21	0.34	0.47	0.25	0.13
D-Melibiose	0.26	0.42	0.44	0.29	0.14
Thymidine	0.21	0.31	0.26	0.20	0.20
L-Asparagine	0.30	0.31	0.24	0.14	0.12
D-Aspartic Acid	0.00	0.04	0.07	0.02	0.01
D-Glucosaminic Acid	0.04	0.11	0.16	0.04	0.05
1,2-Propanediol D5 T	0.06	0.11	0.11	0.04	0.06
Tween 40	0.05	0.08	0.07	0.07	0.08
α-Keto-Glutaric Acid	0.37	0.36	0.26	0.24	0.17
α-Keto-Butyric Acid	0.20	0.20	0.07	0.18	0.09
α-Methyl-DGalactoside	0.41	0.42	0.37	0.34	0.15

	MG1655	BW25113	OP50	HT115	HB101
α-D-Lactose	0.22	0.12	0.41	0.23	0.10
α-D-Lactose	0.33	0.12	0.39	0.26	0.09
α-D-Lactose	0.08	0.14	0.07	0.05	0.03
Uridine	0.32	0.35	0.39	0.33	0.18
L-Glutamine	0.37	0.33	0.24	0.08	0.18
m-Tartaric Acid	0.28	0.31	0.27	0.04	0.13
D-Glucose-1- Phosphate	0.31	0.30	0.40	0.29	0.18
D-Fructose-6- Phosphate	0.34	0.34	0.31	0.21	0.15
Tween 80	0.04	0.01	0.02	0.09	0.09
α-Hydroxy Glutaric Acid-γLactone	0.04	0.03	0.07	0.03	0.02
α-Hydroxy Butyric Acid	0.12	0.18	0.06	0.14	0.05
ß-Methyl-DGlucoside	0.41	0.42	0.22	0.26	0.18
Adonitol	0.04	0.05	0.06	0.03	0.04
Maltotriose	0.23	0.31	0.22	0.23	0.15
2-Deoxy Adenosine	0.27	0.36	0.33	0.19	0.14
Adenosine	0.18	0.23	0.23	0.18	0.15
Glycyl-L-Aspartic Acid	0.38	0.43	0.25	0.29	0.19
Citric Acid	0.03	0.04	0.08	0.01	0.03
myo-Inositol	0.04	0.06	0.12	0.04	0.04
D-Threonine	0.06	0.06	0.08	0.02	0.07
Fumaric Acid	0.35	0.30	0.23	0.03	0.20
Bromo Succinic Acid	0.23	0.19	0.15	0.03	0.09
Propionic Acid	0.32	0.35	0.10	0.20	0.14
Mucic Acid	0.39	0.34	0.30	0.27	0.13
Glycolic Acid	0.35	0.37	0.19	0.24	0.10
Glyoxylic Acid	0.17	0.27	0.24	0.14	0.05
D-Cellobiose	0.02	0.07	0.08	0.03	0.05
Inosine	0.35	0.38	0.34	0.31	0.17
Glycyl-LGlutamic Acid	0.33	0.38	0.28	0.26	0.23
Tricarballylic Acid	0.01	0.03	0.12	0.02	0.07
L-Serine	0.38	0.32	0.35	0.24	0.16
L-Threonine	0.20	0.23	0.26	0.15	0.12
L-Alanine	0.38	0.39	0.23	0.38	0.20
L-Alanyl-Glycine	0.44	0.46	0.28	0.44	0.19
Acetoacetic Acid	0.05	0.04	0.03	0.03	0.03
N-Acetyl-ß-DMannosamine	0.37	0.46	0.38	0.30	0.12
Mono Methyl Succinate	0.02	0.05	0.07	0.04	0.04
Methyl Pyruvate	0.15	0.22	0.22	0.21	0.16
D-Malic Acid	0.33	0.33	0.27	0.03	0.09
L-Malic Acid	0.26	0.28	0.22	0.04	0.16
Glycyl-L-Proline	0.43	0.53	0.46	0.29	0.22
p-Hydroxy Phenyl Acetic Acid	0.01	0.00	0.43	0.01	0.02
m-Hydroxy Phenyl Acetic Acid	0.00	0.02	0.50	0.01	0.02
Tyramine	0.01	0.00	0.01	0.01	0.01

	MG1655	BW25113	OP50	HT115	HB101
D-Psicose	0.05	0.10	0.08	0.04	0.06
L-Lyxose	0.25	0.01	0.23	0.01	0.02
Glucuronamide	0.09	0.10	0.11	0.09	0.04
Pyruvic Acid	0.25	0.21	0.16	0.14	0.20
L-Galactonic Acid-γ-Lactone	0.26	0.27	0.26	0.25	0.14
D-Galacturonic Acid	0.32	0.34	0.25	0.31	0.14
Phenylethylamine	0.01	0.02	0.00	0.00	0.01
2-Aminoethanol	0.00	0.03	0.00	0.01	0.02
Ammonia	0.29	0.31	0.14	0.07	0.05
Nitrite	0.05	0.02	0.01	0.00	0.02
Nitrate	0.03	0.02	0.01	0.02	0.04
Urea	0.02	0.04	0.04	0.02	0.05
Biuret	0.04	0.04	0.04	0.02	0.02
L-Alanine	0.34	0.40	0.36	0.14	0.05
L-Arginine	0.29	0.34	0.16	0.07	0.05
L-Asparagine	0.46	0.44	0.32	0.23	0.13
L-Aspartic Acid	0.32	0.33	0.21	0.05	0.06
L-Cysteine	0.51	0.47	0.28	0.04	0.02
L-Glutamic Acid	0.27	0.23	0.31	0.02	0.04
L-Glutamine	0.41	0.40	0.29	0.24	0.11
Glycine	0.30	0.28	0.31	0.18	0.14
L-Histidine	0.13	0.09	0.10	0.04	0.06
L-Isoleucine	0.11	0.09	0.04	0.03	0.03
L-Leucine	0.10	0.10	0.05	0.01	0.04
L-Lysine	0.31	0.24	0.02	0.06	0.10
L-Methionine	0.13	0.10	0.10	0.07	0.07
L-Phenylalanine	0.17	0.14	0.11	0.06	0.07
L-Proline	0.39	0.39	0.37	0.31	0.16
L-Serine	0.30	0.36	0.37	0.07	0.13
L-Threonine	0.19	0.13	0.30	0.16	0.11
L-Tryptophan	0.39	0.32	0.12	0.12	0.07
L-Tyrosine	0.10	0.11	0.03	0.08	0.07
L-Valine	0.06	0.06	0.08	0.01	0.02
D-Alanine	0.40	0.37	0.40	0.17	0.13
D-Asparagine	0.20	0.14	0.07	0.07	0.10
D-Aspartic Acid	0.05	0.09	0.05	0.02	0.09
D-Glutamic Acid	0.04	0.06	0.06	0.02	0.10
D-Lysine	0.04	0.04	0.06	0.04	0.08
D-Serine	0.31	0.35	0.36	0.11	0.13
D-Valine	0.04	0.07	0.07	0.05	0.07
L-Citrulline	0.12	0.07	0.08	0.04	0.05
L-Homoserine	0.17	0.08	0.05	0.01	0.01
L-Ornithine	0.35	0.34	0.03	0.09	0.03

	MG1655	BW25113	OP50	HT115	HB101
N-Acetyl-LGlutamic Acid	0.03	0.01	0.02	0.09	0.04
N-Phthaloyl-LGlutamic Acid	0.08	0.03	0.07	0.10	0.08
L-Pyroglutamic Acid	0.05	0.05	0.07	0.02	0.08
Hydroxylamine	0.00	0.02	0.05	0.01	0.05
Methylamine	0.01	0.07	0.05	0.01	0.07
N-Amylamine	0.08	0.08	0.09	0.01	0.09
N-Butylamine	0.08	0.09	0.07	0.03	0.10
Ethylamine	0.04	0.09	0.08	0.04	0.09
Ethanolamine	0.02	0.06	0.07	0.03	0.06
Ethylenediamine	0.00	0.00	0.06	0.01	0.02
Putrescine	0.27	0.26	0.05	0.05	0.01
Agmatine	0.28	0.19	0.01	0.00	0.01
Histamine	0.02	0.01	0.00	0.01	0.01
ß-Phenylethylamine	0.06	0.05	0.07	0.03	0.10
Tyramine	0.07	0.06	0.06	0.04	0.11
Acetamide	0.03	0.06	0.06	0.02	0.08
Formamide	0.06	0.07	0.08	0.02	0.08
Glucuronamide	0.39	0.30	0.53	0.15	0.15
D,L-Lactamide	0.03	0.07	0.08	0.02	0.08
D-Glucosamine	0.38	0.40	0.43	0.47	0.17
D-Galactosamine	0.08	0.07	0.09	0.07	0.06
D-Mannosamine	0.15	0.10	0.14	0.03	0.08
N-Acetyl-DGlucosamine	0.38	0.40	0.44	0.33	0.14
N-Acetyl-DGalactosamine	0.00	0.02	0.42	0.01	0.04
N-Acetyl-DMannosamine	0.17	0.12	0.33	0.26	0.07
Adenine	0.21	0.20	0.07	0.01	0.03
Adenosine	0.31	0.32	0.45	0.31	0.15
Cytidine	0.38	0.36	0.45	0.30	0.26
Cytosine	0.23	0.15	0.14	0.07	0.15
Guanine	0.45	0.27	0.25	0.62	0.40
Guanosine	0.25	0.17	0.23	0.32	0.11
Thymine	0.04	0.04	0.06	0.02	0.04
Thymidine	0.04	0.05	0.11	0.06	0.03
Uracil	0.07	0.05	0.06	0.05	0.02
Uridine	0.07	0.06	0.04	0.06	0.02
Inosine	0.03	0.01	0.05	0.02	0.02
Xanthine	0.10	0.06	0.07	0.15	0.04
Xanthosine	0.10	0.04	0.08	0.11	0.08
Uric Acid	0.07	0.04	0.13	0.01	0.03
Alloxan	0.07	0.05	0.11	0.06	0.05
Allantoin	0.07	0.05	0.08	0.03	0.05
Parabanic Acid	0.05	0.06	0.08	0.04	0.04
D,L-α-Amino-NButyric Acid	0.10	0.12	0.05	0.01	0.01
γ-Amino-NButyric Acid	0.39	0.32	0.09	0.04	0.04
ε-Amino-NCaproic Acid	0.12	0.08	0.08	0.03	0.04

	MG1655	BW25113	OP50	HT115	HB101
D,L-α-AminoCaprylic Acid	0.09	0.06	0.09	0.04	0.03
δ-Amino-NValeric Acid	0.36	0.36	0.24	0.03	0.04
α-Amino-NValeric Acid	0.00	0.00	0.00	0.00	0.00
Ala-Asp	0.42	0.42	0.34	0.22	0.07
Ala-Gln	0.44	0.44	0.42	0.22	0.08
Ala-Glu	0.48	0.44	0.38	0.25	0.10
Ala-Gly	0.40	0.44	0.37	0.17	0.07
Ala-His	0.34	0.35	0.27	0.09	0.05
Ala-Leu	0.31	0.28	0.29	0.03	0.01
Ala-Thr	0.45	0.45	0.26	0.32	0.08
Gly-Asn	0.43	0.47	0.32	0.18	0.05
Gly-Gln	0.48	0.47	0.53	0.19	0.06
Gly-Glu	0.36	0.31	0.36	0.11	0.05
Gly-Met	0.27	0.28	0.22	0.01	0.02
Met-Ala	0.31	0.31	0.28	0.02	0.03
Phosphate	0.36	0.34	0.14	0.10	0.03
Pyrophosphate	0.32	0.35	0.14	0.08	0.06
Trimeta Phosphate	0.35	0.33	0.10	0.03	0.03
Tripoly Phosphate	0.36	0.33	0.22	0.09	0.04
Triethyl Phosphate	0.04	0.02	0.01	0.02	0.03
Hypophosphite	0.00	0.01	0.00	0.00	0.02
Adenosine-2'- monophosphate	0.39	0.35	0.25	0.12	0.01
Adenosine-3'- monophosphate	0.38	0.41	0.28	0.15	0.01
Adenosine-5'- monophosphate	0.37	0.39	0.27	0.14	0.02
Adenosine-2',3'- cyclic monophosphate	0.35	0.37	0.25	0.10	0.02
Adenosine-3',5'- cyclic monophosphate	0.03	0.06	0.01	0.01	0.02
Thiophosphate	0.30	0.31	0.17	0.03	0.03
Dithiophosphate	0.29	0.29	0.18	0.08	0.01
D,L-α-Glycerol Phosphate	0.36	0.33	0.20	0.15	0.05
ß-Glycerol Phosphate	0.38	0.33	0.19	0.06	0.03
Carbamyl Phosphate	0.36	0.34	0.17	0.05	0.04
D-2-PhosphoGlyceric Acid	0.37	0.33	0.17	0.05	0.03
D-3-PhosphoGlyceric Acid	0.41	0.34	0.27	0.06	0.03
Guanosine-2'- monophosphate	0.36	0.36	0.28	0.15	0.04
Guanosine-3'- monophosphate	0.37	0.37	0.28	0.19	0.04
Guanosine- 5' - monophosphate	0.37	0.36	0.32	0.18	0.03
Guanosine- 2',3'- cyclic monophosphat	0.35	0.40	0.24	0.11	0.04
Guanosine- 3',5'- cyclic monophosphat	0.01	0.02	0.01	0.00	0.01
Phosphoenol Pyruvate	0.29	0.32	0.11	0.02	0.01
PhosphoGlycolic Acid	0.33	0.34	0.04	0.06	0.05
D-Glucose-1- Phosphate	0.34	0.38	0.31	0.17	0.05
D-Glucose-6- Phosphate	0.37	0.37	0.30	0.20	0.06
2-Deoxy-DGlucose-6- Phosphate	0.10	0.06	0.07	0.03	0.02

	MG1655	BW25113	OP50	HT115	HB101
D-Glucosamine6-Phosphate	0.39	0.37	0.34	0.12	0.07
6-PhosphoGluconic Acid	0.40	0.33	0.24	0.02	0.03
Cytidine-2- monophosphate	0.41	0.41	0.35	0.18	0.02
Cytidine-3- monophosphate	0.10	0.08	0.04	0.02	0.05
Cytidine-5'- monophosphate	0.38	0.42	0.31	0.14	0.04
Cytidine-2',3'- cyclic monophosphate	0.37	0.41	0.36	0.15	0.02
Cytidine-3',5'- cyclic monophosphate	0.04	0.04	0.02	0.00	0.01
D-Mannose-1- Phosphate	0.33	0.33	0.26	0.12	0.02
D-Mannose-6- Phosphate	0.35	0.34	0.21	0.15	0.05
Cysteamine-SPhosphate	0.32	0.33	0.00	0.01	0.01
Phospho-LArginine	0.39	0.36	0.23	0.06	0.05
O-Phospho-DSerine	0.40	0.37	0.30	0.11	0.03
O-Phospho-LSerine	0.41	0.34	0.32	0.09	0.03
O-Phospho-LThreonine	0.42	0.36	0.35	0.09	0.03
D8 Uridine-2'- monophosphat	0.41	0.36	0.21	0.16	0.04
Uridine-3'- monophosphate	0.38	0.37	0.27	0.18	0.04
Uridine-5'- monophosphate	0.36	0.36	0.29	0.16	0.03
Uridine-2',3'- cyclic monophosphate	0.37	0.40	0.24	0.17	0.02
Uridine-3',5'- cyclic monophosphate	0.02	0.03	0.01	0.00	0.00
O-Phospho-DTyrosine	0.35	0.36	0.15	0.05	0.00
O-Phospho-LTyrosine	0.40	0.38	0.09	0.02	0.03
Phosphocreatine	0.36	0.34	0.21	0.03	0.04
Phosphoryl Choline	0.35	0.34	0.18	0.04	0.03
O-PhosphorylEthanolamine	0.38	0.34	0.25	0.05	0.03
Phosphono Acetic Acid	0.10	0.07	0.05	0.02	0.05
2-Aminoethyl Phosphonic Acid	0.13	0.07	0.17	0.01	0.03
Methylene Diphosphonic Acid	0.12	0.12	0.12	0.07	0.06
Thymidine-3'- monophosphate	0.44	0.36	0.19	0.12	0.04
Thymidine-5'- monophosphate	0.40	0.28	0.27	0.15	0.04
Inositol Hexaphosphat	0.29	0.27	0.07	0.07	0.02
Thymidine 3',5'- cyclic monophosphate	0.04	0.04	0.01	0.01	0.01
Sulfate	0.35	0.35	0.16	0.03	0.04
Thiosulfate	0.38	0.33	0.22	0.05	0.02
Tetrathionate	0.39	0.36	0.27	0.08	0.02
Thiophosphate	0.17	0.16	0.15	0.02	0.06
Dithiophosphate	0.21	0.20	0.30	0.06	0.03
L-Cysteine	0.29	0.25	0.29	0.05	0.02
D-Cysteine	0.41	0.37	0.29	0.08	0.05
L-CysteinylGlycine	0.28	0.26	0.17	0.04	0.03
L-Cysteic Acid	0.30	0.29	0.05	0.02	0.05
Cysteamine	0.15	0.08	0.01	0.00	0.05
L-Cysteine Sulfinic Acid	0.34	0.38	0.23	0.04	0.01

	MG1655	BW25113	OP50	HT115	HB101
N-Acetyl-LCysteine	0.05	0.10	0.02	0.01	0.01
S-Methyl-LCysteine	0.08	0.09	0.02	0.01	0.03
Cystathionine	0.29	0.26	0.06	0.08	0.05
Lanthionine	0.38	0.34	0.04	0.00	0.03
Glutathione	0.33	0.35	0.08	0.06	0.06
D,L-Ethionine	0.08	0.10	0.02	0.02	0.06
L-Methionine	0.19	0.20	0.12	0.02	0.04
D-Methionine	0.13	0.13	0.09	0.03	0.06
Glycyl-LMethionine	0.18	0.19	0.12	0.03	0.06
N-Acetyl-D,LMethionine	0.16	0.16	0.12	0.02	0.04
L-Methionine Sulfoxide	0.17	0.15	0.10	0.01	0.03
L-Methionine Sulfone	0.06	0.05	0.01	-0.01	0.02
L-Djenkolic Acid	0.33	0.33	0.04	0.03	0.03
Thiourea	0.10	0.11	0.07	0.01	0.02
1-Thio-ß-DGlucose	0.06	0.08	0.03	0.02	0.02
D,L-Lipoamide	0.07	0.06	0.02	0.01	0.04
Taurocholic Acid	0.07	0.09	0.04	0.03	0.02
Taurine	0.35	0.31	0.11	0.04	0.03
Hypotaurine	0.26	0.31	0.05	0.02	0.03
P-Amino Benzene Sulfonic Acid	0.07	0.07	0.03	0.01	0.03
Butane Sulfonic Acid	0.38	0.29	0.05	0.01	0.04
2-Hydroxyethane Sulfonic Acid	0.39	0.31	0.10	0.03	0.03
Methane Sulfonic Acid	0.30	0.28	0.01	0.01	0.02
Tetramethylene Sulfone	0.05	0.06	0.01	0.01	0.01

Table 2 Genes uniquely present or absent on OP50, HT115 or HB101

Genes uniquely absent in HB101	
gpt	xanthine-guanine phosphoribosyltransferase
phoE	outer membrane porin E
proB	glutamate 5-kinase
proA	glutamate 5-semialdehyde dehydrogenase
trkG	K+ transporter TrkG
ompN	outer membrane pore protein N, non-specific
ldhA	D-lactate dehydrogenase - fermentative
feaB	phenylacetaldehyde dehydrogeanse
tynA	copper containing amine oxide (tyramine oxidase, copper-requiring)
aldA	aldehyde dehydrogenase A, NAD-linked
ydcS	putative periplasmic binding protein ABC family/polyhydroxybutyrate synthase
ydcT	putative transport protein ABC family
ydcU	putative transport protein ABC family
ydcV	putative transport protein ABC family
patD	gamma-aminobutyraldehyde dehydrogenase

ansP	L-asparagine transporter
nhoA	arylamine N-acetyltransferase
narV	nitrate reductase Z subunit gamma
narW	putative private chaperone for NarZ nitrate reductase subunit
narY	nitrate reductase Z subunit beta
narZ	nitrate reductase Z subunit alpha
narU	nitrate/nitrite transporter
yddG	aromatic aminoacid exporter YddG
fdnG	formate dehydrogenase N subunit alpha
fdnH	formate dehydrogenase N subunit beta
fdnI	formate dehydrogenase N subunit gamma
adhP	ethanol dehydrogenase/alchol dehydrogenase
maeA	malate dehydrogenase, NAD-requiring
ddpF	putative D,D-dipeptide ABC transporter membrane protein subunit, DdpF
ddpD	putative D,D-dipeptide ABC transporter membrane protein subunit, DdpD
ddpC	putative D,D-dipeptide ABC transporter membrane protein subunit, DdpC
ddpB	putative D,D-dipeptide ABC transporter membrane protein subunit, DdpB

ddpA	putative D,D-dipeptide ABC transporter periplasmic binding protein
ddpX	D-ala-D-ala-dipeptidase
dosP	c-di-GMP phosphodiesterase
gadC	glutamic acid:4-aminobutyrate antiporter
Genes uniquely absent in HT115	
thrC	4-hydroxy-L-threonine kinase
nadR	ribosylnicotinamide kinase
Genes uniquely absent in OP50	
yeaP	diguanylate cyclase
mmuP	S-methyl-L-methionine transporter
mmuM	homocysteine S-methyltranferase
argF	ornithine carbamoyltransferase
pheP	phenylalanine:H+ symporter
cobC	putative adenosylcobalamin phosphatase/alpha-ribazole phosphatase
dcyD	D-cysteine desulfhydrase, PLP-dependent / 3-chloro-D-alanine dehydrochlorinase

amyA	alpha-amylase
wzzB	regulator of length of O-antigen component of lipopolysaccharide chains
wbbK	putative lipopolysaccharide biosynthesis protein
wbbI	beta-1,6-galactofuranosyltransferase
wbbH	putative O-antigen polymerase
glf	UDP-galactopyranose mutase
rfbX	O-antigen flippase
rfbC	dTDP-4-dehydrorhamnose 3,5-epimerase
mqo	malate:quinone oxidoreductase
atoD	alpha complex
atoA	beta complex
atoE	short chain fatty acid transporter
atoB	acetyl-CoA acetyltransferase
xapB	xanthosine:H+ symporter
xapA	xanthosine phosphorylase
cysM	cysteine synthase B
gabD	galactarate/glucarate/glycerate transporter
gudP	galactarate/glucarate/glycerate transporter

queF	7-cyano-7-deazaguanine reductase
sdaC	serine:H+ symporter
sdaB	L-serine deaminase II
fucO	L-1,2-propanediol oxidoreductase
fucP	fucose:H+ symporter
waaL	O-antigen ligase
waaA	KDO transferase
waaZ	protein involved in KdoIII attachment during lipopolysaccharide core biosynthesis
waaY	lipopolysaccharide core heptose (II) kinase
waaJ	UDP-glucose:(glucosyl)LPS α-1,2-glucosyltransferase
waaO	UDP-D-glucose:(glucosyl)LPS α-1,3-glucosyltransferase
waaB	UDP-D-galactose:(glucosyl)lipopolysaccharide-1,6-D-galactosyltransferase
waaS	lipopolysaccharide core biosynthesis protein
waaQ	lipopolysaccharide core heptosyltransferase III
corA	Ni2+/Co2+/Mg2+ transporter
malG	maltose ABC transporter membrane subunit
malF	maltose ABC transporter membrane subunit

malE	maltose ABC transporter periplasmic binding protein
malK	maltose ABC transporter ATP binding subunit
lamB	maltose outer membrane porin/phage lambda receptor protein

Chapter V: Conclusion chapter

Since the discovery of DNA and genes, molecular biology has made enormous strides to understand the functions and regulation of genes and gene-gene interactions. We understand the basics of gene regulation and the influence many genes and their mutations have on health and disease. However, the way most of the research was conducted so far is to look at the function of a single gene in a single pathway in one biological context. While very valuable to understand the basic biological processes, this kind of view assumes that a given gene-gene interaction will be the same in different contexts, which is not always the case.

The understanding of gene regulation and metabolic pathways increased greatly in recent decades and currently, we have entire databases where we can find information regarding metabolic pathways, like KEGG (237) or Biocyc (238). However, metabolic and gene regulatory pathways presented in the databases are static pathways that were inferred from studies done in different cells or organisms, and in different contexts. Even though we have a detailed picture of the interactions that can happen inside a single cell it doesn't mean that every reaction takes place in every cell. Cells differentiate and specialize in performing only a fraction of the possible metabolic reactions and express only certain genes, but not the others (239–241). Also, as we have shown, transcriptional regulation of the genes differ depending on the context in which a cell or an organism happens to be. Different metabolites and TF are needed when an organism experiences oxidative stress and different when it is starved, so those metabolic and gene interaction

pathways need to be adjusted accordingly to context. This also means that some pathways will be active in one condition, but not the other. Therefore if we make inferences based on experiments in one context, the inference may be incorrect in another context.

The approach of looking at one gene in one context at a time stems from the experimental limitations. Even though our laboratory methods and equipment improved over the years, performing whole-genome screens is a laborious process, and gaining whole-genome data can be expensive. Therefore we are more likely to draw conclusions regarding gene interactions based on a few available data sets obtained in a limited number of contexts. However, recently, obtaining large data sets encompassing data from the entire genome has become easier and cheaper, and we expect improvements in the future. It opens new doors to opportunities that will allow for testing gene interactions in different contexts and gain more knowledge about context-dependent gene interactions.

To be able to make sense of big omics datasets that come from whole-genome screens and how the gene-gene interactions change depending on the context we need to employ computer modeling. Genome-scale models of cell metabolism have already been developed for several organisms (215,242–246). Since the metabolic pathways have been known for decades, computer algorithms can draw on this knowledge and build an initial pan model of metabolism. Based on this model and omics data from a particular context,

the model can be adjusted to fit the data of a given organism or tissue in the particular context.

Many methods have been developed to use omics data and integrate them into models (247–249). Since omics data can be acquired in different contexts, we can build context-specific models that are more interactive and can adjust gene interactions depending on the context (250). Even more advanced models would be able not only to capture different types of data and combine them to propose specific drug targets but should be also able to adapt and change depending on different inputs, eg. stress, fasting, etc.

One of the most common and basic contexts would be tissue-specificity. Tissue-Specific Metabolic Networks have already been constructed for multiple different cell types (251). In next steps we can use models to predict how metabolic networks react to different insults and conditions. Another layer of complexity would be to look at the gene interaction networks of different microbial compositions and test how they interact with human cells (252). It could allow us to test how the microbiome of each patient will metabolize different medications, allowing for even better precision medicine. First steps toward creating context-specific models have already been taken (48).

Context-specific models can be employed not only in basic biology, but also in clinical settings, especially in precision medicine. In precision medicine we look at each

individual as an organism in a specific context, since each one of us has different mutations, different diet and we live in different environments. Studying context-dependence and understanding it at the molecular level can lead to clinically significant discoveries.

Researchers in the field of cancer genetics already realized the importance of context and its implication of the treatment of tumors (91,250,253). Studies looked at cancer tissues taken from multiple patients and compared the different molecular signatures in order to create patient-specific networks and propose drug targets (254). The importance of the context-dependent gene regulation in regard to tissue specificity is evident in some mutations that result in cancer much more frequently in one tissue, but not otters, like BRCA1 and BRCA2 in breast and ovarian tissues (255) (91). Additionally, the same drug used for targeting the same oncogenic mutation can have different efficacy in different cancer tissues, as is the case with drug targeting $BRAF^{V600E}$ mutation which works well in melanoma, non–small-cell lung cancer, and hairy cell leukemia, but not colorectal cancers (91) showing that, just as in the case, of gene interactions, we cannot always extrapolate results obtained from one tumor type line with a given mutation to different cell type with the same mutation. In a CRISPR-Cas9 screen performed on three different cancer cell lines, authors identified differences among the lines. Among the 152 potential synthetic-lethal gene interactions they identified, none of them was common to all three cell lines indicating that gene-gene interactions depend on the context, in this case, different cell lines (256).

In the past, the experimental limitations were often the reason why we needed to limit ourselves to only one gene in a single context. However, the explosion of omics techniques allows us to look at gene-gene interactions on a bigger scale and in several different contexts in a single experiment. Additionally, improvement in computational methods allows for creating the networks of gene-gene interactions on a big scale and adjusting those networks to different biological contexts.

Understanding such complex genetic networks and what influence context has on them, is essential in understanding how complex traits emerge as well as the basis of human disease.

Appendix I: Towards *C. elegans* metabolic models

1. Results

Our collaborators built a computer model of the *C. elegans* metabolism that is able to predict phenotypic outcomes depending on perturbation of the input nutrients or *in silico* inactivation or hyperactivation of single (or multiple) metabolic enzymes, henceforth called MetaboFlux. This model is a 1535-enzymes curated version of the metabolic models of *C. elegans* published by Walhout and Kaleta's labs (232,233). However, this model has not been experimentally validated. One of the most common validations of the metabolic models is the ability to predict genes that are needed for biomass production, that is the production of body mass from egg to adult worm. If a given gene inactivation causes *C. elegans* not to be able to produce biomass that would mean that the metabolic flux in the *C. elegans* is blocked.

Previous models have used publicly available databases to acquire experimentally data regarding lethal genes. However, those data come from different experiments performed in different conditions, therefore they may not accurately represent the lethal genes To remedy this, in our model we used the data generated by another graduate student in the lab, Wenfan Ke. He used high-throughput RNAi and automated microscopy to inactivate each of the 1535 genes in populations of ~75 worms and imaged them at a time point when wild-type worms have reached adulthood. With the help of undergraduate trainees, I analyzed this set and visually scored the *C. elegans* images to

identify *C. elegans* essential genes, that is genes that are necessary for the survival of an organism. We identified genes whose inactivation resulted in reduced biomass production in *C. elegans* measured as smaller size or lack of progeny (eggs).

Among the RNAi-treated worms we identified three phenotypic classes:

1) High-confidence essential genes. Animals that did not produce biomass, that is were arrested in the pre-adulthood stage, after 5 days of incubation at 25°C. High-confidence genes received the score of 5 or above (in 6 independent scorings, see Methods)

2) Medium confidence essential genes, animals did not produce biomass/reached adulthood. Medium-confidence genes received a score of 3 or 4, in 6 independent scorings.

3) Wild-type genes.

This experimental data will be used to inform improvements in the *C. elegans* model.

In the next steps, we can combine the previously created *E. coli* models (described in the 2nd chapter of this thesis) with the *C. elegans* models to create *E. coli*-*C. elegans* holobiont model.

E. coli models predict the metabolites *E. coli* strains are capable (or not) to produce. Thus, they can be used to "feed" *C. elegans in silico* with a pool of nutrients that better resemble their lab food source. The models for these *E. coli* strains can also serve to model microbiota-host interactions, as *E. coli* is the only source of microbiota for *C. elegans* grown in lab conditions. By using the *C. elegans-E. coli* holobiont, we can ask questions regarding microbiota-host crosstalk *in vivo* and with single-molecule (gene) resolution and test those predictions experimentally. In future work these two genetically tractable organisms, the microbe *E. coli* and the nematode *C. elegans* can be used to create functionally validated models of microbiota-host co-metabolism (holobionts), and molecularly dissect the mechanisms by which the microbiota modulates critical host processes such as nutrient sensing.

App. I Table 1. High-confidence essential genes.

Gene name (i.e. lipl-1)	Gene sequence (i.e. F54F3.3)
rpoa-2	F14B4.3
pri-2	W02D9.1
slc-36.5	C44B7.6
fars-3	F22B5.9
R53.4	R53.4
pdha-1	T05H10.6
tars-1	C47D12.6
B0491.5	B0491.5
vha-6	VW02B12L.1
M01F1.3	M01F1.3
lars-1	R74.1
rars-1	F26F4.10
rpb-2	C26E6.4
rpc-2	F09F7.3
ucr-1	F56D2.1
stt-3	T12A2.2
pars-1	T20H4.3
let-754	C29E4.8
atp-2	C34E10.6
nuo-4	K04G7.4
elo-3	D2024.3
F33D4.4	F33D4.4
hyl-1	C09G4.1
F21D5.1	F21D5.1

Gene name (i.e. lipl-1)	Gene sequence (i.e. F54F3.3)
pcp-2	F23B2.12
ogdh-1	T22B11.5
vha-11	Y38F2AL.3
elo-2	F11E6.5
nuo-3	Y57G11C.12
dld-1	LLC1.3
fat-6	VZK822L.1
mars-1	F58B3.5
F01G4.6	F01G4.6
hars-1	T11G6.1
dlst-1	W02F12.5
nuo-5	Y45G12B.1
eat-6	B0365.3
F53F4.10	F53F4.10
lpin-1	H37A05.1
alg-1	F48F7.1
ribo-1	T22D1.4
F44G4.2	2J289
Y51H1A.3	Y51H1A.3
gstk-1	ZK1320.1
vha-2	R10E11.2
vha-1	R10E11.8
hpo-18	F32D1.2
vha-19	Y55H10A.1

App. II Table 2. Medium-confidence essential genes

Gene name (i.e. lipl-1)	Gene sequence (i.e. F54F3.3)
nuo-2	T10E9.7
nuo-6	W01A8.4
aars-2	F28H1.3
atp-3	F27C1.7
pnk-1	C10G11.5
spe-5	Y110A7A.12
fars-1	T08B2.9
asg-1	K07A12.3
F26E4.6	F26E4.6
C34B2.8	C34B2.8
hxk-1	F14B4.2
W09C5.8	W09C5.8
pole-1	F33H2.5
rpb-7	Y54E10BR.6
gcy-21	F22E5.3
pacs-1	B0286.3
F09E5.3	F09E5.3
ndx-6	EEED8.8
R12C12.1	R12C12.1
maoc-1	E04F6.3
T02H6.11	phi-44
gcy-15	ZC239.7
C01F1.3	phi-41
mlt-7	ZK430.8
cgt-3	F59G1.1
nuo-1	C09H10.3
T10F2.2	T10F2.2
emb-8	K10D2.6
F09F7.4	F09F7.4
tdo-2	C28H8.11
C16A3.5	C16A3.5
jhdm-1	T26A5.5

Gene name (i.e. lipl-1)	Gene sequence (i.e. F54F3.3)
set-1	T26A5.7
T20H4.5	T20H4.5
let-767	C56G2.6
gars-1	T10F2.1
rnr-1	T23G5.1
dars-1	B0464.1
cbp-1	R10E11.1
ama-1	F36A4.7
rpc-1	C42D4.8
F42G8.10	F42G8.10
dgk-4	F42A9.1
sars-1	C47E12.1
vha-5	F35H10.4
elo-5	F41H10.7
vha-17	F49C12.13
gln-6	C28D4.3
asb-2	F02E8.1
daf-9	T13C5.1
pcyt-1	F08C6.2
fah-1	K10C2.4
asg-2	C53B7.4
dot-1.2	F54F7.7
sir-2.3	F46G10.3
ucr-11	F57B10.14
sams-1	C49F5.1
dyn-1	C02C6.1
vha-3	Y38F2AL.4
vha-16	C30F8.2
sptl-1	C23H3.4
R04F11.2	R04F11.2
ears-1	ZC434.5

App. II Table 3. Genes which inactivation results in Wild Type phenotype.

Gene name (i.e. lipl-1)	Gene sequence (i.e. F54F3.3)
gst-25	F37F2.3
F53F10.2	F53F10.2
pgk-1	T03F1.3
E01A2.1	E01A2.1
ptps-1	B0041.6
vha-10	F46F11.5
acdh-1	C55B7.4
ahcy-1	K02F2.2
nars-1	F22D6.3
R119.5	R119.5
acs-16	F47G6.2
fbp-1	K07A3.1
tyr-5	Y44E3B.2
lin-59	T12F5.4
ugt-25	C10H11.3
ugt-27	C10H11.5
ugt-26	C10H11.6
coq-1	C24A11.9
T19B4.3	1G247
tyr-4	C34G6.2
pgp-2	C34G6.4
C27A12.9	C27A12.9
abt-6	F56F4.6
pigv-1	T09B4.1
T09B4.8	T09B4.8
T05E7.1	T05E7.1
ech-1.2	T08B2.7
bli-4	K04F10.4
gld-2	ZC308.1
dad-1	F57B10.10
pcbd-1	T10B11.1
idhg-2	C30F12.7
pde-6	Y95B8A.10
gcy-17	W03F11.2
F23C8.5	F23C8.5
W03D8.8	W03D8.8

Gene name (i.e. lipl-1)	Gene sequence (i.e. F54F3.3)
C29E4.10	C29E4.10
ZC262.5	ZC262.5
R05D3.6	R05D3.6
met-2	R05D3.11
lap-1	ZK353.6
mig-22	PAR2.4
ZC155.4	ZC155.4
basl-1	C05D2.3
alh-9	F01F1.6
atgl-1	C05D11.7
T26A5.8	T26A5.8
tyr-1	C02C2.1
sup-18	C02C2.5
gly-3	ZK688.8
pde-2	R08D7.6
nac-2	R107.1
gst-1	R107.7
dgk-3	F54G8.2
dat-1	T23G5.5
elo-4	C40H1.4
F54C8.1	F54C8.1
sod-4	F55H2.1
acox-5	C48B4.1
pri-1	F58A4.4
mett-10	ZK1128.2
div-1	R01H10.1
umps-1	T07C4.1
C38H2.2	C38H2.2
hat-1	M03C11.4
hpd-1	T21C12.2
dpy-18	Y47D3B.10
mif-1	Y56A3A.3
Y56A3A.19	Y56A3A.19
Y49E10.4	Y49E10.4
scav-3	Y49E10.20
cco-2	Y37D8A.14

Gene name (i.e. lipl-1)	Gene sequence (i.e. F54F3.3)
acly-1	D1005.1
Y71H10B.1	Y71H10B.1
aqp-7	M02F4.8
gpd-2	K10B3.8
ugt-18	ZC443.5
ugt-16	ZC443.6
T07F10.1	T07F10.1
dhrs-4	F54F3.4
lap-2	W07G4.4
C56A3.8	C56A3.8
fmo-4	F53F4.5
F09F3.5	F09F3.5
T22G5.1	T22G5.1
sptl-3	T22G5.5
gcy-32	C06B3.8
cept-2	Y49A3A.1
fntb-1	F23B12.6
slc-25A29	C54G10.4
C01G10.7	C01G10.7
C01G10.9	C01G10.9
ugt-30	T01G5.2
cgt-1	T06C12.10
gst-38	F35E8.8
cth-1	F22B8.6
gcy-20	F21H7.9
gst-44	F13A7.10
pus-1	W06H3.2
phy-3	T20B3.7
fat-5	W06D12.3
wars-1	Y80D3A.1
phy-4	Y43F8B.4
ncx-1	Y113G7A.4
slc-36.3	Y38H6C.17
ipla-3	W07A8.2
Y44A6D.5	Y44A6D.5
gcy-22	T03D8.5

ftn-2	D1037.3	Y39E4A.3	Y39E4A.3	T03D8.6	T03D8.6
guk-1	T03F1.8	Y43F4B.5	Y43F4B.5	sqv-6	Y50D4C.4
R12E2.11	R12E2.11	Y43F4B.7	Y43F4B.7	ugt-46	B0310.5
met-1	C43E11.3	qdpr-1	T03F6.1	mrp-2	F57C12.4
ZK973.11	ZK973.11	T03F6.3	T03F6.3	pifk-1	F35H12.4
lpd-5	ZK973.10	lis-1	T03F6.5	dhs-25	F09E10.3
gcy-28	T01A4.1	T27E9.2	T27E9.2	C14E2.4	C14E2.4
got-2.1	C44E4.3	Y76A2B.5	Y76A2B.5	dot-1.5	ZC53.6
F57C9.1	F57C9.1	aldo-1	T05D4.1	gcy-31	T07D1.1
icmt-1	F21F3.3	set-16	T12D8.1	R04B3.2	R04B3.2
paf-1	W03G9.6	tyr-2	K08E3.1	aat-3	F52H2.2
F54C1.1	F54C1.1	K08E3.5	K08E3.5	pfk-1.1	Y71H10A.1
lfe-2	C46H11.4	Y22D7AR.6	Y119D3_465.o	fard-1	Y71H10A.2
pde-5	C32E12.2	Y71H2AM.4	Y71H2AM.4	gpd-3	K10B3.7
ppk-1	F55A12.3	R02D3.1	R02D3.1	ZK563.2	ZK563.2
M01E11.1	M01E11.1	fnta-1	R02D3.5	Y39B6A.3	Y39B6A.3
F46F11.1	F46F11.1	T21D12.7	T21D12.7	acp-1	ZK563.6
hpo-3	F33D11.9	K02D7.1	K02D7.1	paf-2	C52B9.7
vps-34	B0025.1	ears-2	T07A9.2	acp-5	F13D11.1
T27A3.6	T27A3.6	daf-18	T07A9.6	R07E4.3	R07E4.3
pept-3	F56F4.5	glt-7	W03G1.1	nnt-1	C15H9.1
acdh-3	K06A5.6	asm-3	W03G1.7	kynu-1	C15H9.7
acdh-4	T10E9.9	ugt-52	F56B3.7	F38B6.4	F38B6.4
ipgm-1	F57B10.3	Y77E11A.2	Y77E11A.r	pdi-6	B0403.4
tre-1	F57B10.7	mca-2	R05C11.3	sur-5	K03A1.5
dhod-1	W02D3.2	gcy-23	T26C12.4	gly-12	F48E3.1
ant-1.2	W02D3.6	M57.2	M57.2	set-12	K09F5.5
acdh-5	C37A2.3	K06B9.2	K06B9.2	K07E3.4	K07E3.4
T10B11.2	T10B11.2	tat-2	H06H21.10	oga-1	T20B5.3
pdi-3	H06O01.1	ivd-1	C02B10.1	T09B9.3	T09B9.3
nduf-6	F22D6.4	chil-11	C45E5.2	ZC373.5	ZC373.5
M05B5.4	M05B5.4	sams-4	C06E7.3	W07E11.1	W07E11.1
dhp-1	R06C7.3	pck-3	H04M03.1	acl-5	R07E3.5
adsl-1	R06C7.5	ugt-19	K08B4.3	haly-1	F47B10.2
tyr-3	F21C3.2	ugt-20	K08B4.4	F38B2.4	XL906
ttx-7	F13G3.5	F58F9.1	F58F9.1	gst-42	D1053.1
F52A8.5	F52A8.5	acox-6	F58F9.7	mrp-6	F20B6.3
chs-1	T25G3.2	sams-5	T13A10.11	hyl-2	K02G10.6

tag-173	F27D4.5	T12B3.3	T12B3.3	K05B2.4	K05B2.4
glna-3	F30F8.2	F55G1.5	F55G1.5	C31H2.4	C31H2.4
ath-1	K04G2.5	R05G6.5	R05G6.5	F35C8.5	F35C8.5
sod-2	F10D11.1	sqv-1	D2096.4	sulp-2	F14D12.5
idha-1	F43G9.1	T01B11.2	T01B11.2	cat-1	W01C8.6
dhfr-1	C36B1.7	pole-2	F08B4.5	acs-17	C46F4.2
fasn-1	F32H2.5	C33A12.1	C33A12.1	bgal-2	H22K11.2
hgo-1	W06D4.1	cka-1	C28D4.2	dhs-28	M03A8.1
F30A10.3	F30A10.3	drp-1	T12E12.4	C07D8.6	C07D8.6
fce-1	C04F12.10	C31H1.5	C31H1.5	asns-2	M02D8.4
ncx-4	F35C12.2	sams-3	C06E7.1	chup-1	ZK721.1
iars-2	C25A1.7	ugt-24	C49A9.8	acs-22	D1009.1
Y106G6E.4	Y106G6E.4	tre-2	T05A12.2	gly-13	B0416.6
sdha-2	C34B2.7	C06G3.5	C06G3.5	gpx-5	C11E4.1
gpx-8	F55A3.5	pitr-1	C48A7.2	gpx-3	C11E4.2
hxk-2	H25P06.1	F55G1.9	F55G1.9	ipla-2	F47A4.5
glct-4	C47F8.4	sucg-1	C50F7.4	moc-1	T06H11.4
T27F6.6	T27F6.6	klo-1	C50F7.10	F13E6.5	F13E6.5
acox-1	F08A8.1	C46A5.4	C46A5.4	plc-1	F31B12.1
acox-2	F08A8.2	gcy-8	C49H3.1	pxn-2	K09C8.5
C47B2.2	C47B2.2	moc-3	F42G8.6	cht-1	C04F6.3
Y48G10A.1	Y48G10A.1	aagr-1	D2096.3	glt-1	C12D12.2
gpap-1	Y6B3B.5	ant-1.4	T01B11.4	gyg-1	F56B6.4
lagr-1	Y6B3B.10	bre-1	C53B4.7	ckc-1	T27A10.3
hsd-1	Y6B3B.11	C10C5.4	C10C5.4	dgk-2	F46H6.2
hprt-1	Y105E8B.5	C10C5.5	C10C5.5	aqp-8	K02G10.7
T25G3.4	T25G3.4	ugt-21	C33A12.6	hsd-2	ZC8.1
D2030.4	D2030.4	ant-1.3	K01H12.2	ZC8.6	ZC8.6
cyc-1	C54G4.8	fat-4	T13F2.1	pnk-4	C42D8.3
R05D11.9	R05D11.9	fat-3	W08D2.4	T21F4.1	T21F4.1
gld-4	ZK858.1	dnj-15	K08D10.2	mig-23	R07E4.4
slc-36.4	H32K16.1	C01B10.3	C01B10.3	ipp-5	C09B8.1
nmat-2	F26H9.4	T22D1.3	T22D1.3	got-2.2	C14F11.1
nkb-1	C17E4.9	B0478.3	B0478.3	C15B12.1	C15B12.1
T05F1.8	T05F1.8	plc-4	R05G6.8	slc-25A10	K11G12.5
gpx-1	F26E4.12	cdd-2	F49E8.4	alh-10	C54D1.4
sqv-5	T24D1.1	dif-1	F49E8.5	apy-1	F08C6.6
tag-179	T24D1.4	C06A6.4	C06A6.4	C44E12.1	C44E12.1
M04D5.1	M04D5.1	atic-1	C55F2.1	gpx-7	R03G5.5

png-1	F56G4.5	pcp-3	F23B2.11	C39D10.3	C39D10.3
gmd-2	F56H6.5	T20D3.8	T20D3.8	sdha-1	C03G5.1
glct-1	T09E11.1	C10C5.3	C10C5.3	B0272.3	B0272.3
glct-2	E03H4.12	idh-1	F59B8.2	gst-36	R07B1.4
glct-5	C54C8.5	elo-7	F56H11.3	ugt-23	C17G1.3
pars-2	T27F6.5	aat-1	F27C8.1	cysl-1	C17G1.7
asah-1	K11D2.2	pyp-1	C47E12.4	suca-1	F47B10.1
T26E3.7	T26E3.7	dhp-2	C47E12.8	pho-7	T21B6.2
gale-1	C47B2.6	pld-1	C04G6.3	idh-2	C34F6.8
gcy-35	T04D3.4			C49F5.5	C49F5.5
gpi-1	Y87G2A.8	sars-2	W03B1.4	nmat-1	W06B3.1
hpo-13	Y105E8A.10	T28F3.5	T28F3.5	M153.1	M153.1
rpom-1	Y105E8A.23	H25K10.1	H25K10.1	F42F12.4	F42F12.4
mans-1	D2030.1	coq-3	Y57G11C.11	sir-2.2	F46G10.7
abts-1	F52B5.1	nkcc-1	Y37A1C.1	C33G3.4	C33G3.4
ocrl-1	C16C2.3	F52B11.2	F52B11.2	ucr-2.2	T10B10.2
glct-3	T15D6.7	gly-10	Y45F10D.3	gob-1	H13N06.3
amx-2	B0019.1	Y45F10D.4	Y45F10D.4	got-1.2	T01C8.5
acox-3	F08A8.3	fat-2	W02A2.1	tps-1	ZK54.2
acox-4	F08A8.4	cho-1	C48D1.3	cgt-2	F20B4.6
pde-1	T04D3.3	gcy-18	ZK896.8	gip-2	C45G3.5
gpdh-1	F47G4.3	vha-7	C26H9A.1	tyms-1	Y110A7A.4
mys-2	K03D10.3	ZK795.1	ZK795.1	set-4	C32D5.5
Y54E10BR.1	M01B12.e	tag-335	C42C1.5	acs-6	ZK1127.2
acs-13	Y65B4BL.5			Y17G7B.3	Y17G7B.3
K10B4.1	K10B4.1	ent-1	ZK809.4	set-6	C49F5.2
T01D1.4	T01D1.4	sms-1	H21P03.3	ucr-2.1	VW06B3R.1
chs-2	F48A11.1	F01G4.5	F01G4.5	F42F12.3	F42F12.3
W07E6.3	W07E6.3	ugt-44	F01D4.2	ugt-50	T07C5.1
slc-36.2	T27A1.5	iars-1	R11A8.6	alh-13	T22H6.2
acdh-9	F28A10.6	sir-2.1	R11A8.4	ppk-3	VF11C1L.1
alh-6	F56D12.1	ugt-59	R11A8.3	C29F7.3	C29F7.3
chil-24	T10D4.3	gta-1	K04D7.3	cah-4	R01E6.3
gcy-15	Y27F2A.a	hpo-5	T14G10.7	nkat-1	F28H6.3
bcmo-2	F53C3.12	Y38F2AR.12	Y38F2AR.12	idhb-1	C37E2.1
R11F4.1	R11F4.a	gba-3	F11E6.1	F20D1.9	F20D1.9
sod-5	ZK430.3	C30H6.7	C30H6.7	piki-1	F39B1.1
C17C3.1	C17C3.1	Y7A9A.1	Y7A9A.1	suox-1	H13N06.4

upb-1	F13H8.7	F55B11.1	F55B11.1	tbh-1	H13N06.6
art-1	C15F1.6	ugt-22	C08F11.8	ent-2	K09A9.3
kat-1	T02G5.8	seld-1	Y45F10A.4	K09A9.6	K09A9.6
acdh-12	E04F6.5	fat-1	Y67H2A.8	F59F4.1	F59F4.1
aqp-1	F32A5.5	ugt-65	F08G5.5	B0395.3	B0395.3
tph-1	ZK1290.2	acl-13	F08G5.2	ace-1	W09B12.1
ttm-5	Y54E5A.1	dpm-3	F28D1.11	T20F7.3	T20F7.3
F39B2.3	F39B2.3	acs-20	F28D1.9	acdh-10	T08G2.3
C50D2.7	C50D2.7	C42C1.11	AP-1	pcaf-1	Y47G6A.6
cat-2	B0432.5	hpo-12	C42C1.10	acl-11	F28B3.9
C03H5.4	C03H5.4	phy-2	F35G2.4	ace-2	Y44E3A.2
pho-14	T13B5.3	B0001.4	B0001.4	sir-2.4	C06A5.11
gba-1	C33C12.3	ZK822.5	ZK822.5	Y105E8A.20	Y105E8E.w
gba-2	C33C12.8	ZK792.1	ZK792.1	hex-4	Y51F10.5
B0454.6	B0454.6	acl-3	ZK809.2	set-32	C41G7.4
gst-7	F11G11.2	gfat-2	F22B3.4	C31H5.6	C31H5.6
R05F9.6	R05F9.6	gspd-1	B0035.5	B0205.6	B0205.6
pho-4	T16D1.2	cpt-2	R07H5.2	fdps-1	R06C1.2
algn-2	F09E5.2	ard-1	F01G4.2	gst-43	Y71F9AL.5
T28D9.3	T28D9.3	hpo-4	T05E11.6	asm-1	B0252.2
dgk-5	K06A1.6	alh-3	F36H1.6	gbh-1	D2089.5
T02G5.4	T02G5.4	hrg-4	F36H1.5	dtmk-1	R53.2
T02G5.7	T02G5.7	mogs-1	F13H10.4	Y48E1B.3	Y48E1B.3
skpo-3	F32A5.2	aqp-3	Y69E1A.7	ippk-1	Y17G7B.13
acs-15	R07C3.4	inpp-1	T25B9.10	fmo-3	Y39A1A.19
set-11	F34D6.4	ugt-54	T25B9.7	Y48A6B.9	Y48A6B.9
gcy-15	Y27F2A.k	R102.4	R102.4	dot-1.3	W06D11.4
aagr-2	R05F9.12	fmo-2	K08C7.5	cept-1	F22E10.5
frh-1	F59G1.7	fmo-1	K08C7.2	tre-4	F15A2.2
rars-2	C29H12.1	nkb-2	C43F9.6	nkb-3	F55F3.3
C44B7.7	C44B7.7	ugt-43	F01D4.1	mrp-5	F14F4.3
sod-1	C15F1.7	R10H10.6	R10H10.6	slc-25A21	R11.1
pdl-1	C27H5.1	acs-18	R09E10.3	acdh-7	T25G12.5
mthf-1	C06A8.1	thk-1	Y43C5A.5	abt-2	F12B6.1
vha-4	T01H3.1	ech-9	F01G10.3	catp-1	Y105E8A.12
sphk-1	C34C6.5	ech-8	F01G10.2	F26H9.5	F26H9.5
acp-2	F14E5.4	qns-1	C24F3.4	fut-6	T05A7.5
piga-1	D2085.6	gst-3	K08F4.11	hex-3	Y39A1C.4
C18E9.4	C18E9.4	gst-4	K08F4.7	T25C8.1	T25C8.1
eat-3	D2013.5	gst-2	K08F4.6	idi-1	K06H7.9

sdhb-1	F42A8.2	gcy-29	C04H5.3	snf-6	M01G5.5
nlt-1	ZK892.2	W02H5.8	W02H5.a	ugt-60	C07A9.6
pde-4	R153.1	hmgs-1	F25B4.6	trxr-2	ZK637.10
B0228.7	B0228.7	F44E7.2	F44E7.2	Y54F10AM.5	Y54F10AM.5
glna-2	DH11.1	Y41D4A.6	Y41D4A.6	F52C9.3	F52C9.3
C08B11.8	C08B11.8	set-23	Y41D4B.12	pho-9	Y71H2AM.16
decr-1.3	T05C12.3	daao-1	Y69A2AR.5	nars-2	Y66D12A.23
M110.7	M110.7	egl-8	B0348.4	mans-4	ZC410.3
K01C8.1	K01C8.1	abt-4	Y39D8C.1	trxr-1	C06G3.7
tdc-1	K01C8.3	ugt-42	F31F4.7	lmd-4	F07G11.9
C26D10.4	C26D10.4	icl-1	C05E4.9	pho-6	F52E1.8
skpo-1	F49E12.1	H24K24.3	H24K24.3	gly-7	Y46H3A.6
acp-3	F14E5.3	fmo-5	H24K24.5	lin-46	R186.4
gbh-2	M05D6.7	hacd-1	R09B5.6	ZC443.1	ZC443.1
decr-1.2	W01C9.4	R09B5.11	R09B5.11	ugt-10	T19H12.11
pyr-1	D2085.1	F16B4.6	F16B4.6	ugt-49	AC3.2
C34C6.4	C34C6.4	alh-2	K04F1.15	hex-5	Y70D2A.2
agxt-1	T14D7.1	alh-5	T08B1.3	algn-1	T26A5.4
enol-1	T21B10.2	F59A7.7	F59A7.7	ppk-2	Y48G9A.8
gcs-1	F37B12.2	cysl-4	F59A7.9	Y37B11A.2	Y37B11A.2
mtrr-1	C01G6.6	ckb-4	F22F7.5	pstk-1	Y49E10.22
acs-7	C01G6.7	C01B4.6	C01B4.6	pps-1	T14G10.1
gss-1	M176.2	Y45G12B.3	Y45G12B.3	Y73B6BL.29	Y73B6BL.29
chil-13	M176.8	ugt-53	T03D3.1	T25B9.1	T25B9.1
chil-15	R09D1.1	slc-28.2	F27E11.2	ech-5	F56B3.5
chil-16	R09D1.2	ugt-64	C07G3.9	sqrd-1	F02H6.5
chil-17	R09D1.3	T22F3.3	T22F3.3	C27D8.4	C27D8.4
chil-18	R09D1.5	cysl-3	R08E5.2	coq-6	K07B1.2
chil-19	R09D1.6	R08F11.1	R08F11.1	rhr-2	B0240.1
chil-20	R09D1.7	R08F11.7	R08F11.7	ugt-6	ZC455.4
gcy-1	AH6.1	ugt-32	F47C10.6	elpc-3	ZK863.3
ugt-58	F35H8.6	cyp-35A5	K07C6.5	tre-3	W05E10.4
E02H1.6	E02H1.6	cyp-35A4	C49G7.8	acy-4	T01C2.1
T15H9.6	T15H9.6	D2063.1	D2063.e	K09H11.1	K09H11.1
sqv-8	ZK1307.5	F32D1.5	F32D1.5	acs-10	AH10.1
chil-9	ZK938.6	T08H10.1	T08H10.1	cyp-37B1	F28G4.1
C08H9.3	C08H9.3	ugt-61	F39G3.1	C13C4.4	C13C4.4
chil-1	C08H9.4	adss-1	C37H5.6	pitr-3	B0222.3
chil-2	C08H9.6	C37H5.13	C37H5.13	F08F3.4	F08F3.4

chil-3	C08H9.7	ugt-9	T19H12.1	slc-28.1	F27E11.1
chil-4	C08H9.10	T19H12.6	T19H12.6	gcy-9	ZK455.2
chil-5	C08H9.11	ugt-12	T19H12.9	dot-1.4	F55G7.2
chil-6	C08H9.12	ugt-11	T19H12.10	B0272.4	B0272.4
chil-7	C08H9.13	ugt-13	H23N18.1	dpyd-1	C25F6.3
chil-8	C08H9.14	ugt-14	H23N18.2	F52H2.4	F52H2.4
F26C11.1	F26C11.1	ugt-8	H23N18.3	cdo-1	F56F10.3
pho-10	C05C10.1	H23N18.4	H23N18.4	hap-1	ZC395.7
C05C10.3	C05C10.3	catp-2	C02E7.1	Y53G8B.1	Y53G8B.1
pho-11	C05C10.4	ugt-7	C13D9.9	anmt-1	B0303.2
flad-1	R53.1	ugt-63	C04F5.7	B0524.2	B0524.2
let-268	F52H3.1	ugt-51	C03A7.11	C39B5.6	C39B5.6
gpd-4	F33H1.2	C03A7.13	C03A7.13	cht-4	Y22D7AL.14
plc-3	T01E8.3	ncx-2	C10G8.5	hdl-1	ZK829.2
gcy-4	ZK970.5	acl-6	F08F3.2	gstk-2	D2024.7
gcy-5	ZK970.6	ugt-48	C18C4.3	gba-4	Y4C6B.6
C07E3.9	C07E3.9	hex-2	C14C11.3	ugt-45	Y37E11AR.5
gpd-1	T09F3.3	gcst-1	F25B4.1	pnc-1	Y38C1AA.3
C14A4.3	C14A4.3	K09H11.7	K09H11.7	gcy-37	C54E4.3
ech-4	R06F6.9	C53A3.2	C53A3.2	gcy-25	Y105C5B.2
gmps-1	M106.4	galt-1	M03F8.4	F13H10.5	F13H10.5
metr-1	R03D7.1	acy-2	C10F3.3	afmd-1	D2024.2
gst-5	R03D7.6	mcp-1	C10F3.4	prdx-6	Y38C1AA.11
aars-1	W02B12.6	W02F12.2	W02F12.2	gpx-4	Y94H6A.4
hpo-20	Y110A2AL.12	hpo-8	T15B7.2	dars-2	F10C2.6
mboa-6	R155.1	C55H1.1	C55H1.1	rft-2	Y47D7A.14
cchl-1	T06D8.6	mys-1	VC5.4	gana-1	R07B7.11
pcs-1	F54D5.1	lmd-5	T01C4.1	ugt-56	T04H1.8
F45H10.2	F45H10.2	ugt-39	F10D2.2	gcy-14	ZC412.2
Y39G8B.2	Y39G8B.2	ugt-40	F10D2.5	ncx-5	Y32F6B.2
cyp-37A1	F01D5.9	C05C8.7	phi-49	tag-38	B0222.4
ctl-1	Y54G11A.6	ugt-1	AC3.7	acs-3	T08B1.6
mes-2	R06A4.7	pap-1	Y32F6A.3	folt-1	C06H2.4
catp-4	C01G12.8	ZK836.2	ZK836.2	gst-23	T28A11.11
cbs-2	F54A3.4	ugt-55	T04H1.7	fre-1	Y113G7A.8
pisy-1	Y46G5A.5	T28H10.1	T28H10.1	H43I07.3	H43I07.3
spds-1	Y46G5A.19	dhs-21	R11D1.11	cyp-32B1	Y5H2B.5
acl-7	Y46G5A.21	ugt-3	ZC455.3	F49H6.5	F49H6.5
Y51H7C.9	Y51H7C.i	fat-7	F10D2.9	cbs-1	ZC373.1
K02F3.2	K02F3.2	F09G2.8	F09G2.8	acl-1	F59F4.4

ceeh-1	K02F3.6	cyp-32A1	C26F1.2	ZK563.7	ZK563.7
ucr-2.3	T24C4.1	F26D11.1	F26D11.1	hsd-3	ZC449.6
T24C4.5	phi-53	ech-3	F43H9.1	tald-1	Y24D9A.8
sucl-2	F23H11.3	F41E6.5	F41E6.5	Y47G6A.22	Y47G6A.22
ckb-3	B0285.10	H14N18.4	H14N18.4	Y47D9A.1	Y47D9A.1
mlcd-1	F35G12.1	aat-2	F07C3.7	aqp-2	C01G6.1
sdhd-1	F33A8.5	K07B1.4	K07B1.4	gln-3	Y105C5B.28
F40F8.1	F40F8.1	R04B5.5	R04B5.5	Y94H6A.7	Y94H6A.7
cox-15	T06D8.5	gna-1	B0024.12	Y105C5B.15	Y105C5B.15
T06D8.10	T06D8.10	ugt-34	F29F11.2	algn-7	Y60A3A.14
B0491.1	B0491.1	pho-8	R13H4.3	chil-22	R09D1.10
B0491.7	B0491.7	sodh-1	K12G11.3	chil-23	R09D1.11
gfat-1	F07A11.2	mans-2	C52E4.5	chil-27	T19H5.3
F07A11.5	F07A11.5	F10C2.4	F10C2.4	mtm-9	Y39H10A.3
inos-1	VF13D12L.1	kmo-1	R07B7.5	Y39G8B.1	Y39G8B.1
ldh-1	F13D12.2	C27A7.1	C27A7.1	acl-4	F49H12.6
F43G6.5	F43G6.5	C27A7.3	C27A7.3	F23F1.6	F23F1.6
tpi-1	Y17G7B.7	C27A7.5	C27A7.5	chil-25	T19H5.1
polg-1	Y57A10A.15	ugt-37	F10D2.6	gcy-3	R134.1
daf-22	Y57A10C.6	ugt-38	F10D2.7	nsun-5	Y53F4B.4
mecr-1	W09H1.5	ugt-41	F10D2.11	ads-1	Y50D7A.7
alh-7	F45H10.1	pitr-5	F09G2.3	gly-4	Y116F11B.12
C31C9.2	C31C9.2	ugt-36	F09G2.6	C50D2.2	C50D2.2
ace-4	Y48B6A.7	cyp-35A1	C03G6.14	F49E2.1	F49E2.1
ctl-2	Y54G11A.5	cyp-35A2	C03G6.15	Y62E10A.13	Y62E10A.13
agl-1	R06A4.8	ddo-2	F18E3.7	Y47D3A.29	Y47D3A.29
cysl-2	K10H10.2	ftn-1	C54F6.14	F21D5.1	F21D5.1
tps-2	F19H8.1	sptl-2	F43H9.2	moc-2	W01A11.6
glna-1	C09F9.3	vars-1	ZC513.4	gst-6	F11G11.3
elo-9	Y53F4B.2	catp-3	C09H5.2	pho-12	C27A2.4
Y53F4B.3	Y53F4B.3	vha-18	F52E1.10	gln-2	K03H1.1
sqv-2	Y110A2AL.14	pxn-1	ZK994.3	rpc-1	C42D4.8
cox-10	Y46G5A.2	pitr-2	B0222.2	Y41D4A.6	Y41D4A.6
bcmo-1	Y46G5A.24	ucp-4	K07B1.3	F16B4.6	F16B4.6
gsy-1	Y46G5A.31	acl-14	K07B1.5	D2063.1	D2063.e
pck-1	W05G11.6	haao-1	K06A4.5	mdh-1	F46E10.10
crls-1	F23H11.9	acs-14	F11A3.1	dhs-21	R11D1.11
acsd-1	Y71D11A.3	pfk-1.2	C50F4.2	papl-1	F18E2.1
polh-1	F53A3.2	cyp-29A4	B0331.1	tag+A10:B10-96	M01D7.4

gly-14	M01F1.1	aqp-4	F40F9.9	Y54E10BR.1	M01B12.e
gsr-1	C46F11.2	anmt-3	T07C12.9	gcy-21	F22E5.3
pdi-1	C14B1.1	uda-1	K08H10.4	F53C3.13	F53C3.13
amx-1	R13G10.2	acl-2	T06E8.1	alh-1	F54D8.3
C36A4.4	C36A4.4	R04B5.6	R04B5.6	vha-14	F55H2.2
acs-19	C36A4.9	ugt-47	R04B5.9	sqv-3	R10E11.4
nit-1	ZK1058.6	ugt-17	C08B6.1	gpdh-2	K11H3.1
glod-4	C16C10.10	C08B6.4	C08B6.4	K11H3.3	K11H3.3
B0285.6	B0285.6	B0024.13	B0024.13	R01H10.7	R01H10.7
ckb-1	B0285.8	ceeh-2	K07C5.5	mtm-6	F53A2.8
ckb-2	B0285.9	ugt-33	C35A5.2	acs-5	Y76A2B.3
prdx-3	R07E5.2	cat-4	F32G8.6	pfkb-1.2	K02B2.1
ugt-62	M88.1	T21C9.6	T21C9.6	dgk-4	F42A9.1
idhg-1	F35G12.2	aqp-6	C32C4.2	H24K24.3	H24K24.3
asb-1	F35G12.10	sqv-4	F29F11.1	fmo-5	H24K24.5
tag-174	F54D8.2	D1054.1	D1054.1	hacd-1	R09B5.6
prx-10	C34E10.4	secs-1	D1054.13	R09B5.11	R09B5.11
F48E8.3	F48E8.3	F17C11.7	F17C11.7	Y45G12B.3	Y45G12B.3
F56D2.2	F56D2.2	mboa-2	H19N07.4	cyp-35A5	K07C6.5
polq-1	W03A3.2	bgal-1	T19B10.3	acl-8	T05H4.1
mdh-2	F20H11.3	gly-20	C03E10.4	T05H4.4	T05H4.4
rpia-1	B0280.3	snf-11	T03F7.1	hpo-19	T05H4.5
dpy-31	R151.5	daf-11	B0240.3	T05H4.7	T05H4.7
psd-1	B0361.5	bus-18	F55A11.5	alh-4	T05H4.13
algn-11	B0361.8	pyc-1	D2023.2	acl-9	ZK40.1
hmgr-1	F08F8.2	mpst-1	D2023.5	dgtr-1	W01A11.2
pcp-1	ZK112.1	sodh-2	K12G11.4	cpt-6	W01A11.5
gsto-1	C29E4.7	F58H1.3	F58H1.3	K04A8.10	K04A8.10
aco-2	F54H12.1	gcy-33	F57F5.2	ppt-1	F44C4.5
acdh-6	C02D5.1	kmo-2	R07B7.4	asns-1	F25G6.6
ZK370.4	ZK370.4	ugt-15	C44H9.1	anmt-3	T07C12.9
ppat-1	T04A8.5	acly-2	B0365.1	uda-1	K08H10.4
T04A8.7	T04A8.7	F53F1.2	F53F1.2	T28H10.1	T28H10.1
set-2	C26E6.9	F53F1.3	F53F1.3	C14C10.1	C14C10.1
clk-1	ZC395.2	F25H9.6	F25H9.6	cyc-2.2	ZC116.2
ZC395.10	ZC395.10	F47B8.10	F47B8.10	ugt-5	ZC455.6
bas-1	C05D2.4	dlat-1	F23B12.5	F19G12.2	F19G12.2
aldo-2	F01F1.12	plc-2	Y75B12B.6	T03G6.3	T03G6.3
F25B5.6	F25B5.6	chil-12	M01B2.6	gcsh-1	D1025.2

T12A2.1	T12A2.1	aagr-4	F52D1.1	nac-1	F31F6.6
oatr-1	C16A3.10	F25E2.3	F25E2.3	yars-1	Y105E8A.19
mel-32	C05D11.11	D1005.2	D1005.2	abt-5	Y53C10A.9
ddo-3	F20H11.5	hex-1	T14F9.3	T22C1.3	T22C1.3
C13B9.2	C13B9.2	T03G6.3	T03G6.3	ugt-60	C07A9.6
K04C2.2	K04C2.a	pccb-1	F52E4.1	ppk-2	Y48G9A.8
F57B9.1	F57B9.1	F53C11.3	F53C11.3	Y37B11A.2	Y37B11A.2
ger-1	R01H2.5	Y50E8A.6	Y50E8A.6	cyp-37B1	F28G4.1
acs-4	F37C12.7	acs-2	F28F8.2	ZC443.1	ZC443.1
adr-2	T20H4.4	ddo-1	C47A10.5	acs-3	T08B1.6
pho-5	B0361.7	B0250.5	B0250.5	C13C4.4	C13C4.4
alh-12	Y69F12A.2	Y97E10AR.2	Y97E10AR.e	gcy-9	ZK455.2
upp-1	ZK783.2	mrp-1	F57C12.5	hex-5	Y70D2A.2
pcp-5	ZK688.6	T04G9.4	T04G9.4		

2. Materials and Methods

RNAi screen

Hatchlings were seeded on *E. coli* HT115 L4440 control or RNAi and incubated in 15°C for 60h, followed by 24h incubation at 25°C. When animals reached the gravid stage, they were stained with the previously described oil Red O method (164).

Scoring

Each gene was inactivated by RNAi in three independent biological experiments. Images were visually scored to determine growth under the given RNAi gene knockdown. Each image was scored independently by 2 researchers, giving us 6 scores in total (3 independent experiments, each scored by 2 researchers).

Appendix I: Molecular dissection of the soma-to-germ line trade-off in *C. elegans*

1. Introduction

In evolutionary terms, the only purpose of a living organism is to contribute its offspring to the next generation. However, the cost of reproduction for an organism is high (257). To reach reproductive age and achieve optimal reproduction, the organism needs to invest energy to grow and maintain its soma (body parts excluding germ cells). On the other hand, maintaining the germline (the tissues producing gametes) and, at least in some species, sustaining the developing offspring also require big energy investments (257–261). Since reproduction comes at the expense of bodily maintenance (i.e. in the lab, sterile animals are long-lived (262)) this soma-to-germ line "competition" for resources is described as the soma-to-germ line trade-off. Although this tradeoff is observed in most species so far studied (257,261), molecular understanding of how organisms selectively allocate resources to the soma and/or the germline is mostly lacking. I aimed to uncover the genetic pathways that control, and the genes that execute, the energetic trade-off between soma and germline in the soil nematode *Caenorhabditis elegans.*

2. Results

a. Inactivation of several *C. elegans* genes lead to 'Egg Only Fat' phenotype

Our lab developed whole-animal high-content genome-wide RNAi screening for genes controlling fat storage (163,164,263), which allowed us to identify 23 genes that are essential for proper soma-to-germline fat distribution. We identified a phenotype we named 'Egg Only Fat' (EOF). Unlike wild-type animals, which show fat stores in both the soma (mainly in the intestine) and in the developing eggs (germline), animals with an EOF phenotype show fat in the eggs but not in the soma (App. II Fig. 1A, B).

The predicted function of the 23 identified genes range from transcription factors to, kinases, phosphatases, genes involved in metabolism and cell signalling (Full list in App. II Table. 1).

App. II Fig. 1

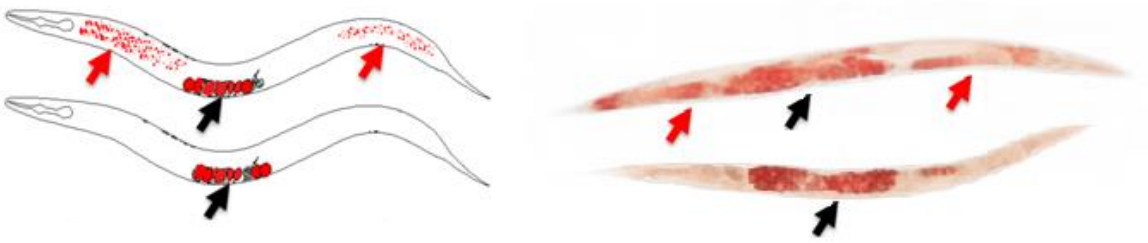

App. II Fig. 1

Schematic representation (left and representative images (right) of normal (top) and EOF (bottom) fat distribution in *C. elegans* as revealed by oil red O staining. Red arrows denote somatic fat, black arrows denote egg fat (germ line)

App. II Table. 1 Genes whose inactivation leads to EOF phenotype

WormBase sequence identifier	**Gene name**	***H. sapiens* homologs**	**Short characterization (based on www.wormbase.org)**
K02B12.1	*ceh-6*	POU3F2 (POU class 3 homeobox 2); POU3F3 (POU class 3 homeobox 3); POU3F4 (POU class 3 homeobox 4)	Predicted to have DNA-binding transcription factor activity. Involved in excretion; transdifferentiation; and water homeostasis. Expressed in body wall musculature; head neurons; hyp7 syncytium; intestine; and tail neurons.
F18F11.5	*drl-1/ mekk-3*	Isoform 1 of Mitogen-activated protein kinase kinase kinase 3	Predicted to have ATP binding activity and protein kinase activity. Expressed in body wall musculature; neurons; seam cell; and vulval muscle.
C06A1.1	*cdc-48.1*	Valosin containing protein	Exhibits ATPase activity and identical protein binding activity. Involved in ER-associated misfolded protein catabolic process; determination of adult lifespan; and positive regulation of mitotic cell cycle, embryonic. Expressed in several structures, including body wall musculature; germline; and gonad.
C41C4.8	*cdc-48.2*	Valosin containing protein	Exhibits ATPase activity and identical protein binding activity. Involved in ER-associated misfolded protein catabolic process; negative regulation of protein localization to centrosome; and protein localization to the nucleus.
C30F12.1	*rege-1*	ZC3H12C (zinc finger CCCH-type containing 12C)	Predicted to have RNA binding activity; endonuclease activity; and metal ion binding activity. Expressed in the tail.
Y47G6A.23	*lpd-3*	Isoform 7 of Uncharacterized protein KIAA1109	Expressed in the intestine. Human orthologs of this gene are implicated in Alkuraya-Kucinskas syndrome.
F33D4.1	*nhr-8*	NR1I2 (nuclear receptor subfamily 1 group I member 2); NR1I3 (nuclear receptor	Predicted to have nuclear receptor activity. Involved in cholesterol homeostasis. Localizes to the nucleus. E Expressed in the intestinal cell.

		subfamily 1 group I member 3); VDR (vitamin D receptor)	Human ortholog(s) of this gene is implicated in osteoporosis and rickets
C02F4.2	*tax-6/ cna-1/ pph2B-A/ pph-3*	PPP3CB (protein phosphatase 3 catalytic subunit beta) PPP3CC (protein phosphatase 3 catalytic subunit gamma)	Exhibits calcium ion binding activity and calmodulin-dependent protein phosphatase activity. Involved in male mating behavior; peptidyl-serine dephosphorylation; and positive regulation of growth rate. Expressed in several structures, including germline; head neurons; muscle cell; tail neurons; and ventral nerve cord. Human ortholog(s) of this gene are implicated in infantile or early childhood epileptic encephalopathy
F11E6.5	*elo-2*	ELOVL3 (ELOVL fatty acid elongase 3) ELOVL6 (ELOVL fatty acid elongase 6)	Predicted to have transferase activity, transferring acyl groups. Involved in the determination of adult lifespan; growth; and lipid metabolic process. Expressed in the intestine; pharyngeal muscle cell; tail; uterus; and ventral nerve cord.
B0348.4	*egl-8/ pbo-2*	PLCB4 (phospholipase C beta 4)	Predicted to have calcium ion binding activity and phosphatidylinositol phospholipase C activity. Involved in positive regulation of acetylcholine secretion, neurotransmission; positive regulation of axon regeneration; and thermotaxis. Expressed in the intestine; nervous system; non-striated muscle; and vas deferens.
B0365.3	*eat-6/ spa-1/ NaK/1*	ATP1A3 (ATPase Na+/K+ transporting subunit alpha 3)	Exhibits sodium:potassium-exchanging ATPase activity. Involved in action potential; establishment or maintenance of transmembrane electrochemical gradient; and monovalent inorganic cation transport. Localizes to membrane. Expressed in several structures, including coelomocyte; intestine; neurons; pharynx; and vulval muscle.
Y80D3A.5	*cyp-42A1*	CYP4V2 (cytochrome P450 family 4 subfamily V member 2)	Predicted to have heme-binding activity; iron ion binding activity; and oxidoreductase activity. Human ortholog(s) of this gene is implicated in Bietti crystalline corneoretinal dystrophy
T13C5.1	*daf-9/ cyp-22A1/ mig-8*	CYP2S1 (cytochrome P450 family 2 subfamily S member 1)	Predicted to have cholestanetriol 26-monooxygenase activity; heme-binding activity; and iron ion binding activity. Involved in cell-cell signaling; dauer larval

			development; and regulation of cell migration. Localizes to the neuronal cell body and perinuclear region of the cytoplasm. Expressed in several structures, including anterior ganglion; excretory cell; head neurons; spermatheca; and vulval muscle.
T01H3.1	*vha-4*	ATP6V0B (ATPase H+ transporting V0 subunit b)	Predicted to have proton transmembrane transporter activity. Involved in embryo development. Expressed in excretory cells and rectum.
Y50D7A.3		PHKG1 (phosphorylase kinase catalytic subunit gamma 1) PHKG2 (phosphorylase kinase catalytic subunit gamma 2).	Predicted to have ATP binding activity; calmodulin-binding activity; and phosphorylase kinase activity. Human ortholog(s) of this gene is implicated in glycogen storage disease IXc.
F37B12.3		NUS1 dehydrodolichyl diphosphate synthase subunit	Predicted to have transferase activity, transferring alkyl or aryl (other than methyl) groups.
Y11D7A.9		PGAP2 (post-GPI attachment to proteins 2)	Enriched in germline precursor cell and hypodermis
C15H9.4		TMCC1 (transmembrane and coiled-coil domain family 1); TMCC2 (transmembrane and coiled-coil domain family 2); TMCC3 (transmembrane and coiled-coil domain family 3)	Enriched in AVK; coelomocyte; excretory cell; and head mesodermal cell. Human TMCC3 exhibits 14-3-3 protein binding activity and identical protein binding activity.
C15C7.5	*bubl-1*		Expressed in head neurons and pharyngeal muscle cell
H04M03.4	*glf-1*		Exhibits UDP-galactopyranose mutase activity. Involved in cellular polysaccharide biosynthetic process. Expressed in hypodermis; muscle cell; and neurons
C50D2.1			Enriched in germline precursor cell and hypodermis
F56B3.2			Enriched in germline and hypodermis
T13F2.6			Enriched in germline; germline precursor cell; and male distal tip cell

b. EOF genes act mainly in intestinal and neuronal tissues

We showed that whole-body RNAi against the EOF genes alters soma-to-germline fat allocation. Then we investigated from which tissues the EOF genes exert their role on soma-to-germline fat allocation. To this, we knocked down the EOF genes one tissue at a time using tissue specific RNAi combined with fat screening as previously described (163,164). We specifically tested a potential role for the EOF genes in the nervous, muscle, digestive, and epithelial systems using already available *C. elegans* strains that enable tissue-specific RNAi in those tissues (264,265).

The results (App. II Table 2) pointed to most EOF genes acting in neurons and intestine rather than in epidermal and muscle systems. Critical role of the intestine in fat distribution is not surprising as the intestine is the major metabolic and fat storage organ is *C. elegans* and many metabolic genes are expressed largely or exclusively in the *C. elegans'* intestine (266). More interestingly, the intestine is also the site for the production of vitellogenins, *C. elegans*' yolk protein. Vitellogenins, after being produced in the intestine, are secreted into the body cavity and then taken up by the gonad to reach oocytes (267), thus linking the intestine to the reproductive system. Similarly *C. elegans'* nervous system has been described to link food sensing to energy storage. Firstly, the nervous system, specifically the motor neuron MC, controls *C. elegans* rate of pumping and rate of pumping determines the amount of food intake of the worm (268). Specifically, pharynx pumping rate is modulated by major neuroendocrine effectors,

serotonin and Transforming Growth Factor β (TGF β) that respond to food availability and sensitise the sensory neurons (269). Serotonin signalling from *C. elegans* chemosensory neurons was also shown to reduce fat levels through increasing the levels of fatty acid oxidation (269).

App. II Table 2

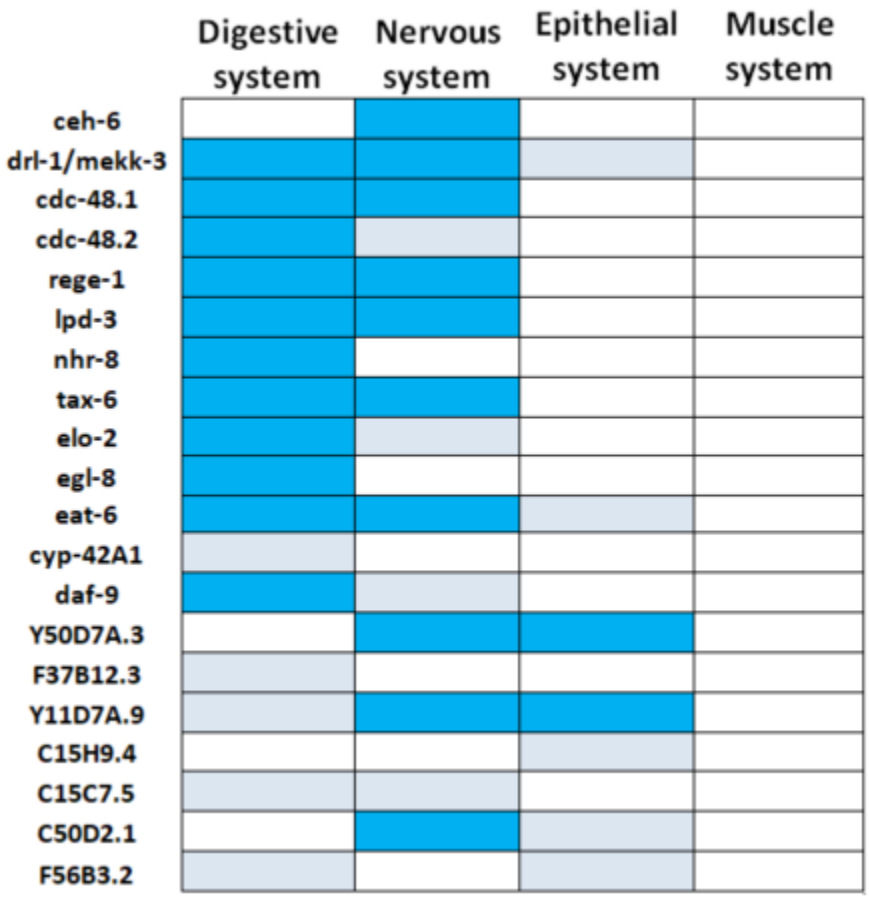

App. II Table 2. EOF genes are acting mainly in intestinal and neuronal tissues. Results of tissue-specific RNAi against EOF genes are depicted according to the following key: White – cannot be distinguished from empty vector RNAi control; Light blue – binomial distribution of phenotypes, as in some animals in the treated population show EOF while others show WT phenotypes; Blue – penetrant Egg Only Fat phenotype. Images of control and treated populations were visually scored.

c. Fat synthesis is reduced in EOF animals

EOF animals show fat stores in the developing embryos, but mostly lack fat in the soma. Hence, we hypothesized that animals exhibiting the EOF phenotype may have:

1) impaired ability to generate fat stores coupled to a prioritized delivery of the scarce fat stores to the germline,

2) excessive burning of their somatic fat stores, and/or

3) exacerbated transfer of nutrient reserves to the germline.

As a proxy for the level of fat breakdown versus build up in the EOF RNAi treated animals, we measured, using qRT-PCR, the transcriptional levels of the fat synthesis genes *sbp-1* (Sterol regulatory element Binding Protein is a transcription factor that activates lipogenesis), *pod-2* (acetyl-CoA carboxylase, catalyzes the first step in de novo fatty acid biosynthesis), *fasn-1* (encodes the rate limiting fatty acid synthase), *acs-1* (ortholog of human ACSF2, acyl-CoA synthetase family member 2), *fat-5* (delta-9 fatty acid desaturase), *fat-6* (Acyl-CoA desaturase), and *fat-7* (delta-9 fatty acid desaturase) (App. II Fig. 2A). On the other hand, to assess the levels of fat breakdown we measured the expression of the genes *lipl-1*, *lipl-3*, and *lipl-4* (encoding lysosomal lipases), *atgl-1* (adipose triglyceride lipase), and *acox-4* (first enzyme of the fatty acid beta-oxidation pathway).

We observed that RNAi against most of the EOF genes lead to a reduction in the expression levels of fat synthesis genes *fasn-1, fat-5, fat-6, fat-7* (App. II Fig. 2B). By

contrast, the expression of genes involved in fat breakdown was more variable among *C. elegans* showing an EOF phenotype (App. II Fig. 2C). By contrast, the expression of genes involved in fat breakdown was either reduced such as for l*ipl-3, atgl-1* and *acox-4* (App. II Fig. 2B) or did not change in animals showing an EOF phenotype. Exceptionally, RNAi against *drl-1*, *eat-2* F56B3.2 led to induction of the lysosomal lipases *lipl-1* and *lipl-4*. However, for the most part the expression of *lipl-1* and *lipl-4* did not change or was reduced in the remaining EOF treatments (App. II Fig. 2C). These preliminary results suggest that inactivation of the EOF genes would mainly impair *C. elegans*' ability to build fat stores. However, in some cases, excessive burning of somatic fat stores may be the principal or an additional mechanism explaining the imbalance of soma-to-germline distribution of fat observed in the EOF animals..

As for the third hypothesis, exacerbated transfer of nutrient reserves to the germline, it awaits testing. The use of fluorescent markers of vitellogenins (lipid-binding proteins that transport fats from the intestine to the developing embryos) and of the germline vitalogenins-receptors RME-1 and RME-2 may aid in further understanding where and how fats are depleted from the soma or overloaded in the germline.

App. II Fig. 2

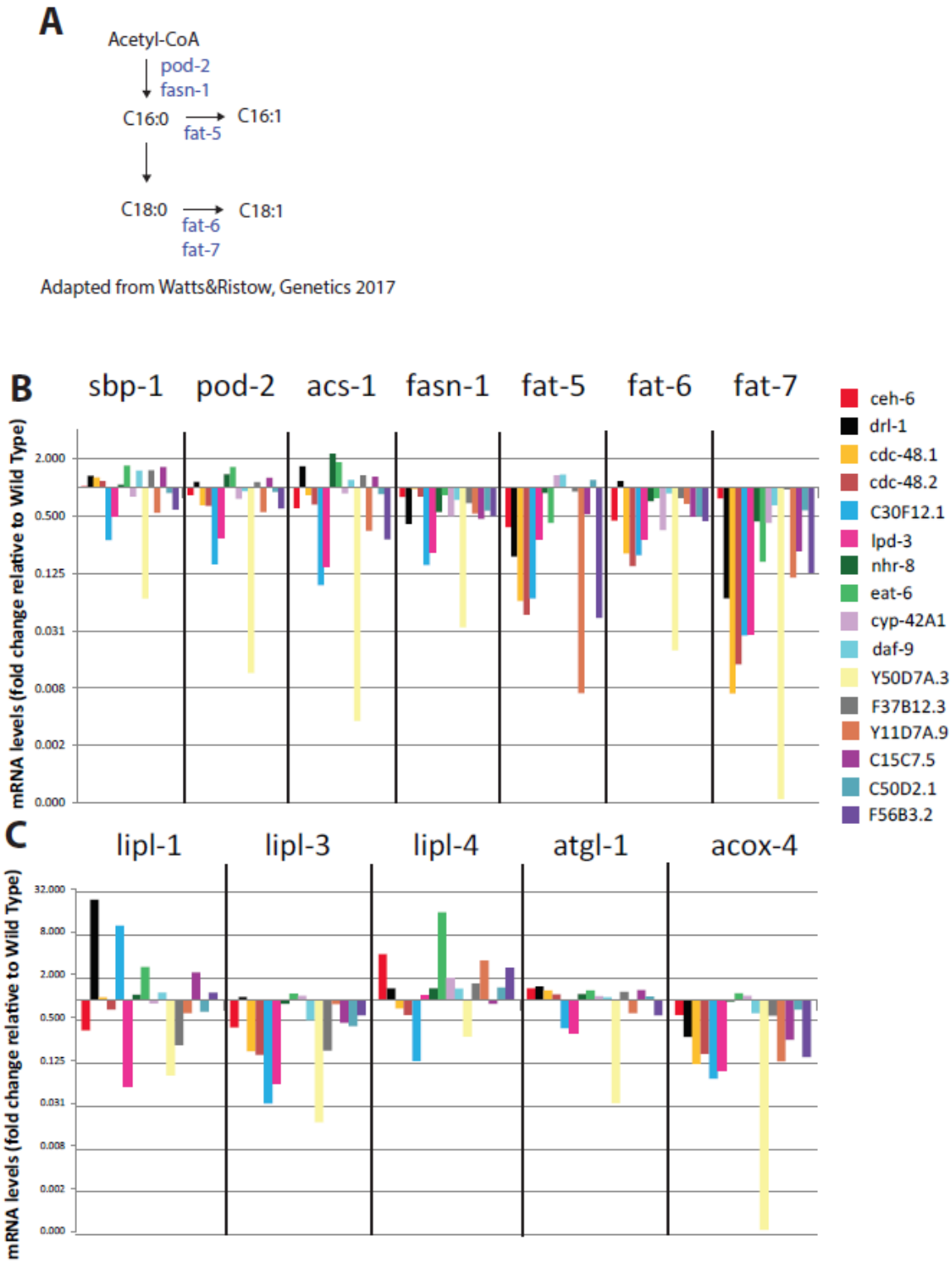
A
Acetyl-CoA
pod-2
fasn-1
C16:0
C16:1
fat-5
C18:0
C18:1
fat-6
fat-7
Adapted from Watts&Ristow, Genetics 2017
B
sbp-1
pod-2
acs-1
fasn-1
fat-5
fat-6
fat-7
mRNA levels (fold change relative to Wild Type)
2.000
0.500
0.125
0.031
0.008
0.002
0.000
ceh-6
drl-1
cdc-48.1
cdc-48.2
C30F12.1
lpd-3
nhr-8
eat-6
cyp-42A1
daf-9
Y50D7A.3
F37B12.3
Y11D7A.9
C15C7.5
C50D2.1
F56B3.2
C
lipl-1
lipl-3
lipl-4
atgl-1
acox-4
mRNA levels (fold change relative to Wild Type)
32.000
8.000
2.000
0.500
0.125
0.031
0.008
0.002
0.000

App. II Fig. 2 Expression of somatic fat synthesis genes is reduced in EOF animals

(A) Molecular pathway of fat synthesis in *C. elegans*

(B) *sbp-1, pod-2, acs-1, fasn-1, fat-5, fat-6, fat-7* expression in animals treated with RNAi against EOF genes (EOF genes tested listed to the right) (n=1)

(C) *lipl-1, lipl-3, lipl-4, atgl-1, acox-4* expression in animals treated with RNAi against EOF genes (EOF genes tested listed to the right) (n=1)

3. Conclusion

The “Egg Only Fat” phenotype is a novel phenotype that is likely to aid in addressing relevant biological questions including how multicellular organism make decisions about nutrient allocation among the different tissues and how the control the actual mobilization of energy across all cells of the body. The preliminary studies presented here suggest that the mechanisms underlying energy allocation between tissues is rather complex since, although grossly EOF animals seem to share the same phenotype, they do not share all the same molecular changes. Further, some EOF genes seem to exert their function from the intestine while others control soma-to-germline fat allocation from the neurons. Therefore, my Initial characterization of the EOF genes points to the notion that this phenotype can be achieved through different molecular pathways. Further exploration of the EOF phenotype may enable building the first atlas of genes controlling and/or executing the fundamental decision of where an animal allocates its energy: soma or reproduction.

4. Materials and Methods

C. elegans growth conditions:

Following *C. elegans* strains were used: N2 (Bristol), MGH171 sid-1(qt9) V;(alxIs9 [vha-6p::sid-1::SL2::GFP])-intestine specific RNAi (264), TU3311 sid-1(qt9) V,(uIs60 [unc-119p::YFP + unc-119p::sid-1])-Hypersensitive neuronal RNAi (265), JM43 rde-1(ne219) V; xkIs99[wrt-2p::rde-1::unc-54 3'UTR]-epidermis specific RNAi (264), SPC272 sid-1(qt9);IS[myo-3::SID-1::RFP]-muscle specific RNAi strain.

C. elegans were grown on Nematode Growth Media at 20°C. They were fed with *E.coli* strain OP50 in a 20 times concentrated S buffer. For RNAi experiments, *E. coli* HT115 bacteria strain was used.

Transcriptional analysis

C. elegans were synchronized by hypochlorite treatment, then grown to adulthood on the 10cm NGM plates. They were fed RNAi for EOF genes from L1 and were harvested as young adults and flash-frozen in liquid nitrogen.

RNA isolation was performed using TRI Reagent (Molecular Research Center) based on phenol-chloroform extraction. The concentration and quality of RNA were evaluated. cDNA was prepared using M-MLV Reverse Transcriptase (Life Technologies) and oligodT primers (Life Technologies). qPCR was performed using iTaq™ Universal SYBR® Green Supermix (BioRad).

References

Bibliography

1. Carlberg C, Molnár F. Overview: what is gene expression? Mechanisms of gene regulation. Dordrecht: Springer Netherlands; 2014. p. 3–15.
2. Hobert O. Common logic of transcription factor and microRNA action. Trends Biochem Sci. 2004 Sep;29(9):462–8.
3. Atkinson TJ, Halfon MS. Regulation of gene expression in the genomic context. Comput Struct Biotechnol J. 2014 Jan 29;9:e201401001.
4. Mitsis T, Efthimiadou A, Bacopoulou F, Vlachakis D, Chrousos G, Eliopoulos E. Transcription factors and evolution: An integral part of gene expression (Review). Wrld Acd Sci. 2020 Jan 17;
5. Lambert SA, Jolma A, Campitelli LF, Das PK, Yin Y, Albu M, et al. The human transcription factors. Cell. 2018 Feb 8;172(4):650–65.
6. Hochheimer A, Tjian R. Diversified transcription initiation complexes expand promoter selectivity and tissue-specific gene expression. Genes Dev. 2003 Jun 1;17(11):1309–20.
7. Gertz J, Reddy TE, Varley KE, Garabedian MJ, Myers RM. Genistein and bisphenol A exposure cause estrogen receptor 1 to bind thousands of sites in a cell type-specific manner. Genome Res. 2012 Nov;22(11):2153–62.
8. Chalbos D, Vignon F, Keydar I, Rochefort H. Estrogens stimulate cell proliferation and induce secretory proteins in a human breast cancer cell line (T47D). J Clin Endocrinol Metab. 1982 Aug;55(2):276–83.
9. Castro-Rivera E, Wormke M, Safe S. Estrogen and aryl hydrocarbon responsiveness of ECC-1 endometrial cancer cells. Mol Cell Endocrinol. 1999 Apr 25;150(1–2):11–21.
10. Dowell RD, Ryan O, Jansen A, Cheung D, Agarwala S, Danford T, et al. Genotype to phenotype: a complex problem. Science. 2010 Apr 23;328(5977):469.
11. Sassetti CM, Boyd DH, Rubin EJ. Comprehensive identification of conditionally essential genes in mycobacteria. Proc Natl Acad Sci USA. 2001 Oct 23;98(22):12712–7.
12. Miller DP, Scott DA. Inherently and Conditionally Essential Protein Catabolism Genes of Porphyromonas gingivalis. Trends Microbiol. 2021 Jan;29(1):54–64.

13. Templeman NM, Murphy CT. Regulation of reproduction and longevity by nutrient-sensing pathways. J Cell Biol. 2018 Jan 2;217(1):93–106.

14. Chantranupong L, Wolfson RL, Sabatini DM. Nutrient-sensing mechanisms across evolution. Cell. 2015 Mar 26;161(1):67–83.

15. Das D, Arur S. Conserved insulin signaling in the regulation of oocyte growth, development, and maturation. Mol Reprod Dev. 2017 Jun;84(6):444–59.

16. Bigas A, Espinosa L. Notch signaling in cell–cell communication pathways. Curr Stem Cell Rep. 2016 Dec;2(4):349–55.

17. Huminiecki L, Goldovsky L, Freilich S, Moustakas A, Ouzounis C, Heldin C-H. Emergence, development and diversification of the TGF-beta signalling pathway within the animal kingdom. BMC Evol Biol. 2009 Feb 3;9:28.

18. Dupont J, Reverchon M, Bertoldo MJ, Froment P. Nutritional signals and reproduction. Mol Cell Endocrinol. 2014 Jan 25;382(1):527–37.

19. Roa J, Tena-Sempere M. Connecting metabolism and reproduction: roles of central energy sensors and key molecular mediators. Mol Cell Endocrinol. 2014 Nov;397(1–2):4–14.

20. Hietakangas V, Cohen SM. Regulation of tissue growth through nutrient sensing. Annu Rev Genet. 2009;43:389–410.

21. Rohde J, Heitman J, Cardenas ME. The TOR kinases link nutrient sensing to cell growth. J Biol Chem. 2001 Mar 30;276(13):9583–6.

22. Siebel C, Lendahl U. Notch signaling in development, tissue homeostasis, and disease. Physiol Rev. 2017 Oct 1;97(4):1235–94.

23. Vander Ark A, Cao J, Li X. TGF-β receptors: In and beyond TGF-β signaling. Cell Signal. 2018 Sep 7;52:112–20.

24. Gangloff Y-G, Mueller M, Dann SG, Svoboda P, Sticker M, Spetz J-F, et al. Disruption of the mouse mTOR gene leads to early postimplantation lethality and prohibits embryonic stem cell development. Mol Cell Biol. 2004 Nov;24(21):9508–16.

25. Shiota C, Woo J-T, Lindner J, Shelton KD, Magnuson MA. Multiallelic disruption of the rictor gene in mice reveals that mTOR complex 2 is essential for fetal growth and viability. Dev Cell. 2006 Oct;11(4):583–9.

26. Vanfleteren JR, Braeckman BP. Mechanisms of life span determination in Caenorhabditis elegans. Neurobiol Aging. 1999 Oct;20(5):487–502.

27. Lapierre LR, De Magalhaes Filho CD, McQuary PR, Chu C-C, Visvikis O,

Chang JT, et al. The TFEB orthologue HLH-30 regulates autophagy and modulates longevity in Caenorhabditis elegans. Nat Commun. 2013;4:2267.

28. Burkewitz K, Zhang Y, Mair WB. AMPK at the nexus of energetics and aging. Cell Metab. 2014 Jul 1;20(1):10–25.

29. Goh GYS, Winter JJ, Bhanshali F, Doering KRS, Lai R, Lee K, et al. NHR-49/HNF4 integrates regulation of fatty acid metabolism with a protective transcriptional response to oxidative stress and fasting. Aging Cell. 2018 Mar 5;17(3):e12743.

30. Aramburu J, Ortells MC, Tejedor S, Buxadé M, López-Rodríguez C. Transcriptional regulation of the stress response by mTOR. Sci Signal. 2014 Jul 1;7(332):re2.

31. Wang Z, Wang N, Liu P, Xie X. AMPK and Cancer. Exp Suppl. 2016;107:203–26.

32. Murugan AK. mTOR: Role in cancer, metastasis and drug resistance. Semin Cancer Biol. 2019 Aug 10;59:92–111.

33. Hopkins BD, Goncalves MD, Cantley LC. Insulin-PI3K signalling: an evolutionarily insulated metabolic driver of cancer. Nat Rev Endocrinol. 2020 Mar 3;16(5):276–83.

34. Honda Y, Honda S. The daf-2 gene network for longevity regulates oxidative stress resistance and Mn-superoxide dismutase gene expression in Caenorhabditis elegans. FASEB J. 1999 Aug;13(11):1385–93.

35. Sarbassov DD, Sabatini DM. Redox regulation of the nutrient-sensitive raptor-mTOR pathway and complex. J Biol Chem. 2005 Nov 25;280(47):39505–9.

36. Wu C-W, Storey KB. mTOR Signaling in Metabolic Stress Adaptation. Biomolecules. 2021 May 1;11(5).

37. LaRue BL, Padilla PA. Environmental and genetic preconditioning for long-term anoxia responses requires AMPK in Caenorhabditis elegans. PLoS ONE. 2011 Feb 3;6(2):e16790.

38. Keating R, McGargill MA. mTOR Regulation of Lymphoid Cells in Immunity to Pathogens. Front Immunol. 2016 May 11;7:180.

39. Mesquita I, Moreira D, Sampaio-Marques B, Laforge M, Cordeiro-da-Silva A, Ludovico P, et al. AMPK in Pathogens. Exp Suppl. 2016;107:287–323.

40. Mohri-Shiomi A, Garsin DA. Insulin signaling and the heat shock response modulate protein homeostasis in the Caenorhabditis elegans intestine during

infection. J Biol Chem. 2008 Jan 4;283(1):194–201.

41. Li L, Thompson LH, Zhao L, Messina JL. Tissue-specific difference in the molecular mechanisms for the development of acute insulin resistance after injury. Endocrinology. 2009 Jan;150(1):24–32.

42. Rask-Madsen C, Kahn CR. Tissue-specific insulin signaling, metabolic syndrome, and cardiovascular disease. Arterioscler Thromb Vasc Biol. 2012 Sep;32(9):2052–9.

43. Sharma N, Castorena CM, Cartee GD. Tissue-specific responses of IGF-1/insulin and mTOR signaling in calorie restricted rats. PLoS ONE. 2012 Jun 6;7(6):e38835.

44. Baar EL, Carbajal KA, Ong IM, Lamming DW. Sex- and tissue-specific changes in mTOR signaling with age in C57BL/6J mice. Aging Cell. 2016 Feb;15(1):155–66.

45. Lage R, Diéguez C, Vidal-Puig A, López M. AMPK: a metabolic gauge regulating whole-body energy homeostasis. Trends Mol Med. 2008 Dec;14(12):539–49.

46. Liu J, Stormo GD. Context-dependent DNA recognition code for C2H2 zinc-finger transcription factors. Bioinformatics. 2008 Sep 1;24(17):1850–7.

47. Lee Y, Zhou Q. Co-regulation in embryonic stem cells via context-dependent binding of transcription factors. Bioinformatics. 2013 Sep 1;29(17):2162–8.

48. Joshi CJ, Schinn S-M, Richelle A, Shamie I, O'Rourke EJ, Lewis NE. StanDep: Capturing transcriptomic variability improves context-specific metabolic models. PLoS Comput Biol. 2020 May 12;16(5):e1007764.

49. Williams GC. Pleiotropy, Natural Selection, and the Evolution of Senescence. Evolution. 1957 Dec;11(4):398.

50. Gems D, Sutton AJ, Sundermeyer ML, Albert PS, King KV, Edgley ML, et al. Two pleiotropic classes of daf-2 mutation affect larval arrest, adult behavior, reproduction and longevity in Caenorhabditis elegans. Genetics. 1998 Sep;150(1):129–55.

51. Larsen PL, Albert PS, Riddle DL. Genes that regulate both development and longevity in Caenorhabditis elegans. Genetics. 1995 Apr;139(4):1567–83.

52. Patel DS, Garza-Garcia A, Nanji M, McElwee JJ, Ackerman D, Driscoll PC, et al. Clustering of genetically defined allele classes in the Caenorhabditis elegans DAF-2 insulin/IGF-1 receptor. Genetics. 2008 Feb 1;178(2):931–46.

53. Kenyon C, Chang J, Gensch E, Rudner A, Tabtiang R. A C. elegans mutant that lives twice as long as wild type. Nature. 1993 Dec 2;366(6454):461–4.

54. Liu JP, Baker J, Perkins AS, Robertson EJ, Efstratiadis A. Mice carrying null mutations of the genes encoding insulin-like growth factor I (Igf-1) and type 1 IGF receptor (Igf1r). Cell. 1993 Oct 8;75(1):59–72.

55. Powell-Braxton L, Hollingshead P, Warburton C, Dowd M, Pitts-Meek S, Dalton D, et al. IGF-I is required for normal embryonic growth in mice. Genes Dev. 1993 Dec;7(12B):2609–17.

56. Holzenberger M, Dupont J, Ducos B, Leneuve P, Géloën A, Even PC, et al. IGF-1 receptor regulates lifespan and resistance to oxidative stress in mice. Nature. 2003 Jan 9;421(6919):182–7.

57. Mao K, Quipildor GF, Tabrizian T, Novaj A, Guan F, Walters RO, et al. Late-life targeting of the IGF-1 receptor improves healthspan and lifespan in female mice. Nat Commun. 2018 Jun 19;9(1):2394.

58. Junnila RK, List EO, Berryman DE, Murrey JW, Kopchick JJ. The GH/IGF-1 axis in ageing and longevity. Nat Rev Endocrinol. 2013 Jun;9(6):366–76.

59. Bartke A, Brown-Borg H. Life extension in the dwarf mouse. Elsevier; 2004. p. 189–225.

60. Clancy DJ, Gems D, Harshman LG, Oldham S, Stocker H, Hafen E, et al. Extension of life-span by loss of CHICO, a Drosophila insulin receptor substrate protein. Science. 2001 Apr 6;292(5514):104–6.

61. Fernandez R, Tabarini D, Azpiazu N, Frasch M, Schlessinger J. The Drosophila insulin receptor homolog: a gene essential for embryonic development encodes two receptor isoforms with different signaling potential. EMBO J. 1995 Jul 17;14(14):3373–84.

62. Chen C, Jack J, Garofalo RS. The Drosophila insulin receptor is required for normal growth. Endocrinology. 1996 Mar;137(3):846–56.

63. Ayyadevara S, Alla R, Thaden JJ, Shmookler Reis RJ. Remarkable longevity and stress resistance of nematode PI3K-null mutants. Aging Cell. 2008 Jan;7(1):13–22.

64. Dorman JB, Albinder B, Shroyer T, Kenyon C. The age-1 and daf-2 genes function in a common pathway to control the lifespan of Caenorhabditis elegans. Genetics. 1995 Dec;141(4):1399–406.

65. Morris JZ, Tissenbaum HA, Ruvkun G. A phosphatidylinositol-3-OH kinase family member regulating longevity and diapause in Caenorhabditis elegans.

Nature. 1996 Aug 8;382(6591):536–9.

66. Zhou X, Takatoh J, Wang F. The mammalian class 3 PI3K (PIK3C3) is required for early embryogenesis and cell proliferation. PLoS ONE. 2011 Jan 20;6(1):e16358.

67. Bi L, Okabe I, Bernard DJ, Wynshaw-Boris A, Nussbaum RL. Proliferative defect and embryonic lethality in mice homozygous for a deletion in the p110alpha subunit of phosphoinositide 3-kinase. J Biol Chem. 1999 Apr 16;274(16):10963–8.

68. Bi L, Okabe I, Bernard DJ, Nussbaum RL. Early embryonic lethality in mice deficient in the p110β catalytic subunit of PI 3-kinase. Mamm Genome. 2002 Mar;13(3):169–72.

69. Foukas LC, Bilanges B, Bettedi L, Pearce W, Ali K, Sancho S, et al. Long-term p110α PI3K inactivation exerts a beneficial effect on metabolism. EMBO Mol Med. 2013 Apr;5(4):563–71.

70. Inuzuka Y, Okuda J, Kawashima T, Kato T, Niizuma S, Tamaki Y, et al. Suppression of phosphoinositide 3-kinase prevents cardiac aging in mice. Circulation. 2009 Oct 27;120(17):1695–703.

71. Zoncu R, Efeyan A, Sabatini DM. mTOR: from growth signal integration to cancer, diabetes and ageing. Nat Rev Mol Cell Biol. 2011 Jan;12(1):21–35.

72. Vellai T, Takacs-Vellai K, Zhang Y, Kovacs AL, Orosz L, Müller F. Genetics: influence of TOR kinase on lifespan in C. elegans. Nature. 2003 Dec 11;426(6967):620.

73. Murakami M, Ichisaka T, Maeda M, Oshiro N, Hara K, Edenhofer F, et al. mTOR is essential for growth and proliferation in early mouse embryos and embryonic stem cells. Mol Cell Biol. 2004 Aug;24(15):6710–8.

74. Jia K, Chen D, Riddle DL. The TOR pathway interacts with the insulin signaling pathway to regulate C. elegans larval development, metabolism and life span. Development. 2004 Aug;131(16):3897–906.

75. Albert PS, Riddle DL. Mutants of Caenorhabditis elegans that form dauer-like larvae. Dev Biol. 1988 Apr;126(2):270–93.

76. Selman C, Tullet JMA, Wieser D, Irvine E, Lingard SJ, Choudhury AI, et al. Ribosomal protein S6 kinase 1 signaling regulates mammalian life span. Science. 2009 Oct 2;326(5949):140–4.

77. Pende M, Um SH, Mieulet V, Sticker M, Goss VL, Mestan J, et al. S6K1(-/-)/S6K2(-/-) mice exhibit perinatal lethality and rapamycin-sensitive 5'-terminal

oligopyrimidine mRNA translation and reveal a mitogen-activated protein kinase-dependent S6 kinase pathway. Mol Cell Biol. 2004 Apr;24(8):3112–24.

78. Carey KL, Paulus GLC, Wang L, Balce DR, Luo JW, Bergman P, et al. TFEB transcriptional responses reveal negative feedback by BHLHE40 and BHLHE41. Cell Rep. 2020 Nov 10;33(6):108371.

79. Repnik U, Borg Distefano M, Speth MT, Ng MYW, Progida C, Hoflack B, et al. L-leucyl-L-leucine methyl ester does not release cysteine cathepsins to the cytosol but inactivates them in transiently permeabilized lysosomes. J Cell Sci. 2017 Sep 15;130(18):3124–40.

80. Thiele DL, Lipsky PE. Mechanism of L-leucyl-L-leucine methyl ester-mediated killing of cytotoxic lymphocytes: dependence on a lysosomal thiol protease, dipeptidyl peptidase I, that is enriched in these cells. Proc Natl Acad Sci USA. 1990 Jan;87(1):83–7.

81. Henkel L, Rauscher B, Boutros M. Context-dependent genetic interactions in cancer. Curr Opin Genet Dev. 2019 Feb;54:73–82.

82. Torrence ME, Manning BD. Nutrient sensing in cancer. Annu Rev Cancer Biol. 2018 Feb;2(1).

83. Dansen TB, Burgering BMT. Unravelling the tumor-suppressive functions of FOXO proteins. Trends Cell Biol. 2008 Sep;18(9):421–9.

84. Sykes SM, Lane SW, Bullinger L, Kalaitzidis D, Yusuf R, Saez B, et al. AKT/FOXO signaling enforces reversible differentiation blockade in myeloid leukemias. Cell. 2011 Sep 2;146(5):697–708.

85. Lapierre LR, Hansen M. Lessons from C. elegans: signaling pathways for longevity. Trends Endocrinol Metab. 2012 Dec 1;23(12):637–44.

86. Michaelson D, Korta DZ, Capua Y, Hubbard EJA. Insulin signaling promotes germline proliferation in C. elegans. Development. 2010 Feb 1;137(4):671–80.

87. Kyriakakis E, Markaki M, Tavernarakis N. Caenorhabditis elegans as a model for cancer research. Mol Cell Oncol. 2015 Jun;2(2):e975027.

88. Berry LW, Westlund B, Schedl T. Germ-line tumor formation caused by activation of glp-1, a Caenorhabditis elegans member of the Notch family of receptors. Development. 1997 Feb;124(4):925–36.

89. Qi W, Huang X, Neumann-Haefelin E, Schulze E, Baumeister R. Cell-nonautonomous signaling of FOXO/DAF-16 to the stem cells of Caenorhabditis elegans. PLoS Genet. 2012 Aug 16;8(8):e1002836.

90. Qi W, Yan Y, Pfeifer D, Donner V Gromoff E, Wang Y, Maier W, et al. C. elegans DAF-16/FOXO interacts with TGF-ß/BMP signaling to induce germline tumor formation via mTORC1 activation. PLoS Genet. 2017 May 26;13(5):e1006801.

91. Schneider G, Schmidt-Supprian M, Rad R, Saur D. Tissue-specific tumorigenesis: context matters. Nat Rev Cancer. 2017 Mar 3;17(4):239–53.

92. Lin X-X, Sen I, Janssens GE, Zhou X, Fonslow BR, Edgar D, et al. DAF-16/FOXO and HLH-30/TFEB function as combinatorial transcription factors to promote stress resistance and longevity. Nat Commun. 2018 Oct 23;9(1):4400.

93. Zhang P, Judy M, Lee S-J, Kenyon C. Direct and indirect gene regulation by a life-extending FOXO protein in C. elegans: roles for GATA factors and lipid gene regulators. Cell Metab. 2013 Jan 8;17(1):85–100.

94. Heimbucher T, Hog J, Gupta P, Murphy CT. PQM-1 controls hypoxic survival via regulation of lipid metabolism. Nat Commun. 2020 Oct 2;11(1):4627.

95. Tepper RG, Ashraf J, Kaletsky R, Kleemann G, Murphy CT, Bussemaker HJ. PQM-1 complements DAF-16 as a key transcriptional regulator of DAF-2-mediated development and longevity. Cell. 2013 Aug 1;154(3):676–90.

96. Ke W, Saba JA, Yao C-H, Hilzendeger MA, Drangowska-Way A, Joshi C, et al. Dietary serine-microbiota interaction enhances chemotherapeutic toxicity without altering drug conversion. Nat Commun. 2020 May 22;11(1):2587.

97. Lynch JB, Hsiao EY. Microbiomes as sources of emergent host phenotypes. Science. 2019 Sep 27;365(6460):1405–9.

98. Holmes E, Li JV, Marchesi JR, Nicholson JK. Gut microbiota composition and activity in relation to host metabolic phenotype and disease risk. Cell Metab. 2012 Nov 7;16(5):559–64.

99. Gérard P. Gut microbiota and obesity. Cell Mol Life Sci. 2016 Jan;73(1):147–62.

100. Fu W, Hall MN. Regulation of mTORC2 Signaling. Genes (Basel). 2020 Sep 4;11(9).

101. Soukas AA, Kane EA, Carr CE, Melo JA, Ruvkun G. Rictor/TORC2 regulates fat metabolism, feeding, growth, and life span in Caenorhabditis elegans. Genes Dev. 2009 Feb 15;23(4):496–511.

102. Xiao R, Chun L, Ronan EA, Friedman DI, Liu J, Xu XZS. RNAi Interrogation of Dietary Modulation of Development, Metabolism, Behavior, and Aging in C. elegans. Cell Rep. 2015 May 19;11(7):1123–33.

103. Mizunuma M, Neumann-Haefelin E, Moroz N, Li Y, Blackwell TK. mTORC2-SGK-1 acts in two environmentally responsive pathways with opposing effects on longevity. Aging Cell. 2014 Oct;13(5):869–78.

104. Jerby L, Shlomi T, Ruppin E. Computational reconstruction of tissue-specific metabolic models: application to human liver metabolism. Mol Syst Biol. 2010 Sep 7;6:401.

105. Schmeichel KL, Bissell MJ. Modeling tissue-specific signaling and organ function in three dimensions. J Cell Sci. 2003 Jun 15;116(Pt 12):2377–88.

106. Vlassis N, Pacheco MP, Sauter T. Fast reconstruction of compact context-specific metabolic network models. PLoS Comput Biol. 2014 Jan 16;10(1):e1003424.

107. Becker SA, Palsson BO. Context-specific metabolic networks are consistent with experiments. PLoS Comput Biol. 2008 May 16;4(5):e1000082.

108. Shlomi T, Cabili MN, Herrgård MJ, Palsson BØ, Ruppin E. Network-based prediction of human tissue-specific metabolism. Nat Biotechnol. 2008 Sep;26(9):1003–10.

109. Clark AJ. The Mode of Action of Drugs on Cells. Canadian Medical Association Journal. 1933 Aug;

110. Henderson ST, Johnson TE. daf-16 integrates developmental and environmental inputs to mediate aging in the nematode Caenorhabditis elegans. Curr Biol. 2001 Dec 11;11(24):1975–80.

111. Zhong M, Niu W, Lu ZJ, Sarov M, Murray JI, Janette J, et al. Genome-wide identification of binding sites defines distinct functions for Caenorhabditis elegans PHA-4/FOXA in development and environmental response. PLoS Genet. 2010 Feb 19;6(2):e1000848.

112. Van Gilst MR, Hadjivassiliou H, Yamamoto KR. A Caenorhabditis elegans nutrient response system partially dependent on nuclear receptor NHR-49. Proc Natl Acad Sci USA. 2005 Sep 20;102(38):13496–501.

113. O'Rourke EJ, Ruvkun G. MXL-3 and HLH-30 transcriptionally link lipolysis and autophagy to nutrient availability. Nat Cell Biol. 2013 Jun;15(6):668–76.

114. Wang MC, O'Rourke EJ, Ruvkun G. Fat metabolism links germline stem cells and longevity in C. elegans. Science. 2008 Nov 7;322(5903):957–60.

115. Steinbaugh MJ, Narasimhan SD, Robida-Stubbs S, Moronetti Mazzeo LE, Dreyfuss JM, Hourihan JM, et al. Lipid-mediated regulation of SKN-1/Nrf in response to germ cell absence. elife. 2015 Aug 24;4.

116. Chen AT-Y, Guo C, Itani OA, Budaitis BG, Williams TW, Hopkins CE, et al. Longevity Genes Revealed by Integrative Analysis of Isoform-Specific daf-16/FoxO Mutants of Caenorhabditis elegans. Genetics. 2015 Oct;201(2):613–29.

117. Lapierre LR, Gelino S, Meléndez A, Hansen M. Autophagy and lipid metabolism coordinately modulate life span in germline-less C. elegans. Curr Biol. 2011 Sep 27;21(18):1507–14.

118. Seah NE, de Magalhaes Filho CD, Petrashen AP, Henderson HR, Laguer J, Gonzalez J, et al. Autophagy-mediated longevity is modulated by lipoprotein biogenesis. Autophagy. 2016;12(2):261–72.

119. O'Rourke EJ, Kuballa P, Xavier R, Ruvkun G. ω-6 Polyunsaturated fatty acids extend life span through the activation of autophagy. Genes Dev. 2013 Feb 15;27(4):429–40.

120. Kimura KD, Riddle DL, Ruvkun G. The C. elegans DAF-2 insulin-like receptor is abundantly expressed in the nervous system and regulated by nutritional status. Cold Spring Harb Symp Quant Biol. 2011 Nov 28;76:113–20.

121. Ogg S, Paradis S, Gottlieb S, Patterson GI, Lee L, Tissenbaum HA, et al. The Fork head transcription factor DAF-16 transduces insulin-like metabolic and longevity signals in C. elegans. Nature. 1997 Oct 30;389(6654):994–9.

122. Robida-Stubbs S, Glover-Cutter K, Lamming DW, Mizunuma M, Narasimhan SD, Neumann-Haefelin E, et al. TOR signaling and rapamycin influence longevity by regulating SKN-1/Nrf and DAF-16/FoxO. Cell Metab. 2012 May 2;15(5):713–24.

123. Taubert S, Van Gilst MR, Hansen M, Yamamoto KR. A Mediator subunit, MDT-15, integrates regulation of fatty acid metabolism by NHR-49-dependent and -independent pathways in C. elegans. Genes Dev. 2006 May 1;20(9):1137–49.

124. Panowski SH, Wolff S, Aguilaniu H, Durieux J, Dillin A. PHA-4/Foxa mediates diet-restriction-induced longevity of C. elegans. Nature. 2007 May 31;447(7144):550–5.

125. Riddle DL, Swanson MM, Albert PS. Interacting genes in nematode dauer larva formation. Nature. 1981 Apr 23;290(5808):668–71.

126. Xu X-Y, Hu J-P, Wu M-M, Wang L-S, Fang N-Y. CCAAT/enhancer-binding protein CEBP-2 controls fat consumption and fatty acid desaturation in Caenorhabditis elegans. Biochem Biophys Res Commun. 2015 Dec 11;468(1–2):312–8.

127. Dowen RH. CEH-60/PBX and UNC-62/MEIS Coordinate a Metabolic Switch that Supports Reproduction in C. elegans. Dev Cell. 2019 Apr 22;49(2):235-250.e7.

128. Goudeau J, Bellemin S, Toselli-Mollereau E, Shamalnasab M, Chen Y, Aguilaniu H. Fatty acid desaturation links germ cell loss to longevity through NHR-80/HNF4 in C. elegans. PLoS Biol. 2011 Mar 15;9(3):e1000599.

129. McGhee JD, Fukushige T, Krause MW, Minnema SE, Goszczynski B, Gaudet J, et al. ELT-2 is the predominant transcription factor controlling differentiation and function of the C. elegans intestine, from embryo to adult. Dev Biol. 2009 Mar 15;327(2):551–65.

130. Altarejos JY, Montminy M. CREB and the CRTC co-activators: sensors for hormonal and metabolic signals. Nat Rev Mol Cell Biol. 2011 Mar;12(3):141–51.

131. Amrit FRG, Steenkiste EM, Ratnappan R, Chen S-W, McClendon TB, Kostka D, et al. DAF-16 and TCER-1 Facilitate Adaptation to Germline Loss by Restoring Lipid Homeostasis and Repressing Reproductive Physiology in C. elegans. PLoS Genet. 2016 Feb 10;12(2):e1005788.

132. Burkewitz K, Morantte I, Weir HJM, Yeo R, Zhang Y, Huynh FK, et al. Neuronal CRTC-1 governs systemic mitochondrial metabolism and lifespan via a catecholamine signal. Cell. 2015 Feb 26;160(5):842–55.

133. Shaw WM, Luo S, Landis J, Ashraf J, Murphy CT. The C. elegans TGF-beta Dauer pathway regulates longevity via insulin signaling. Curr Biol. 2007 Oct 9;17(19):1635–45.

134. Fernandes de Abreu DA, Caballero A, Fardel P, Stroustrup N, Chen Z, Lee K, et al. An insulin-to-insulin regulatory network orchestrates phenotypic specificity in development and physiology. PLoS Genet. 2014 Mar 27;10(3):e1004225.

135. Motola DL, Cummins CL, Rottiers V, Sharma KK, Li T, Li Y, et al. Identification of ligands for DAF-12 that govern dauer formation and reproduction in C. elegans. Cell. 2006 Mar 24;124(6):1209–23.

136. Gerstein MB, Lu ZJ, Van Nostrand EL, Cheng C, Arshinoff BI, Liu T, et al. Integrative analysis of the Caenorhabditis elegans genome by the modENCODE project. Science. 2010 Dec 24;330(6012):1775–87.

137. Sun Y, Li M, Zhao D, Li X, Yang C, Wang X. Lysosome activity is modulated by multiple longevity pathways and is important for lifespan extension in C. elegans. elife. 2020 Jun 2;9.

138. Saxton RA, Sabatini DM. mTOR Signaling in Growth, Metabolism, and Disease. Cell. 2017 Mar 9;168(6):960–76.

139. Tissenbaum HA, Ruvkun G. An insulin-like signaling pathway affects both longevity and reproduction in Caenorhabditis elegans. Genetics. 1998 Feb;148(2):703–17.

140. Miyata S, Begun J, Troemel ER, Ausubel FM. DAF-16-dependent suppression of immunity during reproduction in Caenorhabditis elegans. Genetics. 2008 Feb 1;178(2):903–18.

141. Tullet JMA, Hertweck M, An JH, Baker J, Hwang JY, Liu S, et al. Direct inhibition of the longevity-promoting factor SKN-1 by insulin-like signaling in C. elegans. Cell. 2008 Mar 21;132(6):1025–38.

142. Jünger MA, Rintelen F, Stocker H, Wasserman JD, Végh M, Radimerski T, et al. The Drosophila forkhead transcription factor FOXO mediates the reduction in cell number associated with reduced insulin signaling. J Biol. 2003 Aug 7;2(3):20.

143. Essers MAG, de Vries-Smits LMM, Barker N, Polderman PE, Burgering BMT, Korswagen HC. Functional interaction between beta-catenin and FOXO in oxidative stress signaling. Science. 2005 May 20;308(5725):1181–4.

144. Lehtinen MK, Yuan Z, Boag PR, Yang Y, Villén J, Becker EBE, et al. A conserved MST-FOXO signaling pathway mediates oxidative-stress responses and extends life span. Cell. 2006 Jun 2;125(5):987–1001.

145. Murphy CT, McCarroll SA, Bargmann CI, Fraser A, Kamath RS, Ahringer J, et al. Genes that act downstream of DAF-16 to influence the lifespan of Caenorhabditis elegans. Nature. 2003 Jul 17;424(6946):277–83.

146. Sen I, Zhou X, Chernobrovkin A, Puerta-Cavanzo N, Kanno T, Salignon J, et al. DAF-16/FOXO requires Protein Phosphatase 4 to initiate transcription of stress resistance and longevity promoting genes. Nat Commun. 2020 Jan 9;11(1):138.

147. Oliveira RP, Porter Abate J, Dilks K, Landis J, Ashraf J, Murphy CT, et al. Condition-adapted stress and longevity gene regulation by Caenorhabditis elegans SKN-1/Nrf. Aging Cell. 2009 Sep 1;8(5):524–41.

148. Luz AL, Godebo TR, Smith LL, Leuthner TC, Maurer LL, Meyer JN. Deficiencies in mitochondrial dynamics sensitize Caenorhabditis elegans to arsenite and other mitochondrial toxicants by reducing mitochondrial adaptability. Toxicology. 2017 Jul 15;387:81–94.

149. Masaki N, Kyle ME, Farber JL. tert-butyl hydroperoxide kills cultured

hepatocytes by peroxidizing membrane lipids. Arch Biochem Biophys. 1989 Mar;269(2):390–9.

150. Madsen RR, Vanhaesebroeck B. Cracking the context-specific PI3K signaling code. Sci Signal. 2020 Jan 7;13(613).

151. van Amerongen R, Nusse R. Towards an integrated view of Wnt signaling in development. Development. 2009 Oct;136(19):3205–14.

152. Chi C, Ronai D, Than MT, Walker CJ, Sewell AK, Han M. Nucleotide levels regulate germline proliferation through modulating GLP-1/Notch signaling in C. elegans. Genes Dev. 2016 Feb 1;30(3):307–20.

153. Schuster E, McElwee JJ, Tullet JMA, Doonan R, Matthijssens F, Reece-Hoyes JS, et al. DamID in C. elegans reveals longevity-associated targets of DAF-16/FoxO. Mol Syst Biol. 2010 Aug 10;6:399.

154. Pelham H. Activation of heat-shock genes in eukaryotes. Trends Genet. 1985 Jan;1:31–5.

155. Hsu A-L, Murphy CT, Kenyon C. Regulation of Aging and Age-Related Disease by DAF-16 and Heat-Shock Factor [Internet]. 1999 [cited 2020 Feb 8] p. 2770. Available from: http://science.sciencemag.org/

156. Shemesh N, Shai N, Ben-Zvi A. Germline stem cell arrest inhibits the collapse of somatic proteostasis early in Caenorhabditis elegans adulthood. Aging Cell. 2013 Oct;12(5):814–22.

157. Lee RY, Hench J, Ruvkun G. Regulation of C. elegans DAF-16 and its human ortholog FKHRL1 by the daf-2 insulin-like signaling pathway. Curr Biol. 2001 Dec 11;11(24):1950–7.

158. Servello FA, Apfeld J. The heat shock transcription factor HSF-1 protects Caenorhabditis elegans from peroxide stress. Translational Medicine of Aging. 2020;4:88–92.

159. Morton EA, Lamitina T. Caenorhabditis elegans HSF-1 is an essential nuclear protein that forms stress granule-like structures following heat shock. Aging Cell. 2013 Feb;12(1):112–20.

160. Jarc E, Petan T. Lipid droplets and the management of cellular stress. Yale J Biol Med. 2019 Sep 20;92(3):435–52.

161. Bensaad K, Favaro E, Lewis CA, Peck B, Lord S, Collins JM, et al. Fatty acid uptake and lipid storage induced by HIF-1α contribute to cell growth and survival after hypoxia-reoxygenation. Cell Rep. 2014 Oct 9;9(1):349–65.

162. Bailey AP, Koster G, Guillermier C, Hirst EMA, MacRae JI, Lechene CP, et al. Antioxidant role for lipid droplets in a stem cell niche of drosophila. Cell. 2015 Oct 8;163(2):340–53.

163. Wählby C, Conery AL, Bray M-A, Kamentsky L, Larkins-Ford J, Sokolnicki KL, et al. High- and low-throughput scoring of fat mass and body fat distribution in C. elegans. Methods. 2014 Aug 1;68(3):492–9.

164. Ke W, Drangowska-Way A, Katz D, Siller K, O'Rourke EJ. The Ancient Genetic Networks of Obesity: Whole-Animal Automated Screening for Conserved Fat Regulators. Methods Mol Biol. 2018;1787:129–46.

165. Puertollano R, Ferguson SM, Brugarolas J, Ballabio A. The complex relationship between TFEB transcription factor phosphorylation and subcellular localization. EMBO J. 2018 Jun 1;37(11).

166. Seo K, Choi E, Lee D, Jeong D-E, Jang SK, Lee S-J. Heat shock factor 1 mediates the longevity conferred by inhibition of TOR and insulin/IGF-1 signaling pathways in C. elegans. Aging Cell. 2013 Dec;12(6):1073–81.

167. Martina JA, Chen Y, Gucek M, Puertollano R. MTORC1 functions as a transcriptional regulator of autophagy by preventing nuclear transport of TFEB. Autophagy. 2012 Jun 1;8(6):903–14.

168. Settembre C, Zoncu R, Medina DL, Vetrini F, Erdin S, Erdin S, et al. A lysosome-to-nucleus signalling mechanism senses and regulates the lysosome via mTOR and TFEB. EMBO J. 2012 Mar 7;31(5):1095–108.

169. Vega-Rubin-de-Celis S, Peña-Llopis S, Konda M, Brugarolas J. Multistep regulation of TFEB by MTORC1. Autophagy. 2017 Mar 4;13(3):464–72.

170. Roczniak-Ferguson A, Petit CS, Froehlich F, Qian S, Ky J, Angarola B, et al. The transcription factor TFEB links mTORC1 signaling to transcriptional control of lysosome homeostasis. Sci Signal. 2012 Jun 12;5(228):ra42.

171. Nezich CL, Wang C, Fogel AI, Youle RJ. MiT/TFE transcription factors are activated during mitophagy downstream of Parkin and Atg5. J Cell Biol. 2015 Aug 3;210(3):435–50.

172. Laplante M, Sabatini DM. mTOR signaling at a glance. J Cell Sci. 2009 Oct 15;122(Pt 20):3589–94.

173. Sukumaran A, Choi K, Dasgupta B. Insight on Transcriptional Regulation of the Energy Sensing AMPK and Biosynthetic mTOR Pathway Genes. Front Cell Dev Biol. 2020 Jul 29;8:671.

174. Nakamura S, Karalay Ö, Jäger PS, Horikawa M, Klein C, Nakamura K, et al.

Mondo complexes regulate TFEB via TOR inhibition to promote longevity in response to gonadal signals. Nat Commun. 2016 Mar 22;7:10944.

175. Mao Z, Zhang W. Role of mTOR in Glucose and Lipid Metabolism. Int J Mol Sci. 2018 Jul 13;19(7).

176. Chan SM, Weng AP, Tibshirani R, Aster JC, Utz PJ. Notch signals positively regulate activity of the mTOR pathway in T-cell acute lymphoblastic leukemia. Blood. 2007 Jul 1;110(1):278–86.

177. Barolo S, Posakony JW. Three habits of highly effective signaling pathways: principles of transcriptional control by developmental cell signaling. Genes Dev. 2002 May 15;16(10):1167–81.

178. Senchuk MM, Dues DJ, Schaar CE, Johnson BK, Madaj ZB, Bowman MJ, et al. Activation of DAF-16/FOXO by reactive oxygen species contributes to longevity in long-lived mitochondrial mutants in Caenorhabditis elegans. PLoS Genet. 2018 Mar 9;14(3):e1007268.

179. Qiao A, Jin X, Pang J, Moskophidis D, Mivechi NF. The transcriptional regulator of the chaperone response HSF1 controls hepatic bioenergetics and protein homeostasis. J Cell Biol. 2017 Mar 6;216(3):723–41.

180. Pfaffl MW. A new mathematical model for relative quantification in real-time RT-PCR. Nucleic Acids Res. 2001 May 1;29(9):e45.

181. Albert R, DasGupta B, Dondi R, Kachalo S, Sontag E, Zelikovsky A, et al. A novel method for signal transduction network inference from indirect experimental evidence. J Comput Biol. 2007 Sep;14(7):927–49.

182. Hilbert ZA, Kim DH. Sexually dimorphic control of gene expression in sensory neurons regulates decision-making behavior in C. elegans. elife. 2017 Jan 24;6.

183. Wynn ML, Consul N, Merajver SD, Schnell S. Logic-based models in systems biology: a predictive and parameter-free network analysis method. Integr Biol (Camb). 2012 Nov 1;4(11):1323–37.

184. Laubenbacher R, Hinkelmann F, Murrugarra D, Veliz-Cuba A. Algebraic models and their use in systems biology. In: Jonoska N, Saito M, editors. Discrete and topological models in molecular biology. Berlin, Heidelberg: Springer Berlin Heidelberg; 2014. p. 443–74.

185. Steinway SN, Wang R-S, Albert R. Discrete dynamic modeling: A network approach for systems pharmacology. In: Mager DE, Kimko HHC, editors. Systems pharmacology and pharmacodynamics. Cham: Springer International Publishing; 2016. p. 81–103.

186. Abou-Jaoudé W, Traynard P, Monteiro PT, Saez-Rodriguez J, Helikar T, Thieffry D, et al. Logical modeling and dynamical analysis of cellular networks. Front Genet. 2016 May 31;7:94.

187. Zhang Y, Chen D, Smith MA, Zhang B, Pan X. Selection of reliable reference genes in Caenorhabditis elegans for analysis of nanotoxicity. PLoS ONE. 2012 Mar 15;7(3):e31849.

188. Douglas PM, Baird NA, Simic MS, Uhlein S, McCormick MA, Wolff SC, et al. Heterotypic Signals from Neural HSF-1 Separate Thermotolerance from Longevity. Cell Rep. 2015 Aug 18;12(7):1196–204.

189. Folick A, Oakley HD, Yu Y, Armstrong EH, Kumari M, Sanor L, et al. Aging. Lysosomal signaling molecules regulate longevity in Caenorhabditis elegans. Science. 2015 Jan 2;347(6217):83–6.

190. Avery L. The genetics of feeding in Caenorhabditis elegans. Genetics. 1993 Apr;133(4):897–917.

191. Sohal RS, Weindruch R. Oxidative stress, caloric restriction, and aging. Science. 1996 Jul 5;273(5271):59–63.

192. Mair W, Morantte I, Rodrigues APC, Manning G, Montminy M, Shaw RJ, et al. Lifespan extension induced by AMPK and calcineurin is mediated by CRTC-1 and CREB. Nature. 2011 Feb 17;470(7334):404–8.

193. Greer ER, Pérez CL, Van Gilst MR, Lee BH, Ashrafi K. Neural and molecular dissection of a C. elegans sensory circuit that regulates fat and feeding. Cell Metab. 2008 Aug;8(2):118–31.

194. Lakowski B, Hekimi S. The genetics of caloric restriction in Caenorhabditis elegans. Proc Natl Acad Sci USA. 1998 Oct 27;95(22):13091–6.

195. Carrano AC, Dillin A, Hunter T. A Krüppel-like factor downstream of the E3 ligase WWP-1 mediates dietary-restriction-induced longevity in Caenorhabditis elegans. Nat Commun. 2014 May 8;5:3772.

196. Shore DE, Carr CE, Ruvkun G. Induction of cytoprotective pathways is central to the extension of lifespan conferred by multiple longevity pathways. PLoS Genet. 2012 Jul 19;8(7):e1002792.

197. Park S-K, Link CD, Johnson TE. Life-span extension by dietary restriction is mediated by NLP-7 signaling and coelomocyte endocytosis in C. elegans. FASEB J. 2010 Feb;24(2):383–92.

198. Kuczynski J, Costello EK, Nemergut DR, Zaneveld J, Lauber CL, Knights D, et al. Direct sequencing of the human microbiome readily reveals community

differences. Genome Biol. 2010 May 5;11(5):210.

199. Sekirov I, Russell SL, Antunes LCM, Finlay BB. Gut microbiota in health and disease. Physiol Rev. 2010 Jul;90(3):859–904.

200. Quigley EMM. Microbiota-Brain-Gut Axis and Neurodegenerative Diseases. Curr Neurol Neurosci Rep. 2017 Oct 17;17(12):94.

201. Félix M-A, Duveau F. Population dynamics and habitat sharing of natural populations of Caenorhabditis elegans and C. briggsae. BMC Biol. 2012 Jun 25;10:59.

202. Cabreiro F, Gems D. Worms need microbes too: microbiota, health and aging in Caenorhabditis elegans. EMBO Mol Med. 2013 Sep;5(9):1300–10.

203. Zhang F, Berg M, Dierking K, Félix M-A, Shapira M, Samuel BS, et al. Caenorhabditis elegans as a Model for Microbiome Research. Front Microbiol. 2017 Mar 23;8:485.

204. Brenner S. The genetics of Caenorhabditis elegans. Genetics. 1974 May;77(1):71–94.

205. Boyer HW, Roulland-Dussoix D. A complementation analysis of the restriction and modification of DNA in Escherichia coli. J Mol Biol. 1969 May 14;41(3):459–72.

206. Timmons L, Court DL, Fire A. Ingestion of bacterially expressed dsRNAs can produce specific and potent genetic interference in Caenorhabditis elegans. Gene. 2001 Jan 24;263(1–2):103–12.

207. Han B, Sivaramakrishnan P, Lin C-CJ, Neve IAA, He J, Tay LWR, et al. Microbial genetic composition tunes host longevity. Cell. 2017 Jun 15;169(7):1249-1262.e13.

208. Pang S, Curran SP. Adaptive capacity to bacterial diet modulates aging in C. elegans. Cell Metab. 2014 Feb 4;19(2):221–31.

209. Scott TA, Quintaneiro LM, Norvaisas P, Lui PP, Wilson MP, Leung K-Y, et al. Host-Microbe Co-metabolism Dictates Cancer Drug Efficacy in C. elegans. Cell. 2017 Apr 20;169(3):442-456.e18.

210. García-González AP, Ritter AD, Shrestha S, Andersen EC, Yilmaz LS, Walhout AJM. Bacterial metabolism affects the c. elegans response to cancer chemotherapeutics. Cell. 2017 Apr 20;169(3):431-441.e8.

211. Jhanwar-Uniyal M, Wainwright JV, Mohan AL, Tobias ME, Murali R, Gandhi CD, et al. Diverse signaling mechanisms of mTOR complexes: mTORC1 and

mTORC2 in forming a formidable relationship. Adv Biol Regul. 2019 Apr 11;72:51–62.

212. Hosono R. Sterilization and growth inhibition of Caenorhabditis elegans by 5-fluorodeoxyuridine. Exp Gerontol. 1978;13(5):369–74.

213. Baba T, Ara T, Hasegawa M, Takai Y, Okumura Y, Baba M, et al. Construction of Escherichia coli K-12 in-frame, single-gene knockout mutants: the Keio collection. Mol Syst Biol. 2006 Feb 21;2:2006.0008.

214. Datsenko KA, Wanner BL. One-step inactivation of chromosomal genes in *Escherichia coli* K-12 using PCR products. Proc Natl Acad Sci USA. 2000 Jun 6;97(12):6640–5.

215. Edwards JS, Palsson BO. The Escherichia coli MG1655 in silico metabolic genotype: its definition, characteristics, and capabilities. Proc Natl Acad Sci USA. 2000 May 9;97(10):5528–33.

216. Schellenberger J, Park JO, Conrad TM, Palsson BØ. BiGG: a Biochemical Genetic and Genomic knowledgebase of large scale metabolic reconstructions. BMC Bioinformatics. 2010 Apr 29;11:213.

217. Kanehisa M, Goto S, Furumichi M, Tanabe M, Hirakawa M. KEGG for representation and analysis of molecular networks involving diseases and drugs. Nucleic Acids Res. 2010 Jan;38(Database issue):D355-60.

218. Wang Y, Xiao J, Suzek TO, Zhang J, Wang J, Zhou Z, et al. PubChem's BioAssay Database. Nucleic Acids Res. 2012 Jan;40(Database issue):D400-12.

219. Wang Y, Bryant SH, Cheng T, Wang J, Gindulyte A, Shoemaker BA, et al. PubChem BioAssay: 2017 update. Nucleic Acids Res. 2017 Jan 4;45(D1):D955–63.

220. Caspi R, Altman T, Billington R, Dreher K, Foerster H, Fulcher CA, et al. The MetaCyc database of metabolic pathways and enzymes and the BioCyc collection of Pathway/Genome Databases. Nucleic Acids Res. 2014 Jan;42(Database issue):D459-71.

221. Caspi R, Billington R, Fulcher CA, Keseler IM, Kothari A, Krummenacker M, et al. The MetaCyc database of metabolic pathways and enzymes. Nucleic Acids Res. 2018 Jan 4;46(D1):D633–9.

222. Kim J, Reed JL. Refining metabolic models and accounting for regulatory effects. Curr Opin Biotechnol. 2014 Oct;29:34–8.

223. Bochner BR, Gadzinski P, Panomitros E. Phenotype microarrays for high-throughput phenotypic testing and assay of gene function. Genome Res. 2001

Jul;11(7):1246–55.

224. Lee EJ, Glasgow J, Leu SF, Belduz AO, Harman JG. Mutagenesis of the cyclic AMP receptor protein of Escherichia coli: targeting positions 83, 127 and 128 of the cyclic nucleotide binding pocket. Nucleic Acids Res. 1994 Aug 11;22(15):2894–901.

225. Deo SS, Tseng WC, Saini R, Coles RS, Athwal RS. Purification and characterization of Escherichia coli xanthine-guanine phosphoribosyltransferase produced by plasmid pSV2gpt. Biochim Biophys Acta. 1985 May 8;839(3):233–9.

226. Titz B, Häuser R, Engelbrecher A, Uetz P. The Escherichia coli protein YjjG is a house-cleaning nucleotidase in vivo. FEMS Microbiol Lett. 2007 May;270(1):49–57.

227. Kuznetsova E, Proudfoot M, Gonzalez CF, Brown G, Omelchenko MV, Borozan I, et al. Genome-wide analysis of substrate specificities of the Escherichia coli haloacid dehalogenase-like phosphatase family. J Biol Chem. 2006 Nov 24;281(47):36149–61.

228. McCloskey D, Palsson BØ, Feist AM. Basic and applied uses of genome-scale metabolic network reconstructions of Escherichia coli. Mol Syst Biol. 2013;9:661.

229. Berg EL. Systems biology in drug discovery and development. Drug Discov Today. 2014 Feb;19(2):113–25.

230. Arrell DK, Terzic A. Network systems biology for drug discovery. Clin Pharmacol Ther. 2010 Jul;88(1):120–5.

231. Hefzi H, Ang KS, Hanscho M, Bordbar A, Ruckerbauer D, Lakshmanan M, et al. A Consensus Genome-scale Reconstruction of Chinese Hamster Ovary Cell Metabolism. Cell Syst. 2016 Nov 23;3(5):434-443.e8.

232. Gebauer J, Gentsch C, Mansfeld J, Schmeißer K, Waschina S, Brandes S, et al. A Genome-Scale Database and Reconstruction of Caenorhabditis elegans Metabolism. Cell Syst. 2016 May 25;2(5):312–22.

233. Yilmaz LS, Walhout AJM. A Caenorhabditis elegans Genome-Scale Metabolic Network Model. Cell Syst. 2016 May 25;2(5):297–311.

234. Swainston N, Smallbone K, Hefzi H, Dobson PD, Brewer J, Hanscho M, et al. Recon 2.2: from reconstruction to model of human metabolism. Metabolomics. 2016 Jun 7;12:109.

235. Brunk E, Sahoo S, Zielinski DC, Altunkaya A, Dräger A, Mih N, et al. Recon3D

enables a three-dimensional view of gene variation in human metabolism. Nat Biotechnol. 2018 Mar;36(3):272–81.

236. Bauer E, Thiele I. From network analysis to functional metabolic modeling of the human gut microbiota. mSystems. 2018 Jun;3(3).

237. Kanehisa M, Goto S. KEGG: Kyoto encyclopedia of genes and genomes. Nucleic Acids Res. 2000 Jan 1;28(1):27–30.

238. Karp PD, Billington R, Caspi R, Fulcher CA, Latendresse M, Kothari A, et al. The BioCyc collection of microbial genomes and metabolic pathways. Brief Bioinformatics. 2019 Jul 19;20(4):1085–93.

239. Gray JM, Spiegel I. Cell-type-specific programs for activity-regulated gene expression. Curr Opin Neurobiol. 2019 Jun;56:33–9.

240. Chintapalli VR, Terhzaz S, Wang J, Al Bratty M, Watson DG, Herzyk P, et al. Functional correlates of positional and gender-specific renal asymmetry in Drosophila. PLoS ONE. 2012 Apr 4;7(4):e32577.

241. McClure CD, Southall TD. Getting Down to Specifics: Profiling Gene Expression and Protein-DNA Interactions in a Cell Type-Specific Manner. Adv Genet. 2015 Jul 23;91:103–51.

242. Reed JL, Vo TD, Schilling CH, Palsson BO. An expanded genome-scale model of Escherichia coli K-12 (iJR904 GSM/GPR). Genome Biol. 2003 Aug 28;4(9):R54.

243. Duarte NC, Herrgård MJ, Palsson BØ. Reconstruction and validation of Saccharomyces cerevisiae iND750, a fully compartmentalized genome-scale metabolic model. Genome Res. 2004 Jul;14(7):1298–309.

244. Edwards JS, Palsson BO. Systems properties of the Haemophilus influenzae Rd metabolic genotype. J Biol Chem. 1999 Jun 18;274(25):17410–6.

245. Price ND, Papin JA, Palsson BØ. Determination of redundancy and systems properties of the metabolic network of Helicobacter pylori using genome-scale extreme pathway analysis. Genome Res. 2002 May;12(5):760–9.

246. Yeh I, Hanekamp T, Tsoka S, Karp PD, Altman RB. Computational analysis of Plasmodium falciparum metabolism: organizing genomic information to facilitate drug discovery. Genome Res. 2004 May;14(5):917–24.

247. Ramon C, Gollub MG, Stelling J. Integrating -omics data into genome-scale metabolic network models: principles and challenges. Essays Biochem. 2018 Oct 26;62(4):563–74.

248. Joyce AR, Palsson BØ. The model organism as a system: integrating “omics” data sets. Nat Rev Mol Cell Biol. 2006 Mar;7(3):198–210.

249. Bersanelli M, Mosca E, Remondini D, Giampieri E, Sala C, Castellani G, et al. Methods for the integration of multi-omics data: mathematical aspects. BMC Bioinformatics. 2016 Jan 20;17 Suppl 2:15.

250. Sharma S, Petsalaki E. Large-scale datasets uncovering cell signalling networks in cancer: context matters. Curr Opin Genet Dev. 2019 Jun 11;54:118–24.

251. Fouladiha H, Marashi S-A. Biomedical applications of cell- and tissue-specific metabolic network models. J Biomed Inform. 2017 Feb 24;68:35–49.

252. Sen P, Orešič M. Metabolic modeling of human gut microbiota on a genome scale: an overview. Metabolites. 2019 Jan 28;9(2).

253. Dey N, Williams C, Leyland-Jones B, De P. Mutation matters in precision medicine: A future to believe in. Cancer Treat Rev. 2017 Apr;55:136–49.

254. Drake JM, Paull EO, Graham NA, Lee JK, Smith BA, Titz B, et al. Phosphoproteome Integration Reveals Patient-Specific Networks in Prostate Cancer. Cell. 2016 Aug 11;166(4):1041–54.

255. Nagy R, Sweet K, Eng C. Highly penetrant hereditary cancer syndromes. Oncogene. 2004 Aug 23;23(38):6445–70.

256. Shen JP, Zhao D, Sasik R, Luebeck J, Birmingham A, Bojorquez-Gomez A, et al. Combinatorial CRISPR-Cas9 screens for de novo mapping of genetic interactions. Nat Methods. 2017 Jun;14(6):573–6.

257. Harshman LG, Zera AJ. The cost of reproduction: the devil in the details. Trends Ecol Evol (Amst). 2007 Feb;22(2):80–6.

258. Williams TD. Mechanisms underlying the costs of egg production. Bioscience. 2005;55(1):39.

259. Rose MR, Bradley TJ. Evolutionary physiology of the cost of reproduction. Oikos. 1998 Dec;83(3):443.

260. Zera AJ, Harshman LG. The Physiology of Life History Trade-Offs in Animals. Annu Rev Ecol Syst. 2001 Nov;32(1):95–126.

261. Maklakov AA, Immler S. The expensive germline and the evolution of ageing. Curr Biol. 2016 Jul 11;26(13):R577–86.

262. Arantes-Oliveira N, Apfeld J, Dillin A, Kenyon C. Regulation of life-span by germ-line stem cells in Caenorhabditis elegans. Science. 2002 Jan 18;295(5554):502–5.

263. Wählby C, Kamentsky L, Liu ZH, Riklin-Raviv T, Conery AL, O'Rourke EJ, et al. An image analysis toolbox for high-throughput C. elegans assays. Nat Methods. 2012 Apr 22;9(7):714–6.

264. Melo JA, Ruvkun G. Inactivation of conserved C. elegans genes engages pathogen- and xenobiotic-associated defenses. Cell. 2012 Apr 13;149(2):452–66.

265. Calixto A, Chelur D, Topalidou I, Chen X, Chalfie M. Enhanced neuronal RNAi in C. elegans using SID-1. Nat Methods. 2010 Jul;7(7):554–9.

266. McGhee JD. The C. elegans intestine. WormBook. 2007 Mar 27;1–36.

267. Kimble J, Sharrock WJ. Tissue-specific synthesis of yolk proteins in Caenorhabditis elegans. Dev Biol. 1983 Mar;96(1):189–96.

268. Avery L, You Y-J. C. elegans feeding. WormBook. 2012 May 21;1–23.

269. Srinivasan S. Regulation of body fat in Caenorhabditis elegans. Annu Rev Physiol. 2015;77(1):161–78.